

AD-E800410

AFATL-TR-80-66

② LEVEL III

AD A104989

# Trajectory Prediction Theory Of Supersonic High Fineness Ratio, Cruciform Fin Bodies

Dr Lawrence Lijewski

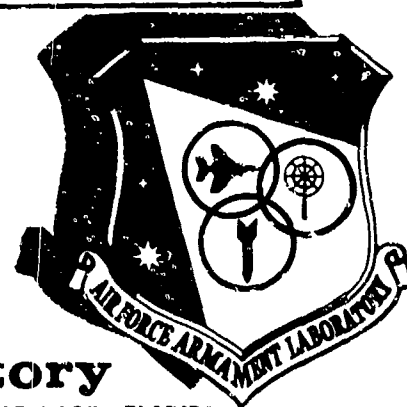
MUNITIONS DIVISION  
AIR FORCE ARMAMENT LABORATORY  
EGLIN AIR FORCE BASE, FLORIDA 32542

DTIC  
ELECTE  
SEP 29 1981  
B

JUNE 1980

FINAL REPORT FOR PERIOD OCTOBER 1972-JULY 1974

APPROVED FOR PUBLIC RELEASE, DISTRIBUTION UNLIMITED.



**Air Force Armament Laboratory**  
AIR FORCE SYSTEMS COMMAND • UNITED STATES AIR FORCE • EGLIN AIR FORCE BASE, FLORIDA

DHC FILE COPY

81 9 28 281

## **NOTICE**

**Please do not request copies of this report from the Air Force Armament Laboratory.  
Additional copies may be purchased from:**

**National Technical Information Service  
5285 Port Royal Road  
Springfield, Virginia 22161**

**Federal Government agencies and their contractors registered with Defense Technical  
Information Center should direct requests for copies of this report to:**

**Defense Technical Information Center  
Cameron Station  
Alexandria, Virginia 22314**

UNCLASSIFIED

SECURITY CLASSIFICATION OF THIS PAGE (When Data Entered)

REPORT DOCUMENTATION PAGE		READ INSTRUCTIONS BEFORE COMPLETING FORM
1. REPORT NUMBER AFATL-TR-80-66	2. GOVT ACCESSION NO. AD-A104989	3. RECIPIENT'S CATALOG NUMBER
4. TITLE (and Subtitle) TRAJECTORY PREDICTION THEORY OF SUPER-SONIC HIGH FINENESS RATIO, CRUCIFORM FIN BODIES		5. TYPE OF REPORT & PERIOD COVERED ANNUAL REPORT: OCTOBER 1973 - JULY 1974
7. AUTHOR(s) Dr. Lawrence Lijewski		8. PERFORMING ORG. REPORT NUMBER
9. PERFORMING ORGANIZATION NAME AND ADDRESS Munitions Division Air Force Armament Laboratory Eglin Air Force Base, Florida 32542		10. PROGRAM ELEMENT, PROJECT, TASK AREA & WORK UNIT NUMBERS PE: 62602F JON: 25670229
11. CONTROLLING OFFICE NAME AND ADDRESS Air Force Armament Laboratory Armament Division Eglin Air Force Base, Florida 32542		12. REPORT DATE June 1980
14. MONITORING AGENCY NAME & ADDRESS (if different from Controlling Office)		13. NUMBER OF PAGES 175
		15. SECURITY CLASS. (of this report) Unclassified
		15a. DECLASSIFICATION/DOWNGRADING SCHEDULE
16. DISTRIBUTION STATEMENT (of this Report)  Approved for public release, distribution unlimited.		
17. DISTRIBUTION STATEMENT (of the abstract entered in Block 20, if different from Report)		
18. SUPPLEMENTARY NOTES  Available in DTIC.		
19. KEY WORDS (Continue on reverse side if necessary and identify by block number) Trajectory Theory                      Six-Degree-of-Freedom Analysis Flight Dynamics Jump Angle Initial Flight Conditions Muzzle Blast Effects		
20. ABSTRACT (Continue on reverse side if necessary and identify by block number) A complete Jump and Dispersion Theory is developed for free flight vehicles. Six-degree-of-freedom computer computations indicate that the theory accurately predicts the jump dispersion of flechettes. The initial conditions and dispersion values are established by range test firings. The raw data is fitted by least squares method and put into initial condition form. Initial conditions are applied to the theory and 6-D numerical computations to evaluate dispersion for eight test rounds. The		

DD FORM 1 JAN 73 1473

UNCLASSIFIED

SECURITY CLASSIFICATION OF THIS PAGE (When Data Entered)

UNCLASSIFIED

SECURITY CLASSIFICATION OF THIS PAGE(When Data Entered)

Item 20 Abstract (Concluded)

results are compared to test firing target data. The agreement between the theory and test results indicate the data analysis and theory provide an accurate means of predicting dispersion of flechettes. Analysis of the firing data indicates that the initial conditions result from an impulse imparted to the flechette in the muzzle blast. The transverse impulse imparted to the flechette initially must be equal to the angular impulse to obtain zero dispersion. Other disturbances in the blast region such as sabot separation influence the initial conditions and hence dispersion. First maximum yaw theory is discussed and disproved.

UNCLASSIFIED

SECURITY CLASSIFICATION OF THIS PAGE(When Data Entered)

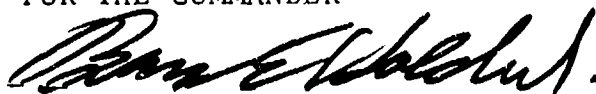
## PREFACE

This study was conducted by Dr. Lawrence Lijewski of the Aircraft Compatibility Branch, Munitions Division, as a dissertation while at the University of Notre Dame.

This report has been reviewed by the Information Officer (OI) and is releasable to the National Technical Information Service (NTIS). At NTIS it will be available to the general public, including foreign nations.

This technical report has been reviewed and is approved for publication.

FOR THE COMMANDER



BARNES E. HOLDER, JR., Colonel, USAF  
Chief, Munitions Division

Accession For	
NTIS GEAR	<input checked="checked" type="checkbox"/>
DTIC TAB	<input type="checkbox"/>
Unannounced	<input type="checkbox"/>
Justification	
By	
Distribution /	
Availability Codes	
Distribution	
A	

# TABLE OF CONTENTS

Section	Title	Page
I	INTRODUCTION . . . . .	1
II	DISPERSION THEORY. . . . .	4
	High Roll Rate Theory . . . . .	8
	Low Roll Rate Theory. . . . .	10
	Very Slow Roll Rate Theory. . . . .	12
III	VALIDATION OF THEORY . . . . .	14
	Phase I . . . . .	14
	Phase II. . . . .	24
	Phase III . . . . .	25
	Comparison: High, Low, Very Slow Roll Rate Theories . . . . .	61
	Phase IV. . . . .	61
IV	FREE FLIGHT DATA ANALYSIS. . . . .	71
V	DISPERSION ANALYSIS. . . . .	111
	Free Flight Versus Theory . . . . .	111
	Dispersion Theory Versus First Maximum Yaw Hypothesis. . . . .	130
VI	PHYSICAL EVALUATION OF DISPERSION. . . . .	139
VII	CONCLUSIONS. . . . .	145
	APPENDIX . . . . .	147
	REFERENCES . . . . .	156

# LIST OF FIGURES

Figure	Title	Page
1	Dispersion: Phase I Cases 10-18. . . . .	17
2	Trajectories, Cases 10-18. . . . .	13
3	Dispersion: Phase I Cases 28-36. . . . .	22
4	Trajectories, Cases 28-36. . . . .	23
5	Dispersion: Phase II Cases 46, 47, 48, 55, 56, and 57 . . . . .	27
6	Dispersion: Phase II Cases 38, 41, 44, 47, 50, 53, and 56 . . . . .	28
7	Dispersion: Phase III Cases 58-68 . . . . .	34
8	Dispersion: Phase III Cases 69-79 . . . . .	35
9	Dispersion: Phase III Cases 80-90 . . . . .	36
10	Dispersion: Phase III Theory, Cases 58-90 . . .	37
11	Trajectory, Case 79. . . . .	38
12	Dispersion: Phase III Cases 91-101 . . . . .	45
13	Dispersion: Phase III Cases 102-112. . . . .	46
14	Dispersion: Phase III Cases 113-123. . . . .	47
15	Dispersion: Phase III Theory, Cases 91-123 . . .	48
16	Trajectory, Case 101 . . . . .	49
17	Dispersion: Phase III Cases 124-134. . . . .	53
18	Dispersion: Phase III Cases 135-145. . . . .	54
19	Dispersion: Phase III Cases 146-156. . . . .	55
20	Dispersion: Phase III Theory, Cases 124-156. . .	56
21	Trajectory, Case 134 . . . . .	57
22	Dispersion: Phase III Cases 157-167. . . . .	62

# LIST OF FIGURES (CONTINUED)

Figure	Title	Page
23	Dispersion: Phase III Cases 168-178 . . . . .	63
24	Dispersion: Phase III Cases 179-189 . . . . .	64
25	Dispersion: Phase III Theory, Cases 157-189 . .	65
26	Trajectory, Case 189. . . . .	66
27	Phase III Theory Equations 24, 28, 30 . . . . .	67
28	Phase III Theory Effective Limits . . . . .	68
29	Ground Point Flechette, With and Without Sabot. .	72
30	Free Flight Test Apparatus and Setup. . . . .	73
31	Raw Translational Data Ground Point-Round 4 . .	75
32	Raw Angular Data Ground Point-Round 4 . . . . .	76
33	Raw Translational Data Ground Point-6 . . . . .	77
4	Raw Angular Data Ground Point-Round 6 . . . . .	78
35	Raw Translational Data Ground Point-Round 7 . .	79
36	Raw Angular Data Ground Point-Round 7 . . . . .	80
37	Raw Translational Data Ground Point-Round 8 . .	81
38	Raw Angular Data Ground Point-Round 8 . . . . .	82
39	Raw Translational Data Ground Point-Round 14. .	83
40	Raw Angular Data Ground Point-Round 14. . . . .	84
41	Raw Translational Data Ground Point-Round 16. .	85
42	Raw Angular Data Ground Point-Round 16. . . . .	86
43	Raw Translational Data Ground Point-Round 17. .	87
44	Raw Angular Data Ground Point-Round 17. . . . .	88
45	Raw Translational Data Ground Point-Round 1. . .	89



# LIST OF FIGURES (CONTINUED)

Figures	Title	Page
46	Raw Angular Data Ground Point-Round 19. . . . .	90
47	Axis Rotation Approximates Pure Pitching Motion	93
48	Fitted Translational Data Ground Point-Round 4.	94
49	Fitted Angular Data Ground Point-Round 4. . . . .	95
50	Fitted Translational Data Ground Point-Round 6.	96
51	Fitted Angular Data Ground Point-Round 6. . . . .	97
52	Fitted Translational Data Ground Point-Round 7.	98
53	Fitted Angular Data Ground Point-Round 7. . . . .	99
54	Fitted Translational Data Ground Point-Round 8.	100
55	Fitted Angular Data Ground Point-Round 8. . . . .	101
56	Fitted Translational Data Ground Point-Round 14	102
57	Fitted Angular Data Ground Point-Round 14 . . . . .	103
58	Fitted Translational Data Ground Point-Round 16	104
59	Fitted Angular Data Ground Point-Round 16 . . . . .	105
60	Fitted Translational Data Ground Point-Round 17	106
61	Fitted Angular Data Ground Point-Round 17 . . . . .	107
62	Fitted Translational Data Ground Point-Round 19	108
63	Fitted Angular Data Ground Point-Round 19 . . . . .	109
64	Dispersion: Ground Point-Round 4 Test Firing Versus Theory, at 50 Feet Downrange . . . . .	113
65	Dispersion: Ground Point-Round 6 Test Firing Versus Theory, at 50 Feet Downrange . . . . .	114
66	Dispersion: Ground Point-Round 7 Test Firing Versus Theory, at 50 Feet Downrange . . . . .	115

# LIST OF FIGURES (CONTINUED)

Figures	Title	Page
67	Dispersion: Ground Point-Round 8 Test Firing Versus Theory, at 50 Feet Downrange. . . . .	116
68	Dispersion: Ground Point-Round 14 Test Firing Versus Theory, at 50 Feet Downrange. . . . .	117
69	Dispersion: Ground Point-Round 16 Test Firing Versus Theory, at 50 Feet Downrange. . . . .	118
70	Dispersion: Ground Point-Round 17 Test Firing Versus Theory, at 50 Feet Downrange. . . . .	119
71	Dispersion: Ground Point-Round 19 Test Firing Versus Theory, at 50 Feet Downrange. . . . .	120
72	Flight Transition Sequence-Round 4 . . . . .	122
73	Flight Transition Sequence-Round 6 . . . . .	123
74	Flight Transition Sequence-Round 7 . . . . .	124
75	Flight Transition Sequence-Round 8 . . . . .	125
76	Flight Transition Sequence-Round 14. . . . .	126
77	Flight Transition Sequence-Round 16. . . . .	127
78	Flight Transition Sequence-Round 17. . . . .	128
79	Flight Transition Sequence-Round 19. . . . .	129
80	Dispersion Versus First Maximum Yaw, Frankford Test Firing Results. . . . .	131
81	Dispersion Versus First Maximum Yaw, Theory- Initial Conditions, 1 Foot Downrange . . . . .	132
82	Dispersion Versus First Maximum Yaw, Theory- Initial Conditions, 3 Feet Downrange . . . . .	133
83	Dispersion Versus First Maximum Yaw Theory- Initial Conditions, 5 Feet Downrange . . . . .	134
84	Jump Angles for Various Initial Conditions . . . . .	138

# LIST OF FIGURES (CONCLUDED)

Figures	Title	Page
85	Flechette In-Bore Position . . . . .	141
86	Typical Flechette Blast Region . . . . .	142
87	Muzzle Blast Effects . . . . .	143
88	Supersonic Free Flight, Ground Point Flechette .	144

# LIST OF TABLES

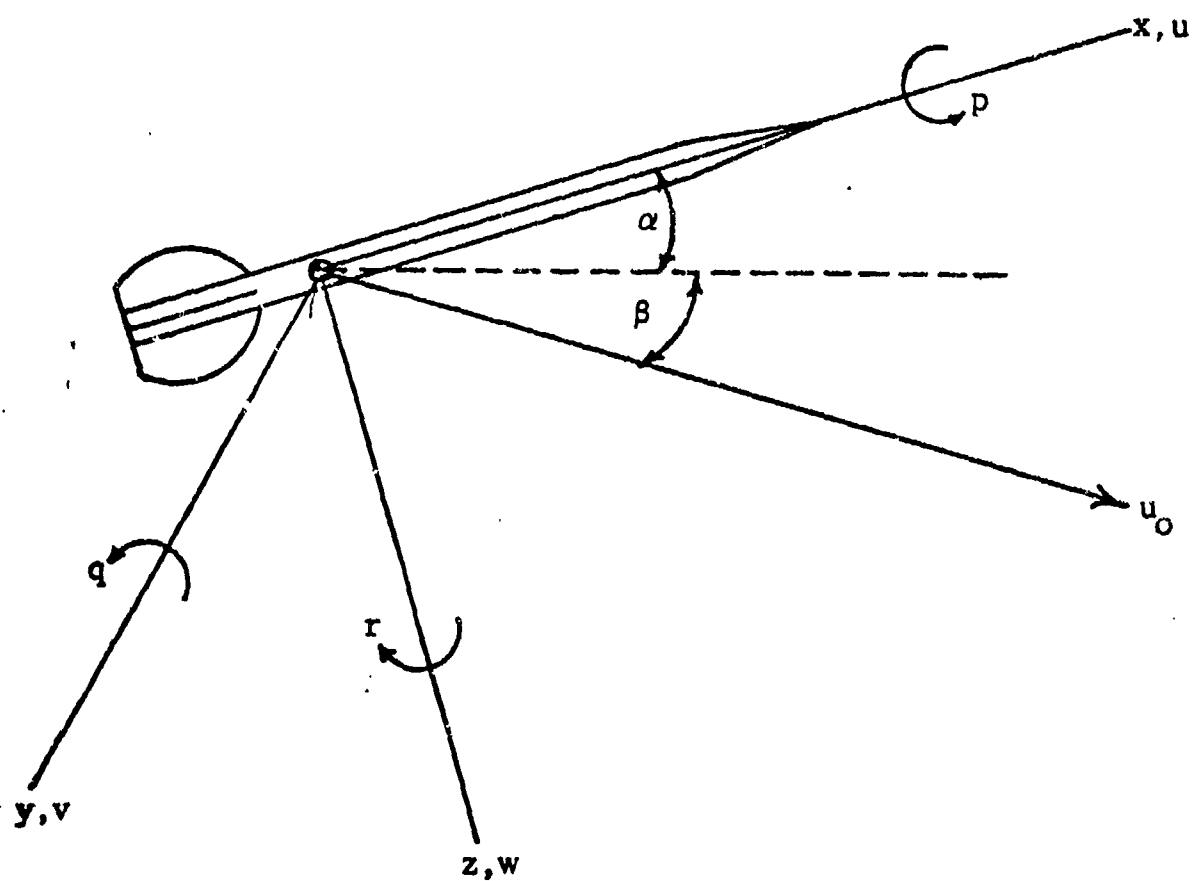
Table	Title	Page
1	Theory Validation, Restoring and Damping Moments, Cases 1-9 . . . . .	15
2	Theory Validation, Restoring and Damping Moments, Cases 10-18 . . . . .	16
3	Theory Validation, Restoring and Damping Moments, Cases 19-27 . . . . .	20
4	Theory Validation, Restoring and Damping Moments, Cases 28-36 . . . . .	21
5	Magnus Coefficients, at Mach 4.5 . . . . .	24
6	Theory Validation, Magnus, Cases 37-57 . . . . .	26
7	Theory Validation, Asymmetries, Cases 58-68. . . . .	30
8	Theory Validation, Asymmetries, Cases 69-79. . . . .	31
9	Theory Validation, Asymmetries, Cases 80-90. . . . .	32
10	Theory Validation, Asymmetries, Cases 91-101 . . . . .	42
11	Theory Validation, Asymmetries, Cases 102-112. . . . .	43
12	Theory Validation, Asymmetries, Cases 113-123. . . . .	44
13	Theory Validation, Asymmetries, Cases 124-134. . . . .	50
14	Theory Validation, Asymmetries, Cases 135-145. . . . .	51
15	Theory Validation, Asymmetries, Cases 146-156. . . . .	52
16	Theory Validation, Asymmetries, Cases 157-167. . . . .	58
17	Theory Validation, Asymmetries, Cases 168-178. . . . .	59
18	Theory Validation, Asymmetries, Cases 179-189. . . . .	60
19	Theory Validation, Gravity Cases 190-201 . . . . .	70
20	Frankford Test Firing Data . . . . .	74
21	Aerodynamic Parameters from Least Squares Fit. . . . .	110

LIST OF TABLE (CONCLUDED)

Table	Title	Page
22	Dispersion Analysis Results . . . . .	112

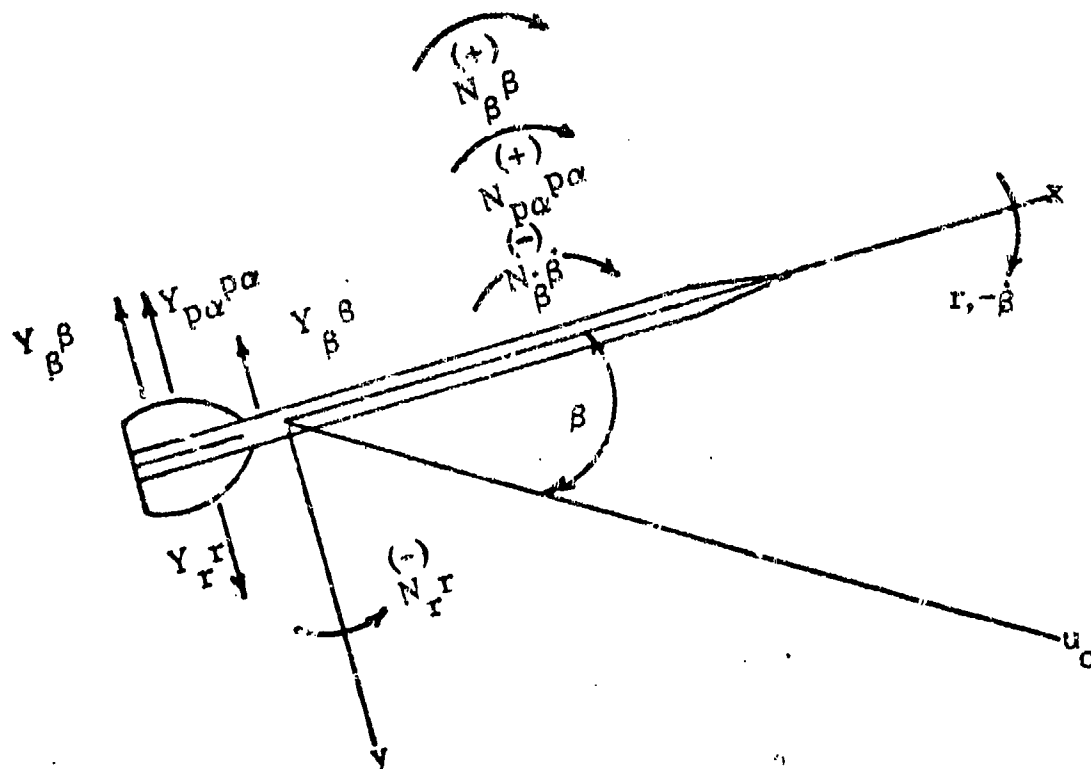
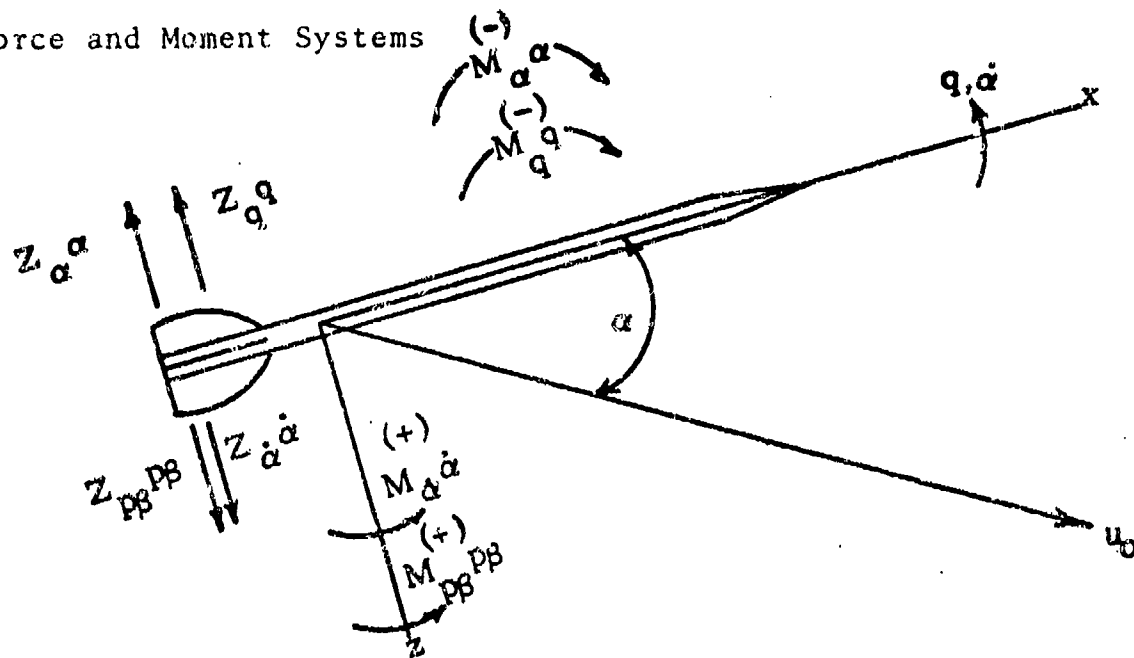
# LIST OF SYMBOLS

Axis System



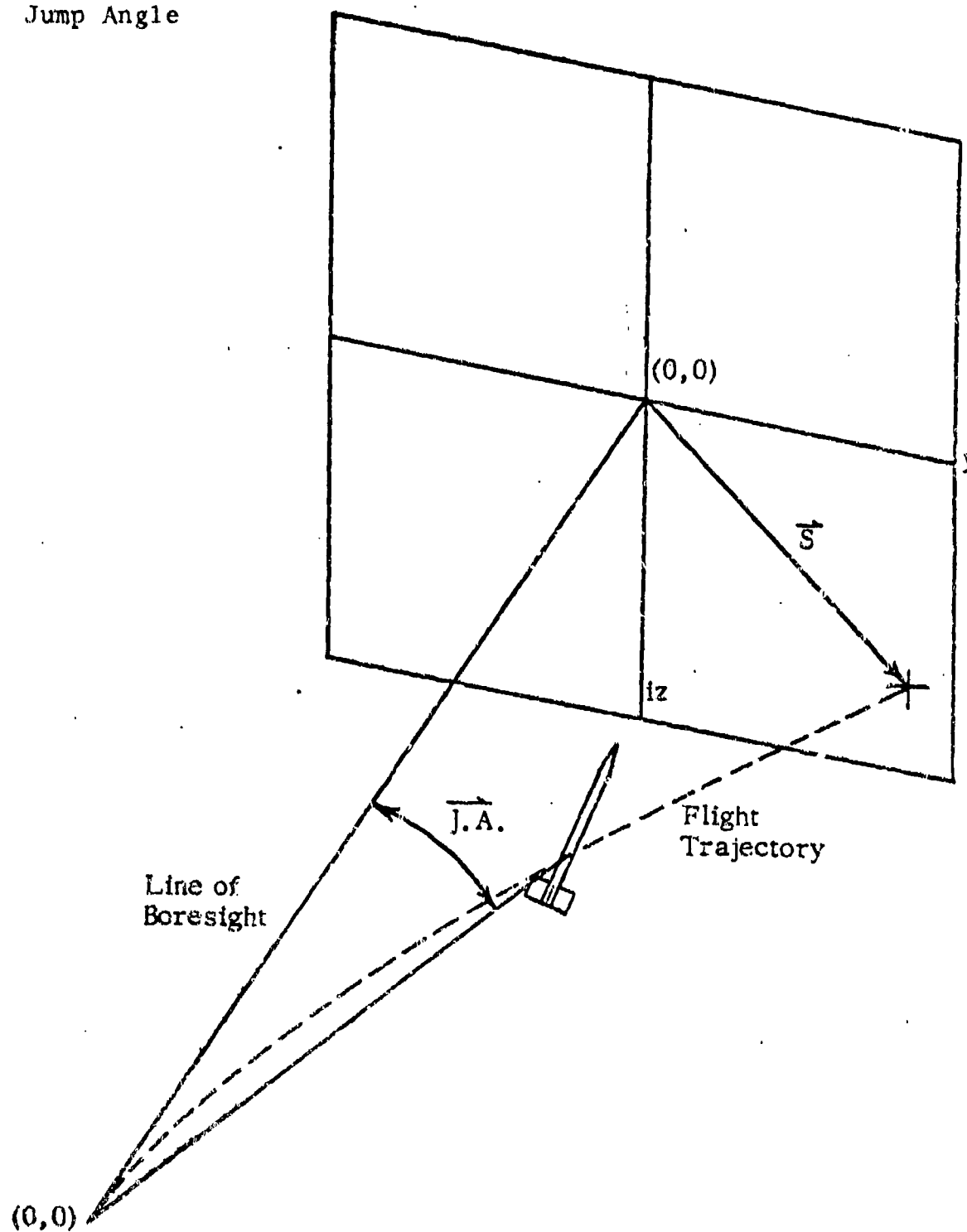
# LIST OF SYMBOLS (CONTINUED)

Force and Moment Systems



# LIST OF SYMBOLS (CONTINUED)

Jump Angle





# LIST OF SYMBOLS (CONTINUED)

$\alpha$  complex angle of attack (degrees or radians)

$$\bar{\alpha} = \beta + i\alpha$$

$\alpha$  pitch angle of attack

$\alpha_0$  initial angle of attack

$\dot{\alpha}_0$  initial angular rate (rad/sec)

$$\bar{\dot{\alpha}}_0 = \dot{\beta}_0 + i\dot{\alpha}_0$$

$\beta$  yaw angle of attack

$C_z$  pitching force coefficients

$$C_z = \frac{Z}{QS}$$

$C_M$  pitching moment coefficients

$$C_M = \frac{M}{QSd}$$

$C_{z\alpha}$  static force stability coefficient ( $\text{rad}^{-1}$ )

$$C_{z\alpha} = \frac{\partial C_z}{\partial \alpha} = \frac{Z_\alpha \alpha}{\alpha QS} = \frac{Y_\beta \beta}{\beta QS}$$

$C_{M\alpha}$  static moment stability coefficient ( $\text{rad}^{-1}$ )

$$C_{M\alpha} = \frac{\partial C_M}{\partial \alpha} = \frac{M_\alpha \alpha}{\alpha QSd} = -\frac{N_\beta \beta}{\beta QSd}$$

$C_{zq}$  damping force stability coefficient ( $\text{rad}^{-1}$ )

$$C_{zq} = \frac{\partial C_z}{\partial \left(\frac{qd}{2u}\right)} = \frac{Z_q q}{\left(\frac{qd}{2u}\right) QS} = -\frac{Y_r r}{\left(\frac{rd}{2u}\right) QS}$$

LIST OF SYMBOLS (CONTINUED)

$C_{Z\dot{\alpha}}$

lag force stability coefficient ( $\text{rad}^{-1}$ )

$$C_{Z\dot{\alpha}} = \frac{\partial C_Z}{\partial \left(\frac{\dot{\alpha} d}{2u}\right)} = \frac{\dot{Z}_{\dot{\alpha}} \dot{\alpha}}{\left(\frac{\dot{\alpha} d}{2u}\right) Q S} = \frac{Y_{\dot{\beta}} \dot{\beta}}{\left(\frac{\dot{\beta} d}{2u}\right) Q S}$$

$C_{M_q}$

damping moment stability coefficient ( $\text{rad}^{-1}$ )

$$C_{M_q} = \frac{\partial C_M}{\partial \left(\frac{q d}{2u}\right)} = \frac{M_{\dot{q}} q}{\left(\frac{q d}{2u}\right) Q S d} = \frac{N_{\dot{r}} r}{\left(\frac{r d}{2u}\right) Q S d}$$

$C_{M\dot{\alpha}}$

lag moment stability coefficient ( $\text{rad}^{-1}$ )

$$C_{M\dot{\alpha}} = \frac{\partial C_M}{\partial \left(\frac{\dot{\alpha} d}{2u}\right)} = \frac{M_{\dot{\alpha}} \dot{\alpha}}{\left(\frac{\dot{\alpha} d}{2u}\right) Q S d} = - \frac{N_{\dot{\beta}} \dot{\beta}}{\left(\frac{\dot{\beta} d}{2u}\right) Q S d}$$

$C_{Z_{p\beta}}$

magnus force stability coefficient ( $\text{rad}^{-2}$ )

$$C_{Z_{p\beta}} = \frac{\partial C_Z}{\partial \beta \partial \left(\frac{p d}{2u}\right)} = \frac{Y_{p\alpha} p \alpha}{\left(\frac{p d}{2u}\right) \alpha Q S} = \frac{Z_{p\beta} p \beta}{\left(\frac{p d}{2u}\right) \beta Q S}$$

$C_{M_{p\beta}}$

magnus moment stability coefficient ( $\text{rad}^{-2}$ )

$$C_{M_{p\beta}} = \frac{\partial C_M}{\partial \beta \partial \left(\frac{p d}{2u}\right)} = \frac{N_{p\alpha} p \alpha}{\left(\frac{p d}{2u}\right) \alpha Q S d} = \frac{M_{p\beta} p \beta}{\left(\frac{p d}{2u}\right) \beta Q S d}$$

$C_{Z_{\delta_e}} \vec{\delta_e}$

aerodynamic asymmetry force, total coefficient

$$C_{Z_{\delta_e}} \vec{\delta_e} = C_{Y_r} \delta_r + i C_{Z_e} \delta_e$$

$C_{M_{\delta_e}} \vec{\delta_e}$

aerodynamic asymmetry moment, total coefficient

$$C_{M_{\delta_e}} \vec{\delta_e} = C_{M_{\delta_e}} \delta_e + i C_{N_{\delta_r}} \delta_r$$

# LIST OF SYMBOLS (CONTINUED)

$d$	flechette body diameter (ft)
$\vec{\delta}_c$	complex aerodynamic asymmetry vector $\vec{\delta}_c = \delta_r + i\delta_e$
$\delta$	phase angle (rad)
$g$	acceleration due to gravity 32.2 ft/sec <sup>2</sup>
$\gamma$	rotation angle between $\alpha, \beta$ axis system and $\alpha', \beta'$ system to approximate pure pitching motion (deg.)
$I_x$	axial moment of inertia (slugs-ft <sup>2</sup> )
$I_y$	transverse moment of inertia (slugs-ft <sup>2</sup> )
$\vec{J.A.}$	jump angle vector (mils)
$\vec{K}_1$	nutation mode amplitude (deg)
$\vec{K}_2$	precession mode amplitude (deg)
$\vec{K}_3, k-T$	trim mode amplitude (deg)
$\vec{K}_4$	yaw of repose amplitude (deg)
$k_{1,2,3,4,5,6}$	dispersion or jump angle amplitude coefficients
$\lambda_1, 2\lambda_{N,P}$	damping factors for nutation and precession modes respectively (rad/sec)
$m$	mass of flechette (slugs)
$p$	roll rate (rad/sec)
$p_0$	initial roll rate (rad/sec)
$\vec{q}$	complex angular velocity (rad/sec) $\vec{q} = q + ir$
$q$	pitching angular velocity (rad/sec)

LIST OF SYMBOLS (CONTINUED)

$Q$	dynamic pressure $\frac{\text{slugs}}{\text{ft} \cdot \text{sec}^2}$
	$Q = \frac{1}{2} \rho u^2$
$r$	yawing angular velocity (rad/sec)
$\rho$	density (slugs/ft <sup>3</sup> )
$S$	reference area $S = \frac{\pi d^2}{4}$
$\overline{S}$	complex translation (ft)
	$\overline{S} = y + iz$
$\overline{S}_0$	initial complex translation (ft)
	$\overline{S}_0 = y_0 + iz_0$
$\dot{\overline{S}}_0$	initial complex velocity (ft/sec)
	$\dot{\overline{S}}_0 = \dot{y}_0 + i\dot{z}_0$
$s$	gyroscopic stability factor
$\tau$	dynamic weight factor
$t$	time (sec)
$u$	axial velocity (ft/sec)
$u_0$	initial axial velocity (ft/sec)
$v, w$	transverse velocities (ft/sec)
$\overline{w}$	complex transverse velocity (ft/sec)
	$\overline{w} = v + iw$

LIST OF SYMBOLS (CONCLUDED)

$\omega, \omega_N, p$	nutation and precession mode frequencies (rad/sec)
$x, y, z$	position components

## SECTION I

### INTRODUCTION

The accuracy and dispersion of free flight vehicles has been a problem in aerodynamics and ballistics for many years. Until the present time, the primary investigations into causes and effects of jump (the angle between the line of boresight and the line connecting the point of launch with the instantaneous position on the trajectory) and dispersion have been directed toward projectiles and, in particular, artillery rounds. A full program to investigate jump and dispersion characteristics of low trajectory finned bodies has been lacking and therefore is the subject of this report. The purpose of this analysis is to develop a basic understanding of the parameters causing the jump and dispersion of flechettes. The flechette, being a gun launched finned body, requires a different approach to the problem. The old concept employed in the analysis of the dispersion of artillery rounds is that the dispersion results from initial launch disturbances imparted by the gun to the shell (References 1 and 2). This concept is no longer valid for flechettes since the flechette is a fin missile, sabot launched, and its dispersion must be tied to the disturbances it encounters when clearing the muzzle blast and sabot separation region. In addition, asymmetries are more prevalent in finned bodies than projectiles and a finned body is more apt to be influenced by the blast. These factors must be taken into account by a theory involving finned bodies.

In order to develop this new approach, (1) a theoretical expression for jump and dispersion had to be developed, (2) the theory had to be validated, (3) free flight test firings had to be undertaken and initial condition data extracted, and (4) the test firing results had to be correlated with the validated theory. The Jump and Dispersion Theory was developed, in general, for both fin and spin stabilized missiles in air. The theory includes the effects of: initial conditions, magnus, aerodynamic asymmetries, and gravity. In the past, theory development for projectiles included only initial angle of attack and initial angular rate (References 1 and 3). Initial transverse velocity was considered non-existent (Reference 4) or negligible. Zaroodny (Reference 5) included a linear momentum term to account for any transverse motion of the projectile but attributed it to the gun during recoil. Any transverse impulse imparted to the projectile by the blast was ignored. Other authors including Sterne (Reference 2) attributed the jump only to bore clearance and therefore only included, effectively, the initial angle of attack. Magnus effects were always neglected

in previous studies either due to lack of familiarity with the subject or lack of data. In general, all cross-forces, except lift, were neglected mainly for convenience sake. Zaroodny, however, cautioning against wholesale simplifying said "it would seem desirable that our formulas allow us to include these other forces as the experimental information on these forces becomes available." Aerodynamic asymmetries were neglected for projectiles but included in Murphy's work (Reference 6). It was not until Nicolaides (References 7, 8, and 9) that all four factors affecting dispersion; initial angle of attack, initial angular rate, initial transverse position and velocity, were put into one theory. The work presented here expands the work of Nicolaides to include all parameters affecting dispersion in detail. Three separate equations comprise the theory to include the complete range of roll rates. Before, only high roll rates were considered; with the study of finned bodies, the roll rate range extends down to zero roll and accurate theories had to be deduced from known aerodynamic equations.

To validate the theory, a six-degree-of-freedom trajectory computer program numerically integrating the equations of motion was utilized (References 10, 11, and 12). The validation consisted of four phases. The procedure began with the most basic theory equation and consecutively added terms to validate the entire theory. Initial conditions, magnus, asymmetries and gravity were successively validated with roll rate and velocity varied in each phase.

Before the advent of adequate photographic material, obtaining test data was often difficult. At first, jump target data was taken separately from yaw data. The thinking was that the yaw data was part of the projectile's characteristics and not affecting jump. As photographic methods improved, and theories developed, the data was correlated. The correlation of the data was often a problem. A fit of the motion to a least squares method was difficult. Fowler, Kent, and Hitchcock developed a method that would plot the magnitude of the yaw separately from the orientation and then fit the curves separately. A better method was developed by McShane-Charters-Turetsky that approximated the yawing motion to a circle. For projectiles the method has been refined and is an excellent method. However, for finned bodies with not always circular angular motions, a different method of data analysis had to be devised. Utilizing the free flight data taken by test engineers at Frankford Arsenal on a number of flechettes, the least squares method was employed to fit the data presented here. The nearly planar oscillations of the flechette in the first few feet downrange were fit to a pure pitching motion (References 13 and 14) and the position downrange fit to a third order

polynomial. From these results, angle of attack, angular rate and transverse position and velocity were determined for the first few feet downrange. Before, there was some controversy as to whether or not the least squares fit could be extrapolated back to the muzzle. Zaroodny contended that the  $x=0$  position had to be taken out of the blast region to allow the aerodynamic equations to be valid. On the other hand, Kent, Hitchcock, Fowler and Sterne held to the fact that the free flight region began the instant the projectile left the bore. In the analysis of flechettes the position  $x=0$  is taken somewhere downrange after the sabot separation sequence has occurred. This is seen to be 3 to 5 feet downrange and assumed clear of any muzzle blast effects.

The striking shortcoming of previous works is the lack of correlation between test data and valid theory. For the flechette, correlation between the theory and test data was undertaken as well as correlation between test results and first maximum yaw data. Currently, the first maximum yaw theory (Reference 15) is held by some to be an accurate method of predicting dispersion. This theory disallows any influence of initial angular rate, transverse position, or velocity on dispersion. The dispersion analysis presented here disproves this theory with actual test data. The details of each of these aspects of this program are developed in the following sections.



## SECTION II

### DISPERSION THEORY

Dispersion relationships for free flight vehicles are embedded in the trajectory equation of any such aeroballistic body. To evaluate the trajectory equation and thus the dispersion, the linear second-order differential equation of angular motion is a logical starting point.

$$\ddot{\vec{w}} + N_1 \dot{\vec{w}} + N_2 \vec{w} = \vec{N}_3 e^{ipt} + \vec{N}_4 \quad (1)$$

where  $N_1$ ,  $N_2$ ,  $\vec{N}_3$ , and  $\vec{N}_4$  are constants.

$$N_1 = \left[ \frac{Z_w + ipZ_{pv}}{Z_{\dot{w}} - m} \right] + \frac{M_{\dot{w}}}{I_y} \left[ \frac{mu + Z_q}{Z_{\dot{w}} - m} \right] \cdot \left[ \frac{ipL_x}{I_y} + \frac{M_q}{I_y} \right] \quad (2)$$

$$N_2 = \left[ \frac{M_w + ipM_{pv}}{I_y} \right] \left[ \frac{mu + Z_q}{Z_{\dot{w}} - m} \right] - \left[ \frac{Z_w + ipZ_{pv}}{Z_{\dot{w}} - m} \right] \left[ \frac{ipL_x}{I_y} + \frac{M_q}{I_y} \right] \quad (3)$$

$$\vec{N}_3 = \left[ \frac{Z_{\delta_\epsilon} \vec{\delta}_\epsilon}{Z_{\dot{w}} - m} \right] \left[ \frac{M_q}{I_y} + \frac{ipL_x}{I_y} - ip \right] - \frac{M_{\delta_\epsilon} \vec{\delta}_\epsilon}{I_y} \left[ \frac{mu + Z_q}{Z_{\dot{w}} - m} \right] \quad (4)$$

$$\vec{N}_4 = \frac{img}{I_y} \left[ \frac{M_q + ipL_x}{Z_{\dot{w}} - m} \right] \quad (5)$$

In this discussion of dispersion theory, it is assumed that,

1. total velocity,  $u_0$ , is constant, equal to  $u$  in the theory development.
2. all force and moment coefficients dependent on angle of attack are considered to be linear with angle of attack.
3. all force and moment coefficients independent of angle of attack are considered to be constant.

4. a linear relationship exists between  $x$  (distance downrange) and time for the nondrag case.
5. roll rate,  $p$ , is considered to be constant.
6. products of force and moment derivatives are negligible, except those involving  $Z_{\delta_\epsilon}$  and  $M_{\delta_\epsilon}$ .

Utilizing these assumptions, and the binomial expansion of  $(Z_{\dot{w}} - m)^{-1}$ , 2, 3, 4, and 5 become:

$$\bar{N}_1 \approx - \left[ \frac{Z_w + ipZ_{pv}}{m} \right] - \left[ \frac{M_q + uM_{\dot{w}}}{I_y} \right] - \frac{ipI_x}{I_y} \quad (2a)$$

$$\bar{N}_2 \approx -u \left[ \frac{M_w + ipM_{pv}}{I_y} \right] + \frac{ipI_x}{I_y} \left[ \frac{Z_w + ipZ_{pv}}{m} \right] \quad (3a)$$

$$\bar{N}_3 \approx \frac{ipZ_{\delta_\epsilon} \hat{\delta}_\epsilon}{m} \left[ 1 - \frac{I_x}{I_y} \right] + \frac{uM_{\delta_\epsilon} \hat{\delta}_\epsilon}{I_y} \quad (4a)$$

$$\bar{N}_4 \approx g \left[ \frac{pI_x}{I_y} \right] \quad (5a)$$

The solution to Equation 1 is that of tricyclic motion; that is,

$$\bar{w} = \bar{K}_1 e^{\phi_1 t} + \bar{K}_2 e^{\phi_2 t} + \bar{K}_3 e^{ipt} + \bar{K}_4 \quad (6)$$

where the complex coefficients are:

$$\bar{K}_{1,2} = \frac{\bar{w}_0 - (\phi_{2,1}) \bar{w}_0 + \bar{K}_3 (\phi_{2,1} - ip)}{\phi_{1,2} - \phi_{2,1}} \quad (7)$$

$$\bar{K}_3 = \frac{\bar{N}_3}{(ip - \phi_1)(ip - \phi_2)} \quad (8)$$

$$\vec{K}_4 = \frac{\vec{N}_4}{N_2} \quad (9)$$

and

$$\phi_{1,2} = -\frac{N_1}{2} \pm \frac{1}{2} \sqrt{N_1^2 - 4N_2} \quad (10)$$

The trajectory equation for free-flight motion:

$$\vec{S} = (\vec{w} - iu\vec{q}) \quad (11)$$

An expression for  $\vec{q}$  is obtained from the equations of motion

$$\begin{aligned} \vec{q} &= i\vec{w} \left[ \frac{Z\dot{w} - m}{mu + Z_q} \right] + i\vec{w} \left[ \frac{Z_w + ipZ_{pv}}{mu + Z_q} \right] + \left[ \frac{iZ_{\delta\epsilon}\vec{\delta\epsilon}}{mu + Z_q} \right] e^{ipt} - \left[ \frac{mg}{mu + Z_q} \right] \\ \vec{q} &= i\vec{w} \left[ 1 - \frac{Z_q + Z\dot{w}}{m} \right] + i\vec{w} \left[ \frac{Z_w + ipZ_{pv}}{mu} \right] + \left[ \frac{iZ_{\delta\epsilon}\vec{\delta\epsilon}}{mu} \right] e^{ipt} - \frac{g}{u} \end{aligned} \quad (12)$$

yielding a solution of the form:

$$\vec{S} = \vec{k}_1 e^{\phi_1 t} + \vec{k}_2 e^{\phi_2 t} + \vec{k}_3 e^{ipt} + \vec{k}_4 t^2 + \vec{k}_5 t + \vec{k}_6 \quad (13)$$

where the entire expression for the solution is:

$$\begin{aligned} \vec{S} &= \vec{K}_1 e^{\phi_1 t} \left[ \frac{1}{\phi_1} \left( \frac{Z_q + uZ\dot{w}}{mu} \right) + \frac{u}{\phi_1^2} \left( \frac{Z_w + ipZ_{pv}}{mu} \right) \right] \\ &+ \vec{K}_2 e^{\phi_2 t} \left[ \frac{1}{\phi_2} \left( \frac{Z_q + uZ\dot{w}}{mu} \right) + \frac{u}{\phi_2^2} \left( \frac{Z_w + ipZ_{pv}}{mu} \right) \right] \\ &+ \left[ \frac{Z_w + ipZ_{pv}}{m} \vec{K}_3 + \frac{Z_{\delta\epsilon}\vec{\delta\epsilon}}{m} \right] \int_0^t \int_0^t e^{ipt} dt dt \\ &+ \left[ \frac{Z_q + uZ\dot{w}}{mu} \right] \vec{K}_3 \int_0^t e^{ipt} + \left[ \frac{\vec{K}_4}{2} \left( \frac{Z_w + ipZ_{pv}}{m} \right) + \frac{ig}{2} \right] t^2 \end{aligned}$$

$$+ t \left[ \vec{S}_0 + \left( \frac{Z_q + uZ_{\dot{w}}}{mu} \right) (\vec{K}_4 - \vec{w}_0) - \left( \frac{Z_w + ipZ_{pv}}{m} \right) \left( \frac{\vec{K}_1}{\phi_1} + \frac{\vec{K}_2}{\phi_2} \right) \right] \quad (14)$$

$$+ \left[ \vec{S}_0 - \left( \frac{Z_q + uZ_{\dot{w}}}{mu} \right) \left( \frac{\vec{K}_1}{\phi_1} + \frac{\vec{K}_2}{\phi_2} \right) - \left( \frac{Z_w + ipZ_{pv}}{m} \right) \left( \frac{\vec{K}_1}{\phi_1^2} + \frac{\vec{K}_2}{\phi_2^2} \right) \right]$$

The term  $\left( \frac{Z_q + uZ_{\dot{w}}}{mu} \right)$  is of an order of magnitude  $10^{-3}$  and thus is

neglected from all further discussion. This reduces 14 to:

$$\begin{aligned} \vec{S} = & \vec{K}_1 e^{\phi_1 t} \left[ \frac{u}{\phi_1^2} \left( \frac{Z_w + ipZ_{pv}}{mu} \right) \right] + \vec{K}_2 e^{\phi_2 t} \left[ \frac{u}{\phi_2^2} \left( \frac{Z_w + ipZ_{pv}}{mu} \right) \right] \quad (15) \\ & + \left[ \frac{Z_w + ipZ_{pv}}{m} \vec{K}_3 + \frac{Z_{\delta\epsilon} \vec{\delta\epsilon}}{m} \right] \int_0^t \int_0^t e^{ipt} dt dt + \left[ \frac{\vec{K}_4}{2} \left( \frac{Z_w + ipZ_{pv}}{m} \right) + \frac{ig}{2} \right] t^2 \\ & + t \left[ \vec{S}_0 - \left( \frac{Z_w + ipZ_{pv}}{m} \right) \left( \frac{\vec{K}_1}{\phi_1} + \frac{\vec{K}_2}{\phi_2} \right) \right] + \left[ \vec{S}_0 - \left( \frac{Z_w + ipZ_{pv}}{m} \right) \left( \frac{\vec{K}_1}{\phi_1^2} + \frac{\vec{K}_2}{\phi_1^2} \right) \right] \end{aligned}$$

By further inspection, terms with  $\phi_1^2$  and  $\phi_2^2$  will be negligible since they contain products of force and moment derivatives. Equation 15

becomes:

$$\begin{aligned} \vec{S} = & \left[ \frac{Z_w + ipZ_{pv}}{m} \vec{K}_3 + \frac{Z_{\delta\epsilon} \vec{\delta\epsilon}}{m} \right] \int_0^t \int_0^t e^{ipt} dt dt + \left[ \frac{\vec{K}_4}{2} \left[ \frac{Z_w + ipZ_{pv}}{m} \right] + \frac{ig}{2} \right] t^2 \\ & + t \left[ \vec{S}_0 - \left( \frac{Z_w + ipZ_{pv}}{m} \right) \left( \frac{\vec{K}_1}{\phi_1} + \frac{\vec{K}_2}{\phi_2} \right) \right] + \vec{S}_0 \quad (16) \end{aligned}$$

Equation 16 contains only the significant terms in dispersion theory.

This equation is valid for all values of roll rate.

# HIGH ROLL RATE THEORY

For roll rates greater than 100 rad/sec, Equation 16 reduces to an approximate solution. Integration of the double integral gives:

$$\int_0^t \int_0^t e^{ipt} dt dt = \frac{e^{ipt}}{(ip)^2} - \frac{t}{ip} - \frac{1}{(ip)^2} \quad (17)$$

For high roll rates, the first and third terms go to zero, leaving only the second term to affect dispersion. Applying this approximation to Equation 16 :

$$\begin{aligned} \vec{S} = & \left[ \frac{\vec{K}_4}{2} \left( \frac{Z_w + ipZ_{pv}}{m} \right) + \frac{ig}{2} \right] t^2 + \left[ \vec{S}_0 - \left( \frac{Z_w + ipZ_{pv}}{m} \right) \left( \frac{\vec{K}_1}{\phi_1} + \frac{\vec{K}_2}{\phi_2} + \frac{\vec{K}_3}{ip} \right) \right. \\ & \left. + \frac{iZ_{\delta\epsilon} \vec{\delta\epsilon}}{mp} \right] t + \vec{S}_0 \end{aligned} \quad (18)$$

where, by applying previous aerodynamic relationships:

$$\left( \frac{\vec{K}_1}{\phi_1} + \frac{\vec{K}_2}{\phi_2} + \frac{\vec{K}_3}{ip} \right) = \left[ \frac{\vec{w}_0 - \vec{w}_0 (\phi_1 + \phi_2)}{-\phi_1 \phi_2} \right] + \left[ \frac{\frac{uM_{\delta\epsilon} \vec{\delta\epsilon}}{I_y} + i \frac{pZ_{\delta\epsilon} \vec{\delta\epsilon}}{m} \left( 1 - \frac{I_x}{I_y} \right)}{(ip) \phi_1 \phi_2} \right] \quad (19)$$

$$\phi_1 + \phi_2 = -N_1$$

$$\phi_1 \phi_2 = N_2$$

$$\vec{K}_4 = -gpI_x \left[ \frac{1}{\left( M_\alpha + \frac{p^2 I_x}{mu} Z_{p\beta} \right) + i \left( pM_{p\beta} - \frac{pI_x}{mu} Z_\alpha \right)} \right] \quad (20)$$

Substituting 19 and 20 into 18 and expanding the various terms:

$$\begin{aligned}
 \vec{S} = & \frac{igt^2}{2} \left[ 1 + \frac{ipl_x}{mud} \left[ \frac{C_{z\alpha} + i\left(\frac{pd}{2u}\right) C_{z_{p\beta}}}{\left(C_{M\alpha} + \frac{pl_x}{mud} \frac{pd}{2u} C_{z_{p\beta}}\right) + i\left(C_{M_{p\beta}} \frac{pd}{2u} - \frac{pl_x}{mud} C_{z\alpha}\right)} \right] \right] \\
 & + ut \left[ \frac{\vec{S}_0}{u} + -\frac{l_y}{mud} \left[ \frac{C_{z\alpha} + i\frac{pd}{2u} C_{z_{p\beta}}}{\left(C_{M\alpha} + \frac{pl_x}{mud} \frac{pd}{2u} C_{z_{p\beta}}\right) + i\left(C_{M_{p\beta}} \frac{pd}{2u} - \frac{pl_x}{mud} C_{z\alpha}\right)} \right] \right. \\
 & \left. + i C_{z_{\delta\epsilon}} \vec{\delta\epsilon} \left[ \frac{\rho u \pi d^2}{8mp} \right] \right] \quad (21) \\
 & \left[ \vec{\alpha}_0 - \alpha_0 \left( \frac{ipl_x}{l_y} \right) - C_{M_{\delta\epsilon}} \vec{\delta\epsilon} \left( \frac{\rho u^2 \pi d^3}{8pl_y} \right) - C_{z_{\delta\epsilon}} \vec{\delta\epsilon} \left( 1 - \frac{l_x}{l_y} \right) \frac{\rho u \pi d^2}{8m} \right] + \vec{S}_0
 \end{aligned}$$

Employing assumption 6 ,

$$\begin{aligned}
 \vec{S} = & \frac{ig}{2} \left( \frac{x}{u} \right)^2 \left[ 1 + \frac{ipl_x}{mud} A \right] + (x) \left[ \frac{\vec{S}_0}{u} + i C_{z_{\delta\epsilon}} \vec{\delta\epsilon} \left( \frac{\rho u \pi d^2}{8mp} \right) \right. \\
 & - \frac{l_y}{mud} A \left[ \vec{\alpha}_0 - \alpha_0 \left( \frac{ipl_x}{l_y} \right) - C_{M_{\delta\epsilon}} \vec{\delta\epsilon} \left( \frac{\rho u^2 \pi d^3}{8pl_y} \right) \right. \\
 & \left. \left. - C_{z_{\delta\epsilon}} \vec{\delta\epsilon} \left( 1 - \frac{l_x}{l_y} \right) \frac{\rho u \pi d^2}{8m} \right] \right] + \vec{S}_0 \quad (22)
 \end{aligned}$$

where

$$A = \frac{C_{z\alpha} + i\left(\frac{pd}{2u}\right) C_{z_{p\beta}}}{\left(C_{M\alpha} + \frac{pl_x}{mud} \frac{pd}{2u} C_{z_{p\beta}}\right) + i\left(C_{M_{p\beta}} \frac{pd}{2u} - \frac{pl_x}{mud} C_{z\alpha}\right)}$$

The mil-relation offers a method to define the Jump Angle from Equation 22.

$$\text{Jump Angle} = \frac{\vec{S}}{x} (10^3) \quad (23)$$

$$\begin{aligned} \vec{J.A.} = & \frac{ig}{2} \left( \frac{x}{u^2} \right) (10^3) \left[ 1 + \frac{ipL_x}{mud} A \right] + (10^3) \left[ \frac{\vec{S}_0}{u} + i C_{Z_{\delta_\epsilon}} \left( \frac{\rho u \pi d^2}{8 m p} \right) \right. \\ & - \frac{I_y}{mud} A \left[ \vec{\alpha}_0 - \vec{\alpha}_0 \left( \frac{ipL_x}{I_y} \right) - C_{M_{\delta_\epsilon}} \left( \frac{\rho u^2 \pi d^3}{8 p I_y} \right) \right. \\ & \left. \left. - C_{Z_{\delta_\epsilon}} \left( 1 - \frac{L_x}{I_y} \right) \frac{\rho u \pi d^2}{8 m} \right] \right] + \frac{1000}{x} \vec{S}_0 \end{aligned} \quad (24)$$

Equation 24 gives an approximation for the Jump Angle for high roll rate cases with gravity, at any position x down range.

#### LOW ROLL RATE THEORY

For roll rates less than 100 rad/sec but having a parameter,  $pt$ , greater than 1, Equation 16 can be reduced to another approximation.

As before, integration of the double integral yields Equation 17

$$\int_0^t \int_0^t e^{ipt} = \frac{e^{ipt}}{(ip)^2} - \frac{t}{ip} - \frac{1}{(ip)^2}$$

For low roll rates all three terms are significant to dispersion.

Equation 16 now becomes:

$$\begin{aligned} \vec{S} = & \left( \frac{Z_w + ipZ_{p\beta}}{m} \vec{K}_3 + \frac{Z_{\delta_\epsilon}}{m} \right) (1 - e^{ipt}) \frac{1}{p^2} + \left[ \frac{\vec{K}_4}{2} \left( \frac{Z_w + ipZ_{p\beta}}{m} \right) + \frac{ig}{2} \right] t^2 \\ & + \left[ \vec{S}_0 - \left( \frac{Z_w + ipZ_{p\beta}}{m} \right) \left( \frac{\vec{K}_1}{\phi_1} + \frac{\vec{K}_2}{\phi_2} \right) + \frac{\vec{K}_3}{ip} + \frac{iZ_{\delta_\epsilon}}{mp} \right] t + \vec{S}_0 \end{aligned} \quad (25)$$

The  $\vec{K}_3$  arm, or rolling trim vector must be separately examined.

From Equation 8,

$$\vec{K}_3 = \frac{\vec{N}_3}{(ip - \phi_1)(ip - \phi_2)}$$

or

$$\vec{K}_3 = \frac{\vec{N}_3}{(ip)^2 - ip(\phi_1 + \phi_2) + \phi_1\phi_2}$$

Numerical inspection of the three denominator terms indicates that the first two terms can be neglected. Each term is not only less than 1 percent of the third term but also they're subtracted from one another to make their contribution even more minimal. Thus  $K_3$  is approximated by,

$$\vec{K}_3 = -\frac{I_y}{md} \left[ \frac{ip C_{Z\delta_\epsilon} \vec{\delta}_\epsilon \left(1 - \frac{I_x}{I_y}\right) + i \frac{mud}{I_y} C_{M_{\delta_\epsilon}} \vec{\delta}_\epsilon}{\left[ C_{M_\alpha} + \frac{p I_x}{mud} \left(\frac{pd}{2u}\right) C_{Z_{p\beta}} \right] + i \left[ C_{M_{p\beta}} \left(\frac{pd}{2u}\right) - \left(\frac{p I_x}{mud}\right) C_{Z_\alpha} \right]} \right]$$

for low roll rates, the second term in the numerator and the first term in the denominator dominate all other terms and become the only significant terms. Thus,

$$\vec{K}_3 = -\frac{u i C_{M_{\delta_\epsilon}} \vec{\delta}_\epsilon}{C_{M_\alpha}} \quad (26)$$

The same approximation holds true for applicable terms in

Equation 25, thus reducing the jump angle equation to:

$$\begin{aligned} \vec{J.A.} = & \left\{ \frac{ig}{2} \left( \frac{x}{u^2} \right) + \frac{\rho u^2 \pi d^2}{8 m p^2} \left[ C_{Z\delta_\epsilon} \vec{\delta}_\epsilon - i \left( \frac{C_{Z_\alpha}}{C_{M_\alpha}} \right) C_{M_{\delta_\epsilon}} \vec{\delta}_\epsilon \right] (1 - e^{ipt}) \right. \\ & + \left[ \frac{\vec{S}_0}{u} + i C_{Z\delta_\epsilon} \vec{\delta}_\epsilon \left( \frac{\rho u \pi d^2}{8 m p} \right) - \frac{I_y}{mud} A \left[ \vec{\delta}_0 - C_{M_{\delta_\epsilon}} \vec{\delta}_\epsilon \left( \frac{\rho u^2 \pi d^3}{8 p I_y} \right) \right. \right. \\ & \left. \left. - C_{Z\delta_\epsilon} \vec{\delta}_\epsilon \left( 1 - \frac{I_x}{I_y} \right) \frac{\rho u \pi d^2}{8 m} \right] + \frac{\vec{S}_0}{x} \right\} (10^3) \end{aligned}$$



Combining terms and dropping the negligible second last term,

$$\begin{aligned} \vec{J.A.} = & \left[ \frac{ig}{2} \left( \frac{x}{u^2} \right) + \frac{\rho u^2 \pi d^2}{8m} \left[ C_{z_{\delta_e}} \vec{\delta_e} - i \left( \frac{C_{z_\alpha}}{C_{M_\alpha}} \right) C_{M_{\delta_e}} \vec{\delta_e} \right] \left[ \frac{1}{p^2 x} + \frac{i}{pu} - \frac{e^{ipt}}{p^2 x} \right] \right. \\ & \left. + \left[ \frac{\dot{S}_0}{u} - \frac{I_y}{mud} \left( \frac{C_{z_\alpha}}{C_{M_\alpha}} \right) \vec{\alpha}_0 \right] + \frac{\vec{S}_0}{x} \right] (10^3) \end{aligned} \quad (27)$$

Expanding  $e^{ipt}$  to  $\cos p \left( \frac{x}{u} \right) + i \sin p \left( \frac{x}{u} \right)$ ,

$$\begin{aligned} \vec{J.A.} = & \left\{ \frac{ig}{2} \left( \frac{x}{u^2} \right) + \frac{\rho u^2 \pi d^2}{8m} \left[ C_{z_{\delta_e}} \vec{\delta_e} - i \left( \frac{C_{z_\alpha}}{C_{M_\alpha}} \right) C_{M_{\delta_e}} \vec{\delta_e} \right] \left[ \frac{1}{p^2} \left( 1 - \cos p \frac{x}{u} \right) \right. \right. \\ & \left. \left. + \frac{i}{p} \left( \frac{x}{u} - \frac{\sin p \frac{x}{u}}{p} \right) \right] + \left[ \frac{\dot{S}_0}{u} - \frac{I_y}{mud} \left( \frac{C_{z_\alpha}}{C_{M_\alpha}} \right) \vec{\alpha}_0 \right] + \frac{\vec{S}_0}{x} \right\} (10^3) \end{aligned} \quad (28)$$

Equation 28 accurately approximates the jump angle for roll rates:

$$p < 100 \text{ rad/sec}$$

$$pt \geq 1.0$$

#### VERY SLOW ROLL RATE THEORY

For very low roll rates; that is,  $p \geq 0$  and  $pt \leq 1$ , Equation 28 is again applicable.

One approximation is used, however, and that is that  $\cos \left( \frac{px}{u} \right)$  and  $\sin \left( \frac{px}{u} \right)$  are approximated by power series.

$$\begin{aligned} \cos \left( \frac{px}{u} \right) &= 1 - \frac{(px)^2}{2u^2} + \frac{(px)^4}{24u^4} - \frac{(px)^6}{720u^6} + \dots \\ \sin \left( \frac{px}{u} \right) &= \frac{px}{u} - \frac{(px)^3}{6u^3} + \frac{(px)^5}{120u^5} - \frac{(px)^7}{5040u^7} + \dots \end{aligned} \quad (29)$$

Substituting and simplifying

$$\begin{aligned}
 \vec{J.A.} = & \left\{ \frac{ig}{2} \left( \frac{x}{u^2} \right) + \frac{\rho \pi d^2 x}{16m} \left[ C_{z\delta_\epsilon} \vec{\delta_\epsilon} - i \left( \frac{C_{z\alpha}}{C_{M\alpha}} \right) C_{M\delta_\epsilon} \vec{\delta_\epsilon} \right] \left[ \left( 1 - \frac{1}{12} \left( \frac{px}{u} \right)^2 \right. \right. \right. \\
 & + \left. \frac{1}{360} \left( \frac{px}{u} \right)^4 \right) + i \left( \frac{px}{3u} - \frac{1}{60} \left( \frac{px}{u} \right)^3 + \frac{1}{2520} \left( \frac{px}{u} \right)^5 \right) \left. \right] \\
 & + \left. \left[ \frac{\vec{S}_0}{u} - \frac{l_y}{mud} \left( \frac{C_{z\alpha}}{C_{M\alpha}} \right) \vec{\delta_0} \right] + \frac{\vec{S}_0}{x} \right\} (10^3)
 \end{aligned} \tag{30}$$

### SECTION III

#### VALIDATION OF THEORY

The theoretical expressions for Jump Angle; Equations 24, 28, and 30; show that the dispersion depends on the initial conditions, aerodynamic coefficients, distance downrange, and mass parameters. Dispersion for this theoretical analysis is defined to be the deviation from the line of fire. By analyzing only one flechette configuration to validate the theory, the producibility Ground Point, and taking all cases to be evaluated at 1000 feet downrange, then the expression for the Jump Angle can only be affected by the initial conditions and aerodynamic coefficients.

To assure that the three equations for Jump Angle are valid and to show the effects for various initial conditions and aerodynamic coefficients, the expressions for the Jump Angle were evaluated for a series of cases and compared to numerical integration of the six-degree-of-freedom equations of motion, (6-D). The series of cases is broken down into various phases of development. Phase I considers various initial conditions but with only the restoring and damping aerodynamic coefficients. This phase validates the use of initial conditions alone. Phase II utilizes a set of constant initial conditions, except for roll rate, and constant restoring and damping coefficients, while varying magnus coefficients to determine their influence. Phase III brings into consideration all the aerodynamic coefficients to include the configurational asymmetry coefficients. Different coefficients are used by varying the initial velocity and roll rates are varied to evaluate high, low, and very low roll theories. Phase IV considers the effects of gravity for various initial velocities and roll rates. No configurational asymmetries are used in order to isolate the gravitational influence. Values for all coefficients are found in the Appendix as well as other data including mass parameters. Since computations were done at 1000 feet downrange, the Jump Angle in mils is equivalent to the deviation from the line of fire in feet for all presented cases. The axis system used throughout this analysis is illustrated in the list of symbols.

#### PHASE I

To validate the effects of initial conditions with restoring and damping coefficients only, 36 cases were evaluated using the high roll rate theory, Equation 24. The cases are divided into four sections isolating different initial conditions and their effects.

### Cases 1-9

The first section shows the effects of roll rate and velocity with zero  $\vec{S}_0$ ,  $\vec{\alpha}_0$  and  $\vec{\dot{\alpha}}_0$ .

Table 1 clearly indicates that no deviation from the line of fire occurs if  $\vec{S}_0$ ,  $\vec{\alpha}_0$ , and  $\vec{\dot{\alpha}}_0$  are set to zero. Roll rate and velocity changes have no effect on the Jump Angle for this particular situation. This is a trivial solution, it being obvious from inspection of Equation 24.

TABLE 1. THEORY VALIDATION, RESTORING AND DAMPING MOMENTS, CASES 1-9

C A S E	Initial Conditions					Coefficients			$\overline{J \cdot A}$ (mils)	
						$C_{Z\alpha}$ $C_{M\alpha}$ $C_{M_q} + C_{M_\alpha}$	$C_{Zp\beta}$ $C_{Mp\beta}$	$C_{YE}$ $C_{ZE}$ $C_{ME}$ $C_{NE}$	6-D	Theory
	$\vec{S}_0$	$\vec{\alpha}_0$	$\vec{\dot{\alpha}}_0$	$p_0$	$u_0$					
1	0	0	0	31416	5000	$\updownarrow$ A1	$\updownarrow$ 0	$\updownarrow$ 0	0 + 0i	0 + 0i
2	0	0	0	18850					0 + 0i	0 + 0i
3	0	0	0	6283					0 + 0i	0 + 0i
4	0	0	0	31416	3000				0 + 0i	0 + 0i
5	0	0	0	18850					0 + 0i	0 + 0i
6	0	0	0	6283					0 + 0i	0 + 0i
7	0	0	0	31416	1000				0 + 0i	0 + 0i
8	0	0	0	18850					0 + 0i	0 + 0i
9	0	0	0	6283					0 + 0i	0 + 0i

### Cases 10-18

The second section gives the effects of initial translational velocity,  $\vec{S}_0 = \dot{y} + iz$ , with various roll rates and velocities. To assure the solution is correct in three dimensional space, the initial translation velocity is given in both y and iz directions. Equation 24 reduces to:

$$\overrightarrow{J.A.} = \frac{1000}{u} \overrightarrow{\dot{S}_0}$$

The correlation between the theory and the 6-D integration for Cases 10-18 is excellent as shown in Table 2. The Jump Angle is seen to be affected by velocity but not roll rate, as would be expected from the reduced Jump Angle equation. Figure 1 illustrates the deviation from the line of fire for initial

TABLE 2. THEORY VALIDATION, RESTORING AND DAMPING MOMENTS, CASES 10-18

C A S E	Initial Conditions					Coefficients		C <sub>YE</sub> C <sub>ZE</sub> C <sub>ME</sub> C <sub>NE</sub>	J.A. (mils)	
						$\begin{matrix} C_{Z\alpha} \\ C_{M\alpha} \end{matrix}$	$\begin{matrix} C_{Zp\beta} \\ C_{Mp\beta} \end{matrix}$		6-D	Theory
	$\vec{\dot{S}}_0$	$\vec{\dot{\alpha}}_0$	$\vec{\dot{\beta}}_0$	$p_0$	$u_0$	$\begin{matrix} C_{Mq} + C_{M\dot{\alpha}} \\ C_{Mp\beta} \end{matrix}$				
10	100+ 100i	0	0	31416	5000	A1	0	0	20.002 + 20.006i	20.000 + 20.000i
11	100+ 100i	0	0	18850					20.002 + 20.006i	20.000 + 20.000i
12	100+ 100i	0	0	6283					20.002 + 20.006i	20.000 + 20.000i
13	100+ 100i	0	0	31416	3000				33.346 + 33.368i	33.333 + 33.333i
14	100+ 100i	0	0	18850					33.346 + 33.368i	33.333 + 33.333i
15	100+ 100i	0	0	6283					33.346 + 33.368i	33.333 + 33.333i
16	100+ 100i	0	0	31416	1000				100.254 + 100.765i	100.000 + 100.000i
17	100+ 100i	0	0	18850					100.254 + 100.764i	100.000 + 100.000i
18	100+ 100i	0	0	6283					100.257 + 100.765i	100.000 + 100.000i

velocities of 5000 ft/sec (Cases 10-12), 3000 ft/sec (Cases 13-15) and 1000 ft/sec (Cases 16-18). Since the theory and 6-D are so close, they are plotted as one point. Figure 2 illustrates the trajectory in both the x-y and x-z planes. The deviation from the line of fire is linear with distance down-range in both planes. This would be expected with no gravitational force acting.

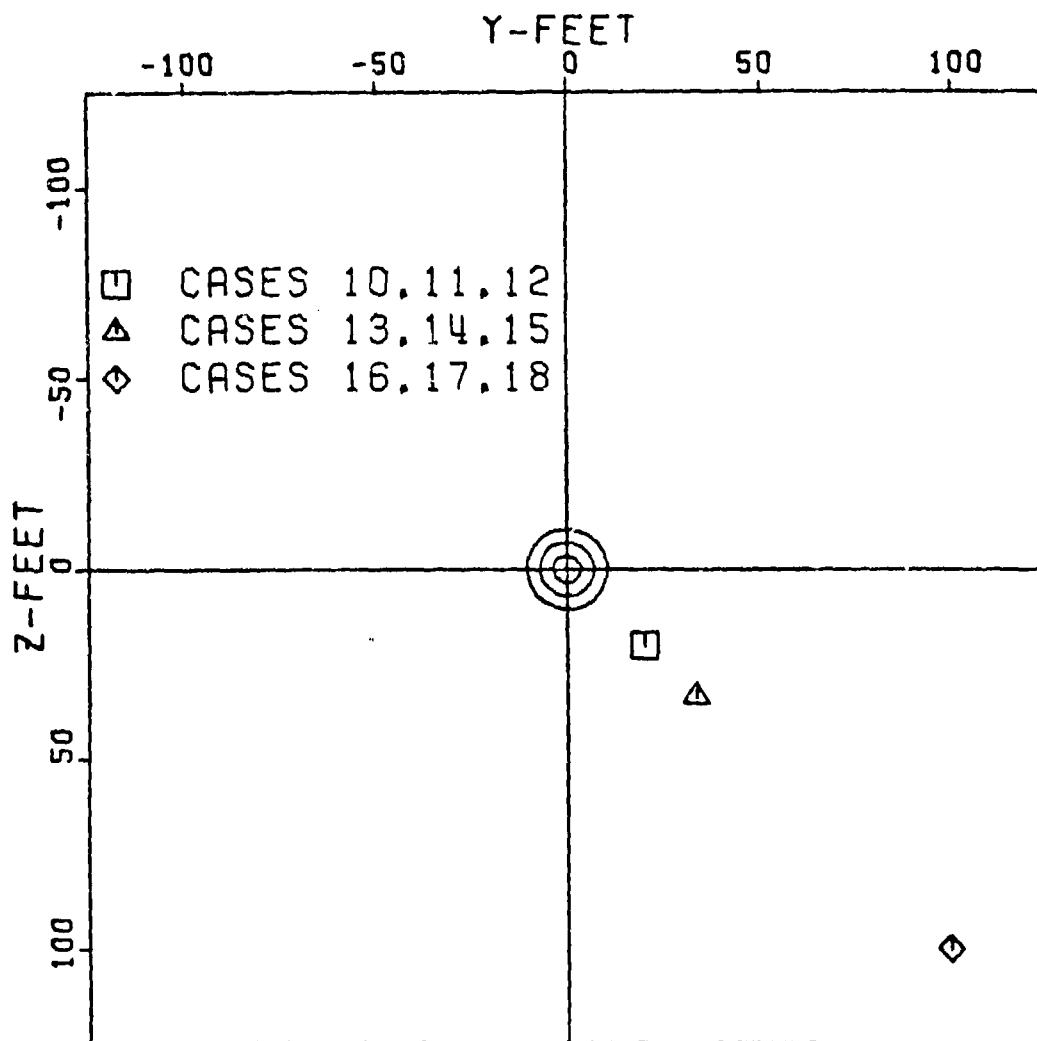


Figure 1. Dispersion: Phase I Cases 10-18

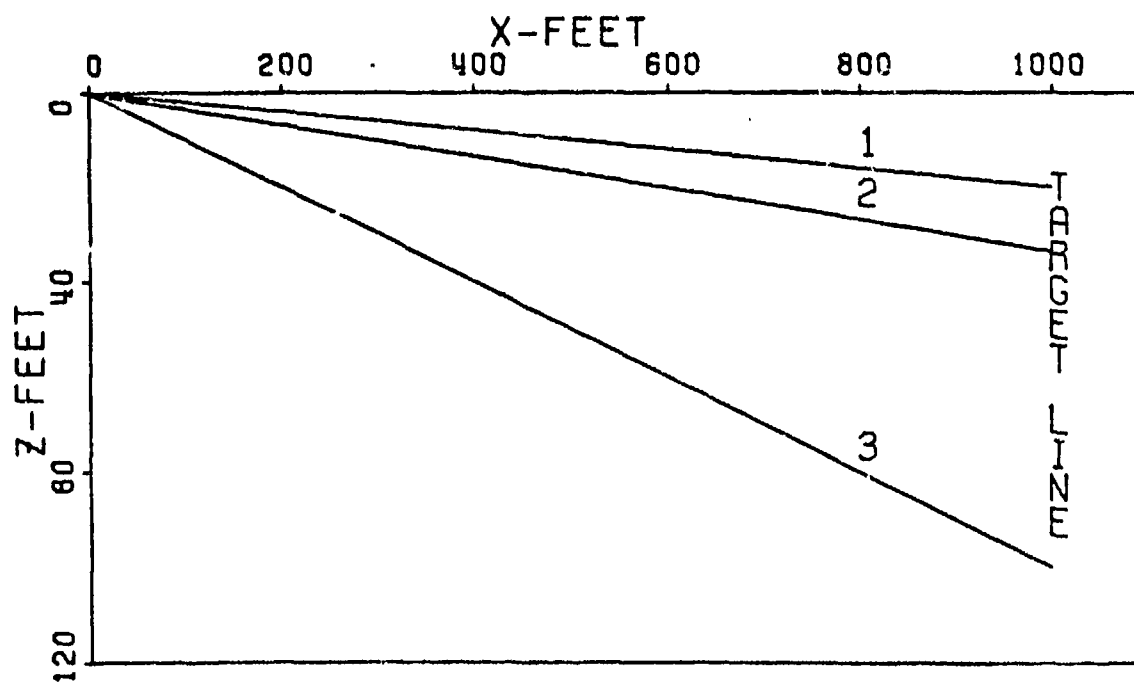
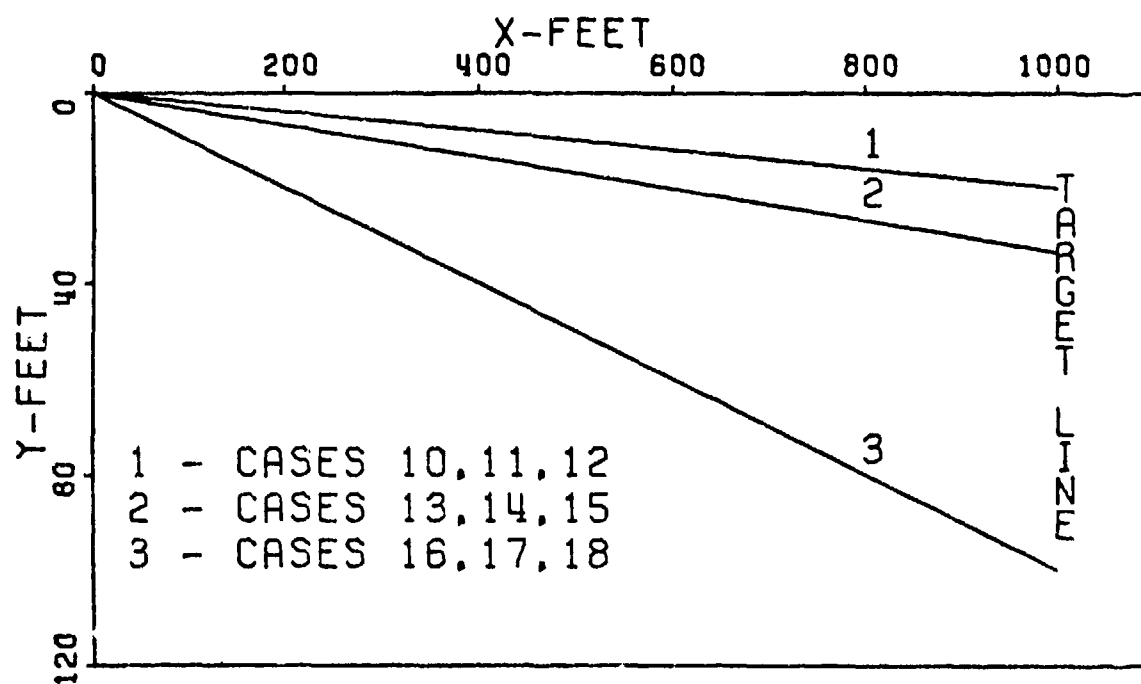


Figure 2. Trajectories, Cases 10-18

#### Cases 19-27

The third section gives the effects of initial angle of attack,  $\vec{\alpha}_0$ , with various roll rates and velocities. Again a complex initial condition is used to validate the theory in three dimensional space. Equation 24 reduces to:

$$\vec{J.A.} = i\vec{\alpha}_0 \left( \frac{pI_x}{\text{mud}} \right) \left[ \frac{C_{Z_\alpha}}{C_{M_\alpha} - i \left( \frac{pI_x}{\text{mud}} \right) C_{Z_\alpha}} \right] 1000$$

Table 3 shows the range of error between the 6-D computation and the theory to be 0.036 to 0.040 mils in the y-direction and 0.038 to 0.041 mils in the z-direction. Although the y-direction deviations differ in sign, the error between them is approximately 0.00225 degrees, an extremely small angle. This angle will give an approximate deviation of 0.04 feet from the line of fire at 1000 feet downrange. With the  $\vec{J.A.}$  being so close to zero it can be expected that the signs may differ due to computational errors. The results do show Jump Angle variance with both roll rate and velocity. The largest changes occur as velocity goes to 1000 ft/sec.

#### Cases 28-36

The fourth section gives the effects of initial angular rate  $\vec{\alpha}_0$ , with varying roll rate and velocity. An angular rate of 250 rad/sec is used in both directions of the complex plane to test validity in three dimensional space. Equation reduces to:

$$\vec{J.A.} = -\vec{\alpha}_0 \left( \frac{I_y}{\text{mud}} \right) \left[ \frac{C_{Z_\alpha}}{C_{M_\alpha} - i \left( \frac{pI_x}{\text{mud}} \right) C_{Z_\alpha}} \right] 1000$$

Table 4 indicates excellent agreement between the theory and 6-D computations. Roll rate is found not to affect the Jump Angle appreciably but velocity does, as would be expected from the reduced Jump Angle equation. Figure 3 shows the dispersion pattern while Figure 4 illustrates the trajectories. Cases 28, 29, and 30 are plotted as one point due to the small difference between the. Cases 31, 32, 33, and 34, 35, and 36 are plotted similarly.



TABLE 3. THEORY VALIDATION, RESTORING AND DAMPING MOMENTS, CASES 19-27

C A S E	Initial Conditions					Coefficients			$\overline{J.A.}$ (mils)	
						$C_{Z\alpha}$ $C_{M\alpha}$ $C_{M_q} + C_{M\dot{\alpha}}$	$C_{Z_{p\beta}}$ $C_{M_{p\beta}}$	$C_{YE}$ $C_{ZE}$ $C_{ME}$ $C_{NE}$		
	$\overline{s}_0$	$\overline{\alpha}_0$	$\overline{\dot{\alpha}}_0$	$p_0$	$u_0$	6-D	Theory			
19	0	1+i	0	31416	5000	A1	0	0	0.012+	-0.027
20	0	1+i	0	18850					0.068i	+0.027i
21	0	1+i	0	6283					0.023+	-0.017
22	0	1+i	0	31416	0.058i				+0.017i	
23	0	1+i	0	18850	3000				0.034+	-0.006
24	0	1+i	0	6283					0.047i	+0.006i
25	0	1+i	0	31416					0.012+	-0.026
26	0	1+i	0	18850	1000				0.067+	+0.026i
27	0	1+i	0	6283					0.022+	-0.016
						0.056i	+0.016i			
						0.033+	-0.005			
						0.046i	+0.005i			
						-0.037+	-0.073			
						0.111i	+0.073i			
						-0.008+	-0.044			
						0.082i	+0.044i			
						0.021+	-0.015			
						0.053i	+0.015i			

TABLE 4. THEORY VALIDATION, RESTORING AND DAMPING MOMENTS, CASES 28-36

C A S E	Initial Conditions					Coefficients			$\overrightarrow{J.A.}$ (mils)				
						$C_{Z\alpha}$ $C_{M\alpha}$ $C_{M_q} + C_{M_{\dot{\alpha}}}$	$C_{Z_{p\beta}}$ $C_{M_{p\beta}}$	$C_{YE}$ $C_{ZE}$ $C_{ME}$ $C_{NE}$	6-D	Theory			
	$\overrightarrow{s}_0$	$\overrightarrow{a}_0$	$\overrightarrow{\dot{a}}_0$	$p_0$	$u_0$								
28	0	0	250+ 250i	31416	5000	A1	0	0	-2.027 -2.034i	-2.073 -2.073i			
29	0	0	250+ 250i	18850					-2.025 -2.030i	-2.073 -2.073i			
30	0	0	250+ 250i	6283					-2.027 -2.029i	-2.073 -2.073i			
31	0	0	250+ 250i	31416	3000				-1.961 -1.967i	-1.970 -1.970i			
32	0	0	250+ 250i	18850					-1.962 -1.966i	-1.970 -1.970i			
33	0	0	250+ 250i	6283					-1.964 -1.964i	-1.970 -1.970i			
34	0	0	250+ 250i	31416	1000				-5.238 -5.274i	-5.540 -5.540i			
35	0	0	250+ 250i	18850					-5.243 -5.264i	-5.540 -5.540i			
36	0	0	250+ 250i	6283					-5.254 -5.260i	-5.540 -5.540i			

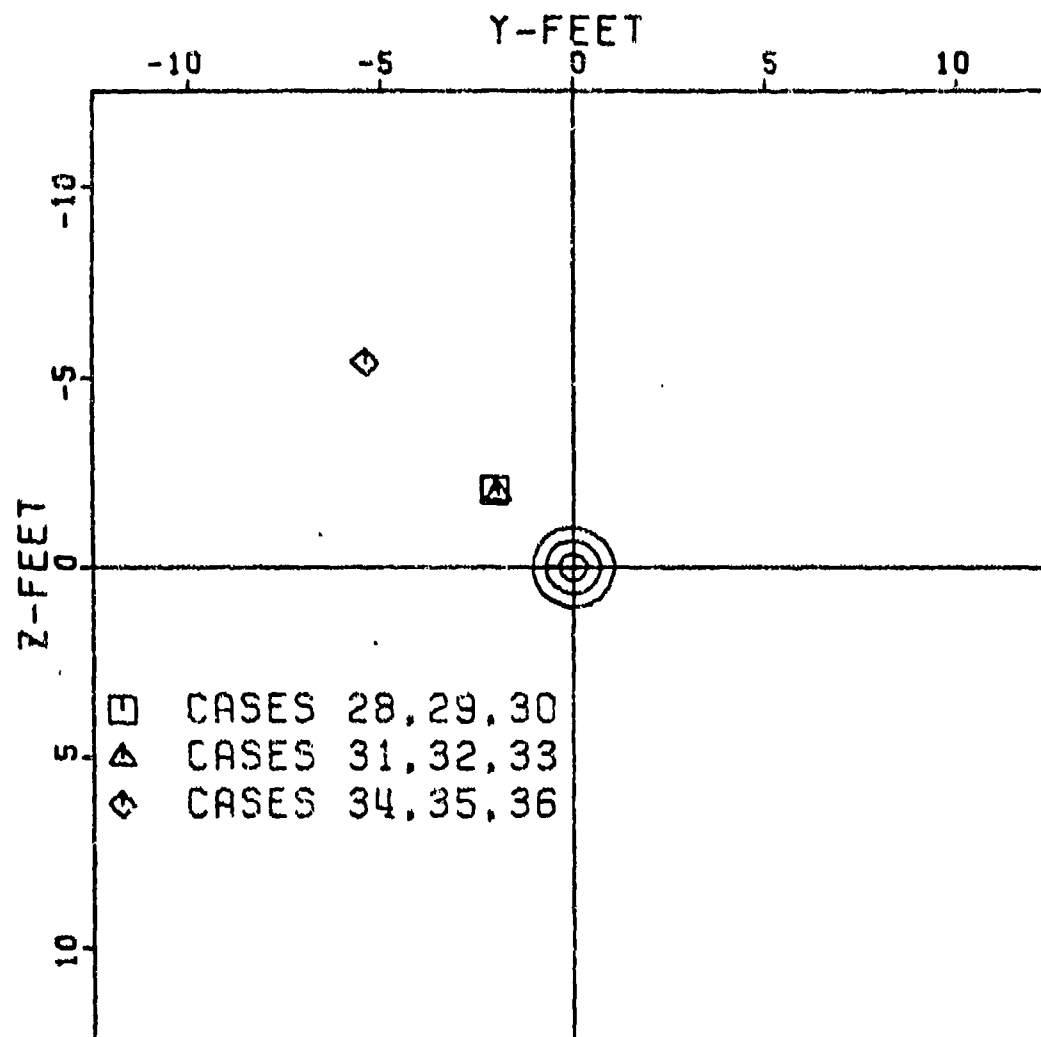


Figure 3. Dispersion: Phase I Cases 28-36

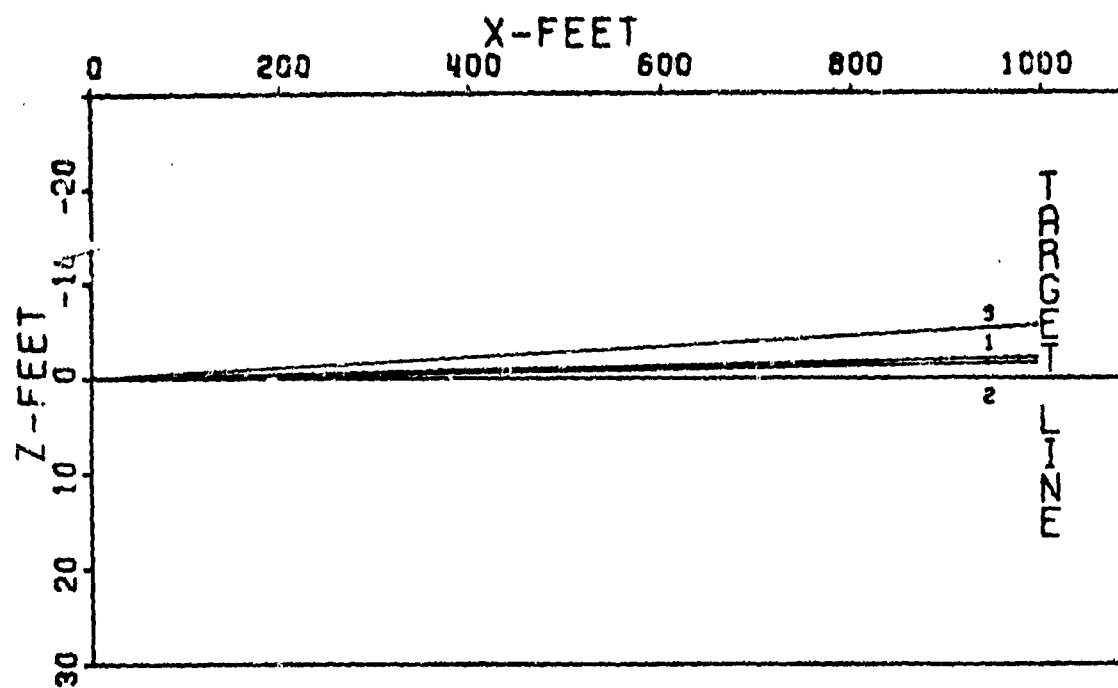
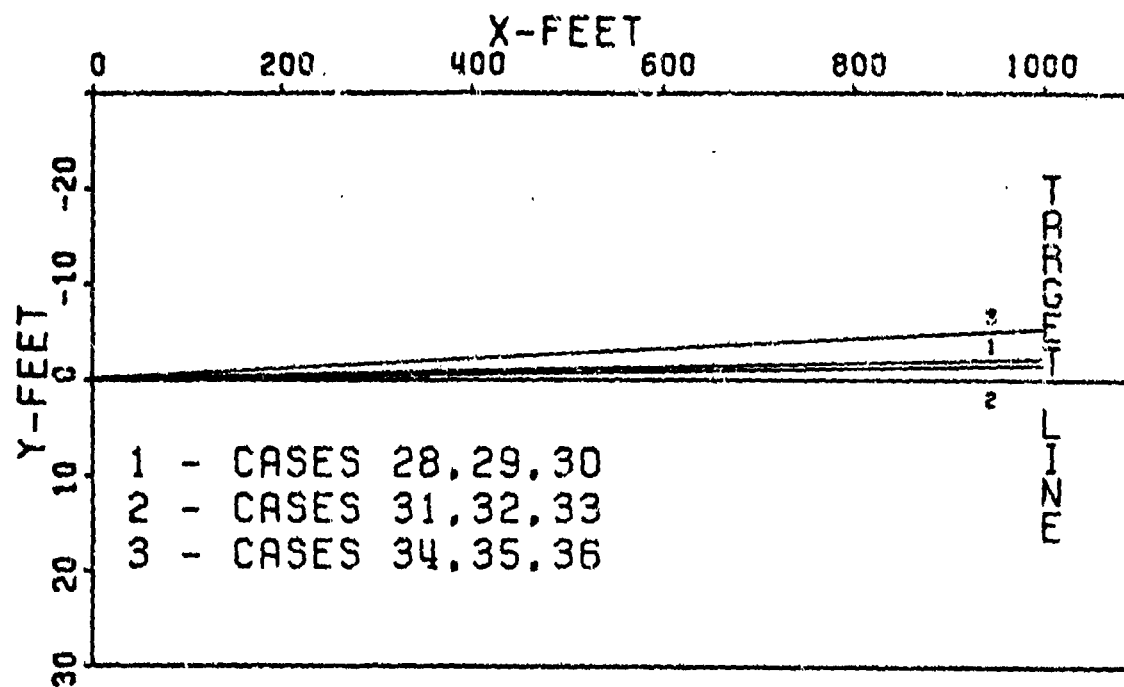


Figure 4. Trajectories, Cases 28-36

## PHASE II

To validate the effect of Magnus Forces and Moments on the dispersion of flechettes, 21 Cases were run varying the initial roll rate and magnus coefficients. All other conditions were held constant. The variance of magnus coefficients with Mach number had to be chosen since no data was available. Arbitrarily, the ratio of  $C_{z_{p\beta}}/C_{M_{p\beta}}$  was chosen to be the same as that

of  $C_{z_{\alpha}}/C_{M_{\alpha}}$ . The magnus coefficients used are presented as

functions of Mach Number in the Appendix with only the values at Mach 4.5 tabulated here for identification sake:

TABLE 5. MAGNUS COEFFICIENTS, AT MACH 4.5

$C_{z_{p\beta}}$	$C_{M_{p\beta}}$
$\pm 34.8$	$\pm 110.0$
$\pm 31.6$	$\pm 100.0$
$\pm 28.4$	$\pm 90.0$

Equation 24 now becomes:

$$\vec{J} \cdot \vec{A} = \left[ \frac{\vec{S}_0}{u} - \frac{I_y}{mud} \left[ \vec{\alpha}_0 - i \vec{\alpha}_0 \left( \frac{p I_x}{I_y} \right) \right] \right] \left[ \frac{C_{z_{\alpha}} + i \left( \frac{pd}{2u} \right) C_{z_{p\beta}}}{\left( C_{M_{\alpha}} + \frac{p I_x}{mud} \frac{pd}{2u} C_{z_{p\beta}} \right) + i \left( C_{M_{p\beta}} \frac{pd}{2u} - \frac{p I_x}{mud} C_{z_{\alpha}} \right)} \right] 1000$$

Initial conditions used in this section are consistent with those of other sections to provide a basis for comparison. Three cases of zero magnus were run, one at each roll rate to provide a standard to judge the influence of magnus.

The effects of magnus coefficients on dispersion are minimal as seen in Table 6. The variance between the zero magnus cases and any other case is found not to be greater than 0.209 mils (or feet at 1000 feet of range). In order to obtain the maximum magnus effects, the largest possible magnus coefficients were used. Hence,  $C_{Z_{p\beta}} = 34.8$  and  $C_{M_{p\beta}} = 110.0$  are the largest possible coefficients since cases 40 and 49 become unstable. Table 6 indicates the effects (for positive magnus coefficients).

1. increasing horizontal dispersion with increasing p
2. decreasing vertical dispersion with increasing p
3. increasing horizontal dispersion with increasing magnus
4. decreasing vertical dispersion with increasing magnus

(for negative magnus coefficients)

5. decreasing horizontal dispersion with increasing p
6. increasing vertical dispersion with increasing p
7. decreasing horizontal dispersion with decreasing magnus
8. increasing vertical dispersion with decreasing magnus

For example, Figure 5 illustrates the effects of roll rate for constant magnus coefficients of  $+90^\circ$  (1,2,5,6 above). Figure 6 illustrates the effects of magnus for a constant sample roll rate (3,4,7,8 above). Obviously, when only a 0.209 mil maximum deviation due to magnus occurs when the situation is geared toward finding the largest effect due to magnus, smaller deviations due to magnus would be found in actual situations. It can be concluded that Magnus has no large effect on dispersion although it could be significant if the total dispersion is close to zero.

### PHASE III

To validate the effects of aerodynamic asymmetries on dispersion of flechettes, a large number of cases were run varying roll rate, velocity, and initial conditions while holding the asymmetry coefficients constant. The asymmetries coefficients were selected to allow 1 degree of non-rolling trim to exist

TABLE 6. THEORY VALIDATION, MAGNUS, CASES 37-57

C A S E	Magnus Forces & Moments	Roll Rate	P <sub>o</sub>	P <sub>o</sub>	P <sub>o</sub>
			31416 rad/sec	18850 rad/sec	6283 rad/sec
37	$C_{Z_{p\beta}} = 0.0$	(6-D) Theory	17.994+ 18.042i 17.900+ 17.954i	(6-D) Theory	(6-D) Theory
38	$C_{M_{p\beta}} = 0.0$				
39					
40	$C_{Z_{p\beta}} = 34.8$	Unstable		18.141+ 17.903i 17.909+ 17.942i	18.057+ 17.979i 17.920+ 17.931i
41	$C_{M_{p\beta}} = 110.0$				
42					
43	$C_{Z_{p\beta}} = 31.6$		18.203+ 17.849i 17.899 17.954i	18.123+ 17.915i 17.909 17.942i	18.053+ 17.982i 17.920+ 17.931i
44	$C_{M_{p\beta}} = 100.0$				
45					
46	$C_{Z_{p\beta}} = 28.4$		18.183+ 17.869i 17.899 17.954i	18.114+ 17.925i 17.909 17.942i	18.050+ 17.987i 17.920+ 17.931i
47	$C_{M_{p\beta}} = 90.0$				
48					
49	$C_{Z_{p\beta}} = -34.8$	Unstable		17.877+ 18.170i 17.090+ 17.942i	17.969+ 18.067i 17.920+ 17.931i
50	$C_{M_{p\beta}} = -110.0$				
51					
52	$C_{Z_{p\beta}} = -31.6$		17.807+ 18.258i 17.899+ 17.954i	17.888+ 18.158i 17.909+ 17.942i	17.973+ 18.063i 17.920+ 17.931i
53	$C_{M_{p\beta}} = -100.0$				
54					
55	$C_{Z_{p\beta}} = -28.4$		17.826+ 18.233i 17.899+ 17.954i	17.900+ 18.144i 17.909+ 17.942i	17.977+ 18.059i 17.820+ 17.931i
56	$C_{M_{p\beta}} = -90.0$				
57					

$\text{CMPB} = \pm 90.0$

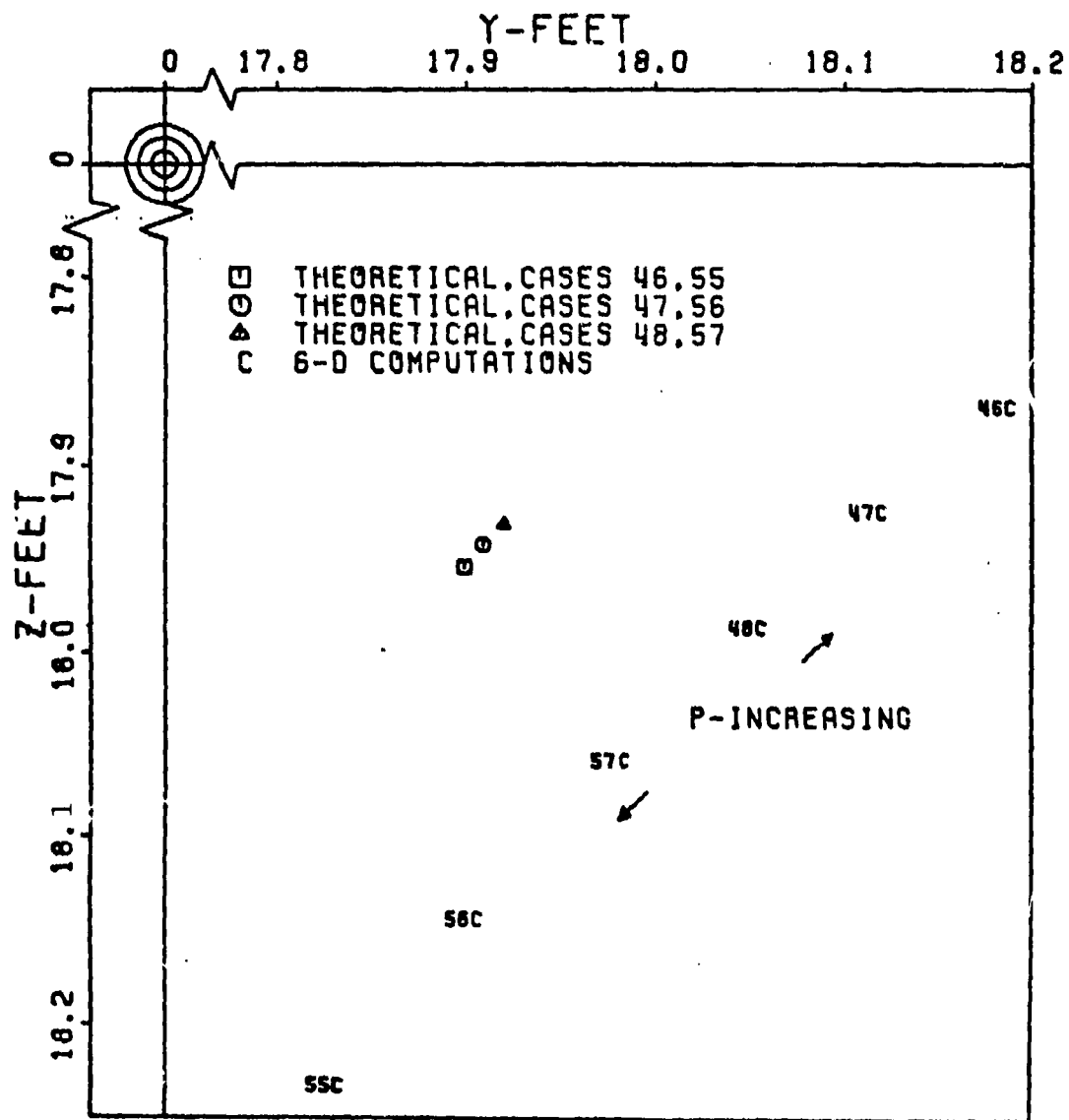


Figure 5. Dispersion; Phase II Cases 46, 47, 48, 55, 56, and 57



$P=18850 \text{ RAD/SEC}$

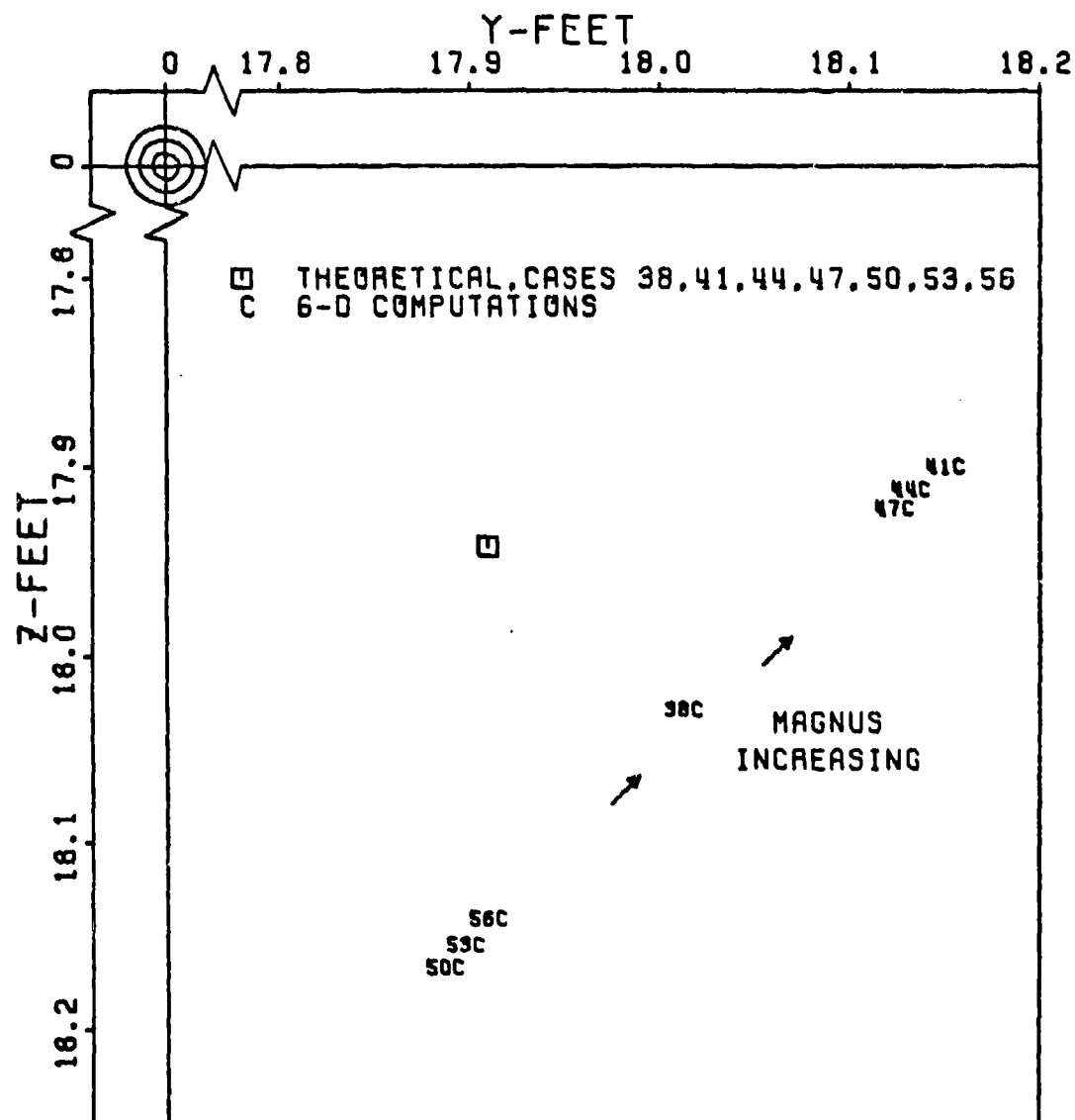


Figure 6. Dispersion: Phase II Cases  
38, 41, 44, 47, 50, 53, and 56

while the flechette was in flight. The asymmetry coefficients,  $C_{YE}$ ,  $C_{ZE}$ ,  $C_{ME}$  and  $C_{NE}$  are presented in the Appendix as a function of mach number. The variance with mach number was chosen arbitrarily: the ratio of asymmetry force to asymmetry moment identical to the ratio of  $C_{Z\alpha}$  to  $C_{M\alpha}$ . The wide range of roll rates makes mandatory use of all three dispersion theories. The governing equations are presented as they apply.

#### Cases 58-90

The first set of cases utilizes zero initial disturbances while varying velocity and roll rate. For roll rates of 31416 rad/sec down to 100 rad/sec the High Roll Rate Theory yields the governing equation,

$$\vec{J} \cdot \vec{A} = \frac{\rho u \pi d^2}{8m} \left[ C_{M_{\delta_\epsilon}} \vec{\delta_\epsilon} \left( \frac{A}{p} \right) + C_{Z_{\delta_\epsilon}} \vec{\delta_\epsilon} \left( \frac{I_y - I_x}{mud} A + \frac{i}{p} \right) \right] 1000$$

For roll rates:  $p < 100$  rad/sec and  $pt \geq 1.0$ , the Low Roll Rate Theory takes effect:

$$\vec{J} \cdot \vec{A} = \frac{\rho u^2 \pi d^2}{8m x} \left[ C_{Z_{\delta_\epsilon}} \vec{\delta_\epsilon} - i \left( \frac{C_{Z\alpha}}{C_{M\alpha}} \right) C_{M_{\delta_\epsilon}} \vec{\delta_\epsilon} \right] \left[ \frac{1}{p^2} \left( 1 - \cos \frac{px}{u} \right) + \frac{1}{p} \left( \frac{x}{u} - \frac{1}{p} \sin \frac{px}{u} \right) \right] 1000$$

Finally, the very Slow Roll Rate Theory applies for values of  $pt < 1.0$ :

$$\vec{J} \cdot \vec{A} = \frac{\rho \pi d^2 x}{16m} \left[ C_{Z_{\delta_\epsilon}} \vec{\delta_\epsilon} - i \left( \frac{C_{Z\alpha}}{C_{M\alpha}} \right) C_{M_{\delta_\epsilon}} \vec{\delta_\epsilon} \right] \left[ \left( 1 - \frac{1}{12} \left( \frac{px}{u} \right)^2 + \frac{1}{360} \left( \frac{px}{u} \right)^4 \right) + i \left( \frac{px}{3u} - \frac{1}{60} \left( \frac{px}{u} \right)^3 + \frac{1}{2520} \left( \frac{px}{u} \right)^5 \right) \right] 1000$$

Tables 7, 8, and 9 list Cases 58-90:

TABLE 7. THEORY VALIDATION. ASYMMETRIES,  
CASES 58-68

C A S E	Initial Conditions					Coefficients			J.A. (mils)	
	$\vec{s}_0$	$\vec{\alpha}_0$	$\vec{\dot{\alpha}}_0$	$p_0$	$u_0$	$C_{Z\alpha}$	$C_{Zp\beta}$	$C_{YE}$	6-D	Theory
						$C_{M\alpha}$		$C_{ZE}$		
						$C_{M_q} + C_{M\dot{\alpha}}$	$C_{M_{p\beta}}$	$C_{ME}$		
58	0	0	0	314'6	5000	A1	A1	A1	0.018-	0.018-
59	0	0	0	18850					0.013i	0.014i
60	0	0	0	6283					0.030-	0.029-
61	0	0	0	500					0.027i	0.025i
62	0	0	0	300					0.060-	0.064-
63	0	0	0	100					0.127i	0.130i
64	0	0	0	50					0.997-	1.013-
65	0	0	0	25					0.992i	1.009i
66	0	0	0	10					1.620-	1.688-
67	0	0	0	5					1.721i	1.683i
68	0	0	0	0					4.574-	4.675-
									4.896i	4.975i
									8.666-	8.780-
									12.280i	12.489i
									20.669-	21.150-
									26.418i	26.927i
									-7.973	-8.210
									-62.197i	-63.210i
									-29.857	-30.372
									-61.459i	-62.353i
									-49.706	-50.427
									-49.706i	-50.427i

TABLE 8. THEORY VALIDATION, ASYMMETRIES  
CASES 69-79

CASE	Initial Conditions					Coefficients			$\overline{J.A.}$ (mils)	
						$C_{Z\alpha}$ $C_{M\alpha}$	$C_{Zp\beta}$	$C_{YE}$ $C_{ZE}$ $C_{ME}$ $C_{NE}$		
	$\vec{s}_o$	$\vec{\alpha}_o$	$\vec{\dot{\alpha}}_o$	$p_o$	$u_o$	$C_{Mq} + C_{M\dot{\alpha}}$	$C_{Mp\beta}$		6-D	Theory
69	0	0	0	31416	3000	A1	A1	A1	0.008- 0.004i	0.009- 0.004i
70	0	0	0	18850					0.013- 0.008i	0.013- 0.008i
71	0	0	0	6283					0.033- 0.028i	0.034- 0.029i
72	0	0	0	500					0.394- 0.398i	0.401- 0.396i
73	0	0	0	300					0.663- 0.659i	0.666- 0.662i
74	0	0	0	100					1.841- 1.998i	1.994- 1.989i
75	0	0	0	50					3.780- 4.513i	3.411- 4.164i
76	0	0	0	25					5.676- 8.457i	5.721- 8.516i
77	0	0	0	10					9.203- 32.628i	9.217 32.897i
78	0	0	0	5					-10.029- -41.985i	-42.273i -42.273i
79	0	0	0	0					-33.014 -33.014i	-33.194 -33.194i

TABLE 9. THEORY VALIDATION. ASYMMETRIES,  
CASES 80-90

C A S E	Initial Conditions					Coefficients			$\overrightarrow{J.A.}$ (mils)	
						$C_{Z\alpha}$ $C_{M\alpha}$ $C_{Mq}+C_{M\dot{\alpha}}$	$C_{Zp\beta}$ $C_{Mp\beta}$	$C_{YE}$ $C_{ZE}$ $C_{ME}$ $C_{NE}$	6-D	Theory
	$\overrightarrow{s}_0$	$\overrightarrow{\alpha}_0$	$\overrightarrow{\dot{\alpha}}_0$	$p_0$	$u_0$					
80	0	0	0	31416	1000	A1	A1	A1	Unstable	
81	0	0	0	18850					Unstable	
82	0	0	0	6283					0.025- 0.010i	0.023- 0.014i
83	0	0	0	500					0.241- 0.229i	0.238- 0.229i
84	0	0	0	300					0.396- 0.380i	0.394- 0.385i
85	0	0	0	100					1.177- 1.160i	1.174- 1.165i
86	0	0	0	50					2.346- 2.329i	2.349- 2.352i
87	0	0	0	25					4.684- 4.672i	4.699- 4.702i
88	0	0	0	10					10.224- 14.447i	10.177- 14.476i
89	0	0	0	5					24.402- 31.013i	24.516- 31.212i
90	0	0	0	0					-58.711 -58.711i	-58.450 -58.450i

Evident from Tables 7, 8, and 9 is the fact that roll rate has tremendous influence on the dispersion of flechettes with aerodynamic asymmetries. Figures 7, 8, and 9 illustrate the dispersion pattern for these cases. The 6-D computations and theory are in very good agreement considering the large deviations involved. It should be noted that the actual flechette with its velocity approaching 5000 ft/sec is affected very little by aerodynamic asymmetries. However, if the flechette were only to roll very slowly, large dispersion ranges in excess of 60 mils could occur. Velocity also has a noticeable effect on dispersion. Figure 10 shows the three theory curves from Figures 7, 8, 9 in composite to illustrate velocity effects. A sample trajectory, Case 79, is shown in Figure 11, illustrating the curved path of flight. This is typical of trajectories involving aerodynamic asymmetries.

#### Cases 91-123

To show the relation between the effects on dispersion for initial transverse velocity and aerodynamic asymmetries a second set of cases were run. Roll rate and velocity were varied as in the first set of cases, but  $\vec{S}_0$  was set at (100 = 100i) ft/sec with  $\vec{\alpha}_0 = 0$  and  $\vec{\delta}_0 = 0$ . Tables 10, 11, and 12 list the results. For high roll rate cases, Equation 24 becomes:

$$\vec{J} \cdot \vec{A} = \left[ \frac{\vec{S}_0}{u} + \frac{\rho u \pi d^2}{8m} \left[ C_{M_{\delta_\epsilon}} \vec{\delta}_\epsilon \left( \frac{A}{p} \right) + C_{Z_{\delta_\epsilon}} \left( \frac{I_y - I_x}{mud} A + \frac{i}{p} \right) \right] \right] 1000$$

For low rate cases, Equation 28 becomes:

$$\vec{J} \cdot \vec{A} = \left[ \frac{\vec{S}_0}{u} + \frac{\rho u \pi d^2}{8mx} \left[ C_{Z_{\delta_\epsilon}} \vec{\delta}_\epsilon - i \left( \frac{C_{Z_\alpha}}{C_{M_\alpha}} \right) C_{M_{\delta_\epsilon}} \vec{\delta}_\epsilon \right] \left[ \frac{1}{p^2} (1 - \cos \frac{px}{u}) + \frac{i}{p} \left( \frac{x}{u} - \frac{1}{p} \sin \frac{px}{u} \right) \right] \right] 1000$$

For very slow roll cases, Equation 30 becomes:

$$\vec{J.A.} = \left[ \frac{\vec{S}_0}{u} + \frac{\rho \pi d^2 x}{16m} \left[ C_{Z_{\delta_\epsilon}} \vec{\delta_\epsilon} - i \left( \frac{C_{Z_\alpha}}{C_{M_\alpha}} \right) C_{M_{\delta_\epsilon}} \vec{\delta_\epsilon} \right] \left[ \left( 1 - \frac{1}{12} \left( \frac{px}{u} \right)^2 + \frac{1}{360} \left( \frac{px}{u} \right)^4 \right) + i \left( \frac{px}{3u} - \frac{1}{60} \left( \frac{px}{u} \right)^3 + \frac{1}{2520} \left( \frac{px}{u} \right)^5 \right) \right] \right] 1000$$

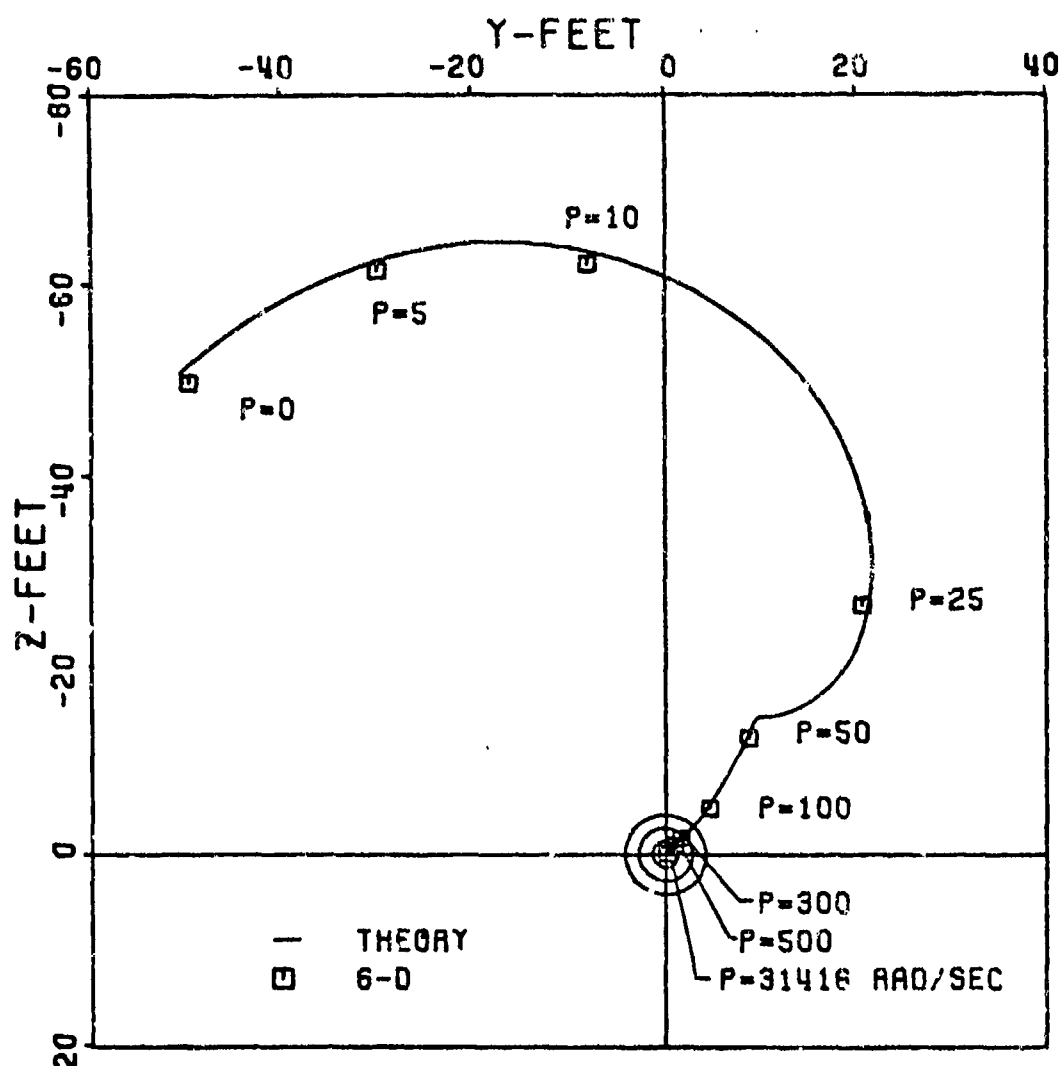


Figure 7. Dispersion: Phase III  
Cases 58-68

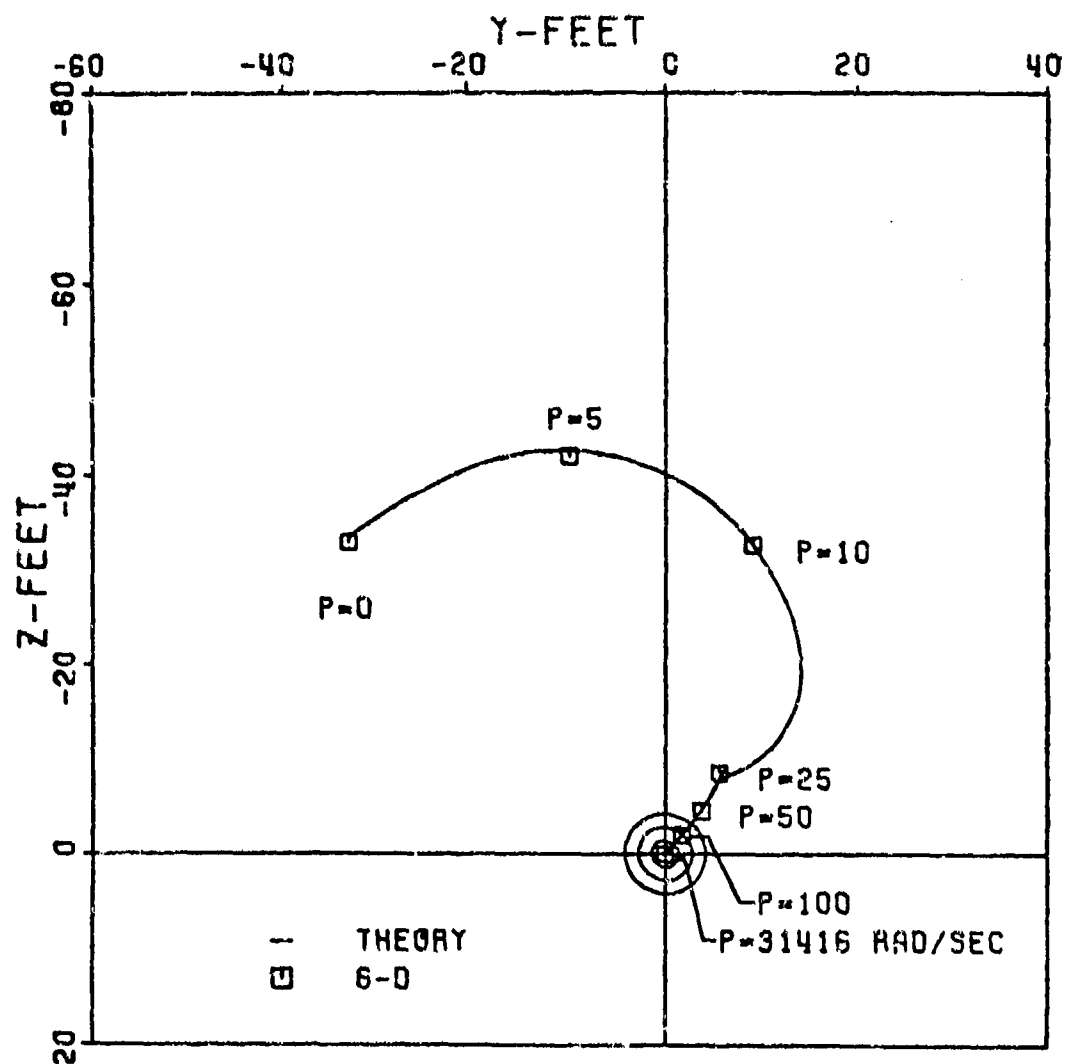


Figure 8. Dispersion: Phase III  
Cases 69-79



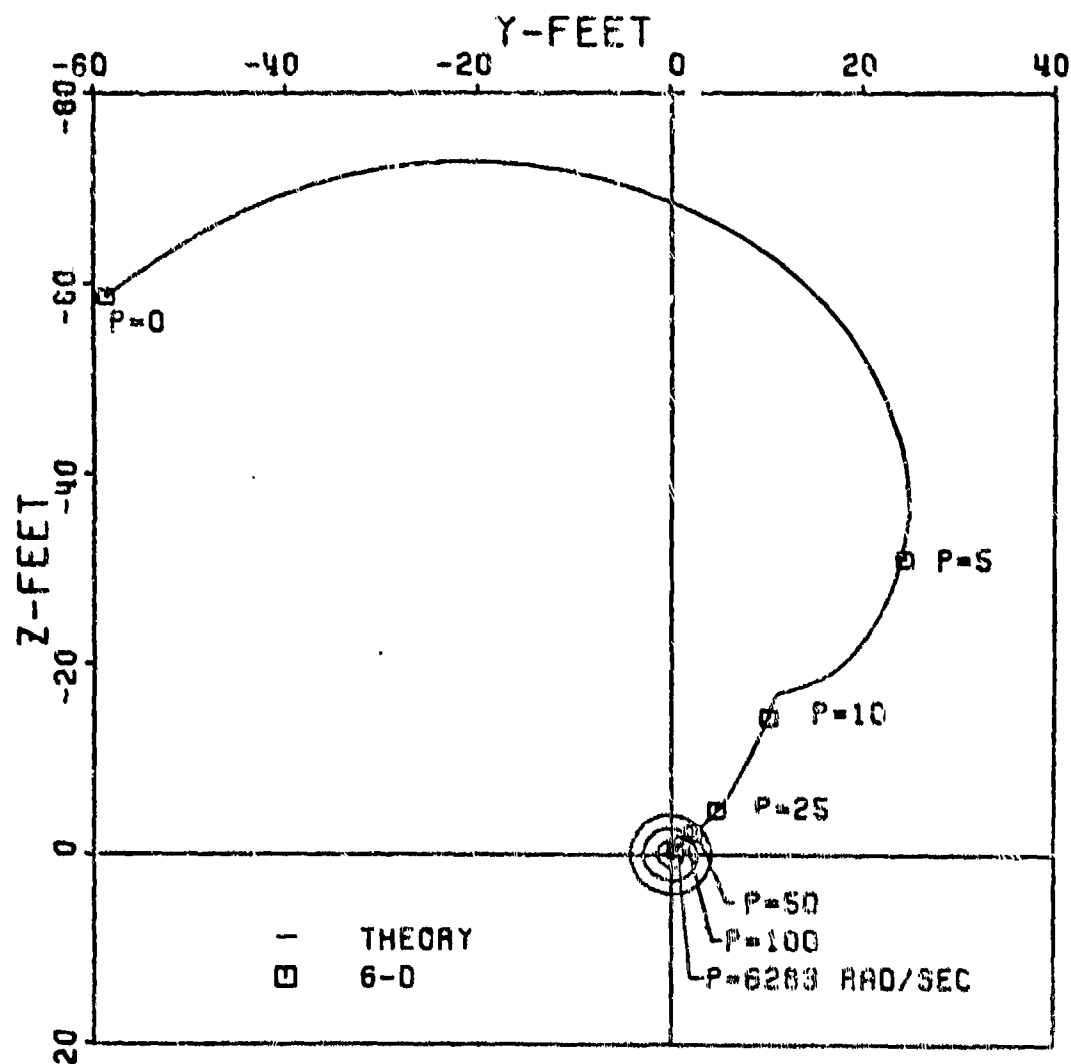


Figure 9. Dispersion: Phase III  
Cases 80-90

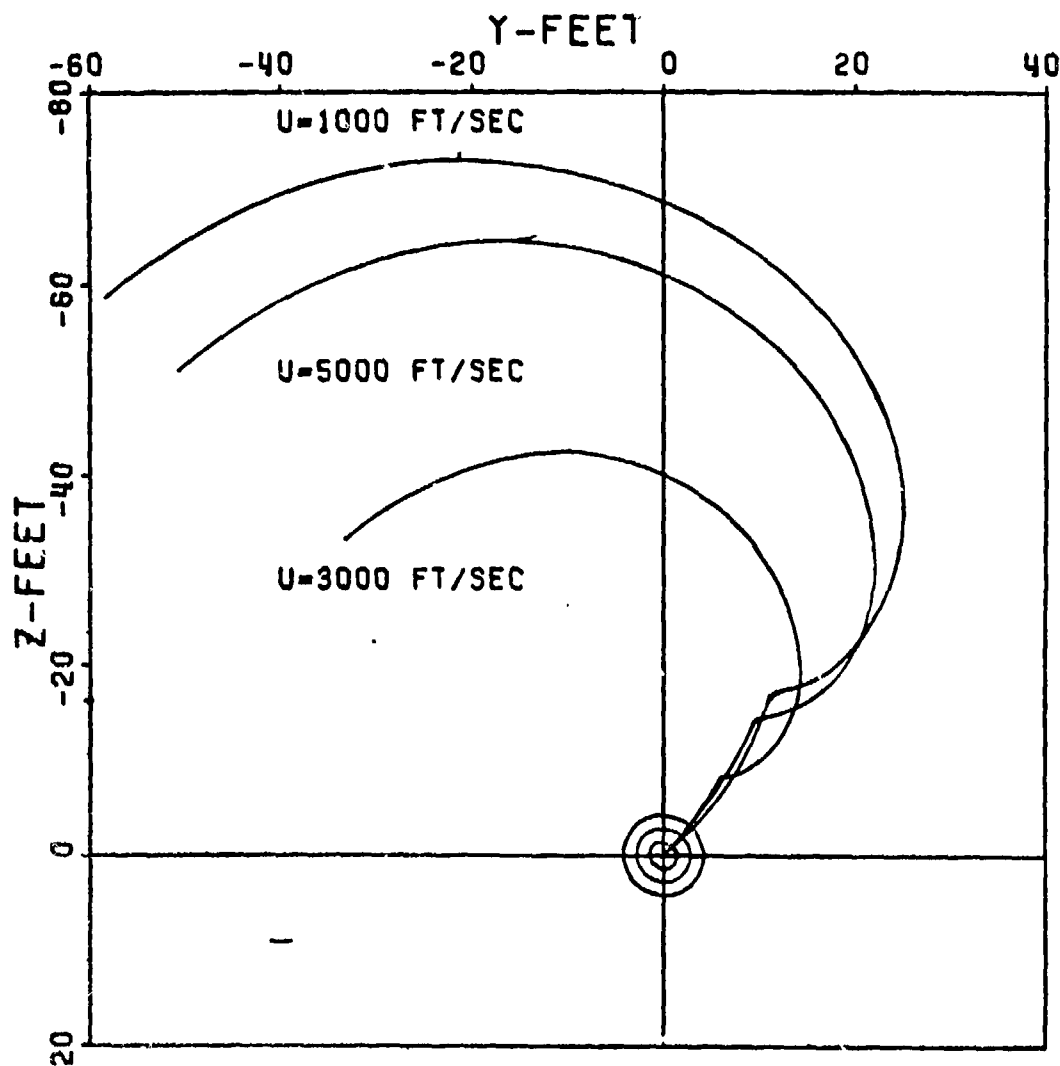


Figure 10. Dispersion: Phase III  
Theory, Cases 58-90

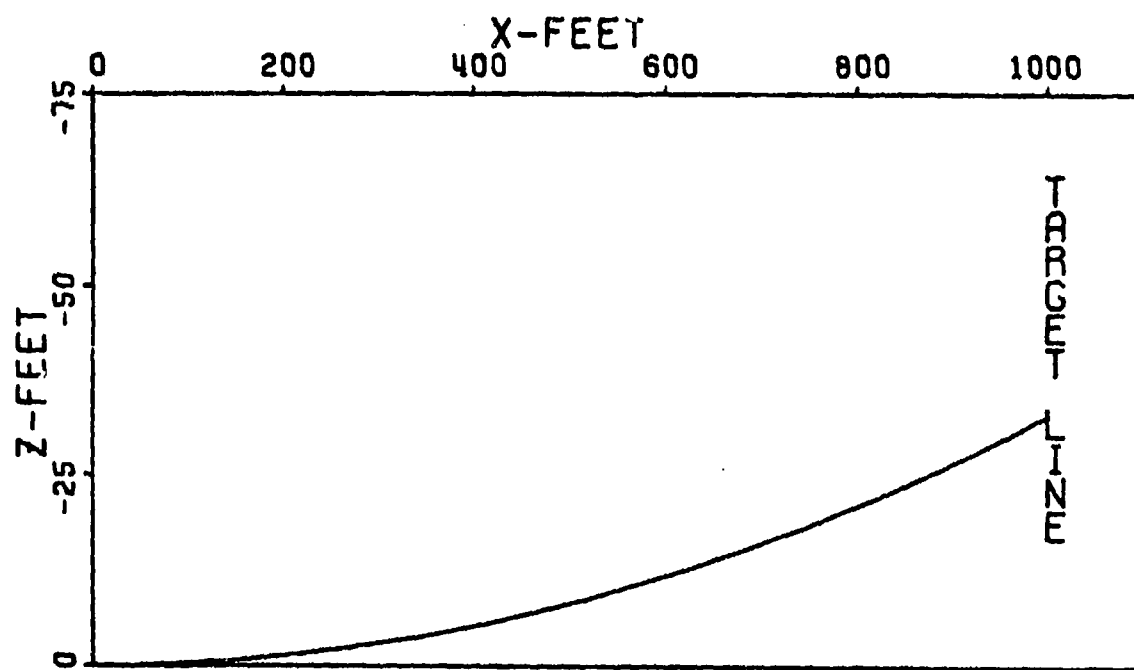
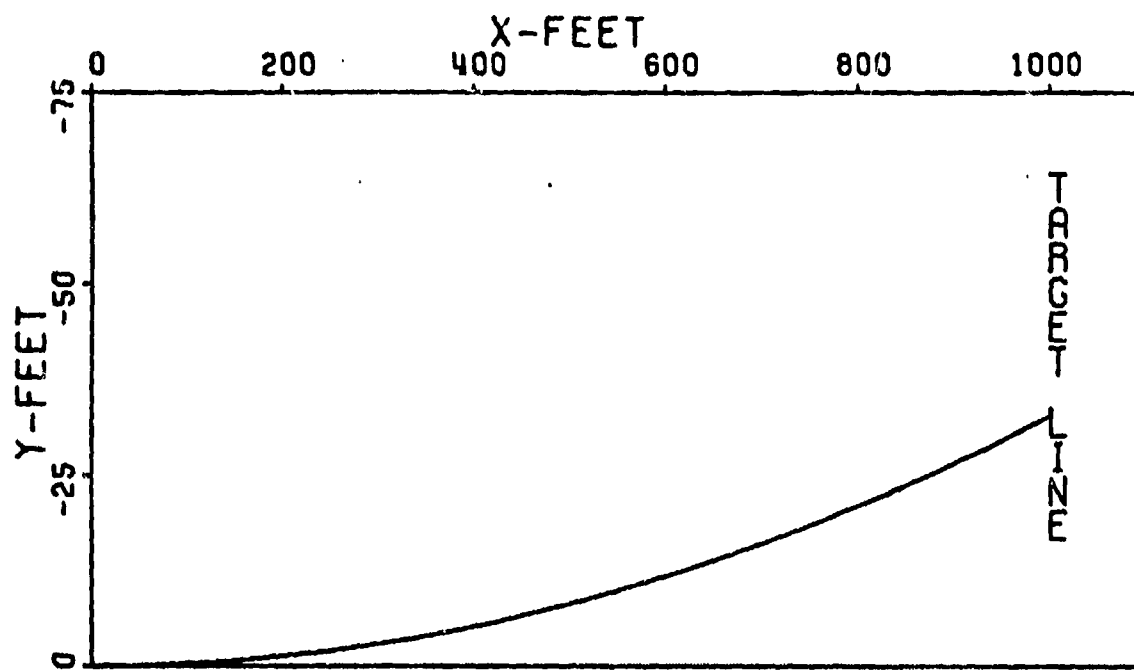


Figure 11. Trajectory, Case 79

Comparing Cases 91, 92, 93 in Table 10 with Cases 10, 11, 12 in Table 2 and Cases 58, 59, 60 in Table 7 it can be concluded that; except for possible computational error, Cases 91, 92, and 93 are the algebraic sum of Cases 10, 11, 12 and 58, 59, 60; that is, for example, Case 91 equals Case 10 plus Case 58. This fact is obviously true of the theory equations and is here shown to be the case for the 6-D computations as well. Similar comparisons can be made with corresponding cases in Tables 2, 8, 11, and 2, 9, 12. Thus, the effects of aerodynamic asymmetries and those of initial transverse velocity are independent of one another.

Figures 12, 13 and 14 illustrate the Cases 91-123. The curves are of the same form as Figures 7, 8, and 9 but differ with the addition of  $\vec{S}_0$ . Maximum effect of all parameters is desired. Cases 113, 114 and 115 show the limit of parameter combinations by 113 and 114 going unstable. Roll rate effects are again large and velocity effects are larger than in Cases 58-90. Figure 15 shows this to be true and also shows the cases involving  $U = 3000$  ft/sec to be ones of smallest dispersion. Such was the case in Figure 10. Figure 16 illustrates a sample trajectory, Case 101.

#### Cases 124-156

To establish the relationship between the effects on dispersion for aerodynamic asymmetries and initial angle of attack, a third set of cases were run. Again roll rate and velocity were varied as done previously but  $\vec{\alpha}_0$  was set at  $(1+i)$  degrees with  $\vec{S}_0=0$  and  $\vec{\alpha}_0=0$ . Tables 13, 14, and 15 tabulate the results. For all high roll rate cases, Equation 24 reduces to:

$$\vec{J} \cdot \vec{A} = \left[ \frac{ipI_x}{mud} A \vec{\alpha}_0 + \frac{\rho u \pi d^2}{8m} \left[ C_{M_{\delta_\epsilon}} \vec{\delta}_\epsilon \left( \frac{A}{p} \right) + C_{Z_{\delta_\epsilon}} \vec{\delta}_\epsilon \left( \frac{I_y - I_x}{mud} A + \frac{i}{p} \right) \right] \right] 1000$$

For low roll rate cases, Equation 28 reduces to:

$$\vec{J} \cdot \vec{A} = \frac{\rho u^2 \pi d^2}{8m \alpha} \left[ C_{Z_{\delta_\epsilon}} \vec{\delta}_\epsilon - i \left( \frac{C_{Z_\alpha}}{C_{M_\alpha}} \right) C_{M_{\delta_\epsilon}} \vec{\delta}_\epsilon \right] \left[ \frac{1}{p^2} (1 - \cos \frac{px}{u}) + \frac{i}{p} \left( \frac{x}{u} - \frac{1}{p} \sin \frac{px}{u} \right) \right] 1000$$

For very low roll rates, Equation 30 reduces to:

$$\vec{J} \cdot \vec{A} = \frac{\rho \pi d^2 x}{16m} \left[ C_{Z_{\delta_\epsilon}} \vec{\delta_\epsilon} - i \left( \frac{C_{Z_\alpha}}{C_{M_\alpha}} \right) C_{M_{\delta_\epsilon}} \vec{\delta_\epsilon} \right] \left[ \left( 1 - \frac{1}{12} \left( \frac{px}{u} \right)^2 + \frac{1}{360} \left( \frac{px}{u} \right)^4 \right) + i \left( \frac{px}{3u} - \frac{1}{60} \left( \frac{px}{u} \right)^3 + \frac{1}{2520} \left( \frac{px}{u} \right)^5 \right) \right] 1000$$

Only for high roll rates does the  $\vec{\alpha}_0$  term appear.  $\vec{\alpha}_0$  should have no noticeable effect on dispersion for  $p < 100$  rad/sec.

Comparing Cases 124, 125, 126 in Table 13 with Cases 19, 20, 21 in Table 3 and Cases 58, 59, 60 in Table 7 it can be concluded that Cases 124, 125 and 126 are the algebraic sum of Cases 19, 20, 21 and 58, 59, 60; that is, for example, Case 124 equals Case 19 plus Case 58. This is obvious from the reduced theoretical equations for Cases 124-156. It is shown here to be also true for the 6-D computations; allowing for some computational error. Similar comparisons can be made with corresponding cases in Tables 3, 8, 14 and 3, 9, 15. Thus the effects of aerodynamic asymmetries and those of initial angle of attack are independent of one another.

Figures 17, 18 and 19 illustrate Cases 124-156. The curves are very similar to those in Figures 7, 8 and 9 with the only difference being the very small  $\alpha_0$  contribution in Figures 17, 18 and 19. Cases 135, 146, and 147 result in instabilities, indicating that maximum effect of the various parameters has been accomplished. Effects of roll rate are essentially the same as in Case 58-90 and effects of velocity, Figure 20, the same as in Figure 10. Cases with  $U = 3000$  ft/sec again have the smallest dispersion. Figure 21 shows a typical trajectory, Case 134.

#### Cases 157-189

To validate the relationship between the effects on dispersion for aerodynamic asymmetries and those of initial angular rate, a fourth set of cases were run. As before, roll rate and velocity were varied, but  $\vec{\alpha}_0$  set at  $(250 + 250i)$  rad/sec with  $\vec{S}_0 = 0$  and  $\vec{\alpha}_0 = 0$ . Tables 16, 17, 18 give the results. For high roll rates, the governing equation becomes:

$$\vec{J} \cdot \vec{A} = \left[ \frac{\rho u \pi d^2}{8m} \left[ C_{M_{\delta_\epsilon}} \vec{\delta_\epsilon} \left( \frac{A}{p} \right) + C_{Z_{\delta_\epsilon}} \vec{\delta_\epsilon} \left( \frac{I_y - I_x}{mud} A + \frac{i}{p} \right) - \frac{I_y}{mud} A \vec{\alpha}_0 \right] \right] 1000$$

For low roll rates, the governing equation:

$$\begin{aligned} \overrightarrow{J.A.} = & \left[ \frac{\rho u^2 \pi d^2}{8 m x} \left[ C_{Z_{\delta \epsilon}} \vec{\delta \epsilon} - i \left( \frac{C_{Z_{\alpha}}}{C_{M_{\alpha}}} \right) C_{M_{\delta \epsilon}} \vec{\delta \epsilon} \right] \left[ \left( 1 - \cos \frac{px}{u} \right) \right. \right. \\ & \left. \left. + \frac{1}{p} \left( \frac{x}{u} - \frac{1}{p} \sin \frac{px}{u} \right) \right] - \frac{I_y}{m u d} \left( \frac{C_{Z_{\alpha}}}{C_{M_{\alpha}}} \right) \vec{\alpha}_o \right] 1000 \end{aligned}$$

For very slow roll rate, the governing equation:

$$\begin{aligned} \overrightarrow{J.A.} = & \left[ \frac{\rho u d^2 x}{16 m} \left[ C_{Z_{\delta \epsilon}} \vec{\delta \epsilon} - i \left( \frac{C_{Z_{\alpha}}}{C_{M_{\alpha}}} \right) C_{M_{\delta \epsilon}} \vec{\delta \epsilon} \right] \left[ \left( 1 - \frac{1}{12} \left( \frac{px}{u} \right)^2 + \frac{1}{360} \left( \frac{px}{u} \right)^4 \right) \right. \right. \\ & \left. \left. + i \left( \frac{px}{3u} - \frac{1}{60} \left( \frac{px}{u} \right)^3 + \frac{1}{2520} \left( \frac{px}{u} \right)^5 \right) \right] - \frac{I_y}{m u d} \left( \frac{C_{Z_{\alpha}}}{C_{M_{\alpha}}} \right) \vec{\alpha}_o \right] 1000 \end{aligned}$$

Comparing Cases 157, 158, and 159 in Table 16 with Cases 28, 29, 30 in Table 4 and Cases 58, 59, 60 in Table 7, it can be concluded that Cases 157, 158, and 159 are the algebraic sum of Cases 28, 29, 30 and 58, 59, 60; that is, for example, Case 157 equals Case 28 plus Case 58. This is obvious from the reduced theoretical equations for Cases 157-189. Here it is shown to be true for 6-D computations also. Any discrepancy can be attributed to computational error. Similar comparisons can be made with corresponding cases in Table 4, 8, and 17. Thus the effects of aerodynamic asymmetries and those of initial angular rate are independent of one another.

TABLE 10. THEORY VALIDATION, ASYMMETRIES,  
CASES 91-101

C A S E	Initial Conditions					Coefficients			$\vec{J.A.}$ (mils)	
	$\vec{s}_0$	$\vec{\alpha}_0$	$\vec{\dot{\alpha}}_0$	$p_0$	$u_0$	$C_{Z\alpha}$ $C_{M\alpha}$	$C_{Zp\beta}$	$C_{YE}$ $C_{ZE}$ $C_{ME}$ $C_{NE}$	6-D	Theory
						$C_{M_q} + C_{M_{\dot{\alpha}}}$	$C_{M_{p\beta}}$			
91	$100+100i$	0	0	31416	5000	A1	A1	A1	20.011+	20.018+
92				18850					19.987i	19.986i
93				6283					20.026+	20.029+
94				500					19.972i	19.975i
95				300					20.056+	20.083+
96				100					19.872i	19.922i
97				50					21.004+	21.013+
98				25					19.012i	18.991i
99				10					21.626+	21.688+
100				5					18.286i	18.317i
101				0					24.593+	24.675+
									15.099i	15.025i
									28.702+	28.780+
									7.687i	7.511i
									40.766-	41.150-
									6.492i	6.927i
									11.983-	11.790-
									42.325i	43.210i
									-9.908-	-10.372
									41.503i	-42.353i
									-29.727	-30.427
									-29.743i	-30.427i

TABLE 11. THEORY VALIDATION, ASYMMETRIES,  
CASES 102-112

C A S E	Initial Conditions					Coefficients			$\vec{J.A.}$ (mils)	
	$\vec{s}_0$	$\vec{\alpha}_0$	$\vec{\dot{\alpha}}_0$	$p_0$	$u_0$	$C_{Z\alpha}$	$C_{Zp\beta}$	$C_{YE}$	6-D	Theory
						$C_{M\alpha}$ $C_{Mq} + C_{M\dot{\alpha}}$	$C_{M_{p\beta}}$	$C_{ZE}$ $C_{ME}$ $C_{NE}$		
102	$100 + 100i$	0	0	31416	3000	A1	A1	A1	33.352+	33.342+
									33.362i	33.329i
103				18850					33.366+	33.345+
									33.364i	33.325i
104				6283					33.388+	33.367+
									33.347i	33.304i
105				500					33.740+	33.734+
									32.964i	32.937i
106				300					34.009+	34.000+
									33.705i	32.761i
107				100					35.188+	35.327+
									31.361i	31.344i
108				50					37.139+	36.744+
									28.850i	29.169i
109				25					39.029+	39.054+
									24.892i	24.817i
110				10					42.575+	42.550+
									0.716i	0.436i
111				5					23.312-	23.159-
									8.612i	8.940i
112				0					0.380+	0.139+
									0.362i	0.139i



TABLE 12. THEORY VALIDATION, ASYMMETRIES,  
CASES 113-123

C A S E	Initial Conditions					Coefficients			$\overline{J.A.}$ (mils)	
	$\overrightarrow{s}_0$	$\overrightarrow{\alpha}_0$	$\overrightarrow{\dot{\alpha}}_0$	$p_0$	$u_0$	$C_{Z\alpha}$	$C_{Zp\beta}$	$C_{YE}$	6-D	Theory
						$C_{M\alpha}$		$C_{ZE}$		
						$C_{M_q} + C_{M_{\dot{\alpha}}}$	$C_{M_{p\beta}}$	$C_{ME}$ $C_{NE}$		
113	$100 + 100i$	0	0	31416	$1000$	A1	A1	A1	Unstable	
114				18850					Unstable	
115				6283					100.351+ 100.814i	100.023+ 99.986i
116				500					100.559+ 100.587i	100.238+ 99.771i
117				300					100.710+ 100.431i	100.394+ 99.615i
118				100					101.492+ 99.658i	101.174+ 98.835i
119				50					102.668+ 98.495i	102.349+ 97.648i
120				25					105.019+ 96.164i	104.699+ 95.298i
121				10					110.862+ 86.275i	110.177+ 85.524i
122				5					125.216+ 69.958i	124.516+ 68.788i
123				0					41.499+ 41.413i	41.550+ 41.550i

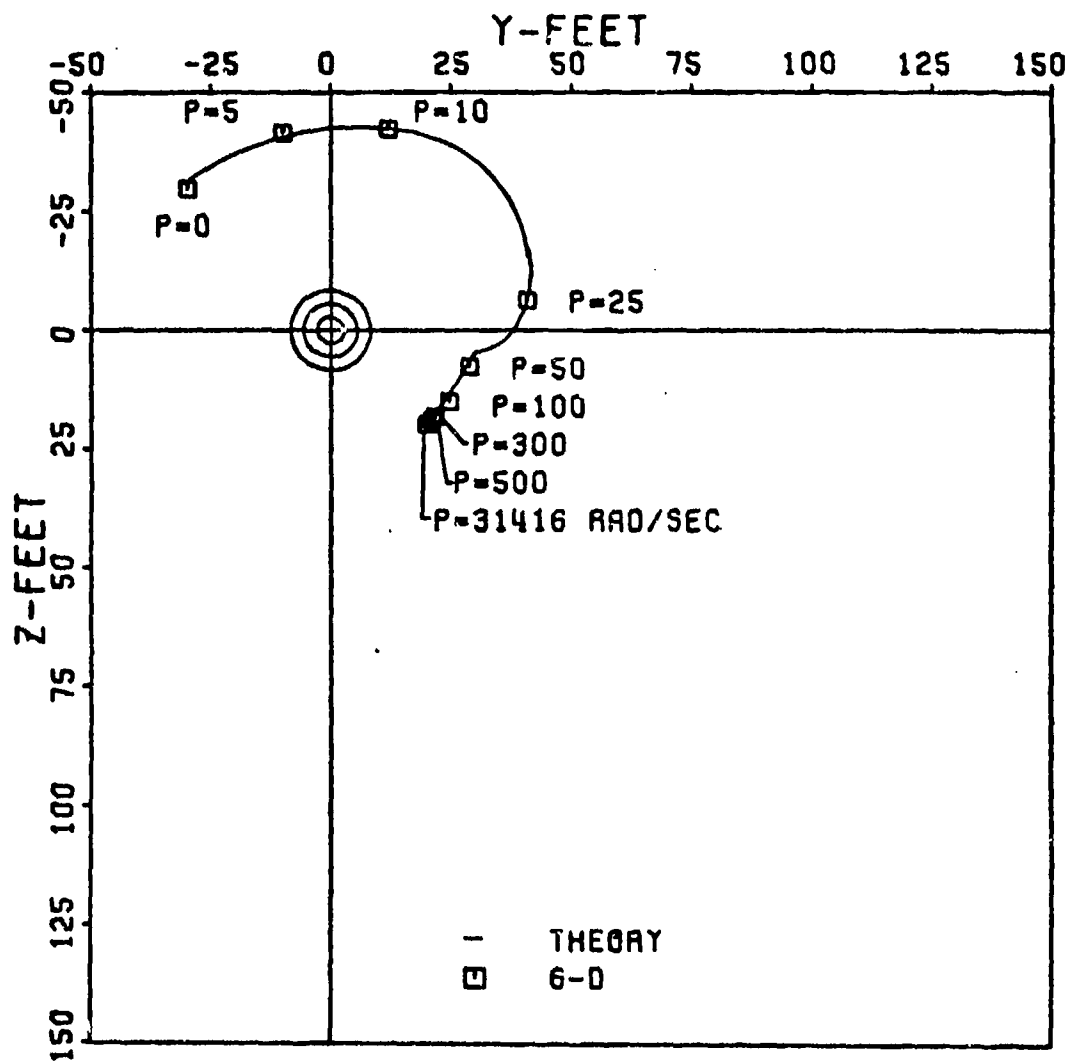


Figure 12. Dispersion: Phase III  
Cases 91-101

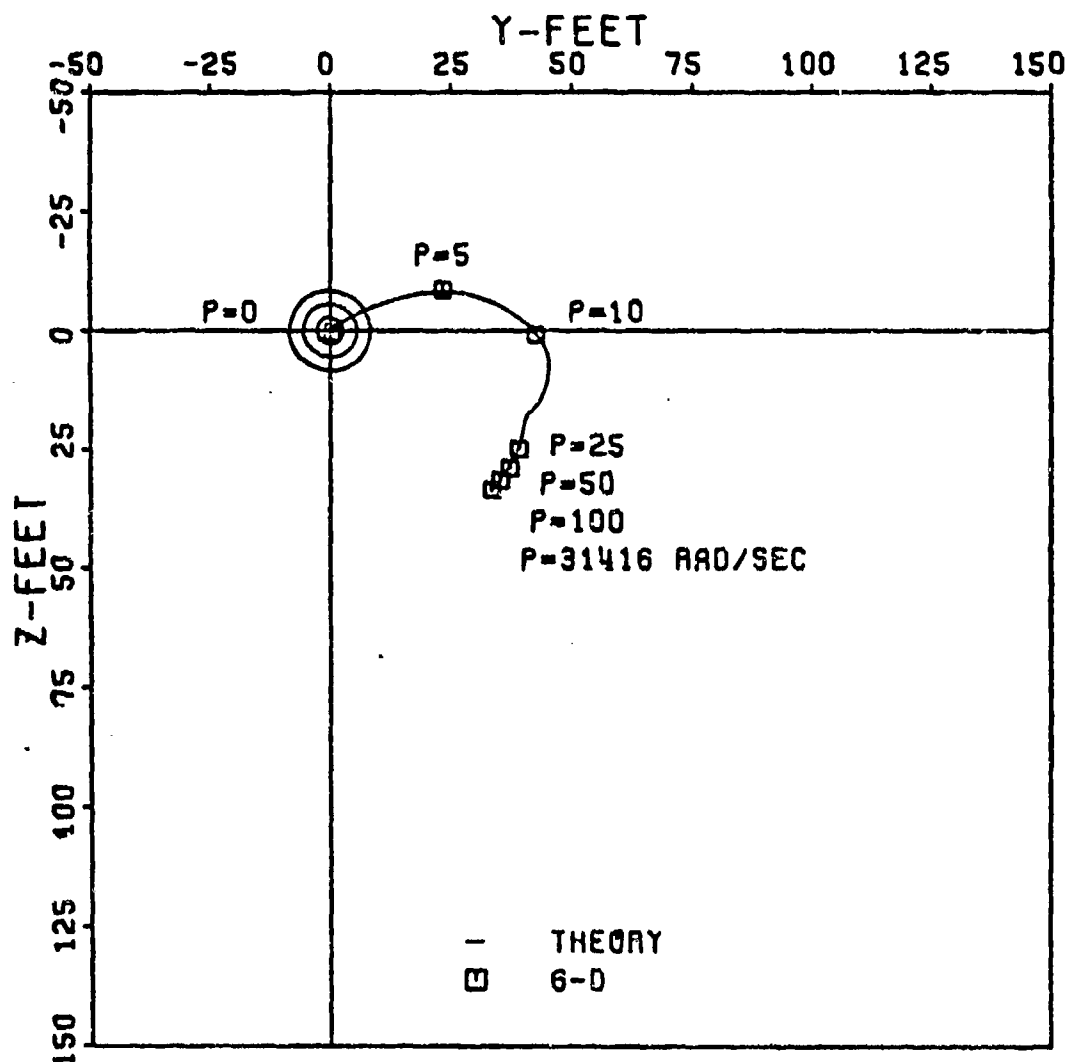


Figure 13. Dispersion: Phase III  
Cases 102-112

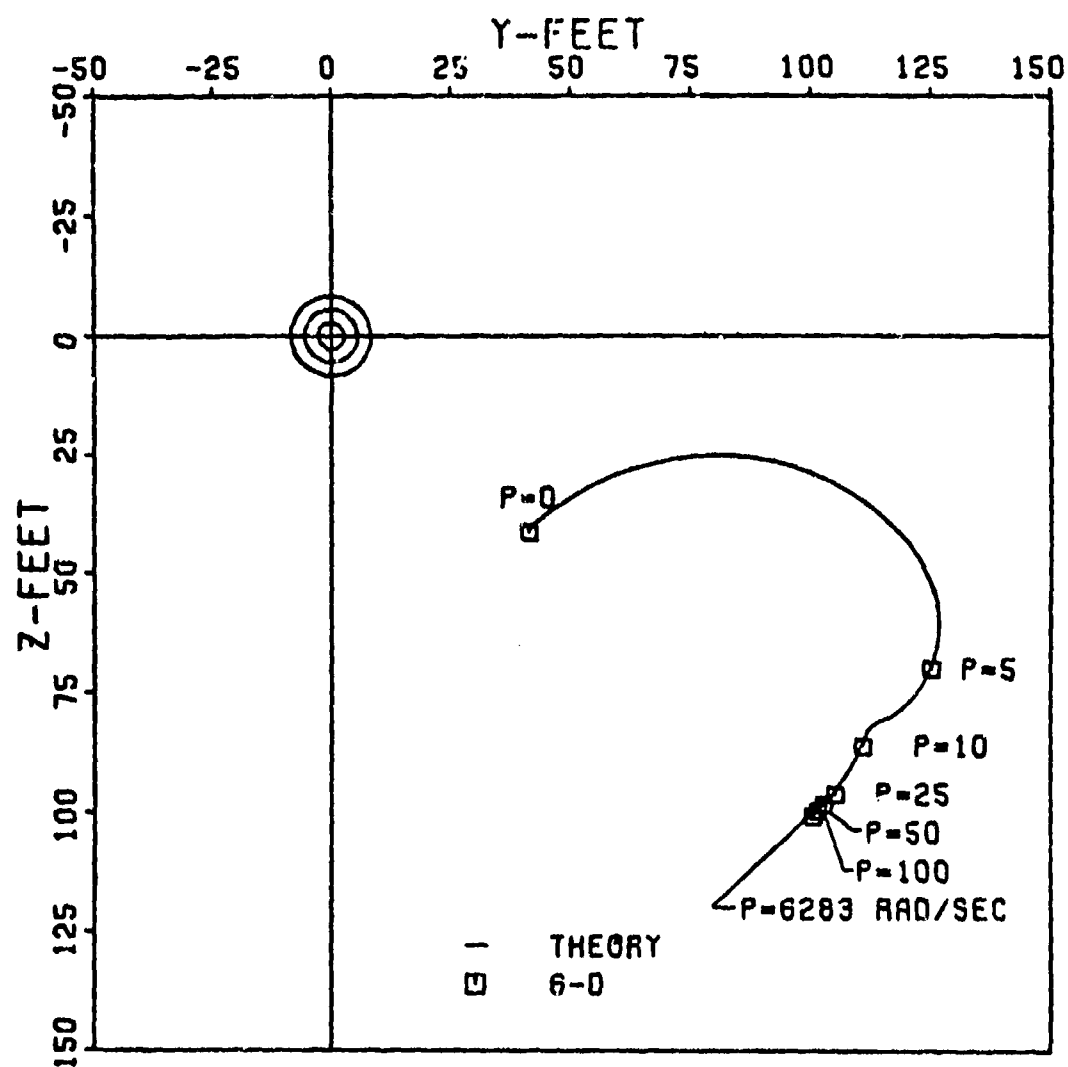


Figure 14. Dispersion: Phase III  
Cases 113-123

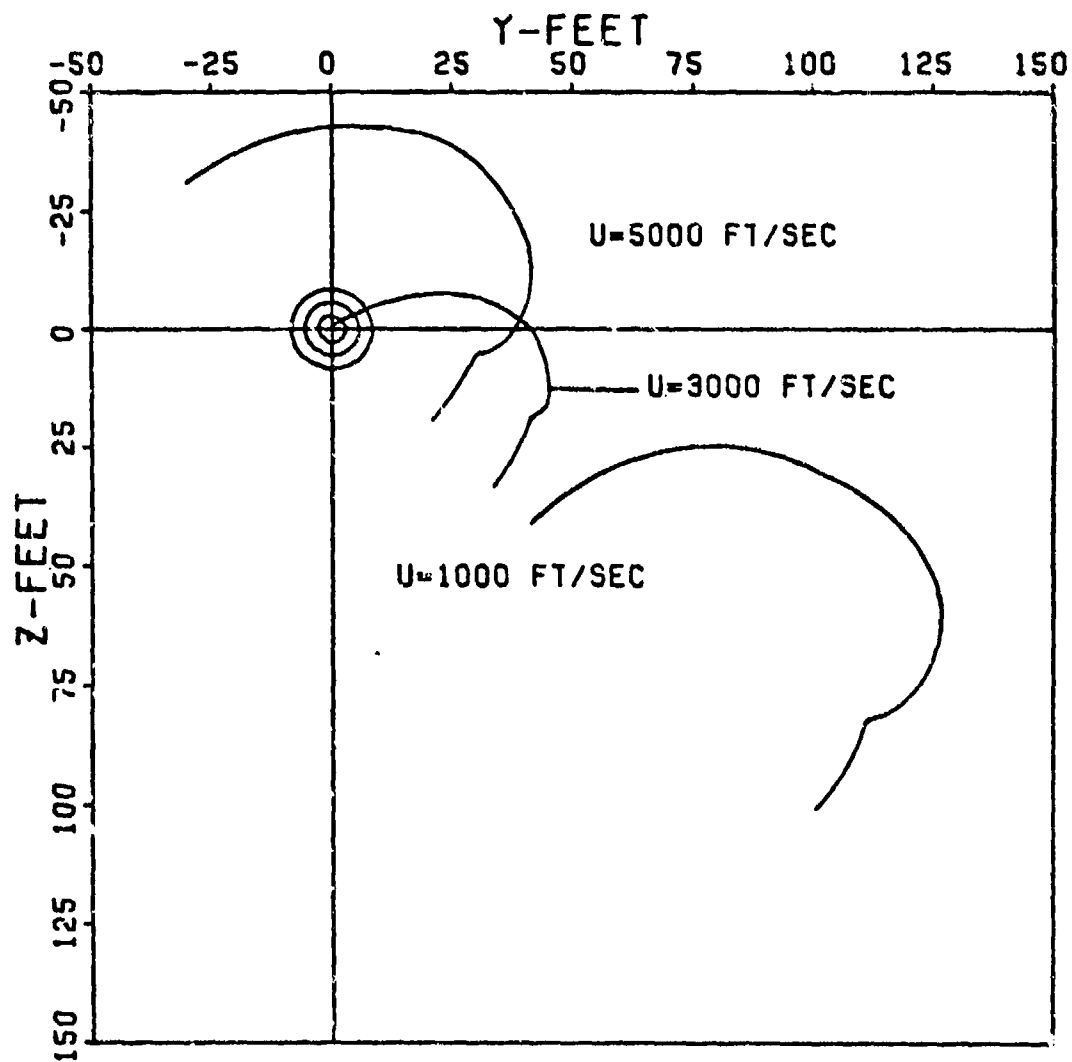


Figure 15. Dispersion: Phase III  
Theory, Cases 91-123

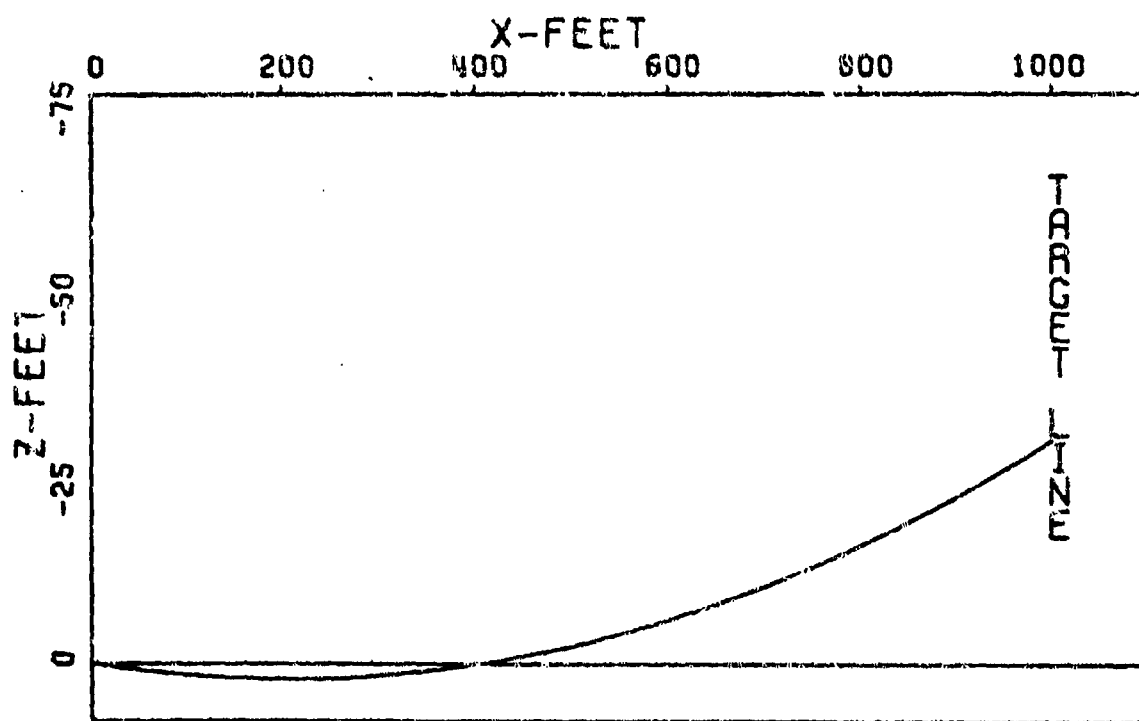
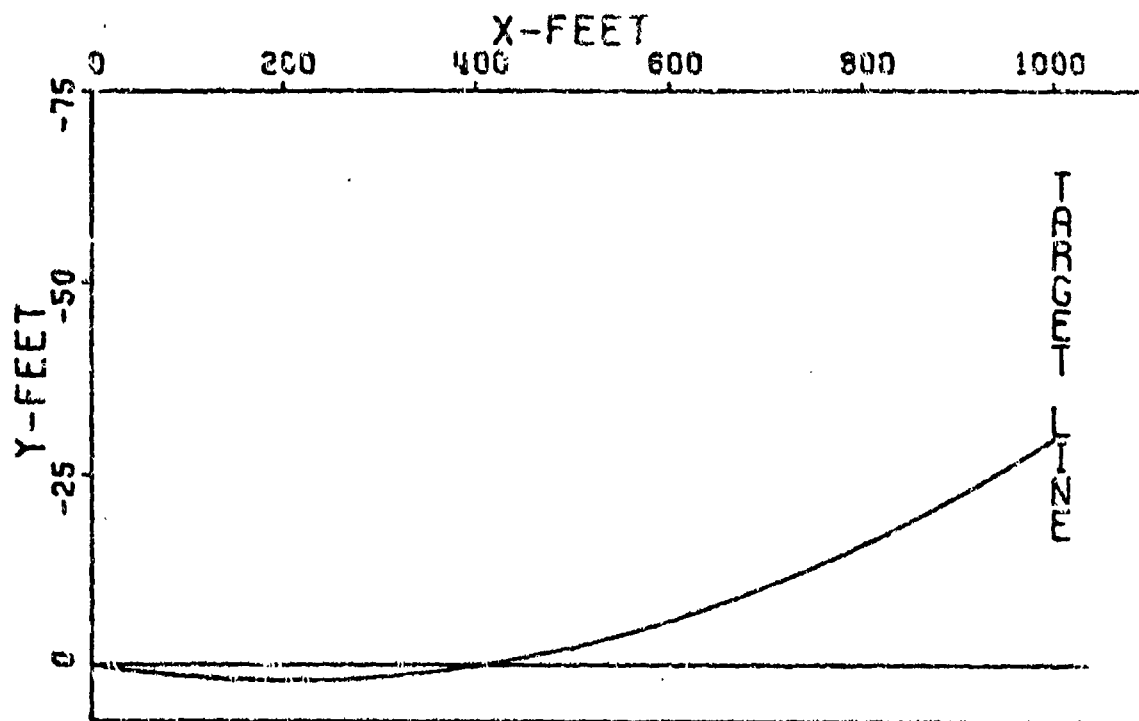


Figure 16. Trajectory, Case 101

TABLE 13. THEORY VALIDATION, ASYMMETRIES,  
CASES 124-134

C A S E	Initial Conditions					Coefficients			$\vec{J.A.}$ (mils)	
						$C_{Z\alpha}$ $C_{M\alpha}$ $C_{Mq} + C_{M\dot{\alpha}}$	$C_{Zp\beta}$ $C_{Mp\beta}$	$C_{YE}$ $C_{ZE}$ $C_{ME}$ $C_{NE}$		
	$\vec{s}_0$	$\vec{\alpha}_0$	$\vec{\dot{\alpha}}_0$	$p_0$	$u_0$				6-D	Theory
124	$\uparrow$	$\uparrow$	$\uparrow$	31416	$\uparrow$	$\uparrow$	$\uparrow$	$\uparrow$	0.028+ 0.052i	0.009- 0.013i
125				18850					0.052+ 0.029i	0.013- 0.009i
126				6283					0.094- 0.080i	0.078- 0.073i
127				500					1.040- 0.954i	1.013- 1.009i
128				300					1.660- 1.680i	1.688- 1.683i
129				100					4.628- 4.868i	4.675- 4.975i
130				50					8.732- 12.279i	8.780- 12.489i
131				25					20.784- 26.468i	21.150- 26.927i
132				10					-7.954- 62.367i	-8.210- 63.210i
133				5					-29.912 -61.629i	-30.372 -62.353i
134				0					-49.828 -49.840i	-50.427 -50.427i

TABLE 14. THEORY VALIDATION, ASYMMETRIES,  
CASES 135-145

C A S E	Initial Conditions					Coefficients			$\vec{J.A.}$ (mils)								
						$C_{Z\alpha}$ $C_{M\alpha}$ $C_{M_q} + C_{M\dot{\alpha}}$	$C_{Z_{p\beta}}$ $C_{M_{p\beta}}$	$C_{YE}$ $C_{ZE}$ $C_{ME}$ $C_{NE}$	6-D	Theory							
	$\vec{s}_0$	$\vec{\alpha}_0$	$\vec{\dot{\alpha}}_0$	$p_0$	$u_0$												
135	$\uparrow$ $\downarrow$	$\uparrow$ $\downarrow$	$\uparrow$ $\downarrow$	31416	$\uparrow$ $\downarrow$	$\uparrow$ $\downarrow$	$\uparrow$ $\downarrow$	$\uparrow$ $\downarrow$	Unstable								
136				18850					0.035+ 0.046i	-0.003 +0.008i							
137				6283					0.066+ 0.017i	0.029- 0.024i							
138				500					0.432- 0.357i	0.401- 0.396i							
139				300					0.701- 0.618i	0.666- 0.662i							
140				0					1+i	0	100	3000	A1	A1	A1	1.879- 1.958i	1.994- 1.989i
141											50					3.819- 4.473i	3.411- 4.164i
142											25					5.714- 8.416i	5.721- 8.516i
143											10					9.247- 32.586i	9.217- 32.897i
144											5					-9.985- 41.948i	-10.174 -42.273i
145											0					-32.973 -32.981i	-33.194 -33.194i



TABLE 15. THEORY VALIDATION, ASYMMETRIES,  
CASES 146-156

C A S E	Initial Conditions					Coefficients			$\vec{J.A.}$ (mils)	
						$C_{Z\alpha}$ $C_{M\alpha}$ $C_{M_q} + C_{M\dot{\alpha}}$	$C_{Z_{p\beta}}$ $C_{M_{p\beta}}$	$C_{YE}$ $C_{ZE}$ $C_{ME}$ $C_{NE}$		
	$\vec{s}_0$	$\vec{\alpha}_0$	$\vec{\dot{\alpha}}_0$	$p_0$	$u_0$				6-D	Theory
146	$\uparrow$	$\uparrow$	$\uparrow$	31416	$\uparrow$	$\uparrow$	$\uparrow$	Unstable		
147	$\uparrow$	$\uparrow$	$\uparrow$	18850	$\uparrow$	$\uparrow$	$\uparrow$	Unstable		
148	$\uparrow$	$\uparrow$	$\uparrow$	6283	$\uparrow$	$\uparrow$	$\uparrow$	0.046+ 0.039i	0.008+ 0.001i	
149	$\uparrow$	$\uparrow$	$\uparrow$	500	$\uparrow$	$\uparrow$	$\uparrow$	0.275- 0.188i	0.237- 0.228i	
150	$\uparrow$	$\uparrow$	$\uparrow$	300	$\uparrow$	$\uparrow$	$\uparrow$	0.432- 0.342i	0.393- 0.384i	
151	0	1+i	0	100	1000	A1	A1	A1	1.213- 1.123i	1.174- 1.165i
152	$\uparrow$	$\uparrow$	$\uparrow$	50	$\uparrow$	$\uparrow$	$\uparrow$	$\uparrow$	2.381- 2.294i	2.349- 2.352i
153	$\uparrow$	$\uparrow$	$\uparrow$	25	$\uparrow$	$\uparrow$	$\uparrow$	$\uparrow$	4.719- 4.637i	4.699- 4.702i
154	$\uparrow$	$\uparrow$	$\uparrow$	10	$\uparrow$	$\uparrow$	$\uparrow$	$\uparrow$	10.258- 14.411i	10.177- 14.476i
155	$\uparrow$	$\uparrow$	$\uparrow$	5	$\uparrow$	$\uparrow$	$\uparrow$	$\uparrow$	24.440- 30.976i	24.516- 31.212i
156	$\downarrow$	$\downarrow$	$\downarrow$	0	$\downarrow$	$\downarrow$	$\downarrow$	$\downarrow$	-58.669 -58.684i	-58.450 -58.450i

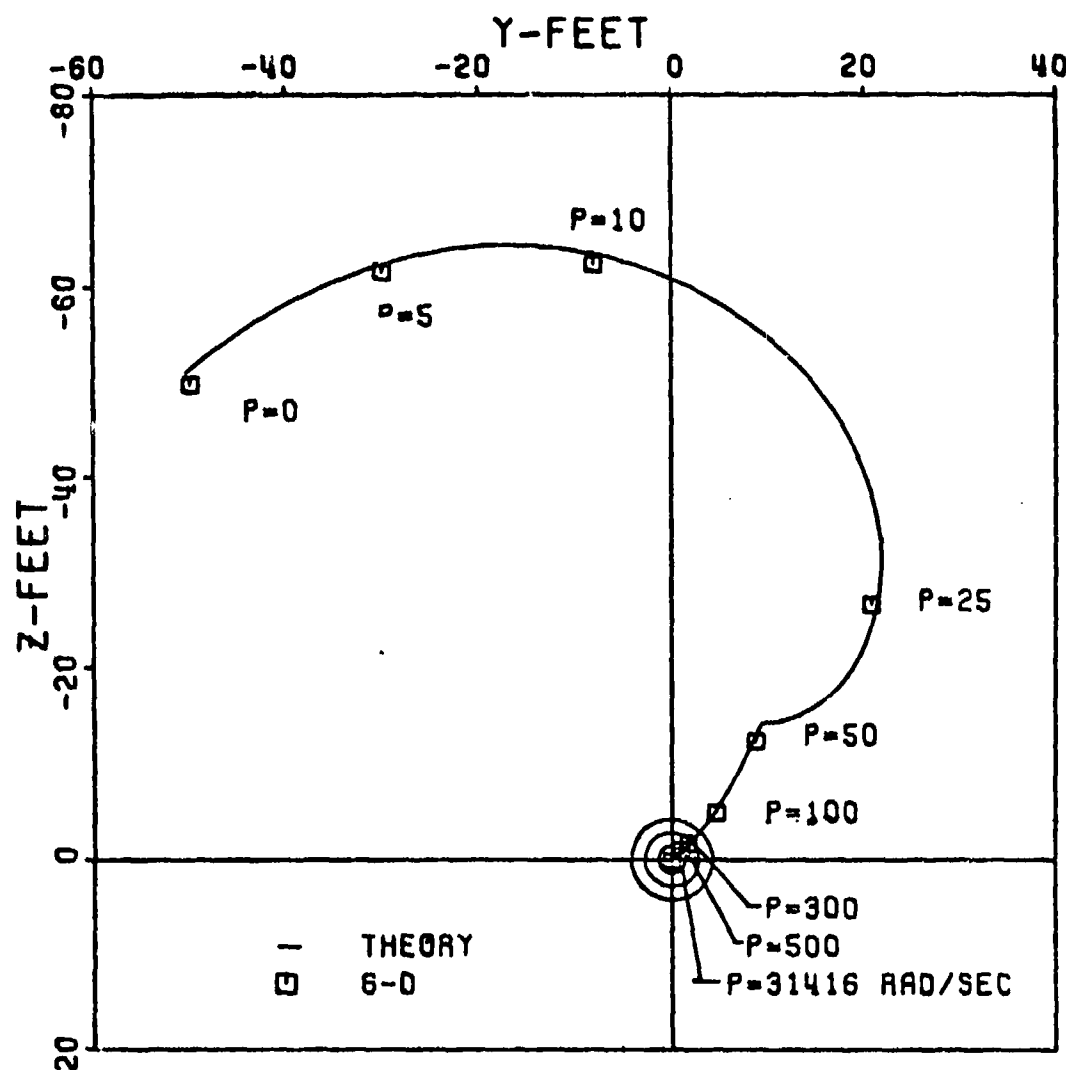


FIGURE 17. DISPERSION: PHASE III  
CASES 124-134

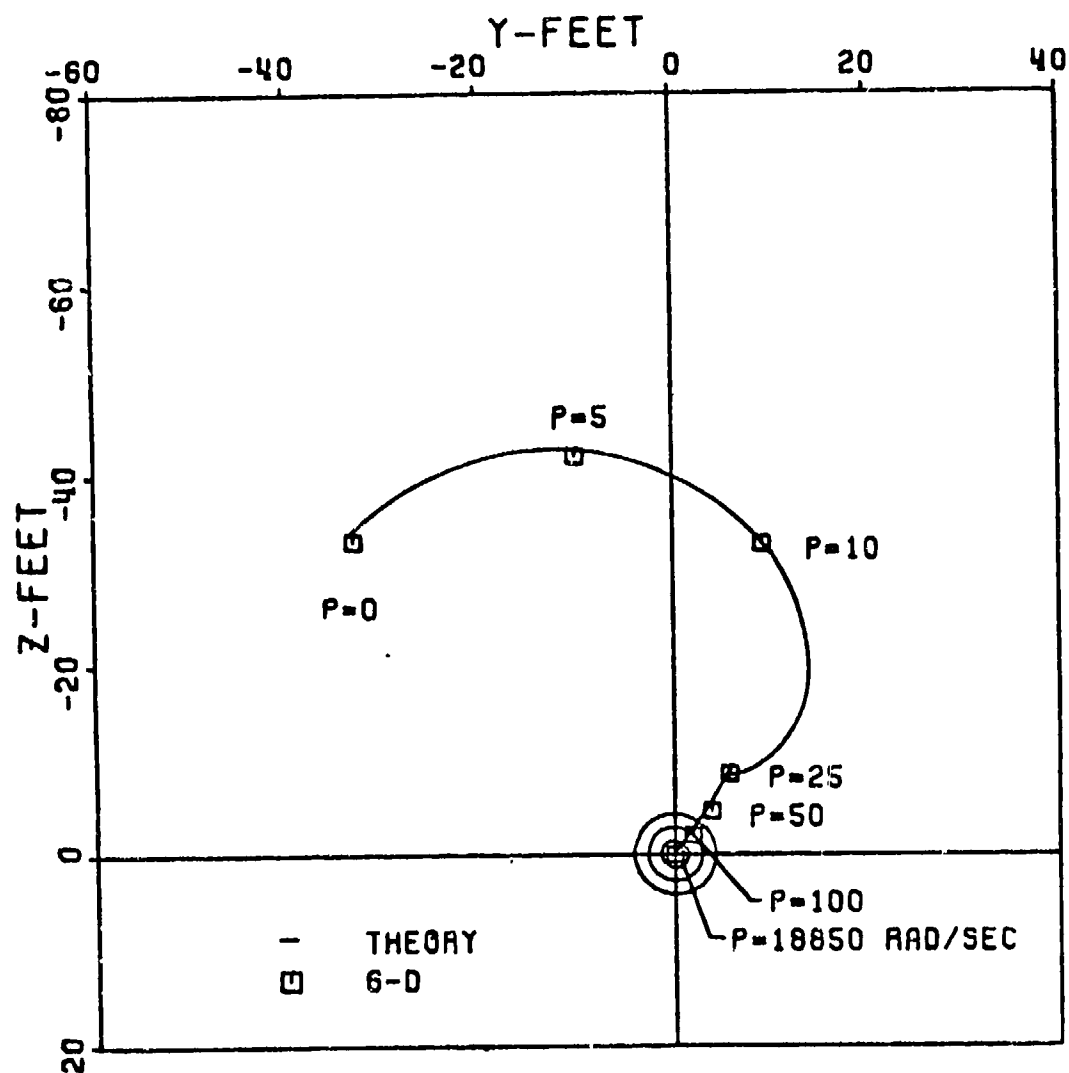


Figure 18. Dispersion: Phase III  
Cases 135-145

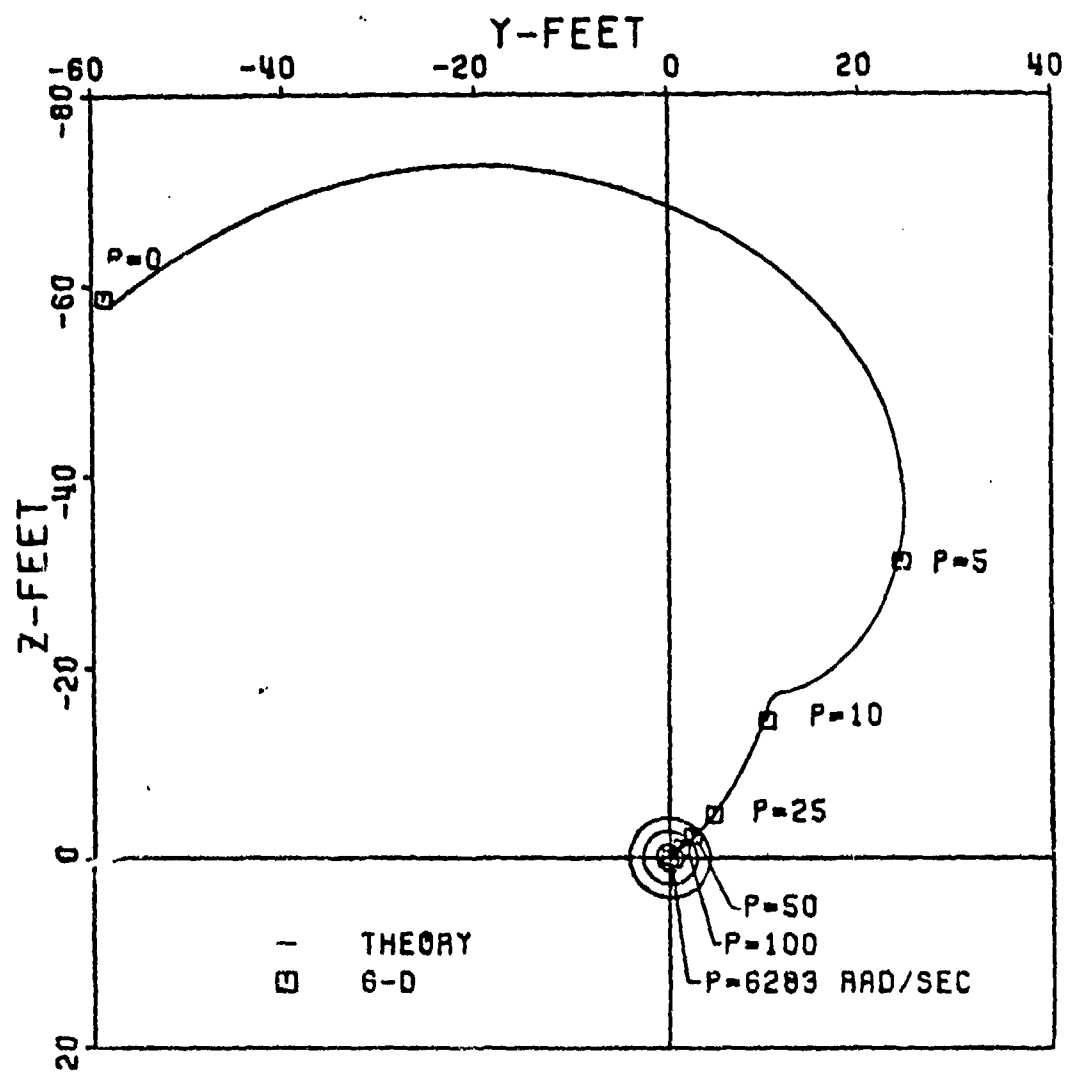


Figure 19. Dispersion: Phase III  
Cases 146-156

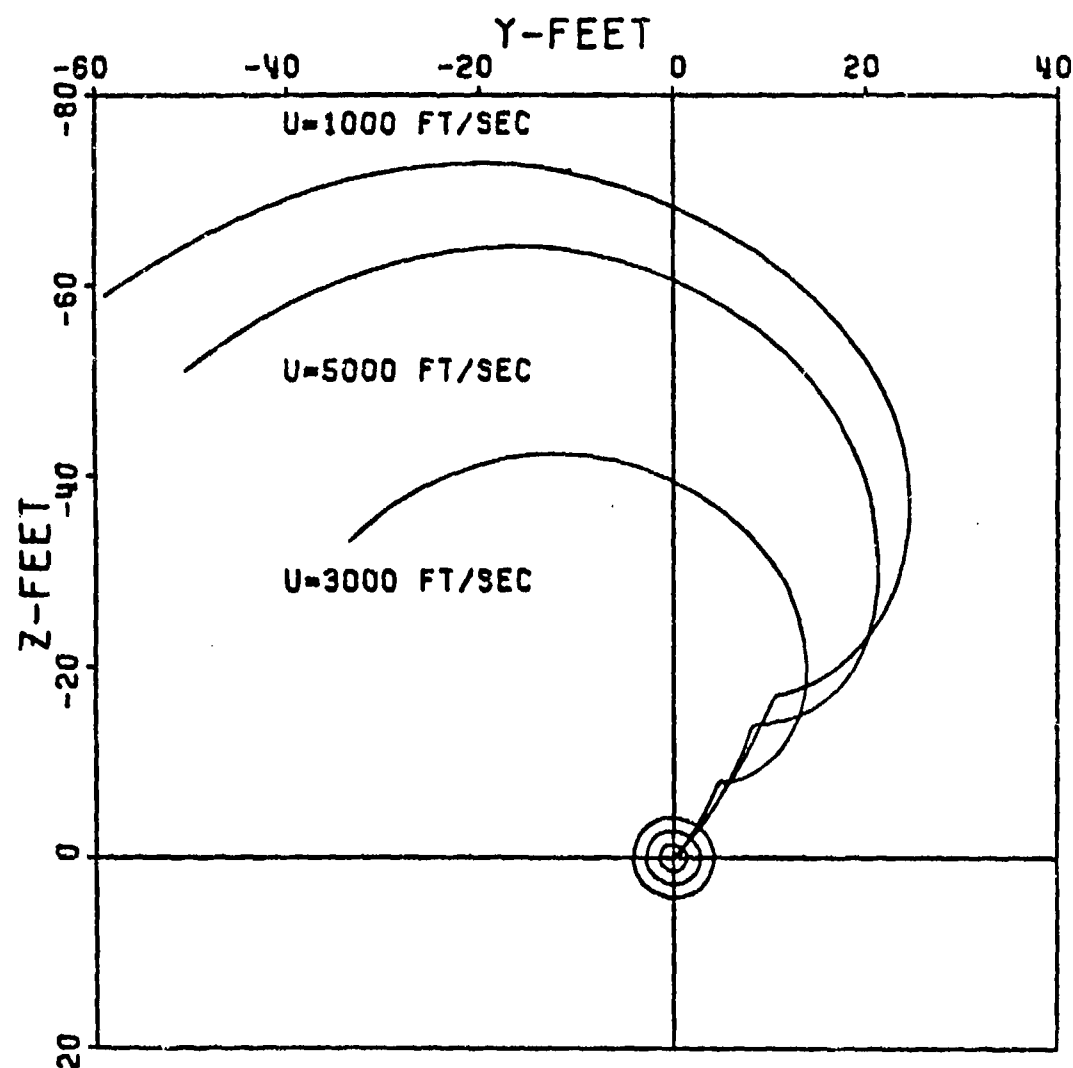


Figure 20. Dispersion: Phase III  
Theory, Cases 124-156

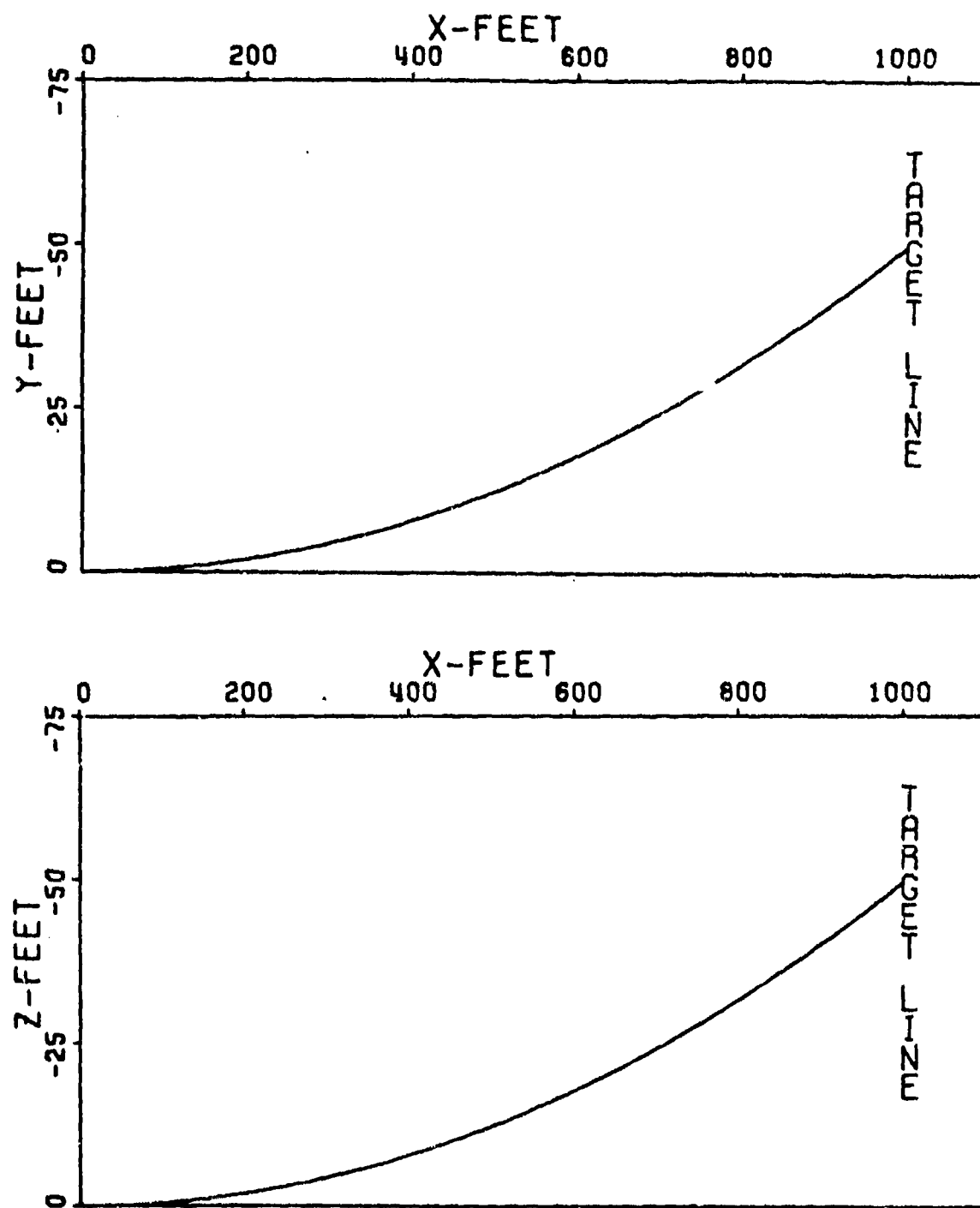


Figure 21. Trajectory, Case 134

TABLE 16. THEORY VALIDATION, ASYMMETRIES,  
CASES 157-167

C A S E	Initial Conditions					Coefficients			$\vec{J} \cdot \vec{A}$ . (mils)	
	$\vec{s}_0$	$\vec{\alpha}_0$	$\vec{\alpha}_0$	$p_0$	$u_0$	$C_{Z\alpha}$	$C_{Zp\beta}$	$C_{YE}$	6-D	Theory
						$C_{M\alpha}$		$C_{ZE}$		
						$C_{Mq} + C_{M\dot{\alpha}}$	$C_{Mp\beta}$	$C_{ME}$		
157	↑	↑	↑	31416	↑	↑	↑	↑	-1.799	-2.055
158	↑	↑	↑	18850	↑	↑	↑	↑	-2.236i	-2.087i
159	↑	↑	↑	6283	↑	↑	↑	↑	-1.873	-2.044
160	↑	↑	↑	500	↑	↑	↑	↑	-2.169i	-2.098i
161	↑	↑	↑	300	↑	↑	↑	↑	-1.924	-1.990
162	0	0	250+	100	5000	A1	A1	A1	-2.190i	-2.151i
163	↑	↑	250i	50	↑	↑	↑	↑	-1.049	-1.060
164	↑	↑	↑	25	↑	↑	↑	↑	-3.000i	-3.082i
165	↑	↑	↑	10	↑	↑	↑	↑	-0.419	-0.385
166	↑	↑	↑	5	↑	↑	↑	↑	-3.716i	-3.756i
167	↑	↑	↑	0	↑	↑	↑	↑	2.457-	2.602-
									6.836i	7.048i
									6.576-	6.707-
									14.075i	14.562i
									18.366-	19.077-
									27.827i	29.000i
									-9.690-	-10.283
									63.387	-65.283i
									-31.387	-32.445
									-62.730i	-64.426i
									-51.094	-52.500
									-51.094i	-52.500i

TABLE 17. THEORY VALIDATION, ASYMMETRIES,  
CASES 168-178

C A S E	Initial Conditions					Coefficients			$\vec{J.A.}$ (mils)	
						$CZ_\alpha$ $CM_\alpha$ $CM_q + CM_{\dot{\alpha}}$	$CZ_{p\beta}$ $CM_{p\beta}$	$C_{YE}$ $C_{ZE}$ $C_{ME}$ $C_{NE}$	6-D	Theory
	$\vec{s}_0$	$\vec{\alpha}_0$	$\vec{\dot{\alpha}}_0$	$p_0$	$u_0$					
168	↑	↑	↑	31416	↑	↑	↑	Unstable		
169	↑	↑	↑	18850	↑	↑	↑	-1.755 -2.154i	-1.957 -1.978i	
170	↑	↑	↑	6283	↑	↑	↑	-1.866 -2.054i	-1.936 -1.999i	
171	↑	↑	↑	500	↑	↑	↑	-1.572 -2.351i	-1.569 -2.366i	
172	↑	↑	↑	300	↑	↑	↑	-1.308 -2.595i	-1.304 -2.632i	
173	0	0	250+ 250i	100	3000	A1	A1	A1	-0.114 -3.912i	-0.024 -3.959i
174	↑	↑	↑	50	↑	↑	↑	↑	1.873- 6.399i	1.441- 6.134i
175	↑	↑	↑	25	↑	↑	↑	↑	3.755- 10.393i	3.751- 10.486i
176	↑	↑	↑	10	↑	↑	↑	↑	7.435- 34.530i	7.247- 34.867i
177	↑	↑	↑	5	↑	↑	↑	↑	-11.870 -44.054i	-12.144 -44.243i
178	↑	↑	↑	0	↑	↑	↑	↑	-35.054 -35.053i	-35.164 -35.164i



TABLE 18. THEORY VALIDATION, ASYMMETRIES,  
CASES 179-189

C A S E	Initial Conditions					Coefficients			$\vec{J.A.}$ (mils)	
						$CZ_\alpha$ $C_{M\alpha}$ $C_{M_q} + C_{M\dot{\alpha}}$	$CZ_{p\beta}$ $C_{M_{p\beta}}$	$C_{YE}$ $C_{ZE}$ $C_{ME}$ $C_{NE}$	6-D	Theory
	$\vec{s}_o$	$\vec{\alpha}_o$	$\vec{\dot{\alpha}}_o$	$p_o$	$u_o$					
179				31416					Unstable	
180				18850					Unstable	
181				6283					Unstable	
182				500					-5.015 -5.503i	-5.302 -5.769i
183				300					-4.884 -5.572i	-5.144 -5.925i
184	0	0	250+ 250i	100	1000	A1	A1	A1	-4.208 -6.135i	-4.366 -6.705i
185				50					-3.056 -7.031i	-3.191 -7.892i
186				25					-0.741 -9.079i	-0.841 -10.242i
187				10					5.244- 18.344i	4.637- 20.016i
188				5					18.563- 33.158i	18.976- 36.752i
189				0					-61.894 -61.894i	-63.990 -63.990i

Figures 22, 23 and 24 illustrate Cases 157-189. The curves are similar to those in Figures 7, 8 and 9 but are displaced by the  $\alpha_0$  contribution. Cases 168, 179, 180 and 181 indicate that maximum effects of the various parameters have been achieved in other stable cases. The effects of roll rate and velocity follow the same trends as those in Cases 58-90. Figure 25 shows the effects of velocity for Cases 157-189. Cases with  $U = 3000$  ft/sec exhibit the smallest dispersion. A sample trajectory, Case 189, is shown in Figure 26.

#### COMPARISON: HIGH, LOW, VERY SLOW ROLL RATE THEORIES

In Cases 58-189 the High, Low, and Very Slow Roll Rate Theories are validated for various initial conditions and parameters. The theories have been applied for certain ranges in roll rate and roll rate times time (pt). The range of pt, ( $pt \leq 1.0$ ) are governed by the inherent requirements of power series expansion. However, the ranges of p are arbitrary (to a certain extent) and are based on accuracy of the theories themselves. Each theory approximates the solution very well for a certain range of p and then begins to diverge and become inaccurate. The range of p for which the very slow roll rate theory is accurate is fairly well cut and dried;  $p < 0$ ,  $pt < 1.0$ . For any  $pt < 1.0$  we must now use the low roll rate theory. The question now arises, how high a roll rate can this theory accommodate? At what value of p must we change to the high roll rate theory? These questions are answered by a plot of sample 6-D computations, Figure 27, and all three theories extended beyond the limits used in the previous validation. The high roll rate theory is a straight line going off to infinity as p goes to zero. Although the length of the curve in which it is an effective theory is short graphically, the range of roll rates it encompasses is tremendous. Figure 28 illustrates the effective limits of each theory; that is, on the spectrum of possible roll rates it shows where each theory is the most effective. The low roll rate theory handles the largest graphical area but only roll rates less than 100 rad/sec and greater than 5 rad/sec. The upper limit of 100 rad/sec was chosen since here the low roll theory attaches itself to the 6-D results while the high roll theory diverges. The lower limit of 5 rad/sec corresponds to  $pt < 1.0$ . Figures 27 and 28 depict Cases 58-68 where  $u_0 = 5000$  ft/sec or  $t = 0.2$  sec. Therefore  $p = 5$  rad/sec corresponds to  $pt = 1.0$ . The very low roll rate theory has the smallest range but is essential in predicting dispersion as the roll rate goes to zero. As  $pt > 1$ , the theory diverges as would be expected from a power series; Equation 29. The sharp turn occurs at  $p \approx 20$  rad/sec or  $pt \approx 4$  for Cases 58-68. Although Cases 58-68 were illustrated here, this analysis of the effective limits of the roll theories was found to be similar for all other cases. For the  $u = 3000$  ft/sec cases the low roll theory limits were  $3.0 < p < 50$  for  $u_0 = 1000$  ft/sec cases:  $1.0 < p < 25.0$ .

#### PHASE IV

To validate the effects of gravity on dispersion, a final set of cases were run using the high roll rate theory, Equation 24. Ordinarily, one

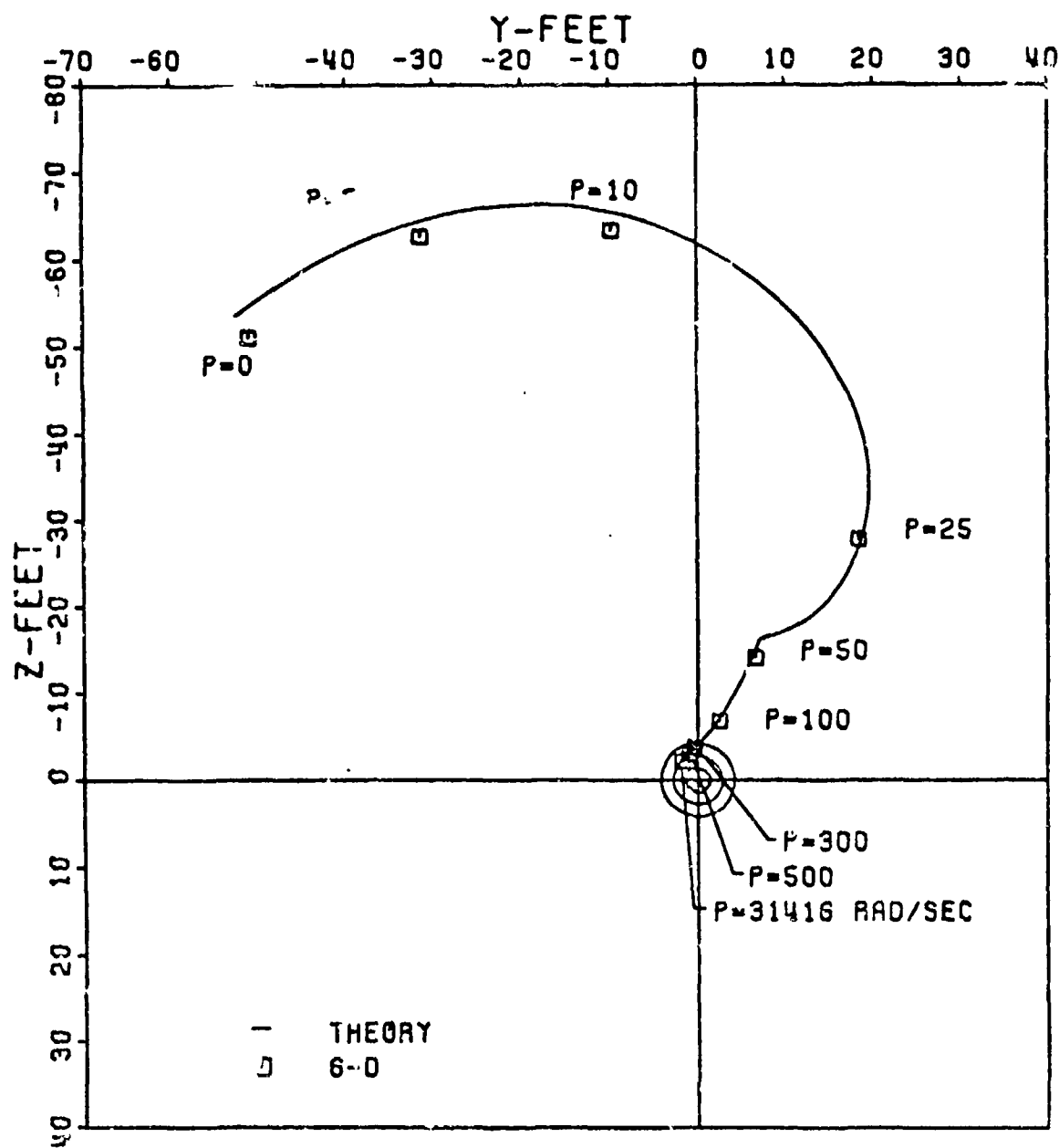


Figure 22. Dispersion: Phase III  
Cases 157-167

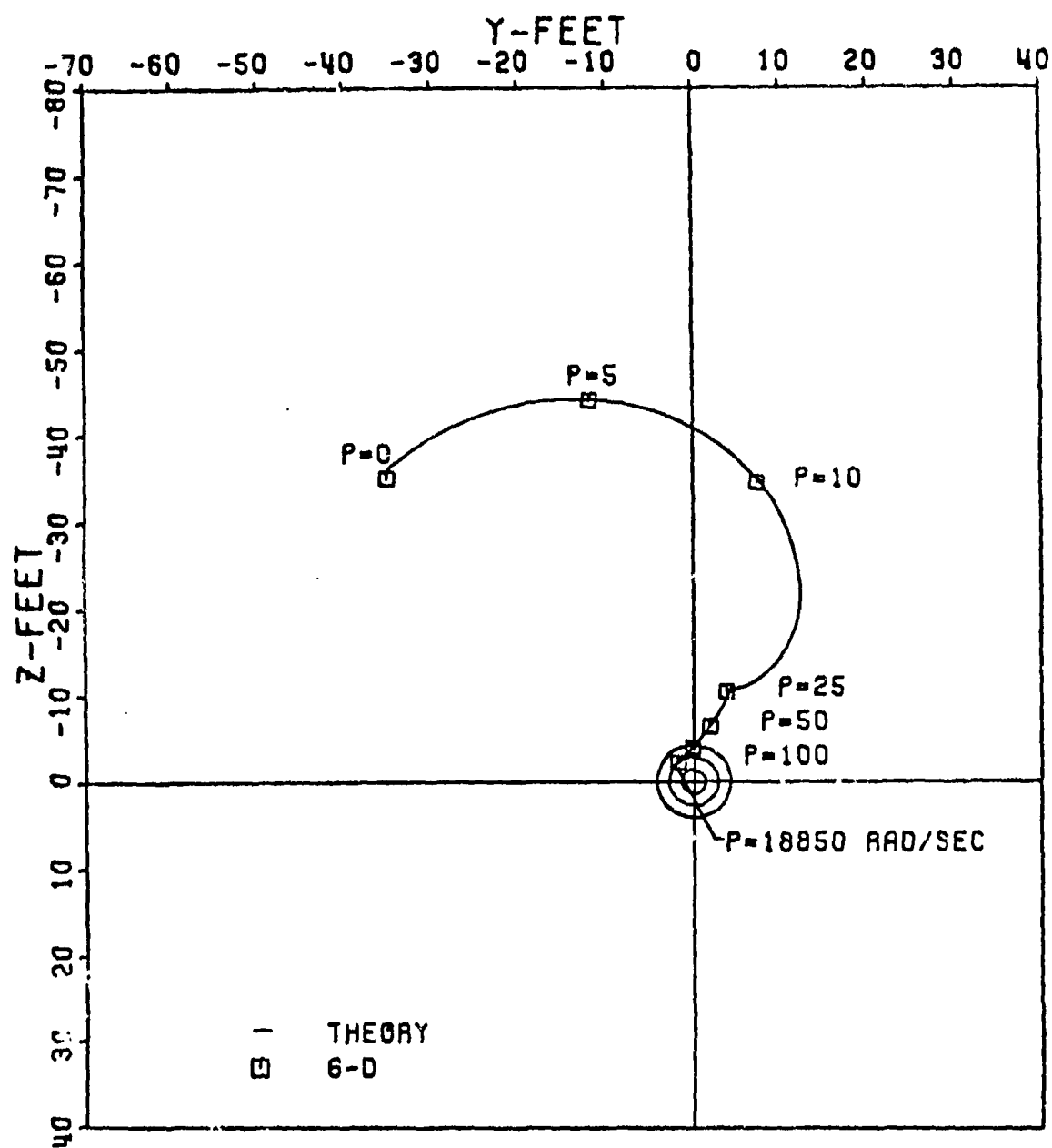


Figure 23. Dispersion: Phase III  
Cases 168-178

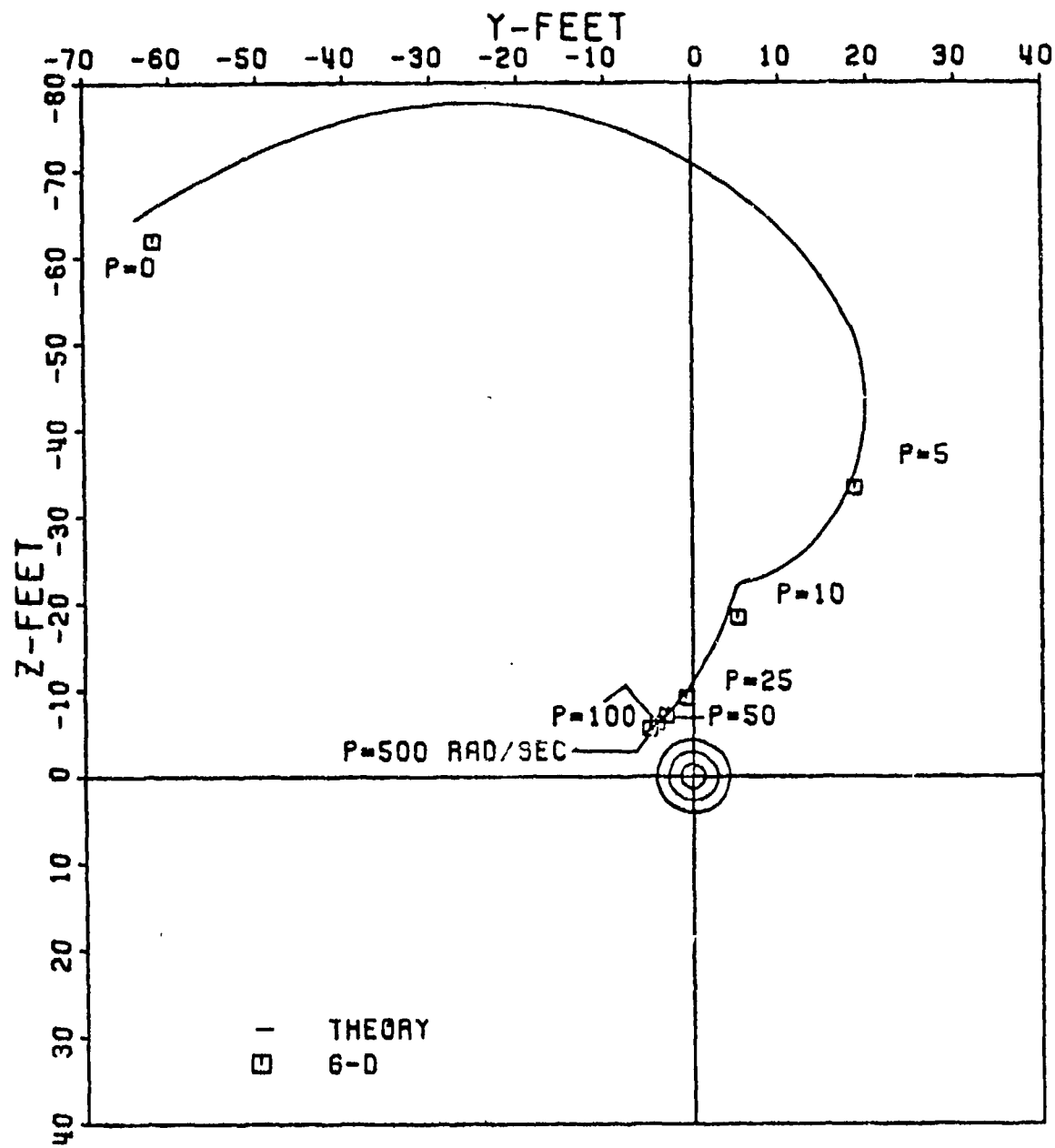


Figure 24. Dispersion: Phase III  
Cases 179-189

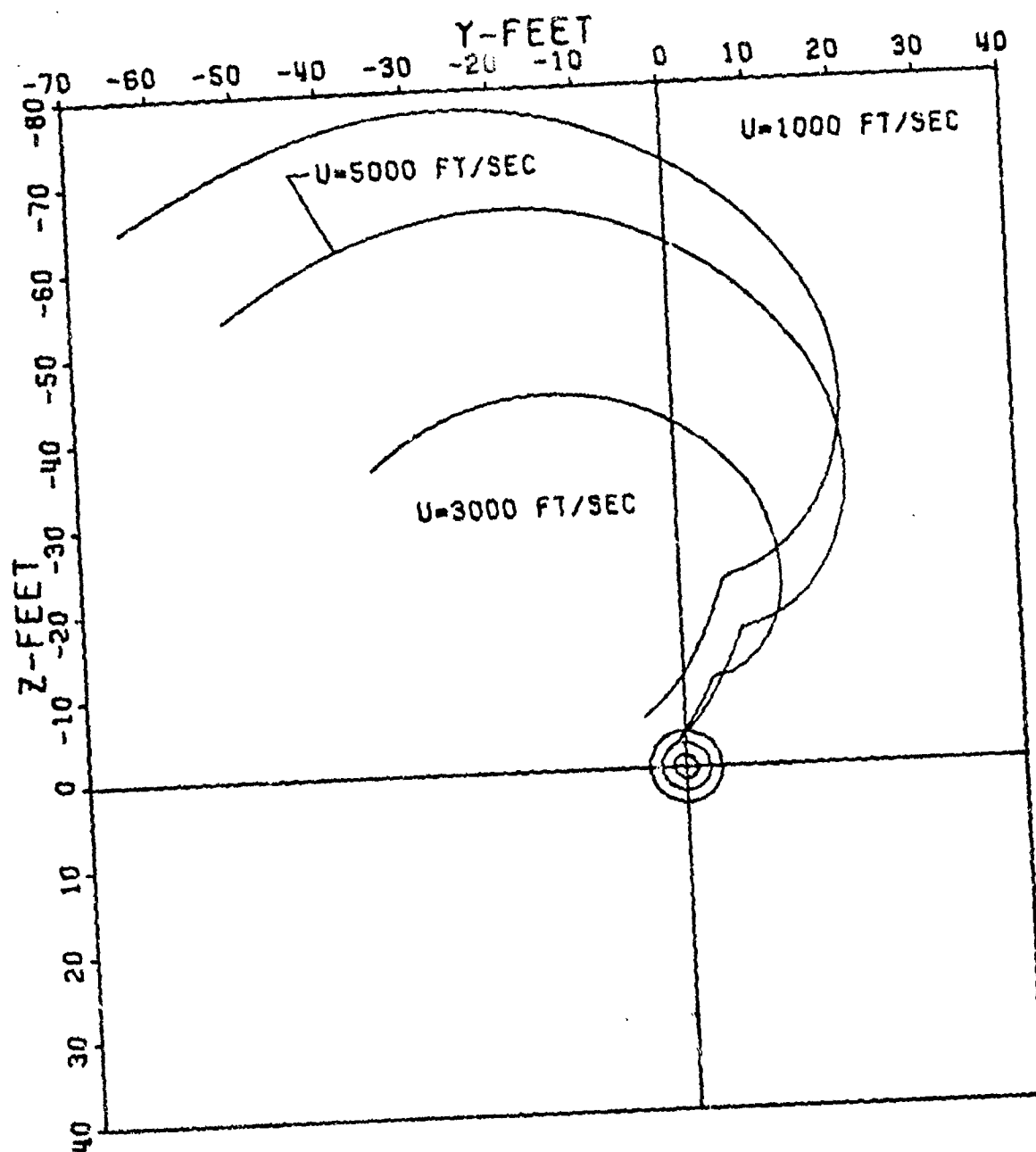


Figure 25. Dispersion: Phase III  
Theory, Cases 157-189

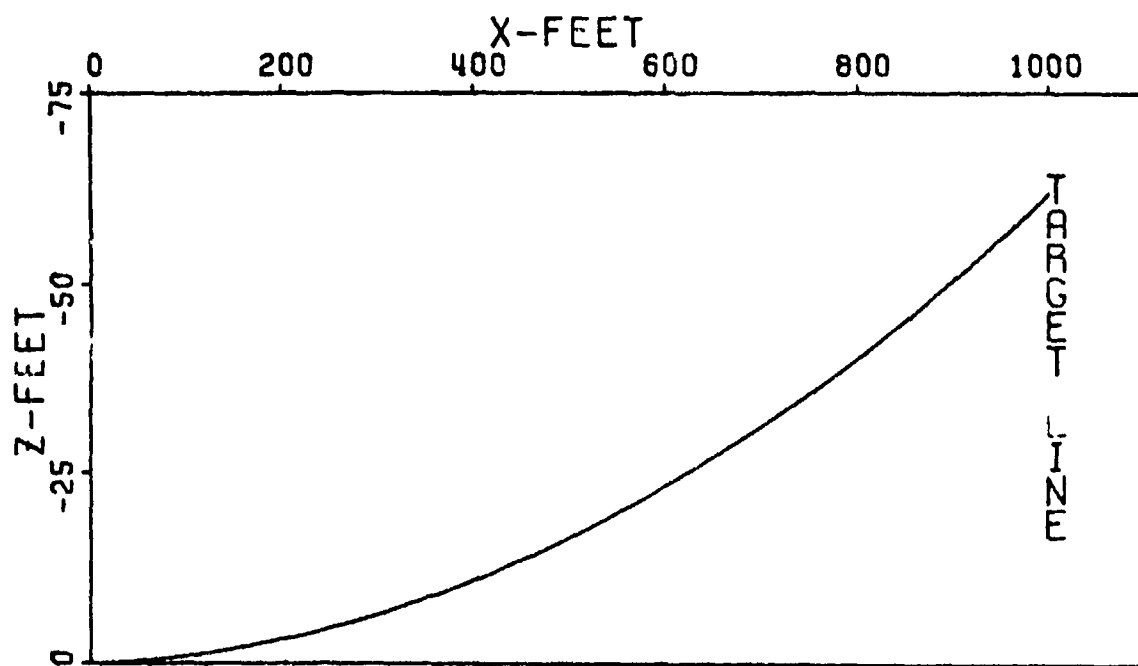
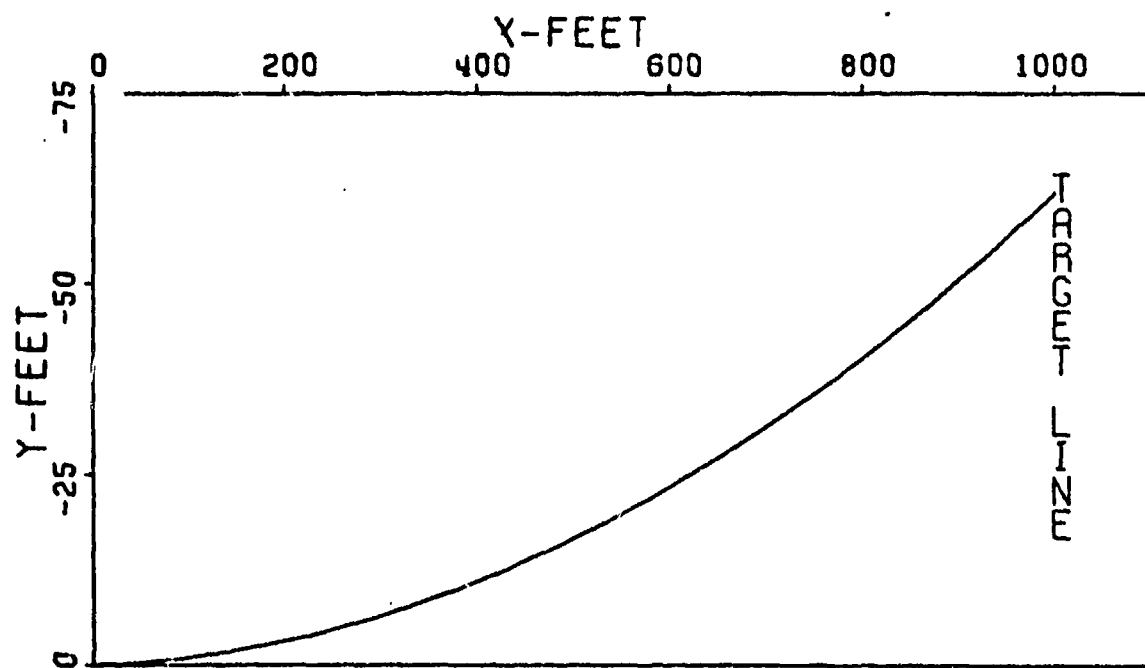


Figure 26. Trajectory, Case 189

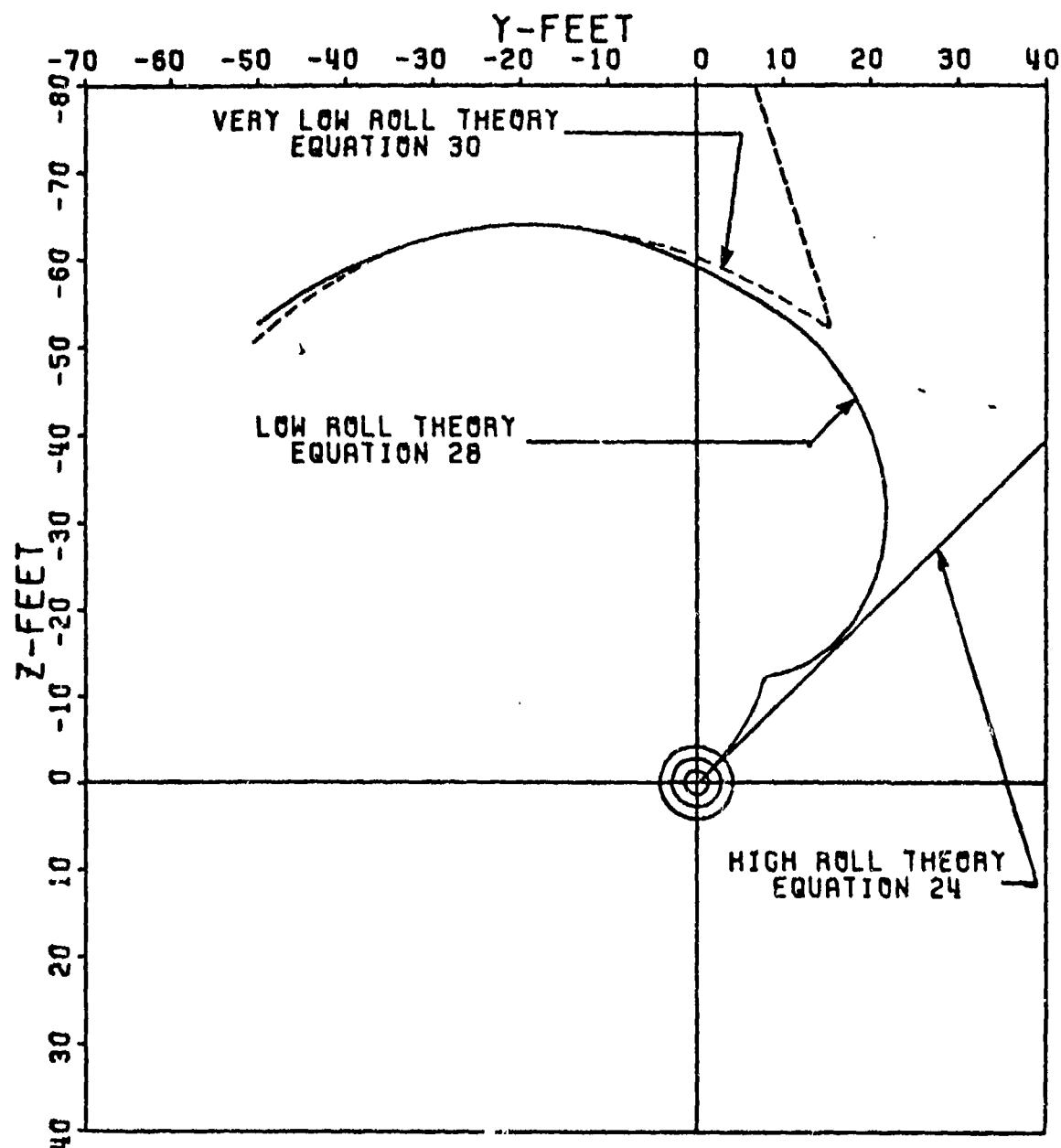


Figure 27. Phase III Theory;  
Equations 24, 28, 30



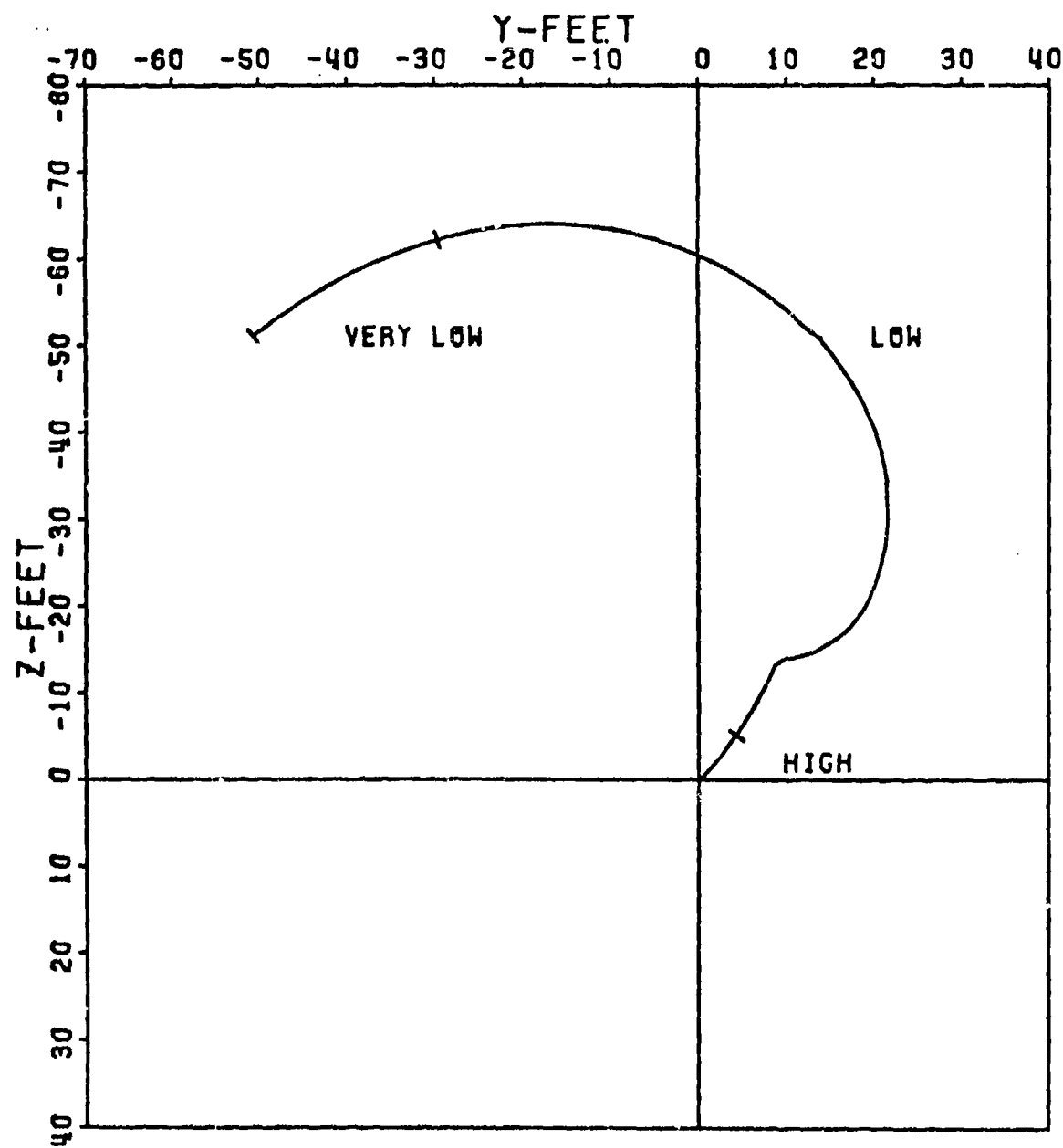


Figure 28. Phase III Theory  
Effective Limits

would think that gravity would only introduce a constant term; one that could be factored out. However integration of the equations of motion produce a gravity term dependent upon roll rate. Determination of its validity and consequence is what is important here.  $\vec{S}_0, \vec{\alpha}_0$ , and  $\vec{\alpha}_0$  were set to zero in order to allow determination of the effects due to roll rate and velocity. The reduced governing equation becomes:

$$\vec{J} \cdot \vec{A} = \frac{ig}{2} \left( \frac{x}{u^2} \right) \left[ 1 + \frac{ipl_x}{mud} A \right] 1000$$

No aerodynamic asymmetries were present and the effects of gravity were assumed independent of effects due to  $\vec{S}_0, \vec{\alpha}_0, \vec{\alpha}_0$ ; a logical assumption. Table 19 lists the results.

Table 19 indicates that the effects due to gravity occur largely in the vertical plane, as would be expected. The transverse contribution is minimal but is affected by both velocity and roll rate. The vertical contribution is only affected by velocity. The unstable cases indicate maximum use of magnus and thus maximum traverse effects on dispersion. It can be concluded from this brief but thorough treatment that gravity effects dispersion only in the vertical plane (for all practical purposes) and that its contribution is constant with

velocity. The roll dependent term,  $\frac{ipl_x}{mud} A$ , has been shown to exist but become negligible for the flechette. This term would possibly become important for projectile dispersion and other missile applications. Projectile motion with gravity is typified by a cocking right or left of the projectile in flight with a positive  $C_{M_{\alpha}}$  but negative  $C_{z_{\alpha}}$ ; the parameter A would become

negative and the entire roll dependent term, positive; that is, cocked to the right, dispersion to the right. For a finned missile the opposite would occur due to the agreement in sign between  $C_{M_{\alpha}}$   $C_{z_{\alpha}}$ .

TABLE 19. THEORY VALIDATION, GRAVITY  
CASES 190-201

C A S E	Initial Conditions					Coefficients			$\vec{J.A.}$ (mils)	
						$CZ_{\alpha}$ $CM_{\alpha}$ $CM_q + CM_{\dot{\alpha}}$	$CZ_{p\beta}$ $CM_{p\beta}$	$C_{YE}$ $C_{ZE}$ $C_{ME}$ $C_{NE}$	6-D	Theory
	$\vec{s}_0$	$\vec{\alpha}_0$	$\vec{\dot{\alpha}}_0$	$p_0$	$u_0$					
190	0	0	0	31416	5000	A1	A1	0	-0.001 +0.644i	-0.001 +0.644i
191				18850					-0.001 +0.644i	-0.001 +0.644i
192				6283					-0.001 +0.644i	-0.001 +0.644i
193				0					0.000 +0.644i	0.000 +0.644i
194				31416	3000				-0.002 +1.788i	-0.003 +1.789i
195				18850					-0.001 +1.789i	-0.002 +1.789i
196				6283					0.000 +1.788i	-0.001 +1.789i
197				0					0.000 +1.788i	0.000 +1.789i
198				31416	1000				Unstable	
199				18850					Unstable	
200				6283					0.001+ 16.100i	0.001+ 16.100i
201				0					0.000+ 16.100i	0.000+ 16.100i

## SECTION IV

### FREE FLIGHT DATA ANALYSIS

In order to analyze actual test firings as to jump and dispersion and correlate them with the validated theory, the initial conditions of each test firing must be obtained and put into the proper form. To obtain raw experimental data, test firings were conducted by the U.S. Army, Frankford Arsenal. The configuration tested was the Producibility Ground Point Flechette, Figure 29. The raw data required was both translational and angular; that is, data was needed to determine position as a function of time and angle of attack of the flechette as a function of time. To accomplish this, Frankford Arsenal devised the test apparatus shown in Figure 30. The gun barrel was mounted on a steel girder to eliminate "barrel whip" due to recoil and boresighted on a target 50 meters down range. At positions, 1, 3, 5, 7, 9, and 11 feet downrange, dual high speed cameras were placed to photograph the flechette as it passed its station. One camera was placed to allow a top view at each station and provide a means of obtaining swerve and yaw data. The other camera allowed a side view at each station to obtain heave and pitch data. At each station reference marks oriented the flechette as to its exact position downrange. This was to allow for any camera timing error and/or variation in muzzle velocity.

From the battery of testing firings, eight separate rounds were chosen at random to be analyzed. The eight rounds along with velocity, roll rates and target positions are given in Table 20.

Raw translational and angular data are shown in Figures 31 through 46. The figures illustrate the position and complex angle of attack of the flechette for each station.

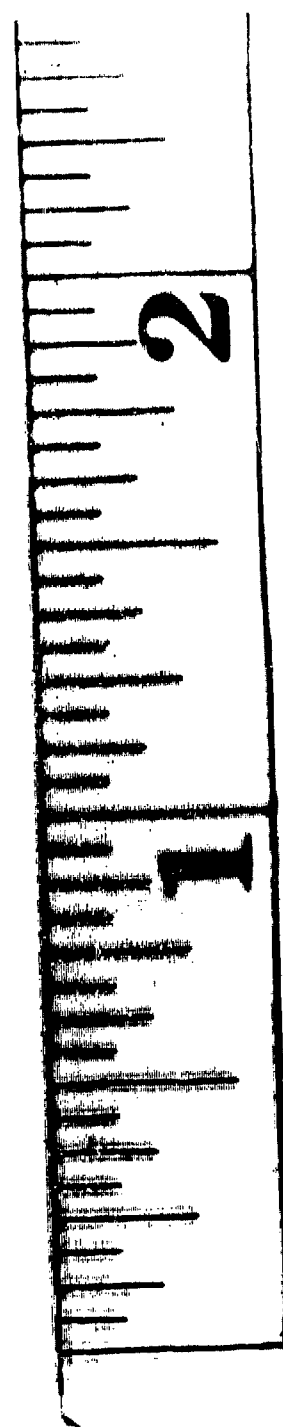
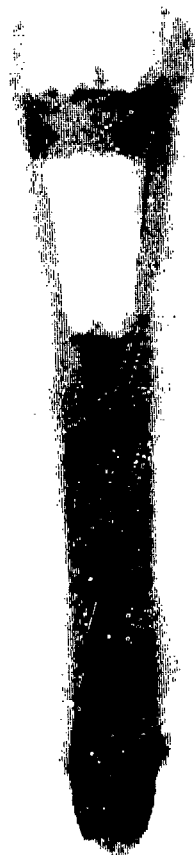


Figure 29. Ground Point Flechette, With and Without Sabot

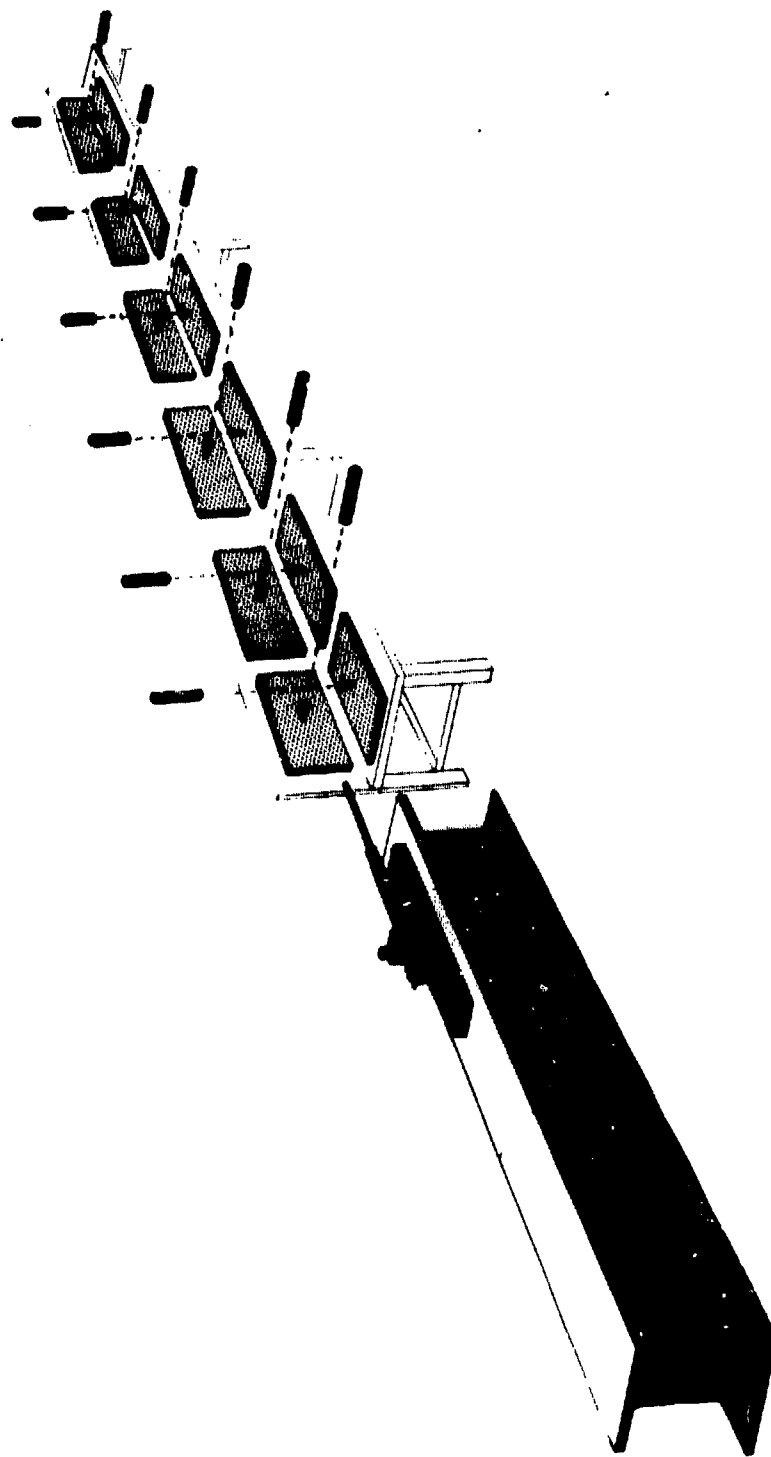


Figure 30. Free Flight Test Apparatus and Setup

TABLE 20. FRANKFORD TEST FIRING DATA

R O U N D	$u_0$	$p_0$	Target at 50 ft	
			Y (ft)	iZ (ft)
4	4747	11,454	0.117	-0.038
6	4662	13,201	0.053	-0.010
7	4642	14,219	0.141	-0.004
8	4662	13,000	0.053	0.099
14	4758	13,289	0.053	0.016
16	4753	17,354	0.084	-0.004
17	4677	16,613	0.070	-0.019
19	4679	11,913	0.089	0.059

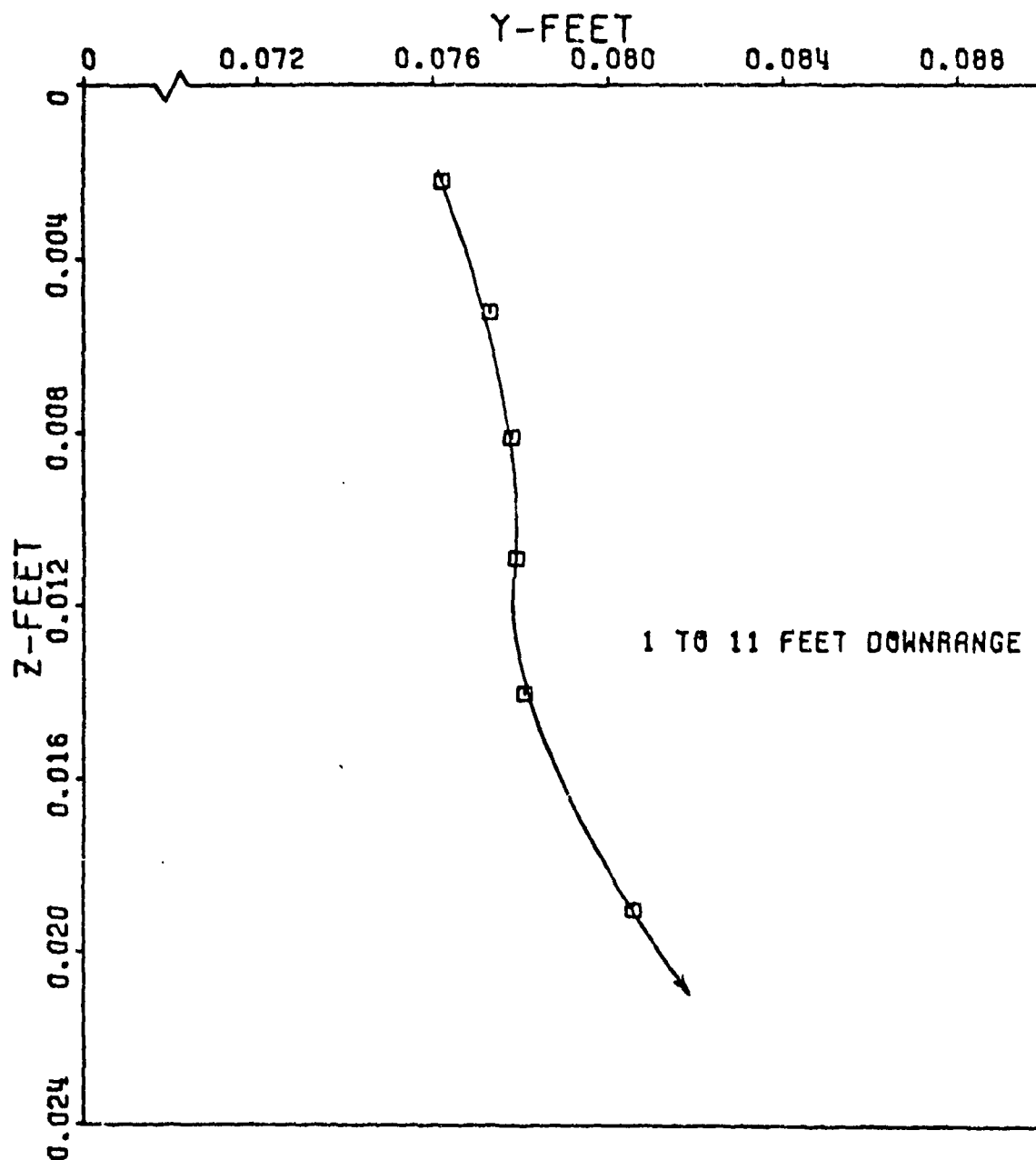


Figure 31. Raw Translational Data  
Ground Point Round 4



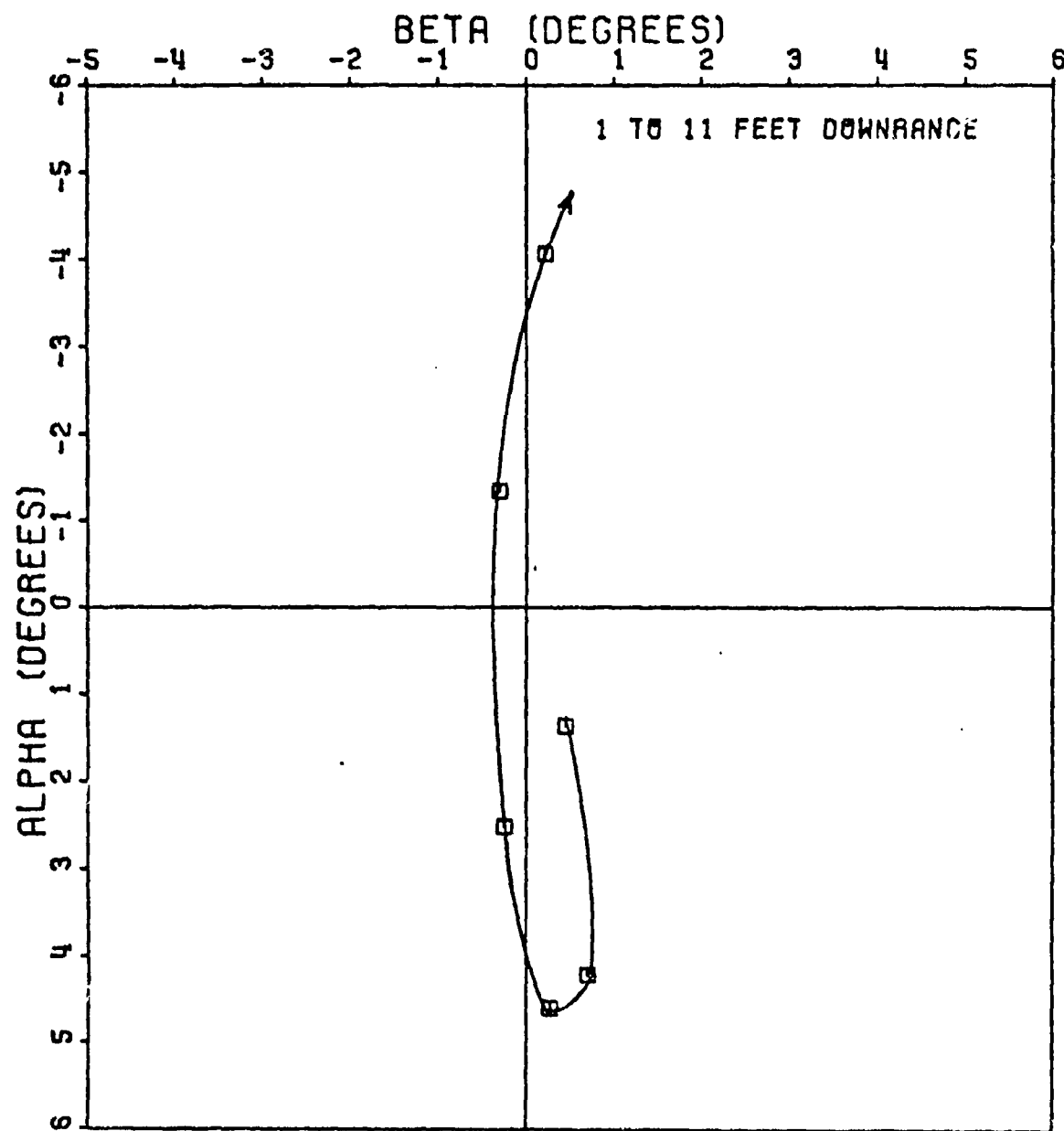


Figure 32. Raw Angular Data  
Ground Point Round 4

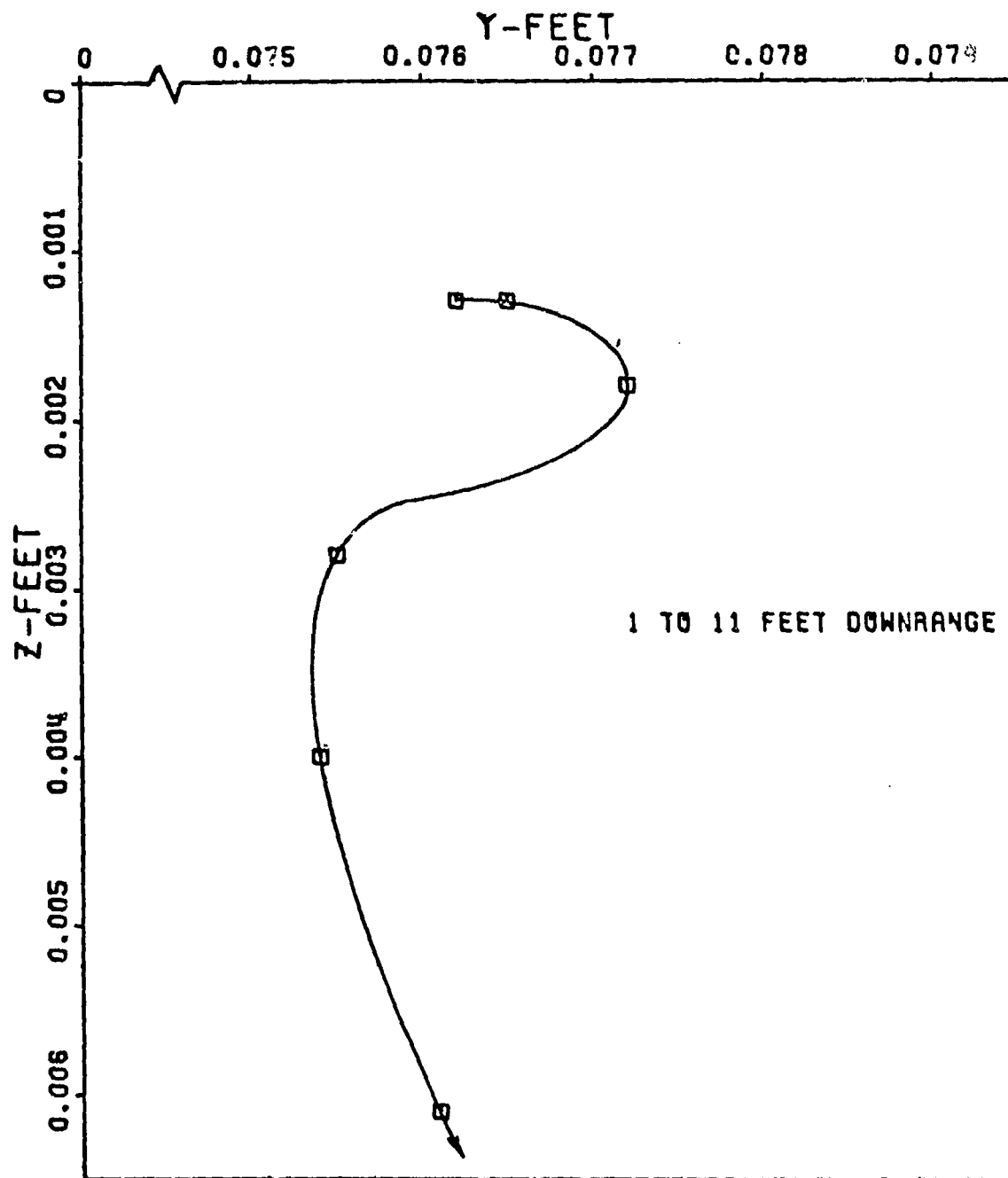


Figure 33. Raw Translational Data  
Ground Point Round 6

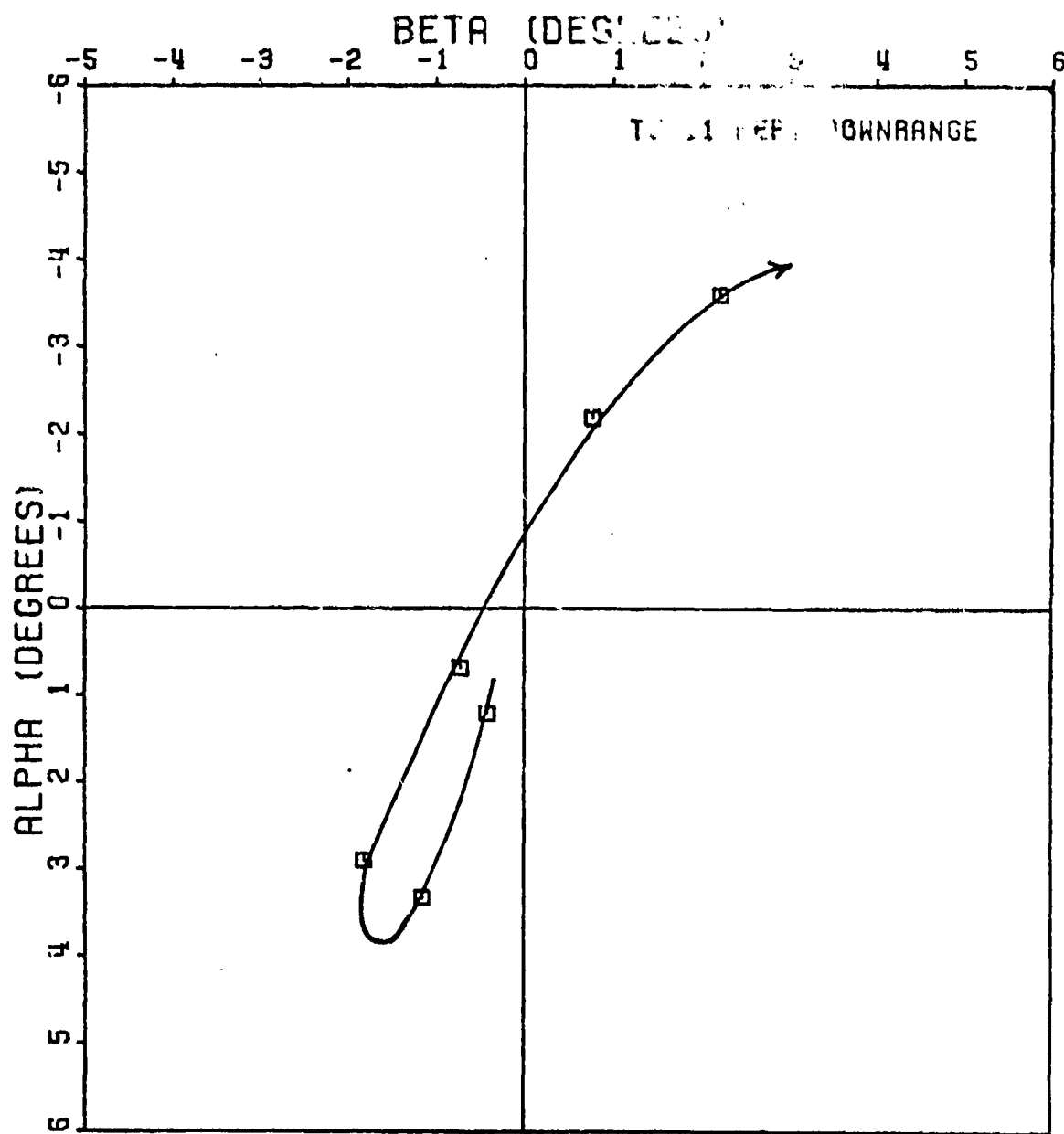


Figure 34. Raw Angular Data  
Ground Point Round 6

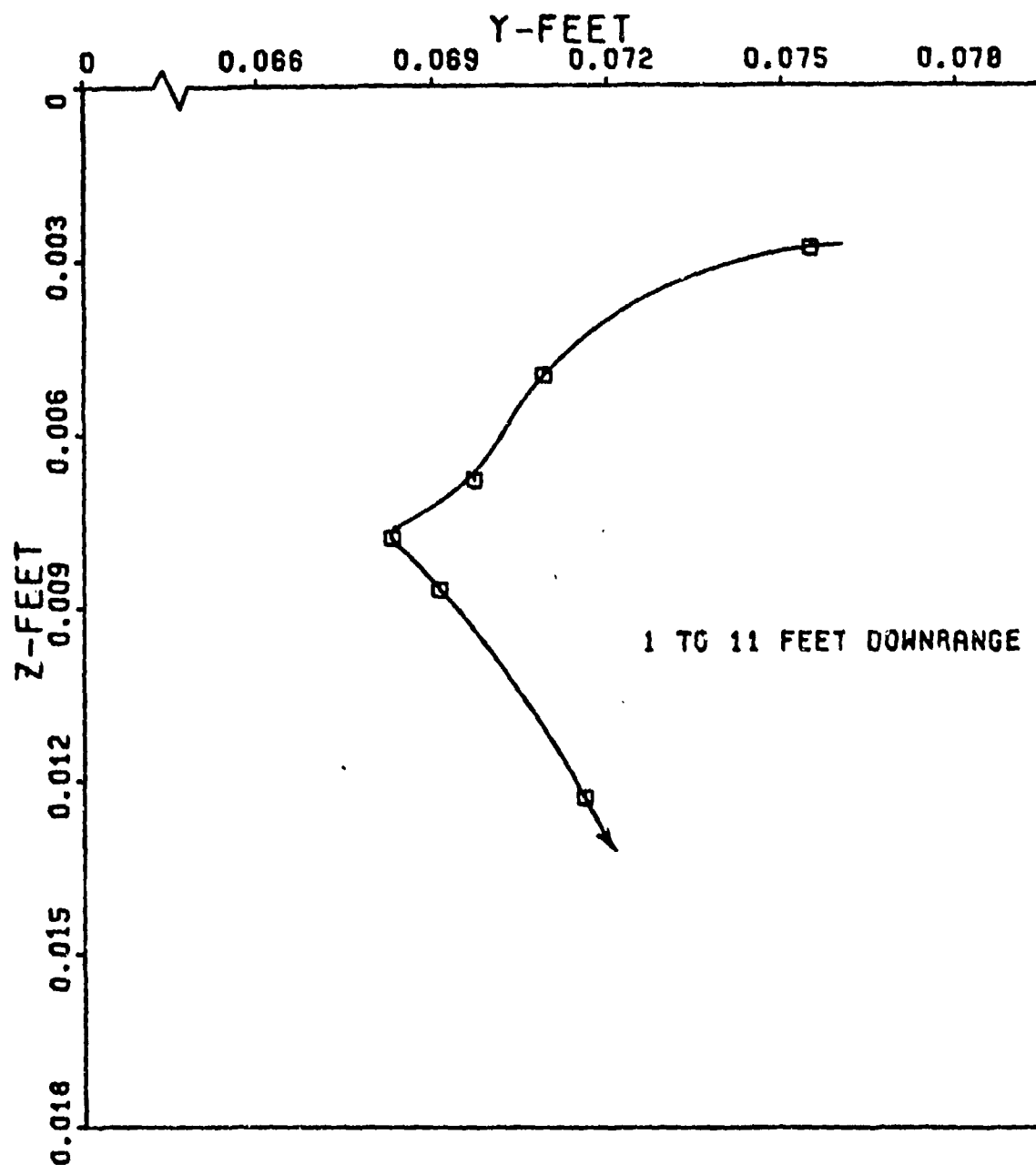


Figure 35. Raw Translational Data  
Ground Point Round 7

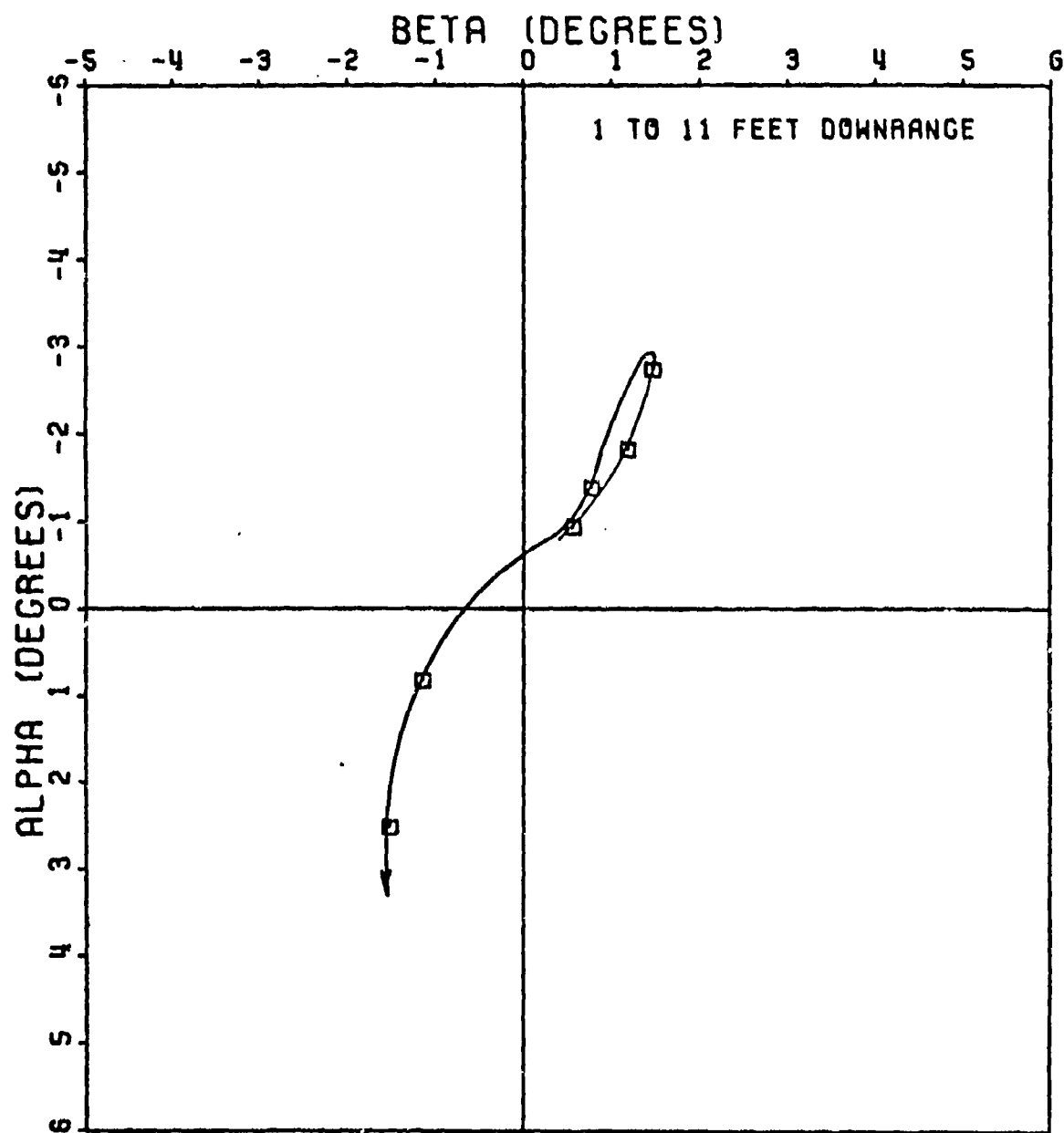


Figure 36. Raw Angular Data  
Ground Point Round 7

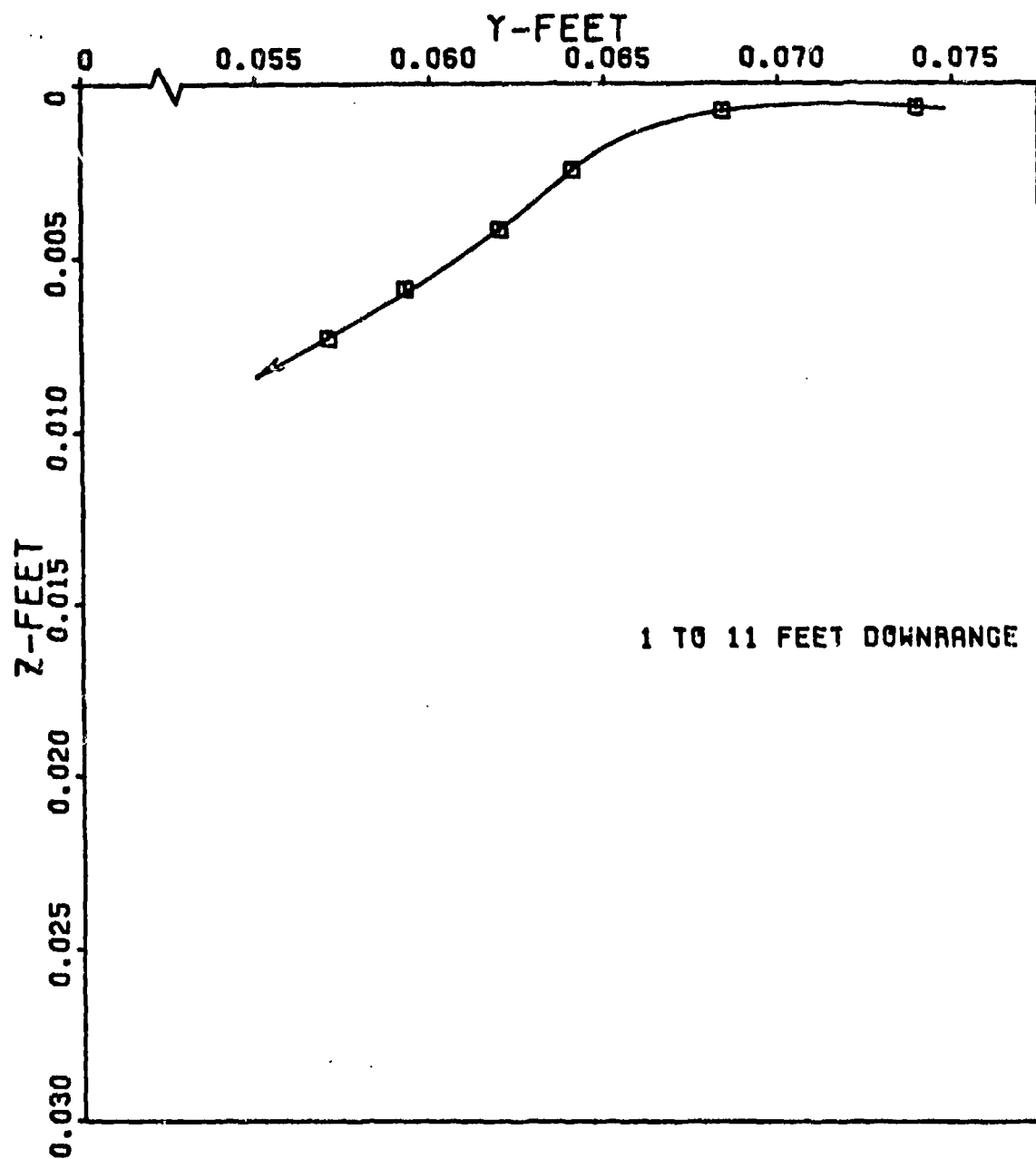


Figure 37. Raw Translational Data  
Ground Point Round 8

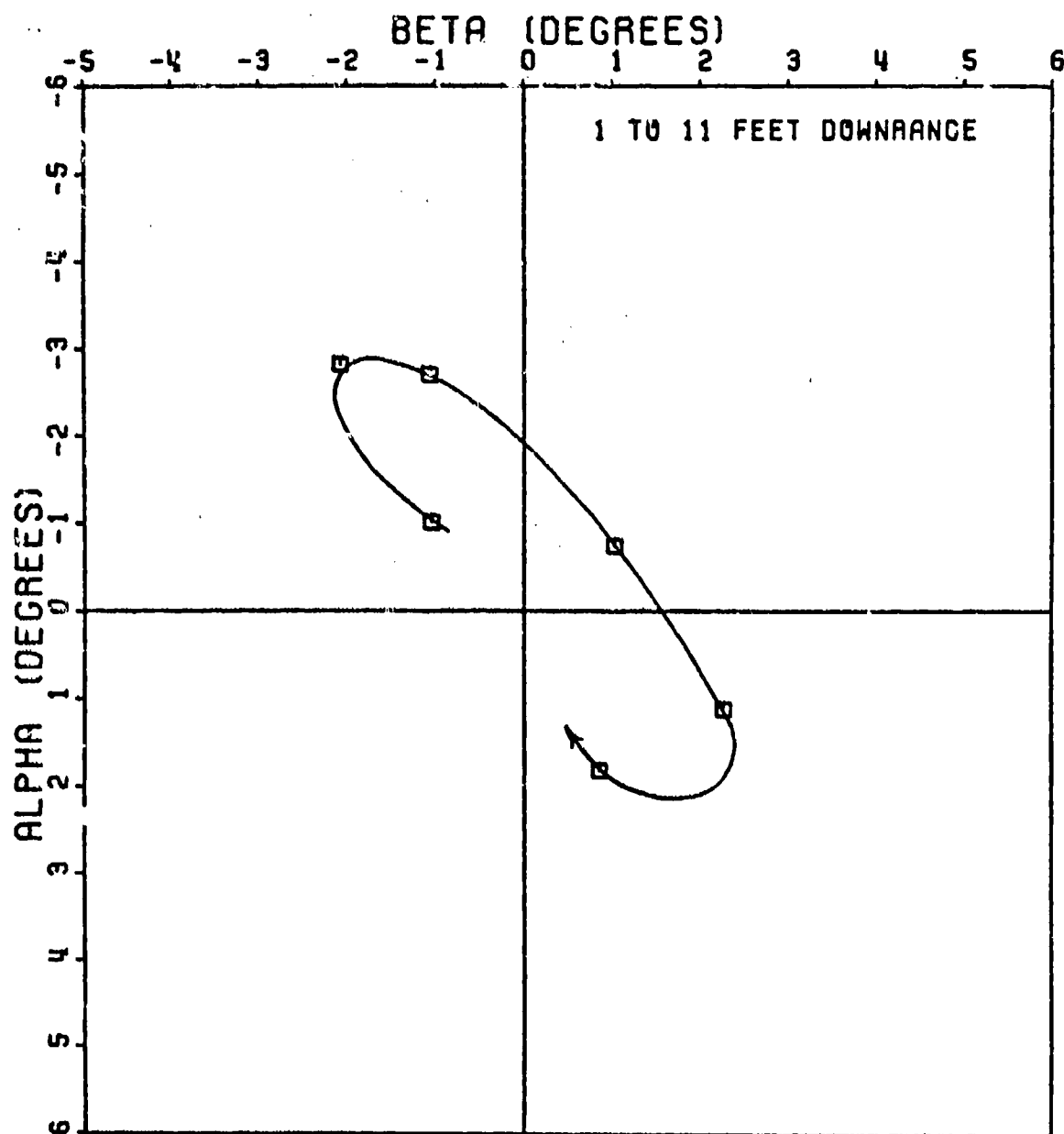


Figure 38. Raw Angular Data  
Ground Point Round 8

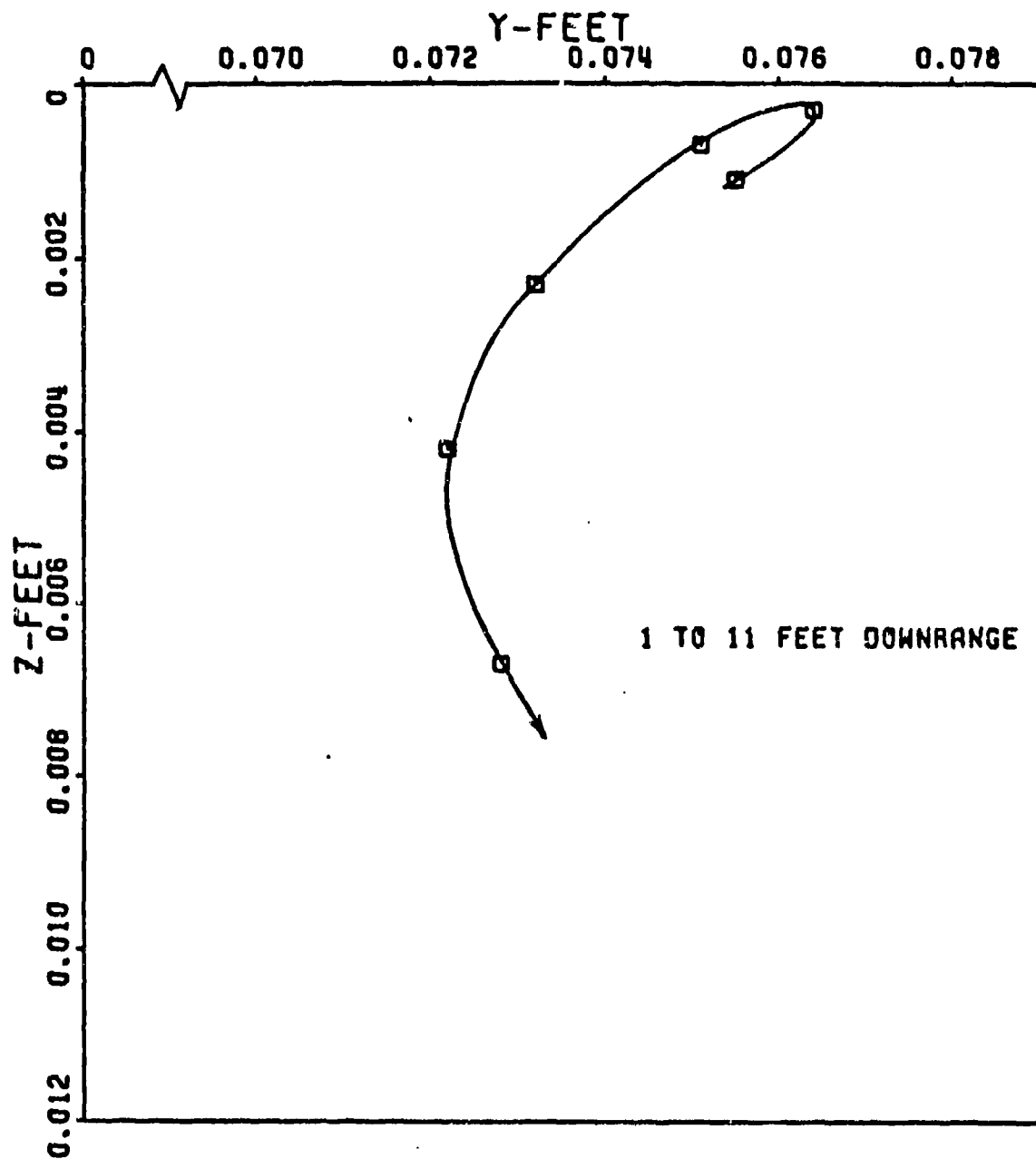


Figure 39. Raw Translational Data  
Ground Point Round 14



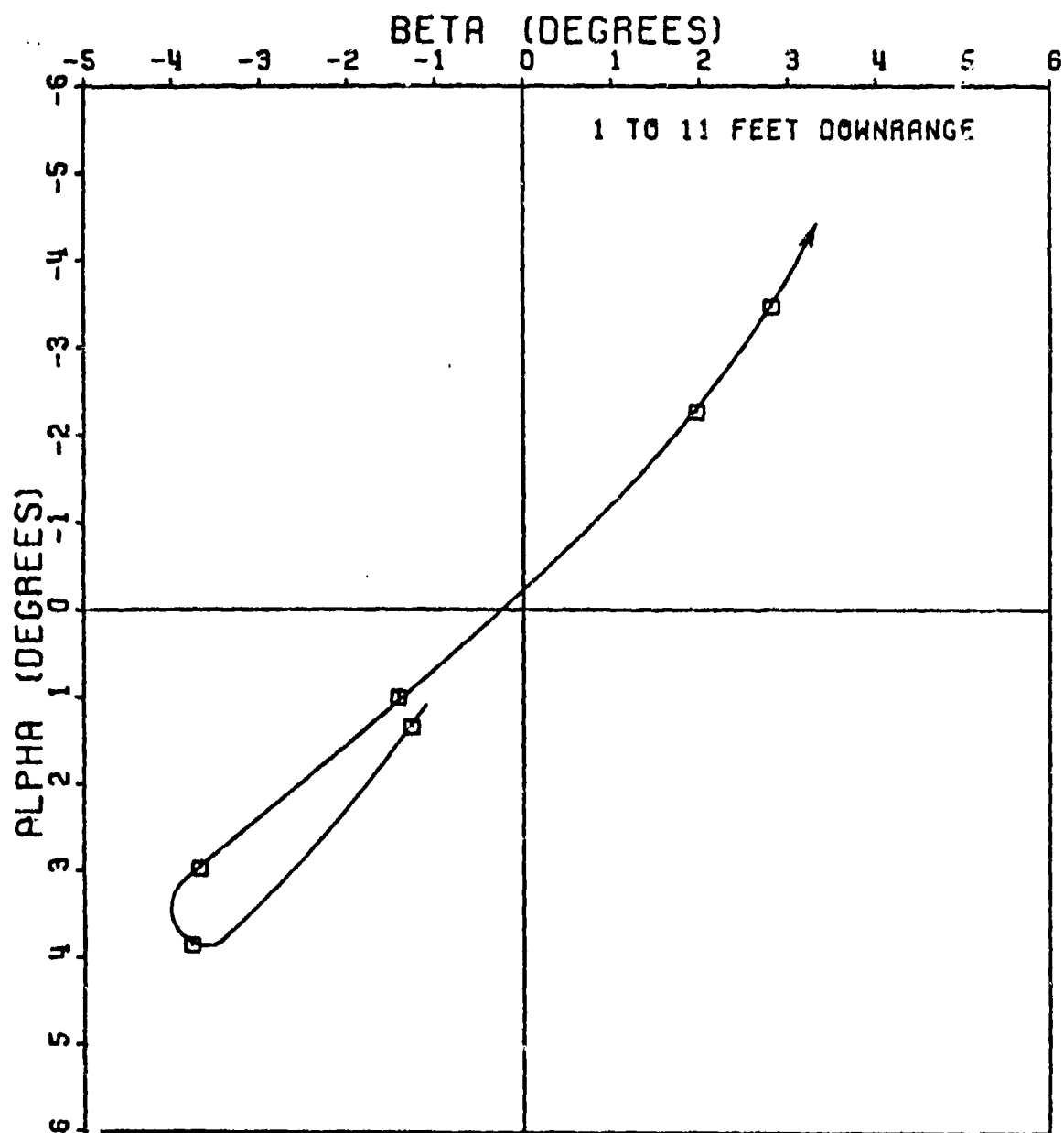


Figure 40. Raw Angular Data  
Ground Point Round 14

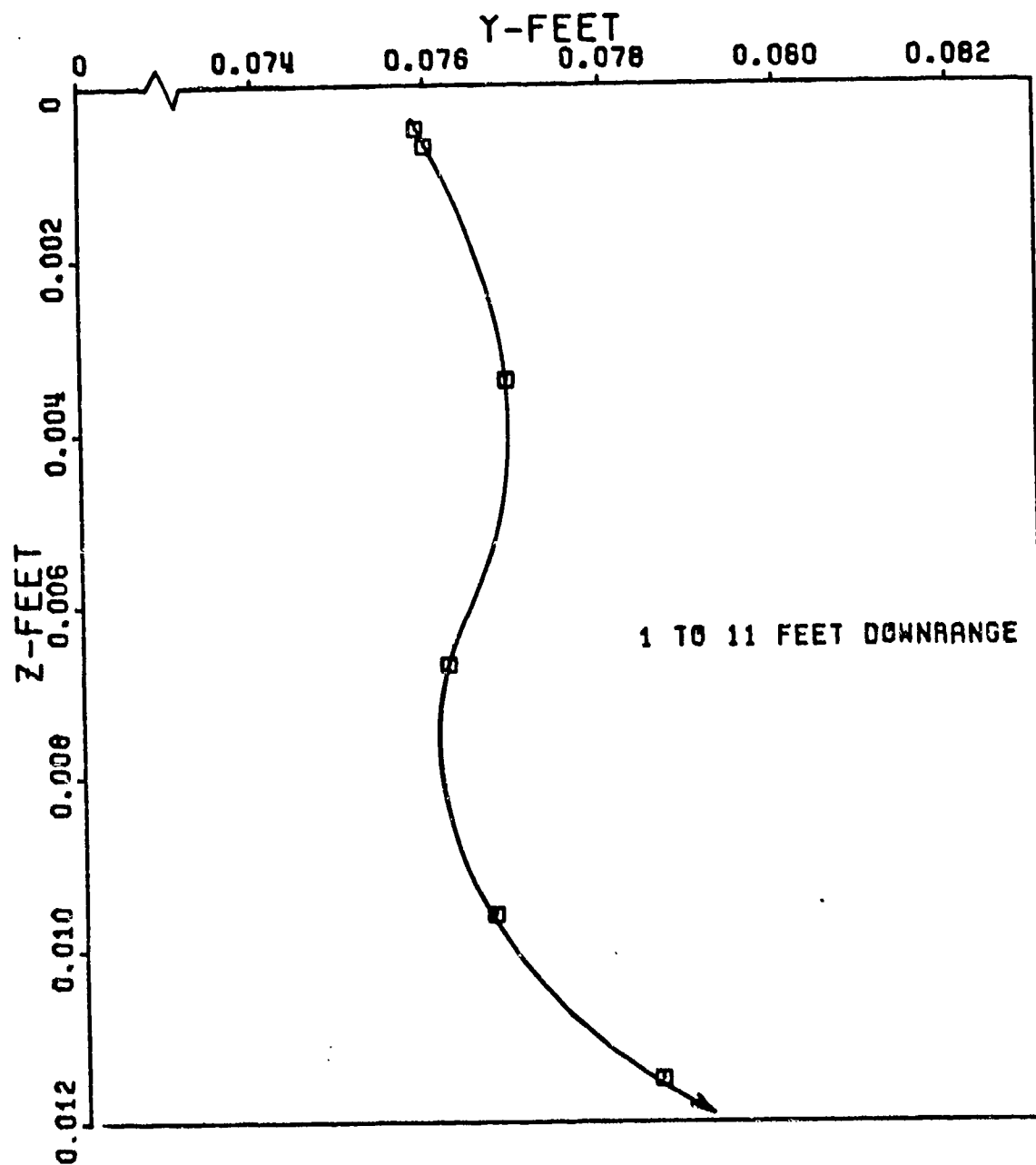


Figure 41. Raw Translational Data  
Ground Point Round 16

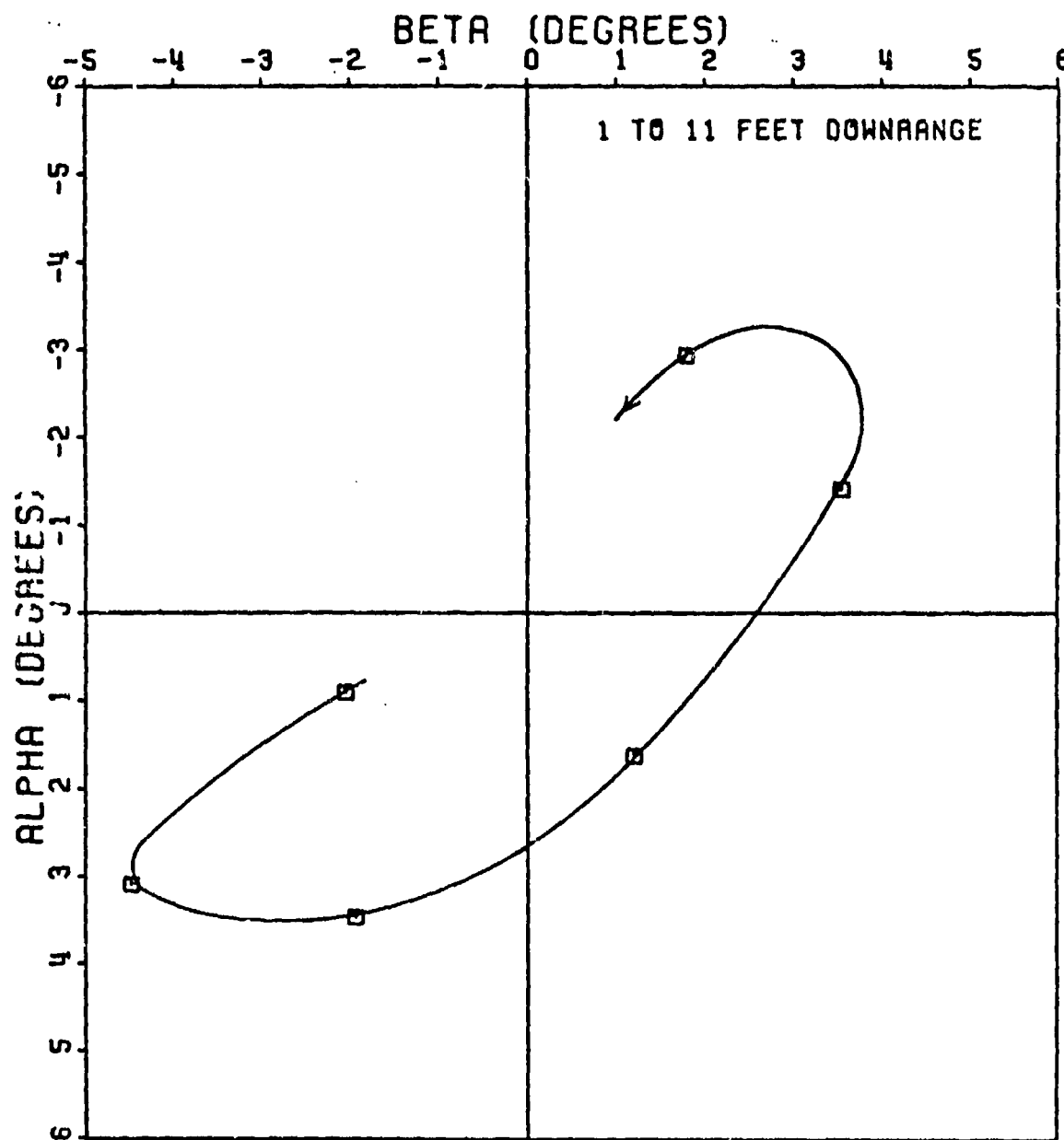


Figure 42. Raw Angular Data  
Ground Point Round 16

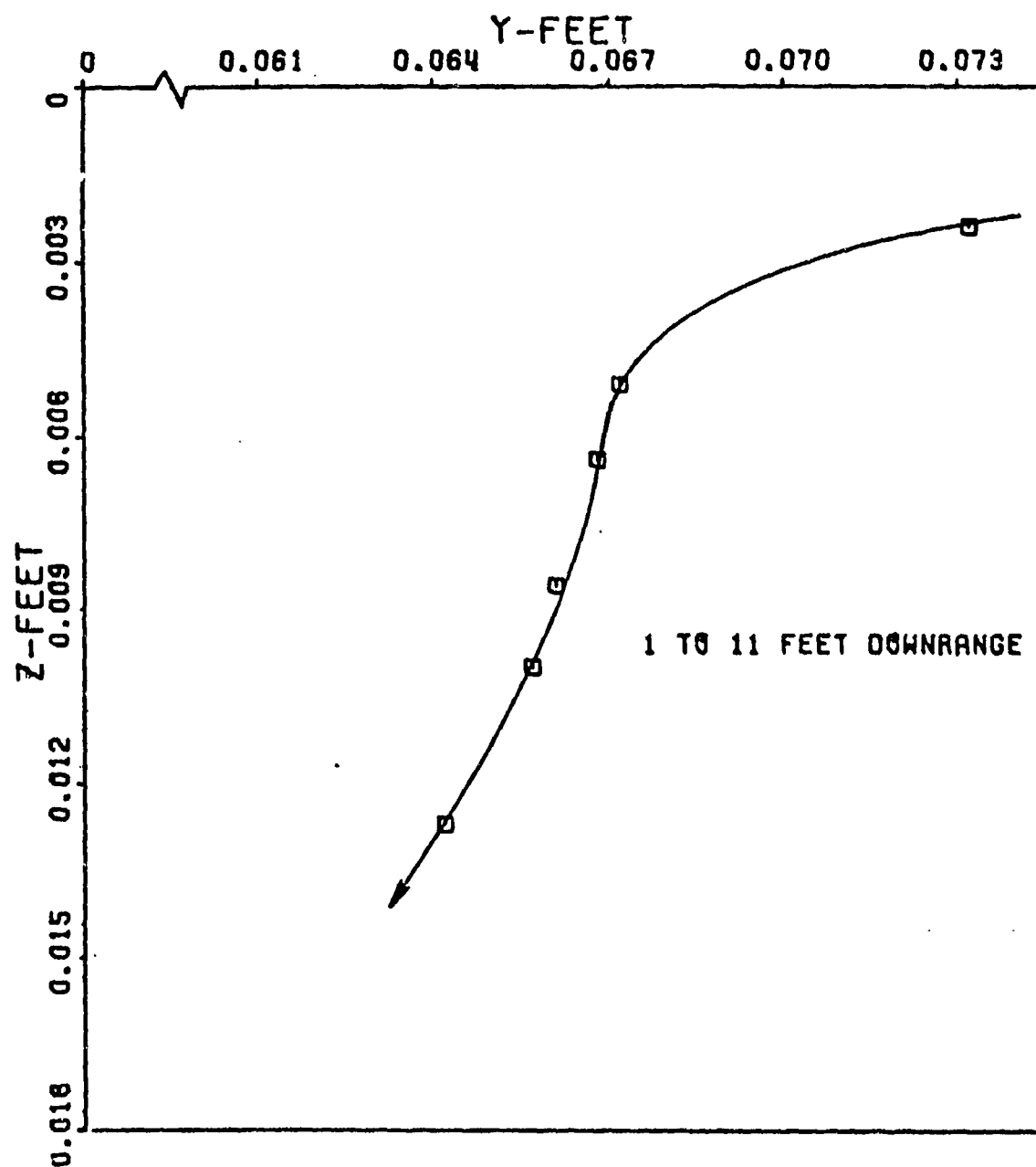


Figure 43. Raw Translational Data  
Ground Point Round 17

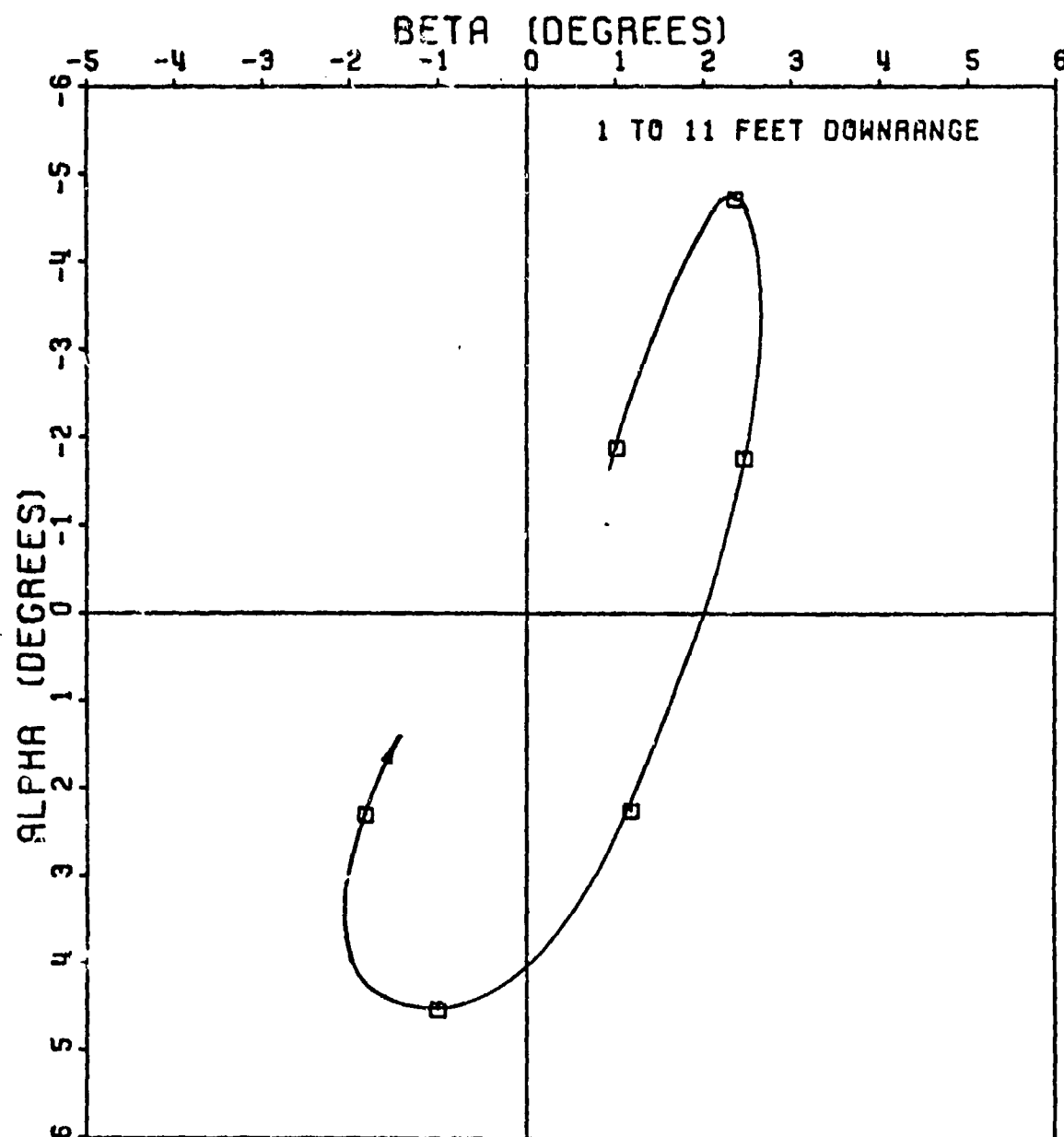


Figure 44. Raw Angular Data  
Ground Point Round 17

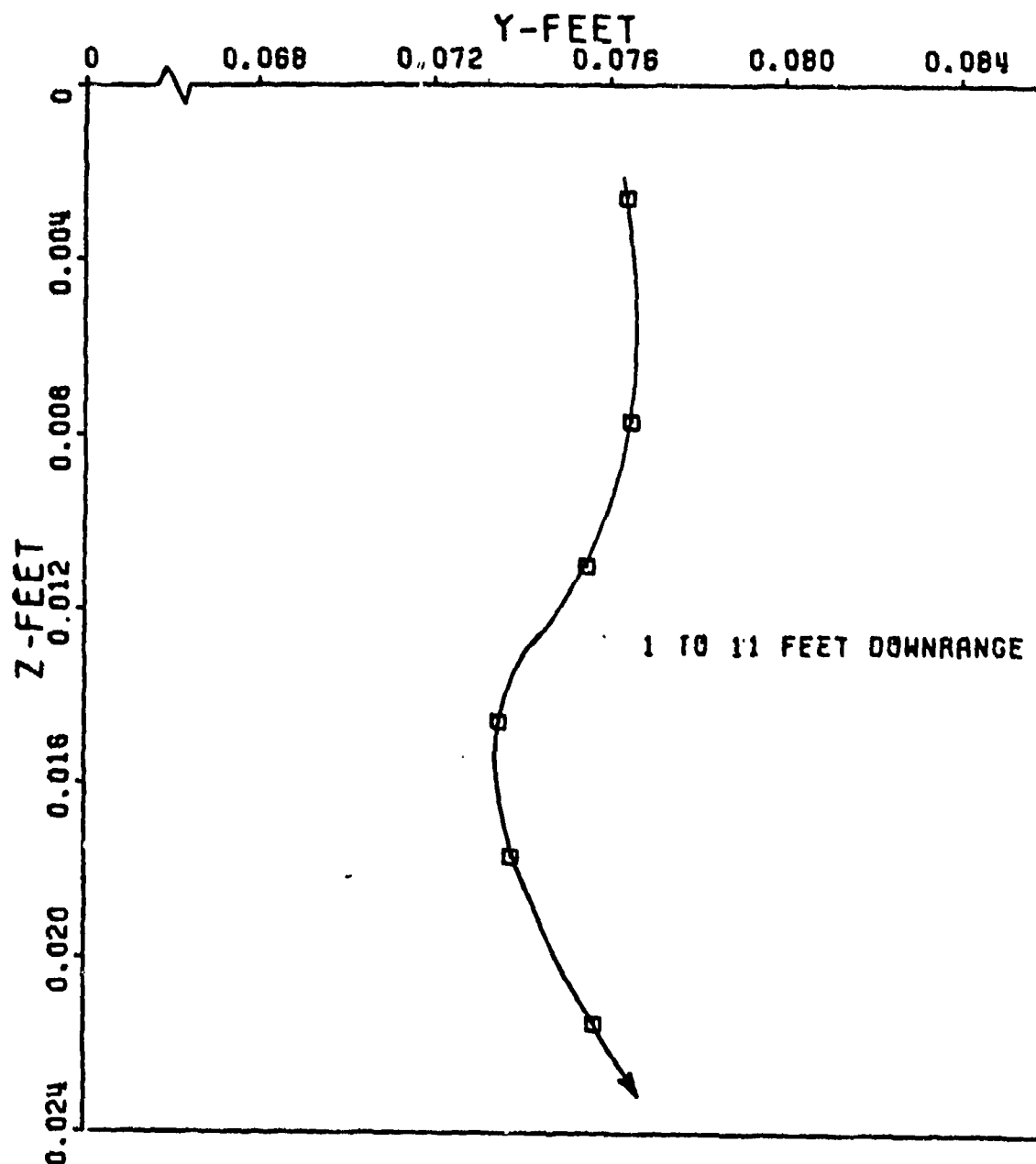


Figure 45. Raw Translational Data  
Ground Point Round 1.9

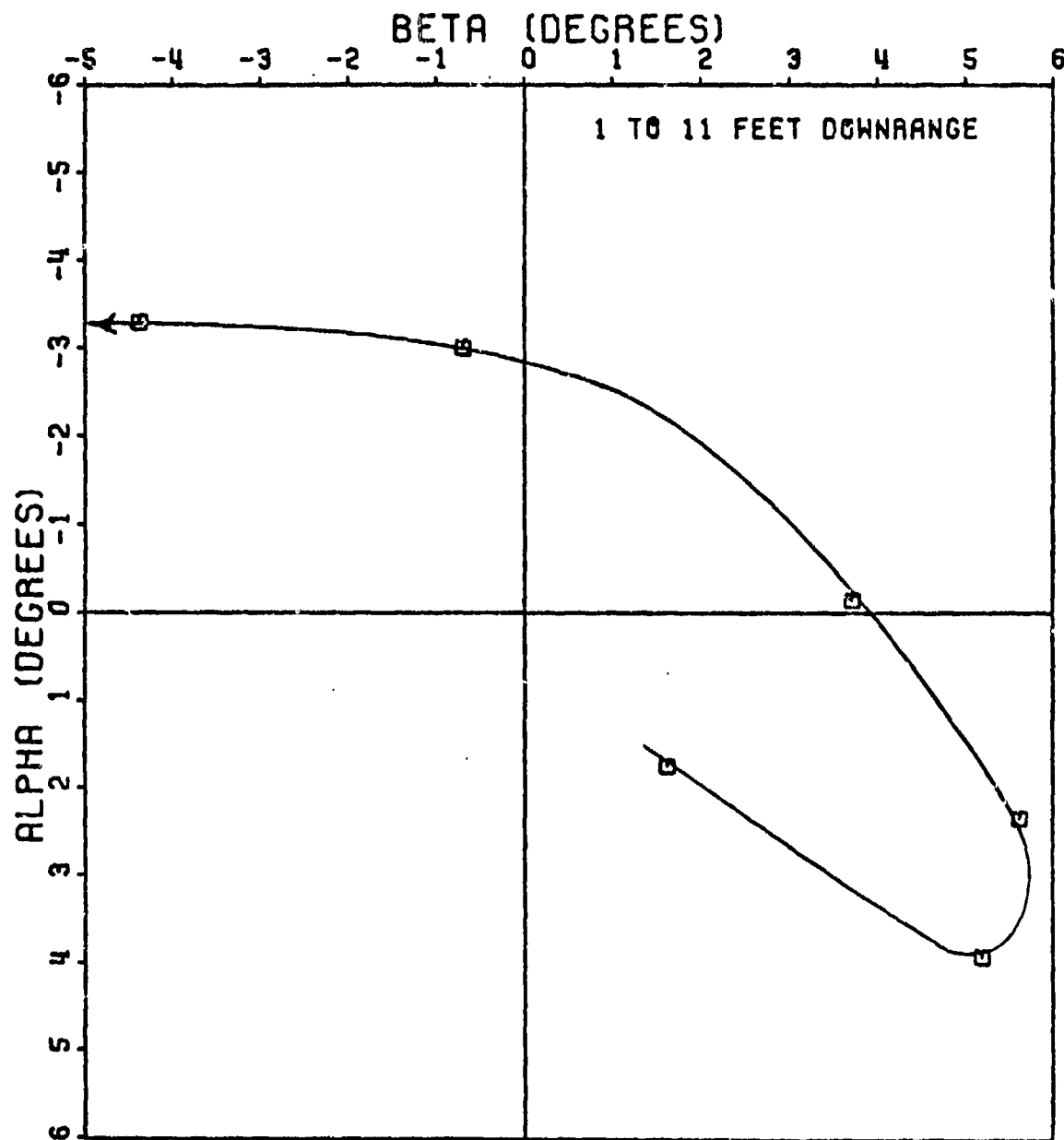


Figure 46. Raw Angular Data  
Ground Point Round 19

Once the raw data was obtained, it had to be converted into a form such that initial conditions  $\vec{S}_0, \dot{\vec{S}}_0, \vec{\alpha}_0$  and  $\dot{\vec{\alpha}}_0$  could be extracted from it. To eventually arrive at values for  $\vec{S}_0$  and  $\dot{\vec{S}}_0$ , the translational parameters, the raw position or translational data had to be approximated by equations. The raw data was fitted to a polynomial equation of third degree by a least squares method. The data in the y-direction was fit separately from that in the z-direction to distinguish between the swerve and heave contributions. With the equations obtained, a simple differentiation yielded equations for the velocities in the y and z directions. The initial conditions  $\vec{S}_0$  and  $\dot{\vec{S}}_0$  are now readily obtainable:

$$\vec{S}_0 \text{ (ft)} = y_0 + iz_0$$

$$\dot{\vec{S}}_0 \text{ (ft/sec)} = \dot{y}_0 + i\dot{z}_0$$

Obtaining  $\vec{\alpha}_0$  and  $\dot{\vec{\alpha}}_0$  from the raw angular data was more difficult. The traditional way of analyzing any missile motion with pitch, yaw, and roll is by a three-degree-of-freedom least squares fit to the tricyclic motion, Equation 6. However, the availability of only 6 data points made this technique impossible, so another, approximate method, had to be employed. The solution was to approximate the pitching and yawing motion to one-degree-of-freedom while holding the roll rate constant. In order to do this, the  $\beta$ - $\alpha$  axis system had to be rotated to coincide with the more dominant angular mode. Figure 47 illustrates a typical raw angular data plot. Since the angular motion of the flechette tends to approximate an ellipse, the  $\beta$ - $\alpha$  axes are rotated some angle  $\gamma$  to coincide with the major and minor axes of the ellipse, as shown. The angular data is retabulated for this new axes system,  $\beta'$ - $\alpha'$ . To fit the data to the one-degree-of-freedom equation:

$$\alpha = K_1 e^{\lambda t} \cos(\omega t + \delta)$$

only the dominant mode can be considered. For example, in Figure 47 the dominant mode occurs along the  $\alpha'$  axis; therefore, only  $\alpha'$  coordinates are utilized in the least squares fit, corresponding  $\beta'$  coordinates are ignored. Table 21 lists the parameters obtained for the eight flechette rounds. Once an equation for  $\alpha'$  is obtained, it represents one dimensional oscillatory motion along the  $\alpha'$  axis. A simple differentiating of the  $\alpha'$  equation yields an equation for  $\dot{\alpha}'$ . The initial



conditions  $\vec{\alpha}_0$  and  $\vec{\dot{\alpha}}_0$ , however, are complex whereas  $\alpha'$  and  $\dot{\alpha}'$  are only one dimensional. Therefore, the rotation angle  $\gamma$  is taken into account and the  $\alpha'$  equation is projected back into the  $\beta, \alpha$  axes system:

$$\alpha = \alpha' \cos \gamma$$

$$\dot{\alpha} = \dot{\alpha}' \cos \gamma$$

$$\beta = \alpha' \sin \gamma$$

$$\dot{\beta} = \dot{\alpha}' \sin \gamma$$

Thus the complex initial conditions are approximated.

$$\vec{\alpha}_0 = \beta_0 + i\alpha_0$$

$$\vec{\dot{\alpha}}_0 = \dot{\beta}_0 + i\dot{\alpha}_0$$

Figures 48-63 illustrate the fitted data both translational and angular for the eight rounds. The transitional data includes the pertinent equations.

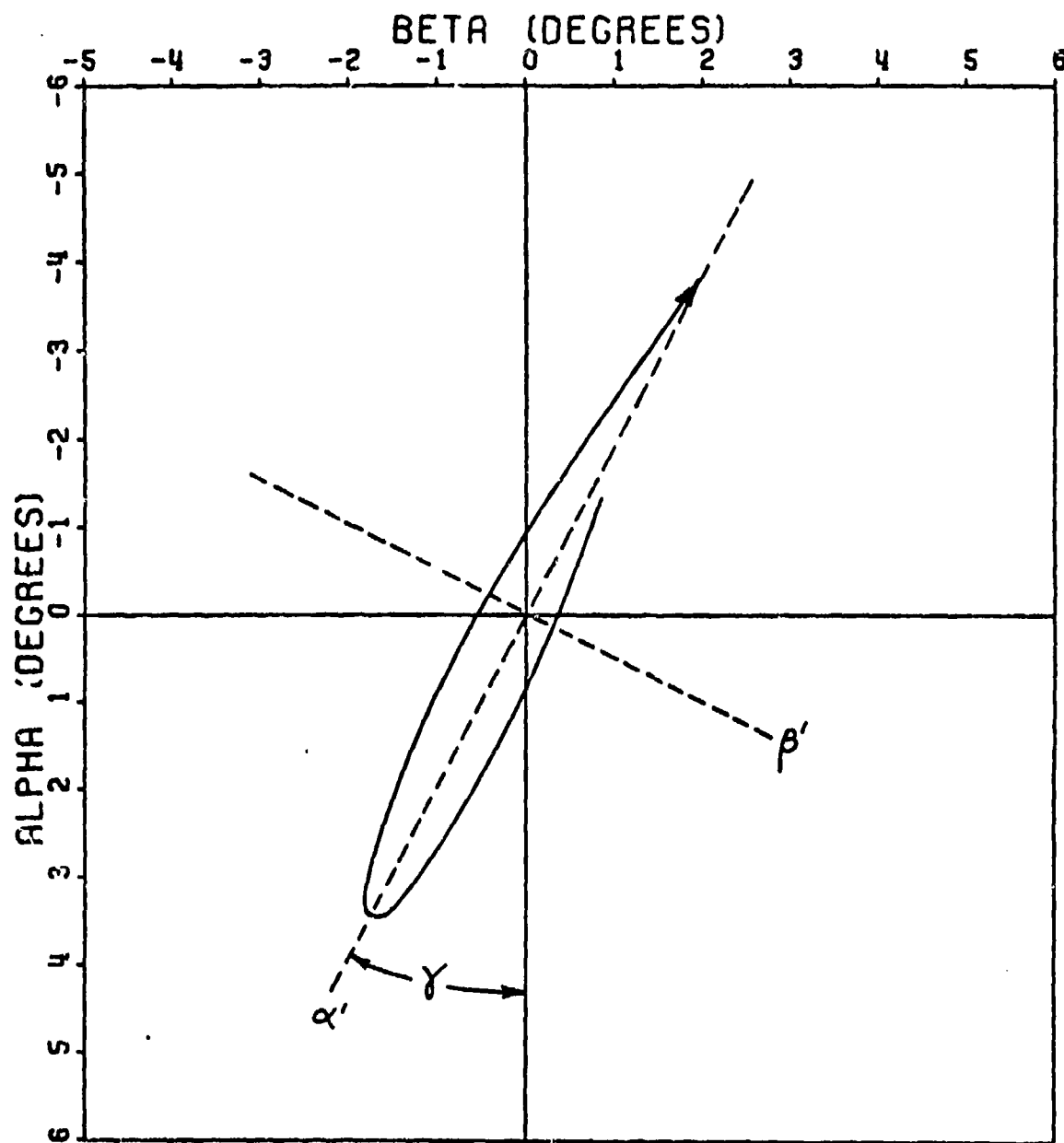


Figure 47. Axis Rotation Approximates Pure Pitching Motion

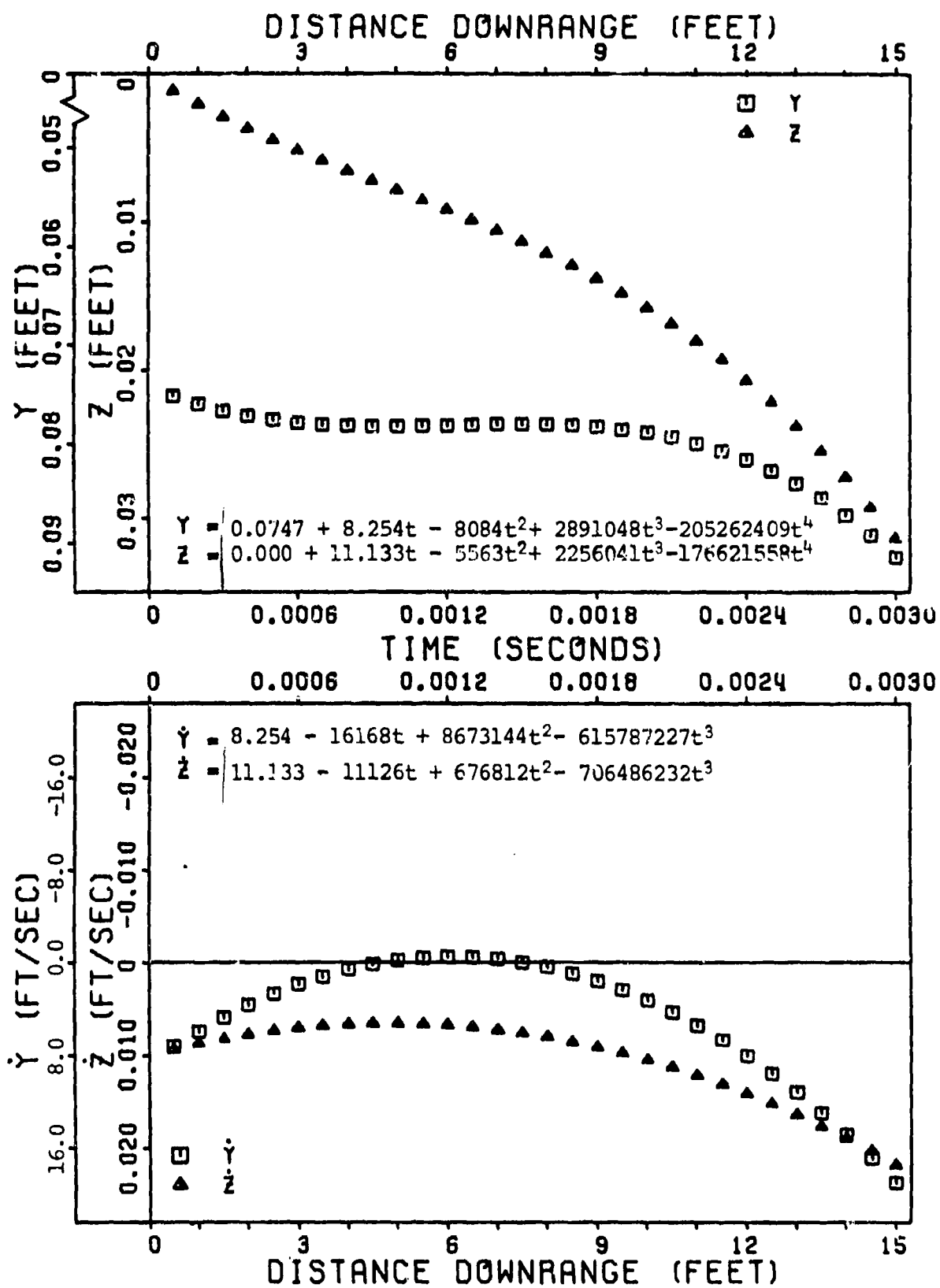


Figure 48. Fitted Translational Data  
Ground Point Round 4

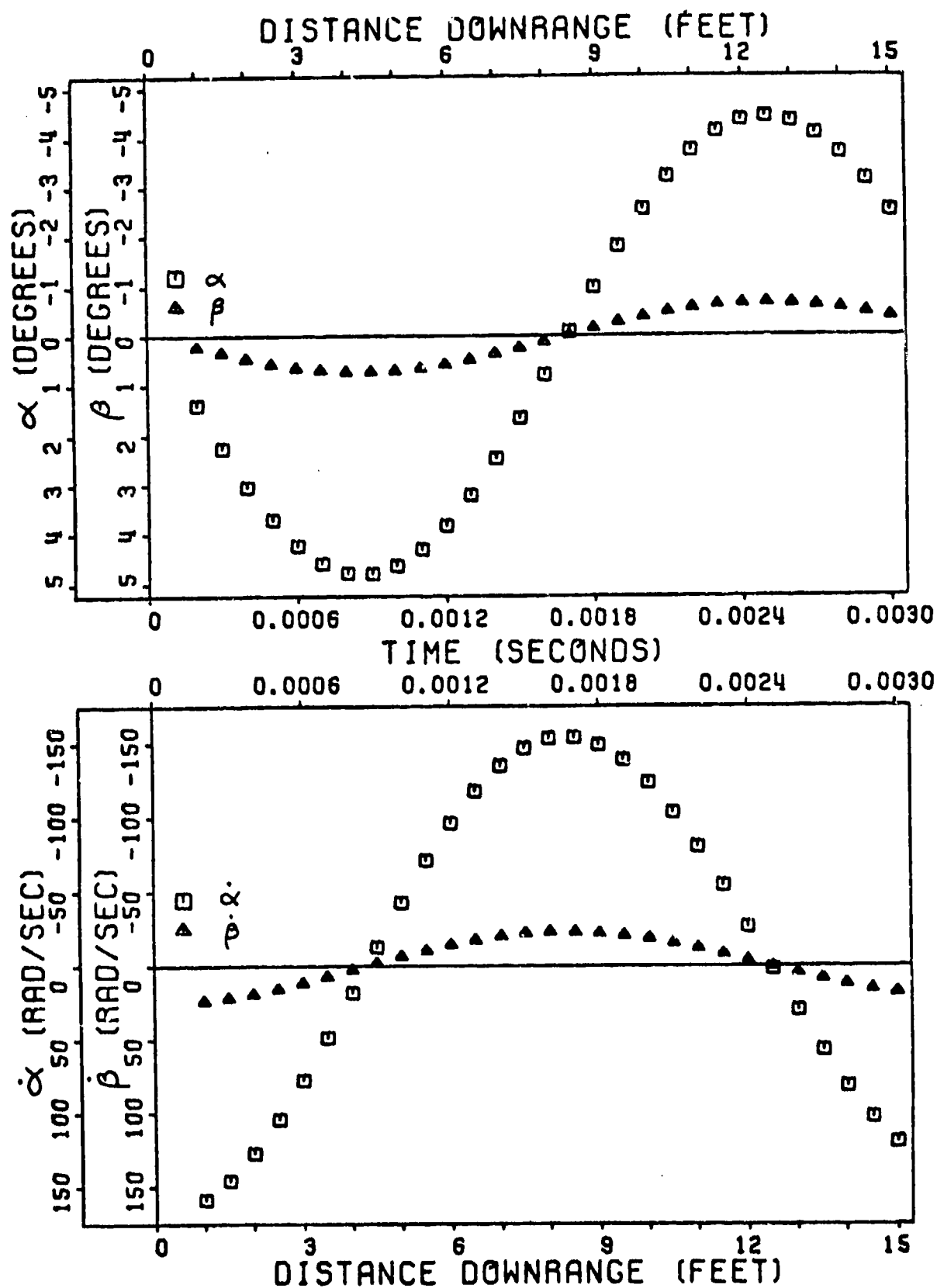


Figure 49. Fitted Angular Data Ground  
Point Round 4

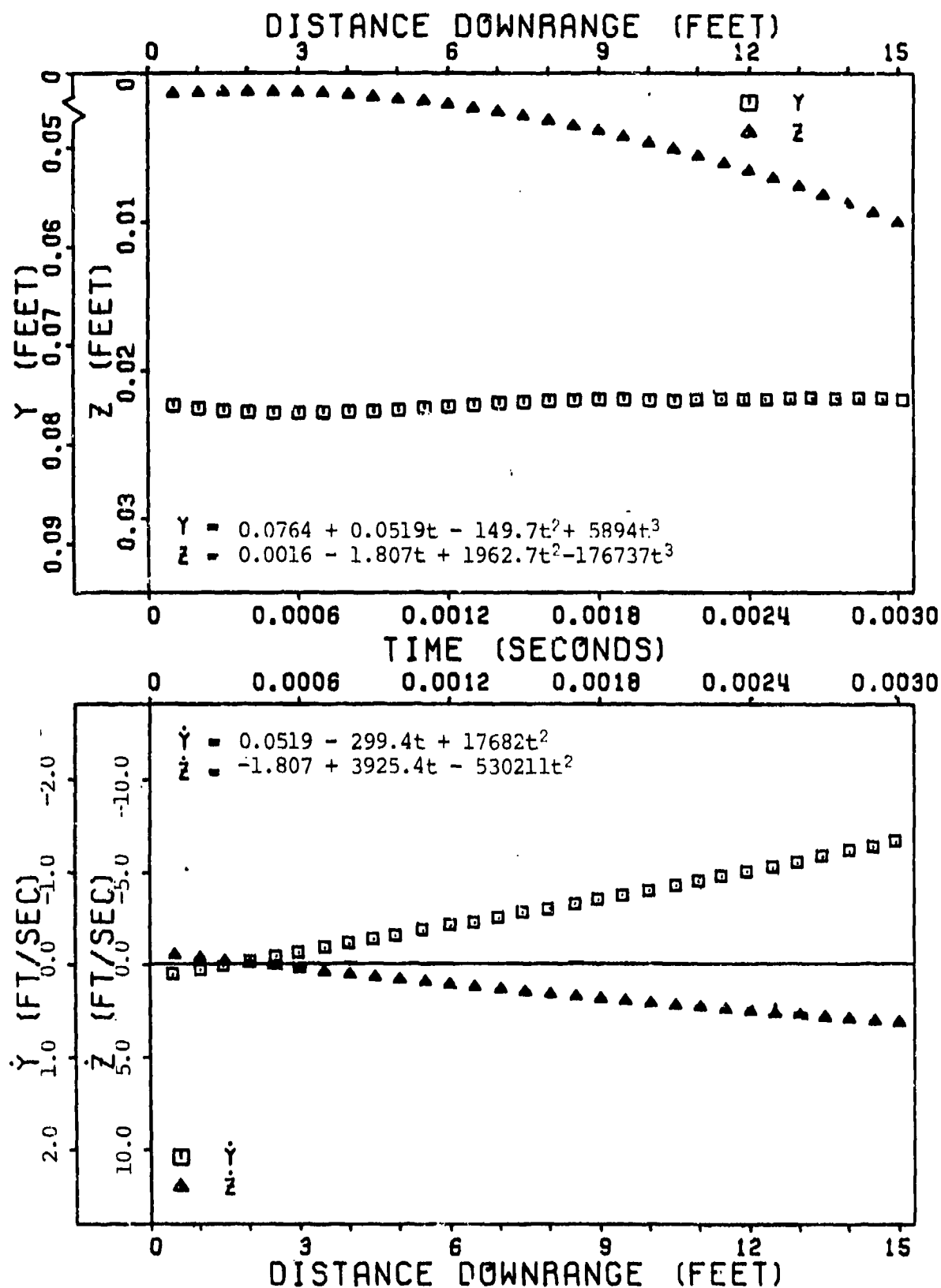


Figure 50. Fitted Translational Data Ground Point Round 6

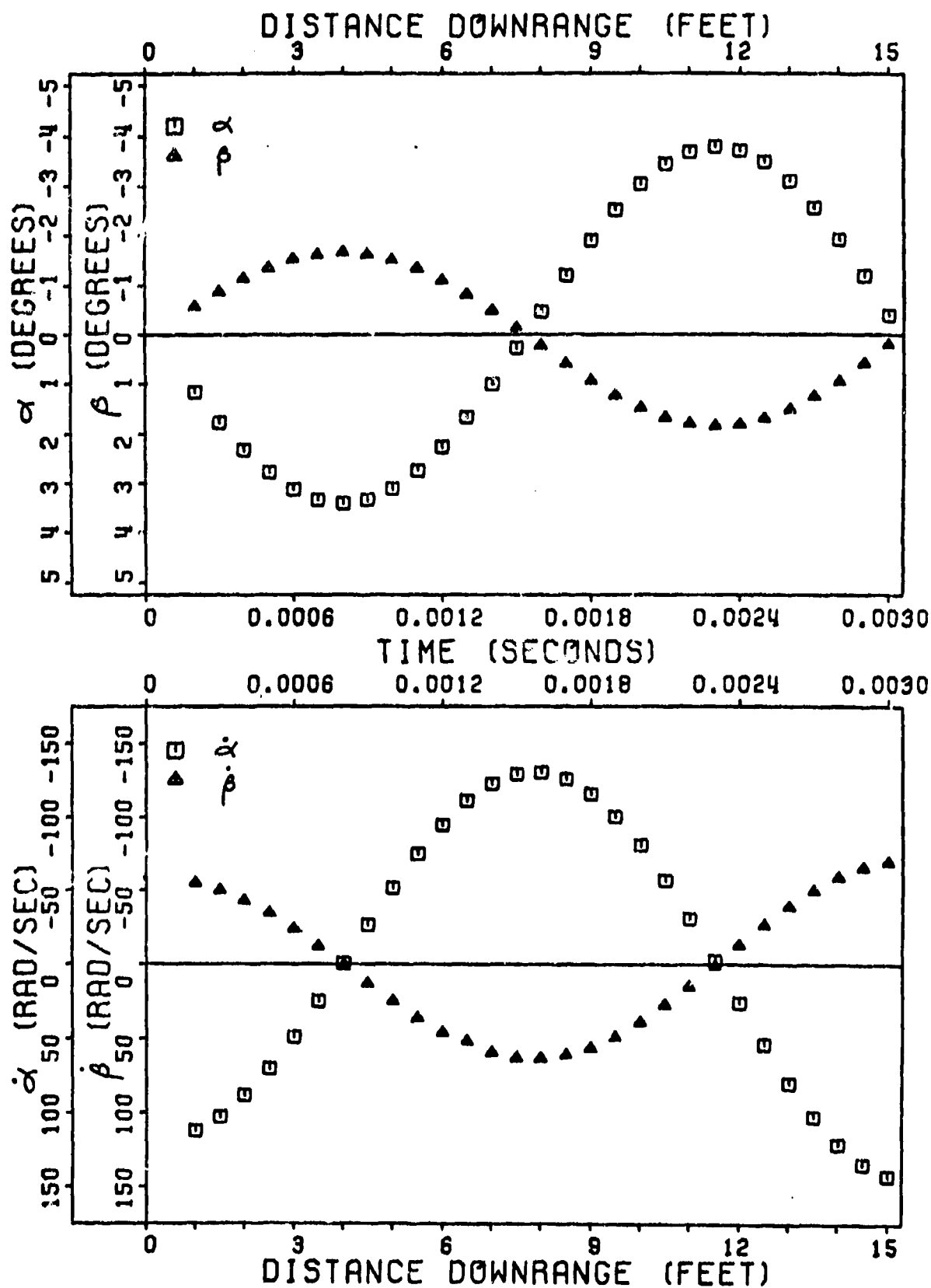


Figure 51. Fitted Angular Data Ground Point Round 6

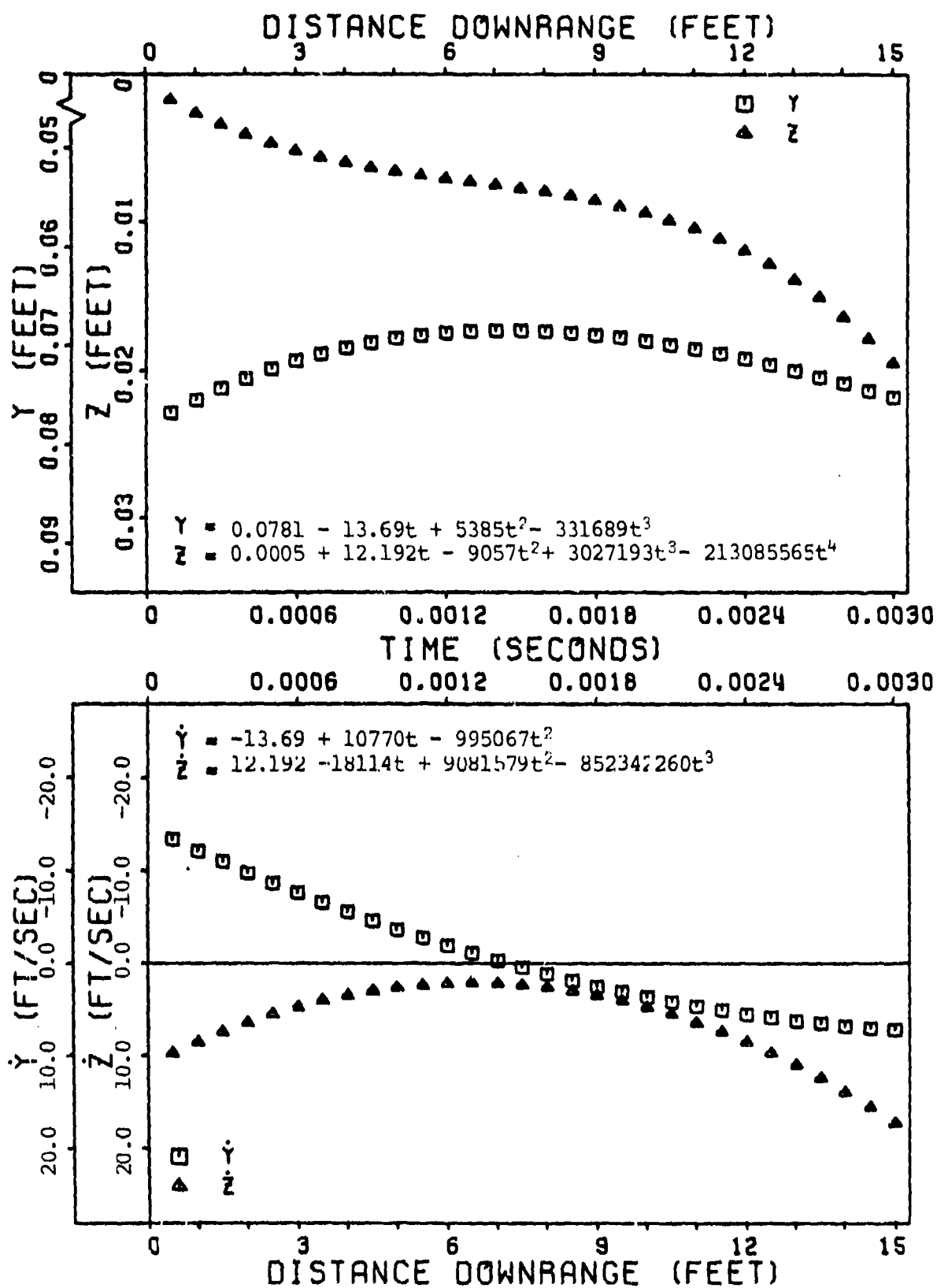


Figure 52. Fitted Translational Data  
Ground Point Round 7

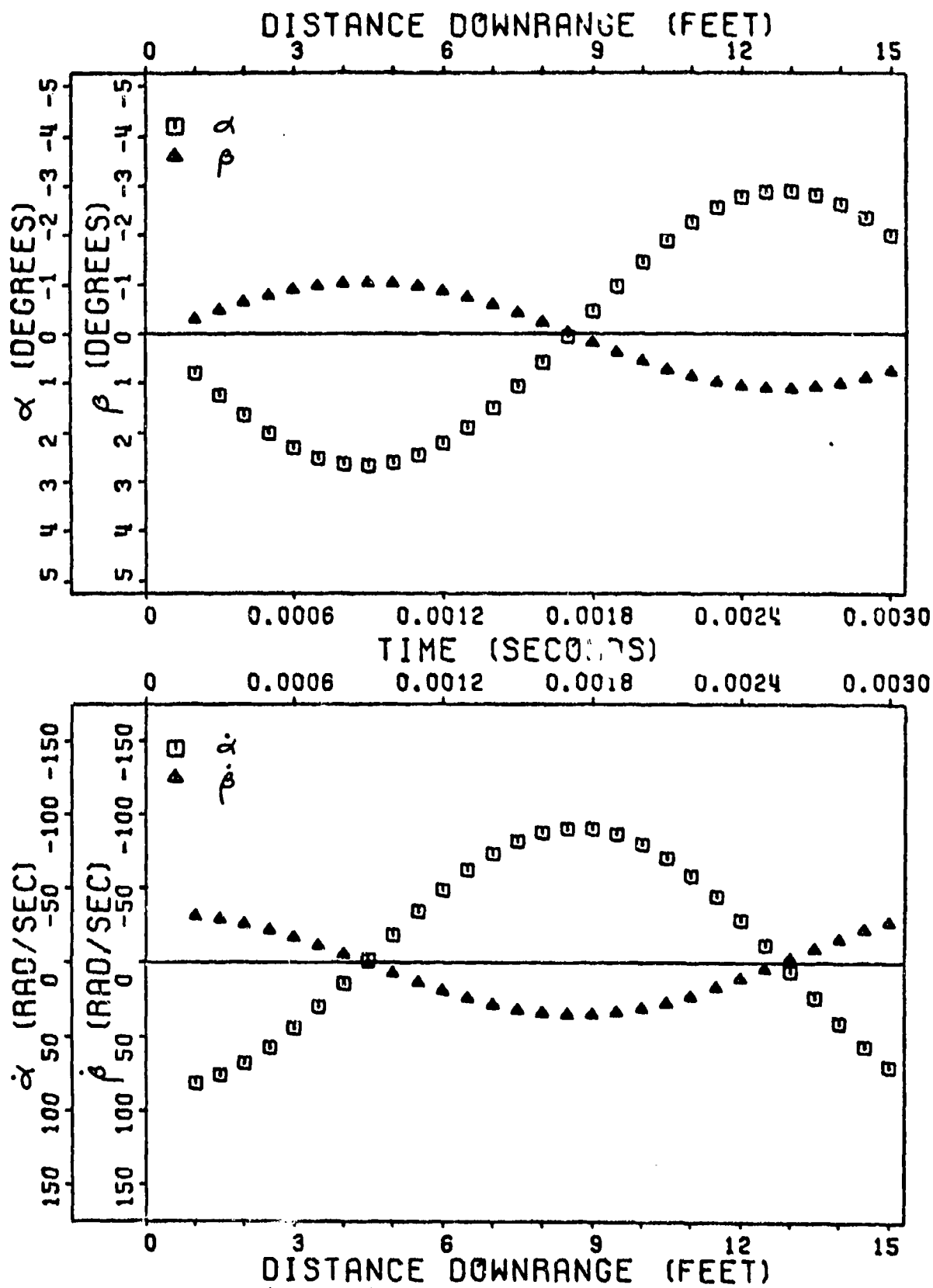


Figure 53. Fitted Angular Data  
Ground Point Round 7



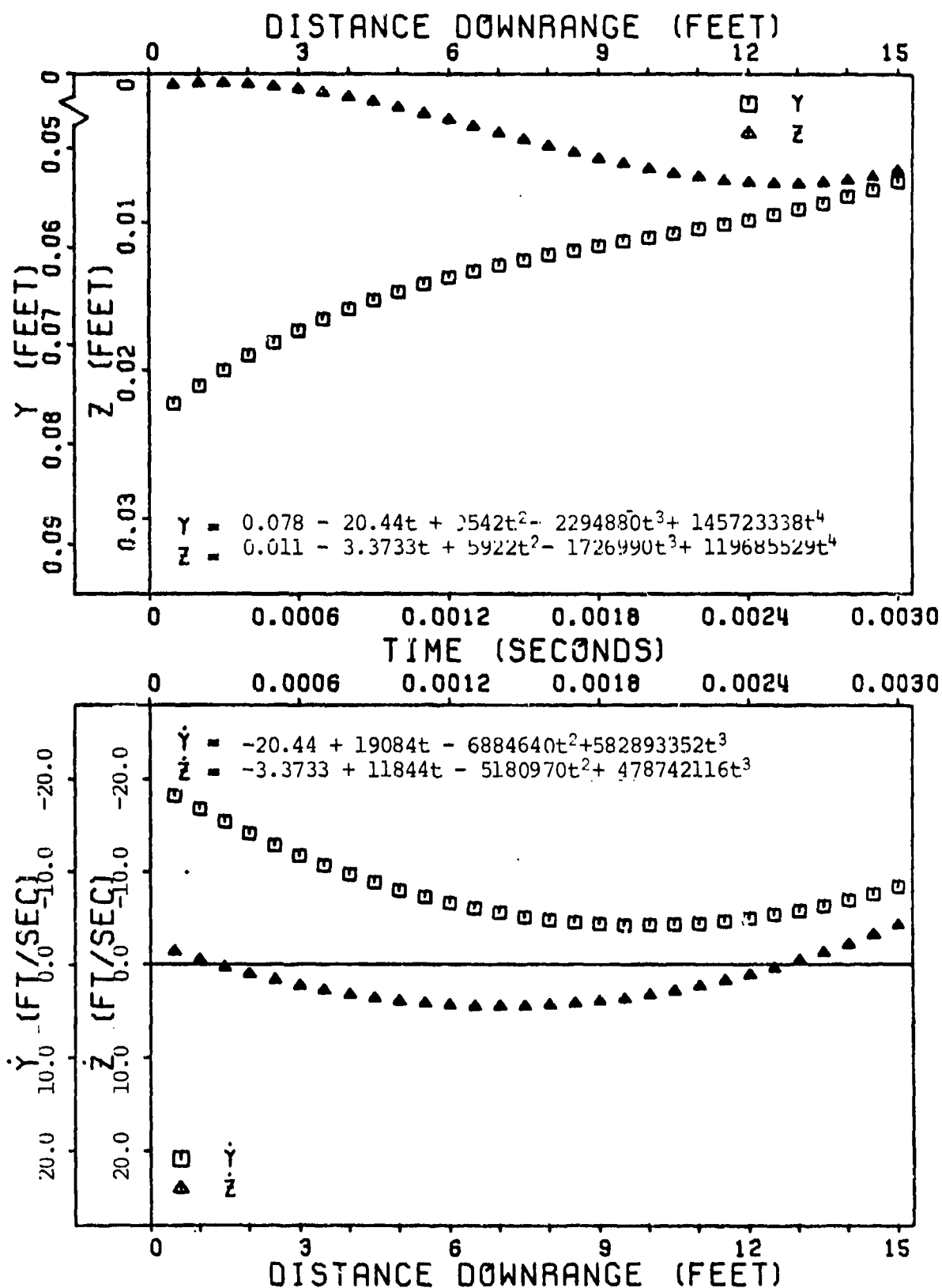


Figure 54. Fitted Translational Data  
Ground Point Round 8

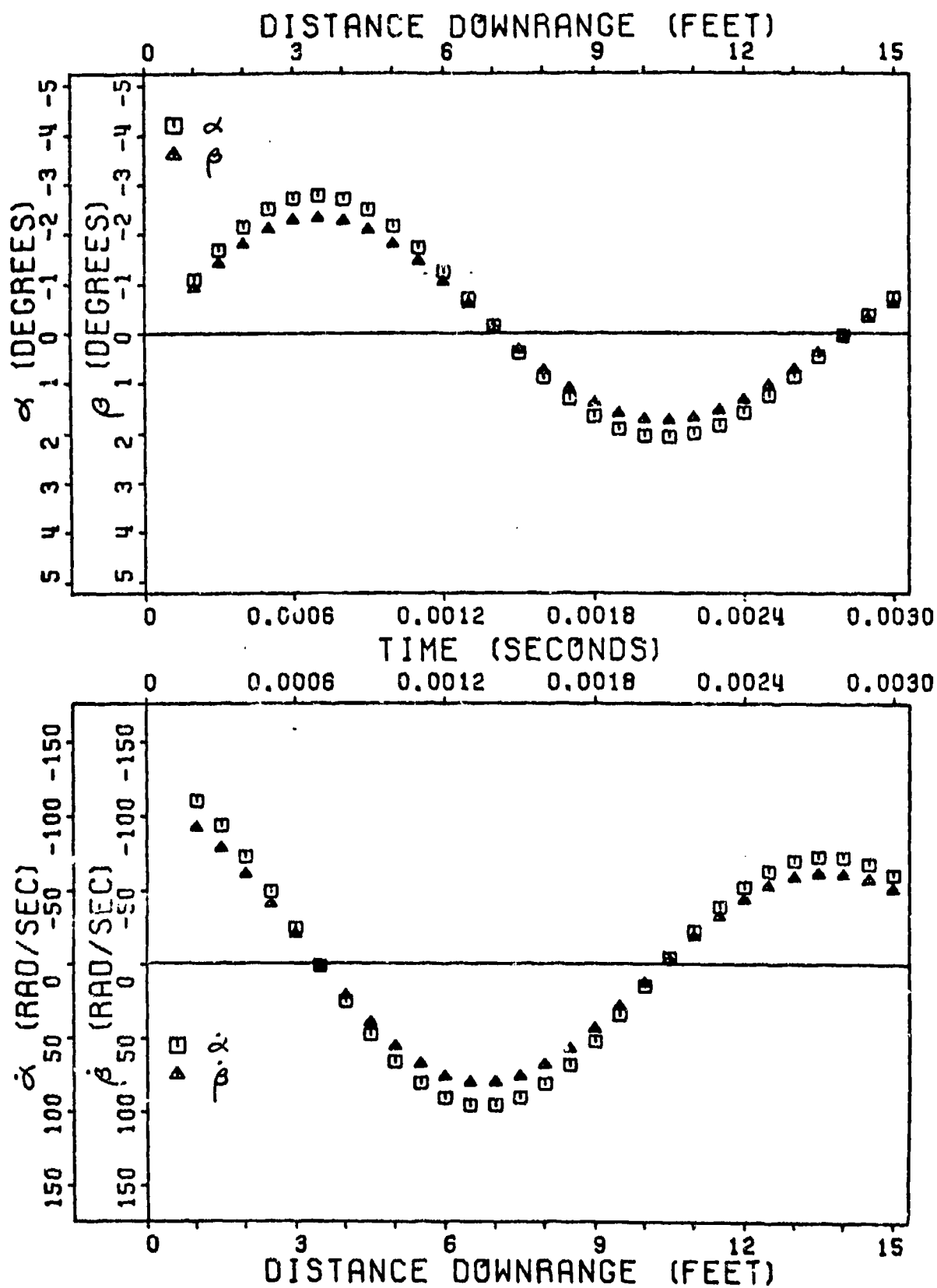


Figure 55. Fitted Angular Data  
Ground Point Round 8

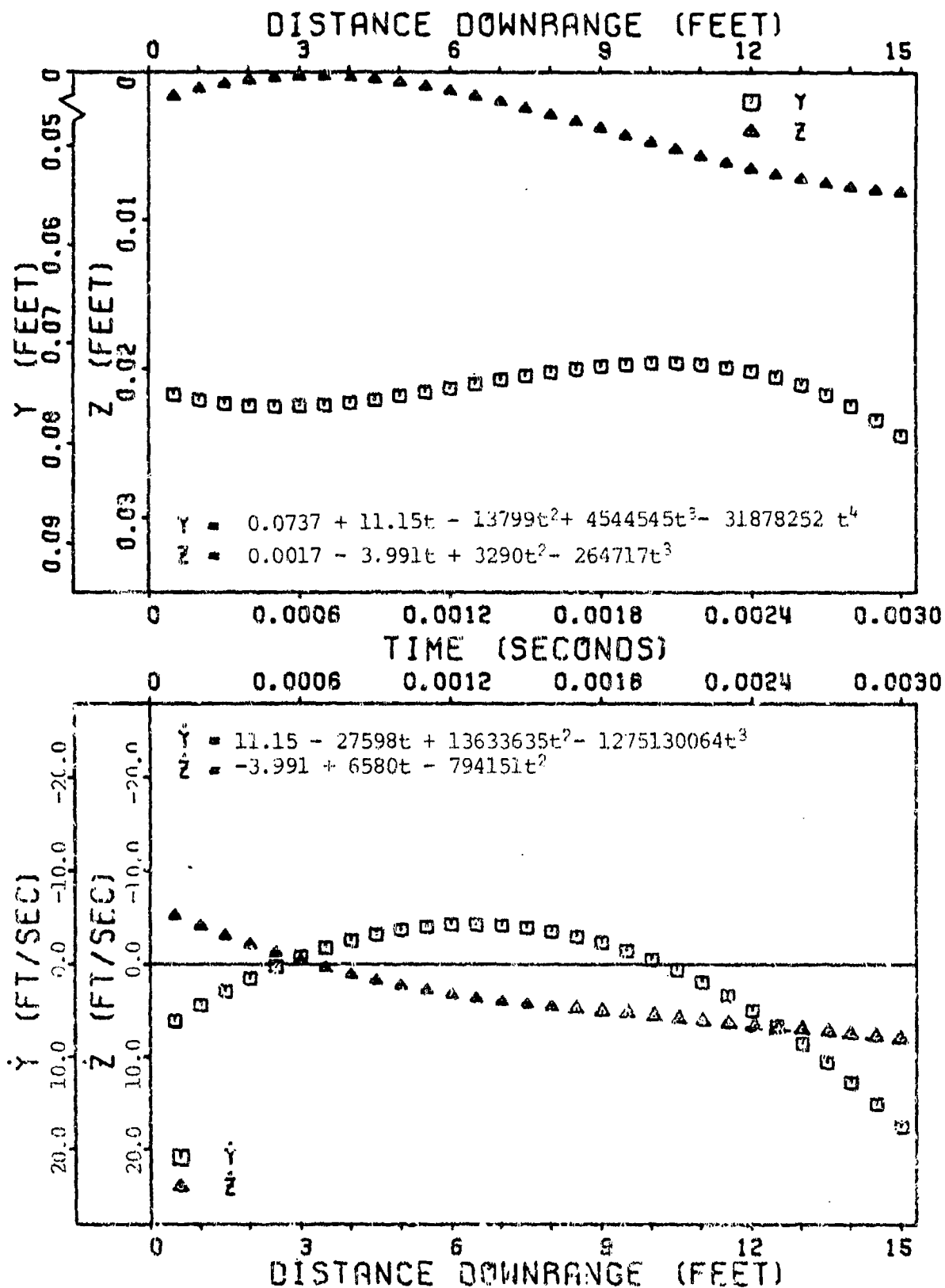


Figure 56. Fitted Translational Data  
Ground Point Round 14

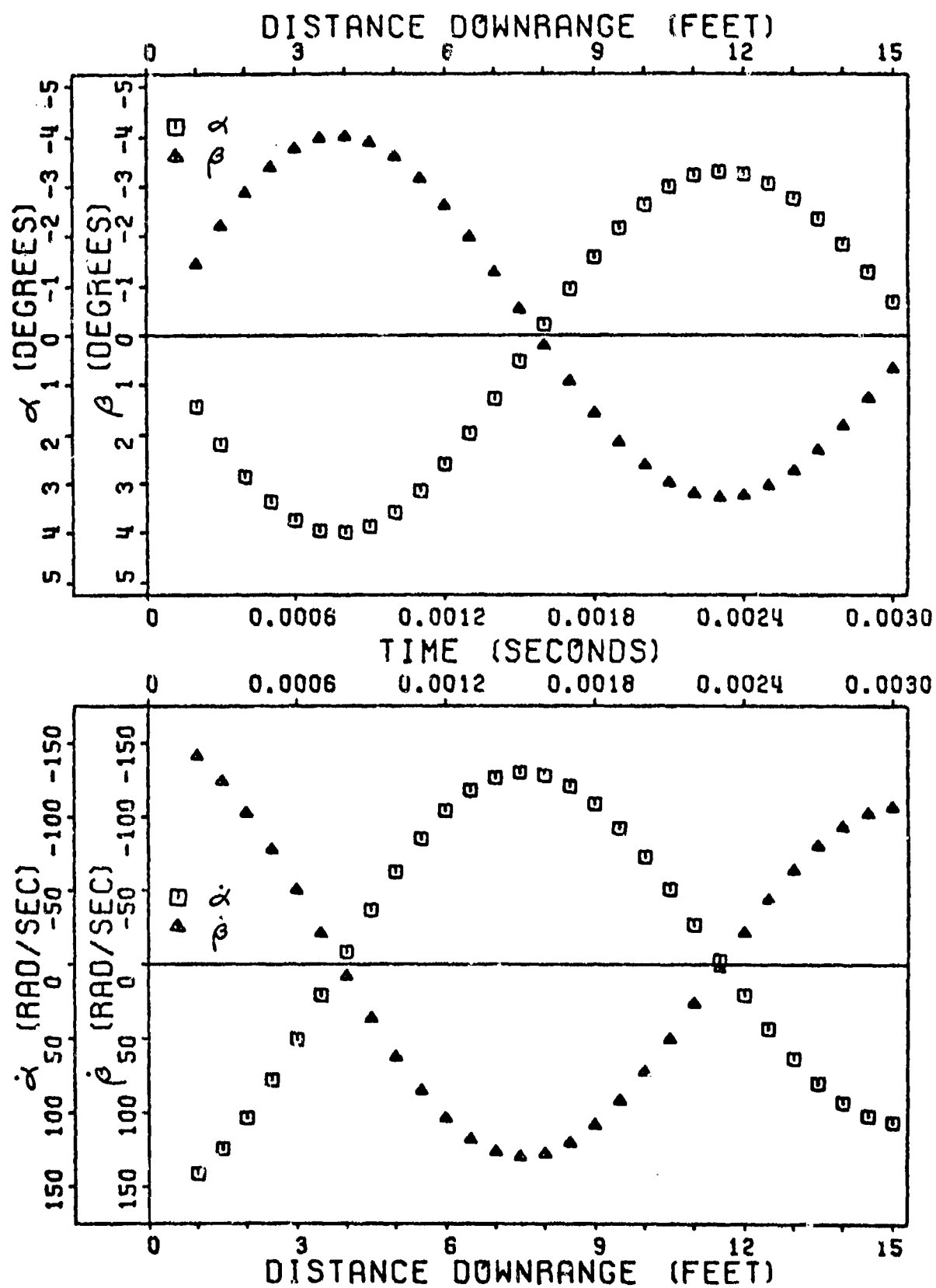


Figure 57. Fitted Angular Data  
Ground Point Round 14

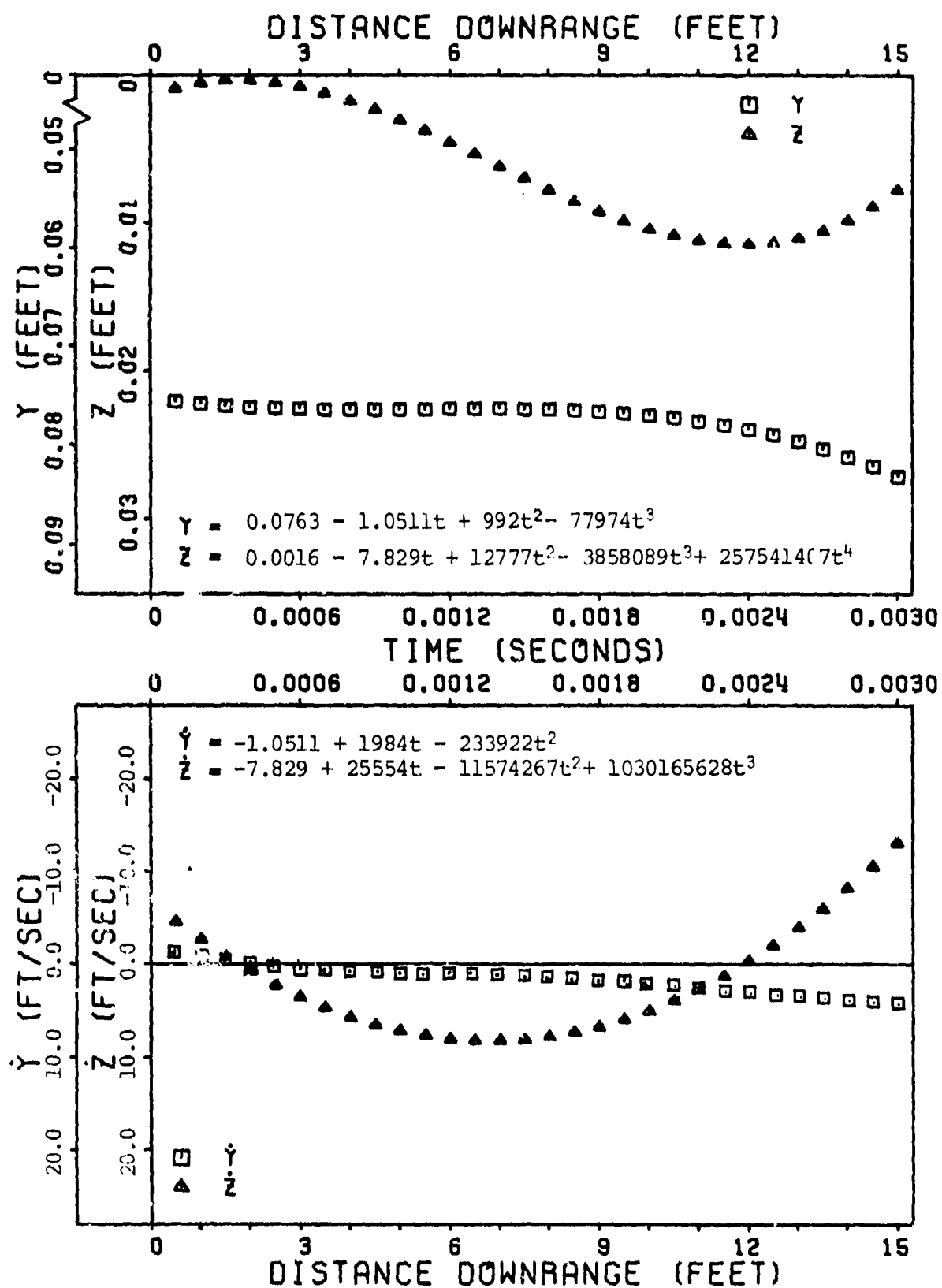


Figure 58. Fitted Translational Data  
Ground Point Round 16

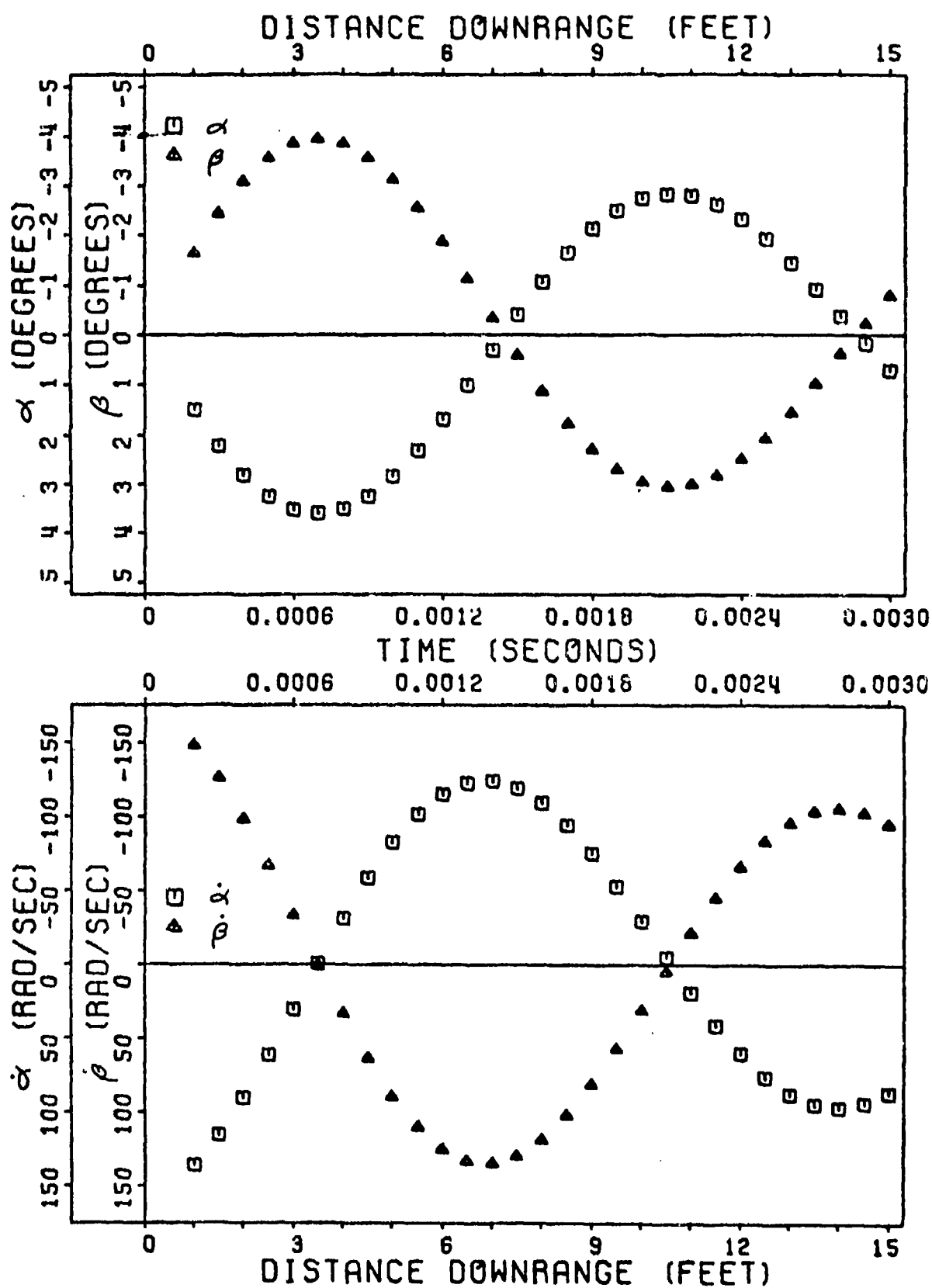


Figure 59. Fitted Angular Data  
Ground Point Round 16

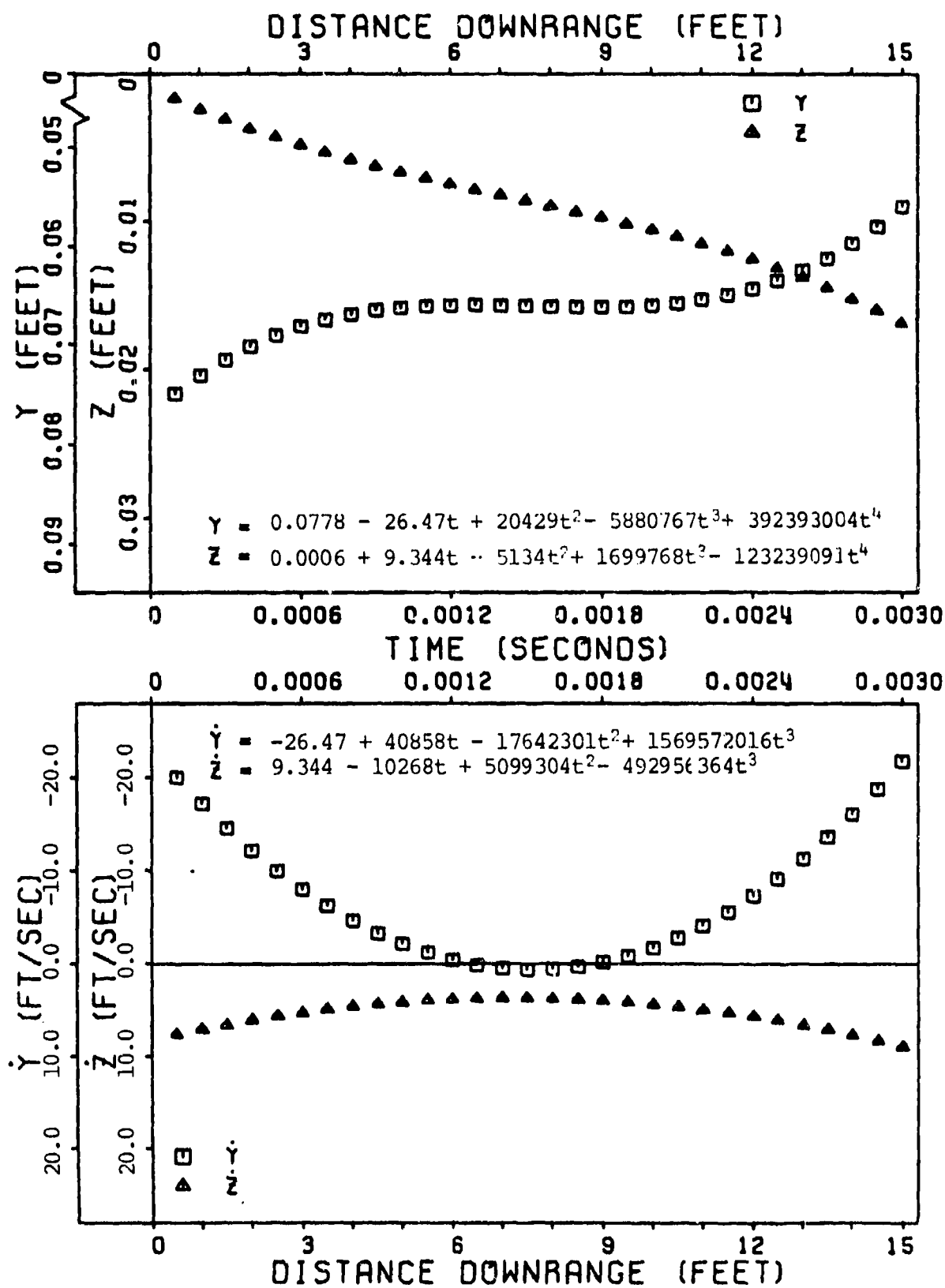


Figure 60. Fitted Translational Data  
Ground Point Round 17

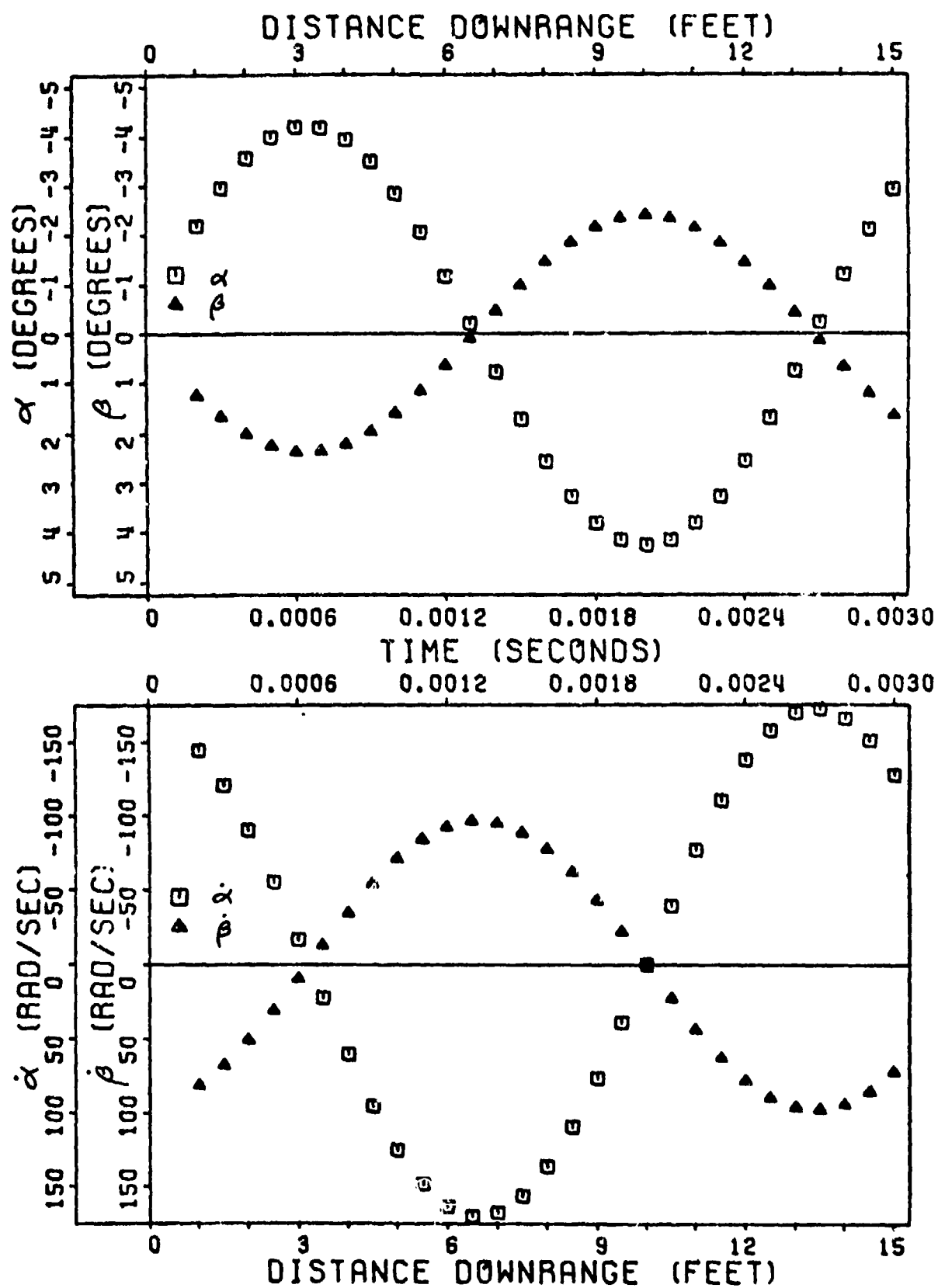


Figure 61. Fitted Angular Data  
Ground Point Round 17



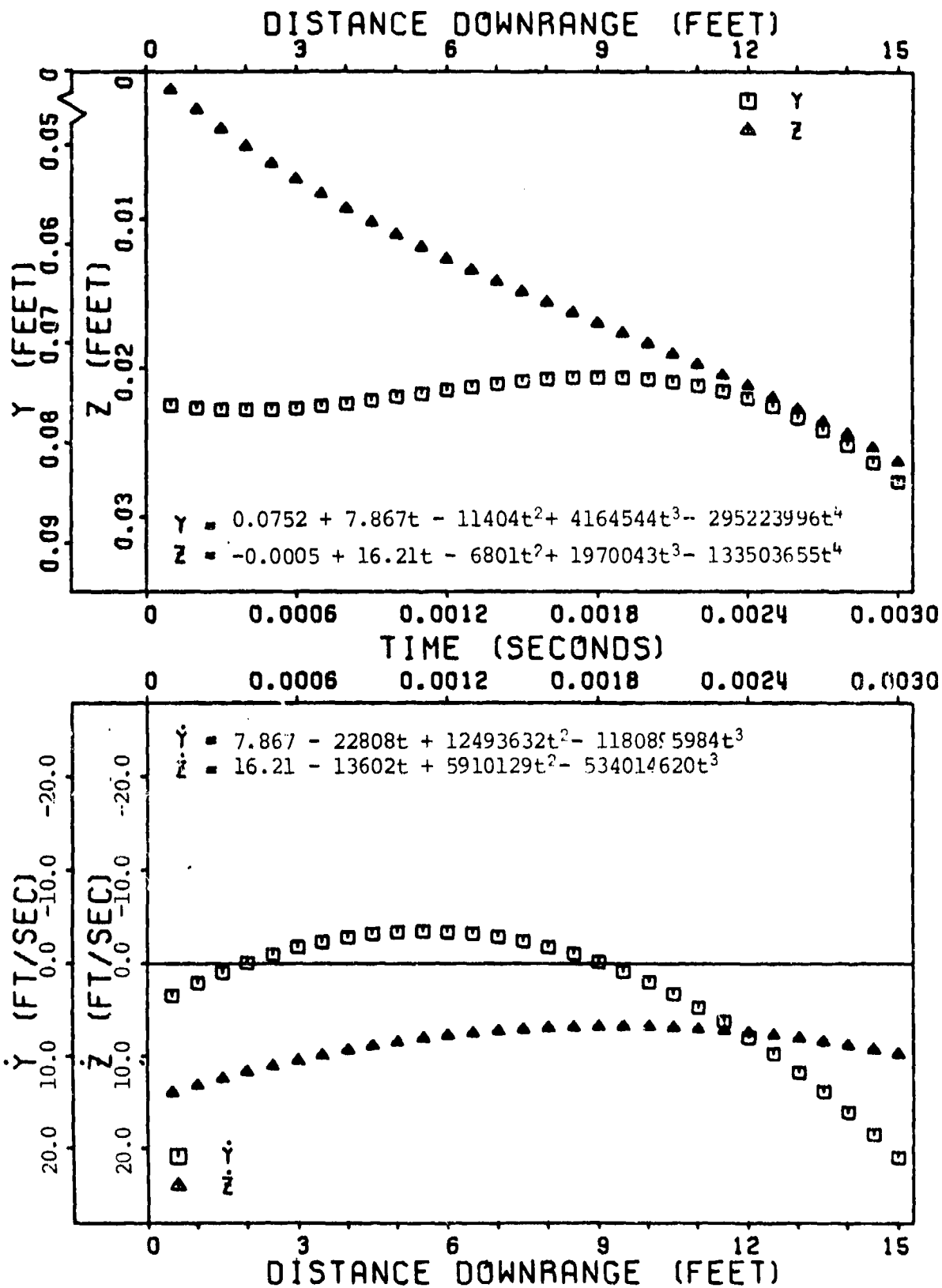


Figure 62. Fitted Translational Data  
Ground Point Round 19

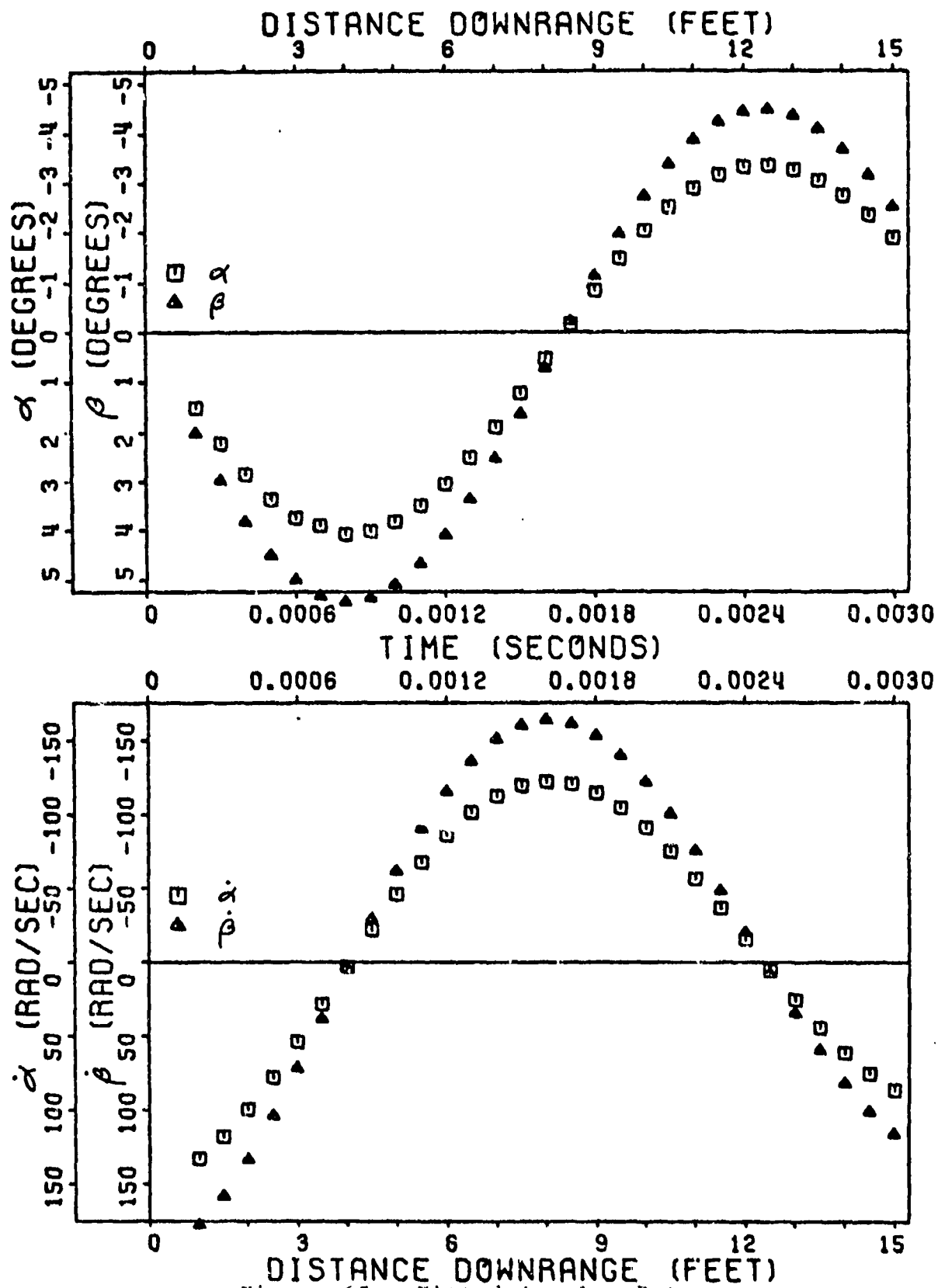


Figure 63. Fitted Angular Data  
Ground Point Round 19

TABLE 21. AERODYNAMIC PARAMETERS FROM  
LEAST SQUARES FIT

R O U N D	K <sub>1</sub> (degrees)	λ (rad/sec)	ω (rad/sec)	δ (rad)
4	5.01	-49.48	1921.3	-1.29
6	3.64	68.24	2079.8	-1.21
7	-2.78	46.48	1871.4	-1.26
8	-4.02	-203.19	2267.6	-1.21
14	6.09	-126.37	2042.0	-1.23
16	5.84	-174.7	2211.7	-1.18
17	-4.81	8.53	2314.5	-1.02
19	7.35	-121.62	1889.9	-1.22

$$\alpha = K_1 e^{\lambda t} \cos(\omega t + \delta)$$

$$\dot{\alpha} = K_1 e^{\lambda t} \left[ \lambda \cos(\omega t + \delta) - \omega \sin(\omega t + \delta) \right]$$

## SECTION V

### DISPERSION ANALYSIS

#### FREE FLIGHT VERSUS THEORY

Once the initial conditions are determined as in the previous section, they are applied to the theory and compared to the dispersion of each test fired round. To utilize the theory, the fitted data must be chosen for a given time; that is,

$\vec{S}_0, \vec{\dot{S}}_0, \vec{\alpha}_0, \vec{\dot{\alpha}}_0$  must be selected for one given point in time-position downrange. Since the question of what point in time the initial conditions occur, 3 sets of initial conditions were chosen to correspond with positions 1, 3, 5 feet downrange. This span of position downrange may or may not be sufficient to include the actual time corresponding to the initial conditions for each round. The following analysis will determine each round's effective time for its initial conditions.

For each set of initial conditions, theory and 6-D computations were done and compared to target data for the Frankford test firings. The results are tabulated in Table 22 in mils and plotted in Figures 64-71 in feet; deviation from the time of fire at 50 feet downrange. The relationship between the deviations in feet and mils at 50 feet downrange is:

$$\vec{J.A.} \text{ (mils)} = \frac{\vec{S} \text{ (ft)}}{x} (1000)$$

or 
$$\vec{J.A.} \text{ (mils)} = (20) \vec{S} \text{ (ft)}$$

To accurately and concisely analyze the complex and large amount of data in Table 22, the positions downrange in which the initial conditions were selected must be simultaneously analyzed with the dispersion results at 50 feet downrange. The problem in choosing initial conditions is where they should be taken; at what point downrange. Normally, one would think that the initial conditions would occur immediately after leaving the gun barrel. However, the flechette being a finned body needs a sabot configuration to guide it down the barrel, Figure 29. The sabot causes the initial condition location problem since the sabot must separate from the flechette outside of the gun barrel. The exact time and place where this occurs is not constant; varying from round to round. Not only does the sabot separate from the flechette instantaneously different every time, the sabot may not separate cleanly or the same way every time. Interference with the fins after sabot separation can

TABLE 22. DISPERSION ANALYSIS RESULTS

R O U N D	INITIAL CONDITIONS			TARGET IMPACTS					
	x <sub>o</sub> (ft)	u <sub>c</sub> (ft/sec)	P <sub>o</sub> (rad/sec)	FRANKFORD FIRINGS		HIGH ROLL THEORY		6-D COMPUTER PROGRAM	
				mils	mils	mils	mils	mils	mils
4	1	4747	11454	2.333- 0.750i	2.451	2.41+0.72i	2.52	2.45+0.71i	2.55
	3					1.69+0.91i	1.92	1.68+0.81i	1.87
	5					1.55+1.71i	2.31	1.50+1.58i	2.18
	7					1.87+2.47i	3.06	1.76+2.40i	2.98
6	1	4662	13201	1.050- 0.200i	1.069	1.91-1.01i	2.16	1.96-1.00i	2.20
	3					1.61-0.19i	1.62	1.70-0.24i	1.72
	5					1.23+0.80i	1.47	1.32+0.74i	1.51
	7					1.04+1.41i	1.75	1.00+1.38i	1.70
7	3	4642	14219	2.817- 0.083i	2.818	-0.10+1.22i	1.22	-0.13+1.25i	1.26
	5					0.85+0.37i	0.93	0.82+0.42i	0.92
	7					1.64+0.11i	1.64	1.65+0.14i	1.66
	9					2.19+0.54i	2.26	2.22+0.52i	2.28
8	5	4662	12998	1.067+ 1.983i	2.249	-0.51+0.29i	0.59	-0.42+0.30i	0.52
	7					-0.25+0.30i	0.39	-0.21+0.26i	0.33
	9					0.12+0.58i	0.59	0.08+0.52i	0.53
	11					0.33+0.75i	0.82	0.28+0.72i	0.77
14	1	4758	13289	1.067+ 0.317i	1.113	3.78-1.61i	4.11	3.85-1.56i	4.15
	3					1.58-0.38i	1.63	1.82-0.44i	1.87
	5					0.16+0.87i	0.88	0.36+0.76i	0.84
	7					-0.12+1.61i	1.61	-0.10+1.52i	1.52
16	1	4753	17354	1.683- 0.083i	1.685	2.49-1.65i	2.99	2.58-1.58i	3.03
	3					1.68+0.57i	1.77	1.92+0.52i	1.99
	5					0.95+2.07	2.28	1.06+1.96i	2.23
	7					0.90+2.39i	2.55	0.88+2.32i	2.48
17	1	4677	16613	1.400- 0.383i	1.451	-2.99+2.66i	4.00	-3.06+2.64i	4.04
	3					-0.05+1.12i	1.12	-0.18+1.18i	1.19
	5					1.68-0.09i	1.68	1.70-0.02i	1.70
	7					1.97-0.17i	1.98	2.06-0.18i	2.07
19	1	4679	11913	1.783+ 1.183i	2.140	0.96+1.95i	2.17	0.96+1.88i	2.11
	3					0.67+1.83i	1.95	0.40+1.72i	1.77
	5					1.29+2.15i	2.51	1.02+2.08i	2.32
	7					2.07+2.40i	3.17	2.00+2.40i	3.12

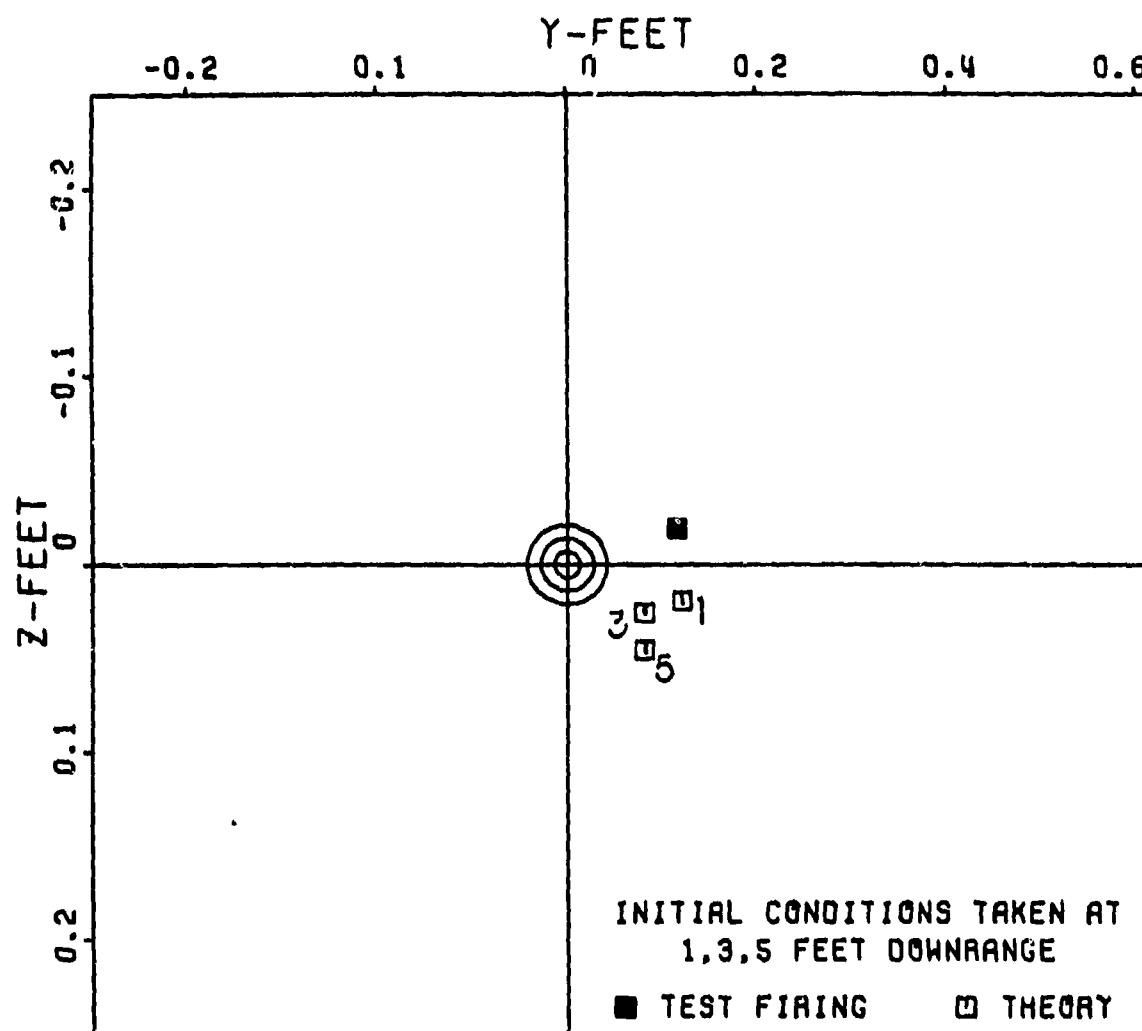


Figure 64. Dispersion: Ground Point-Round 4 Test Firing Versus Theory at 50 Feet Downrange

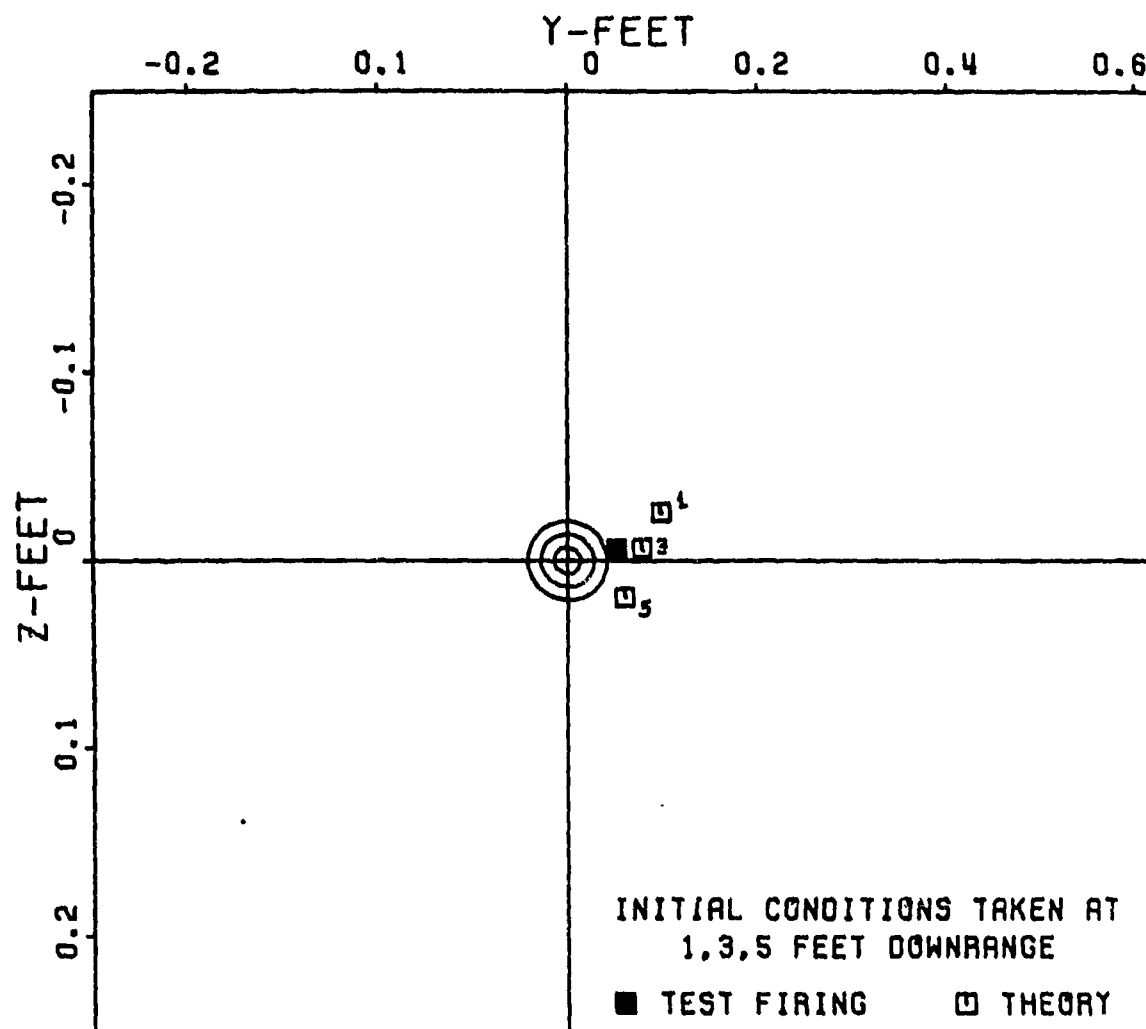


Figure 65. Dispersion: Ground Point Round 6 Test Firing Versus Theory, at 50 Feet Downrange

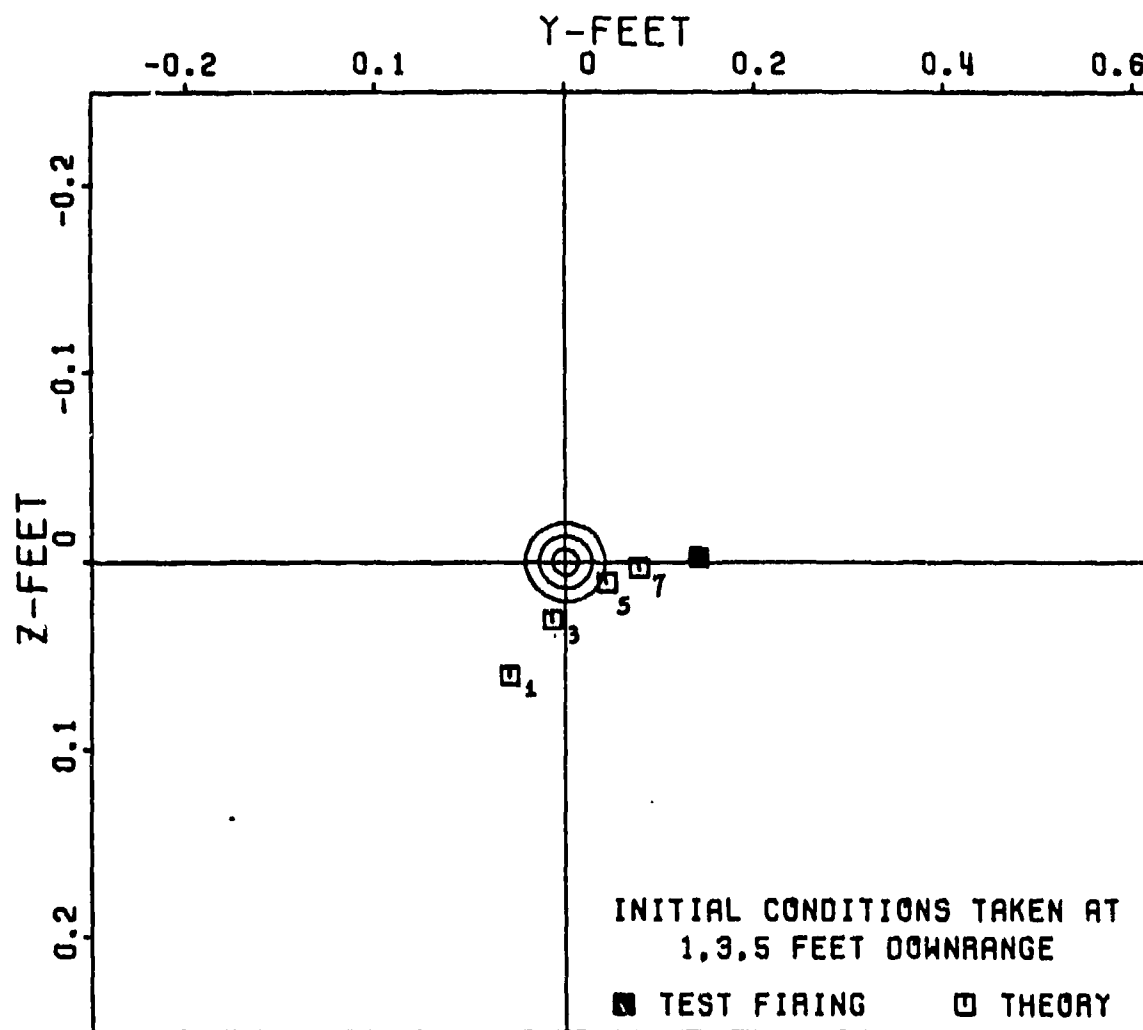


Figure 66. Dispersion: Ground Point Round 7 Test Firing Versus Theory, at 50 Feet Downrange



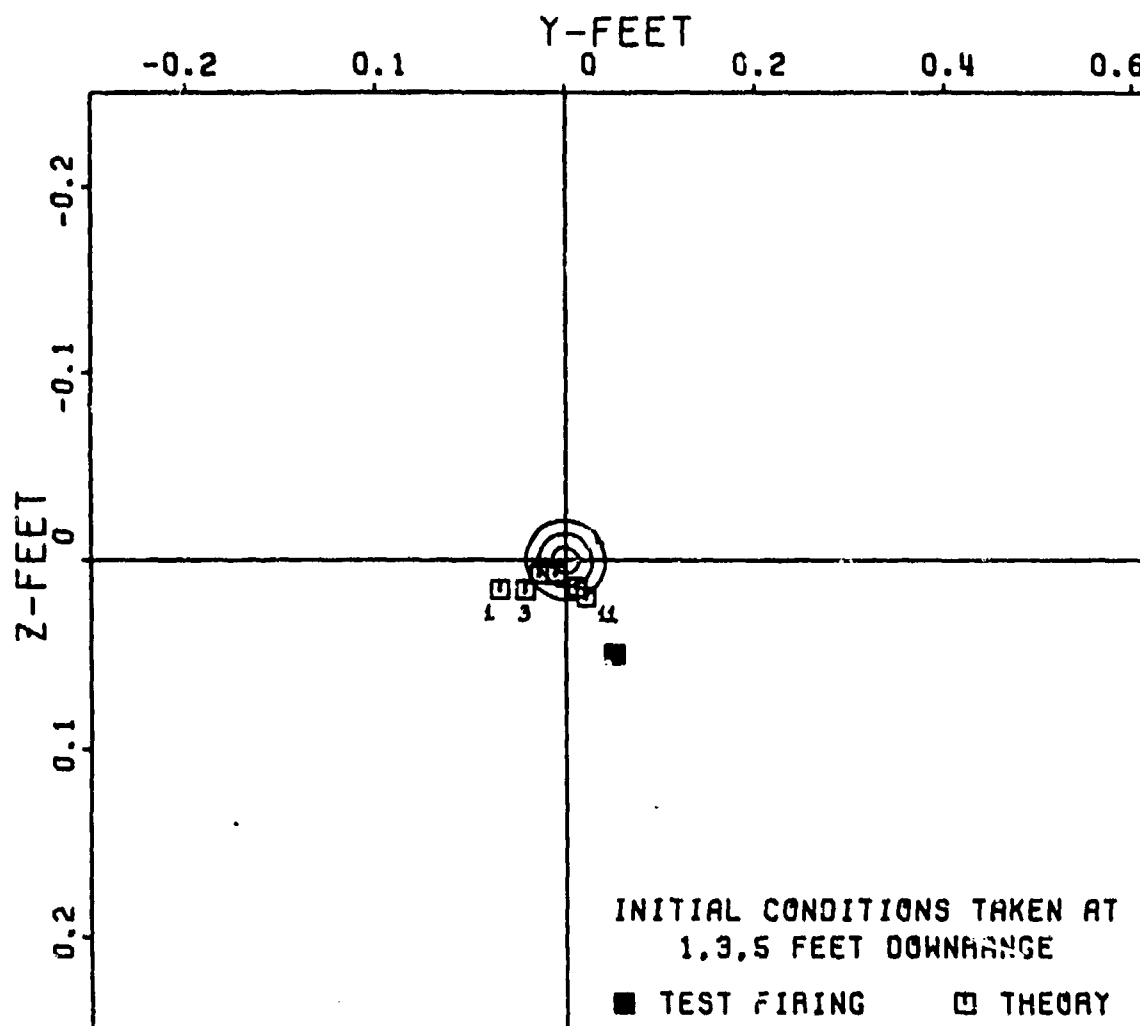


Figure 67. Dispersion: Ground Point Round 8 Test  
Firing Versus Theory, at 50 Feet Downrange

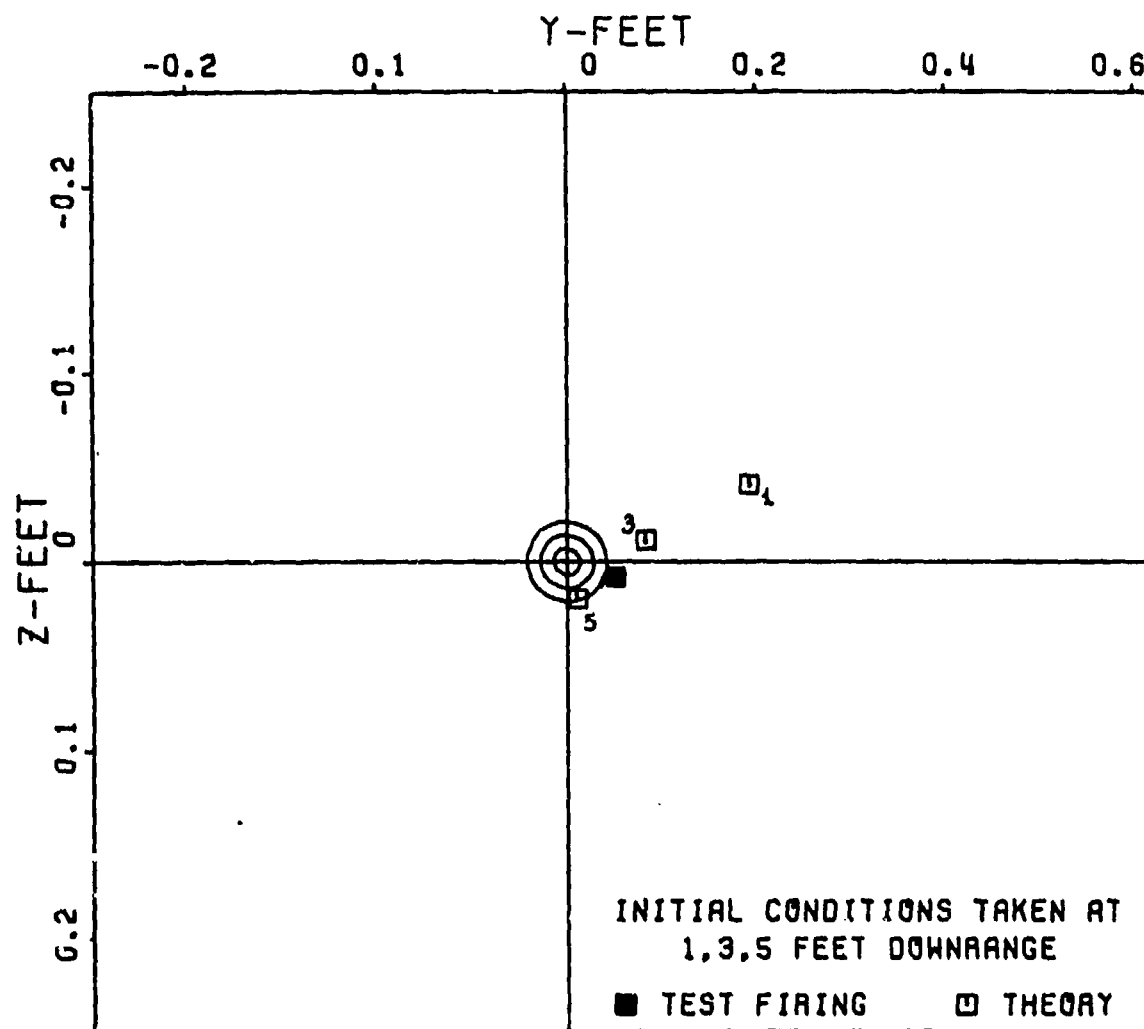


Figure 68. Dispersion: Ground Point Round 14 Test Firing Versus Theory, at 50 Feet Downrange

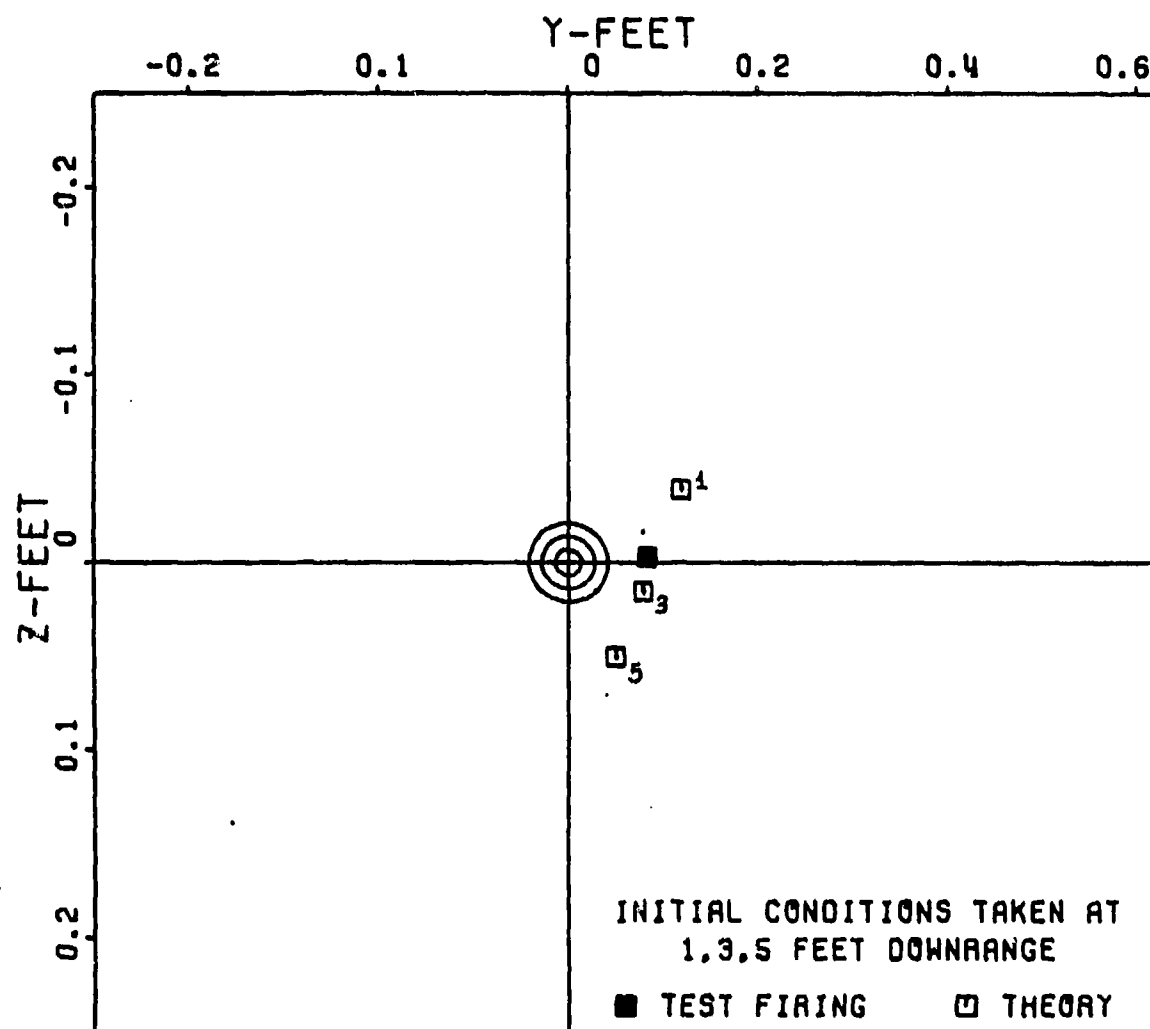


Figure 69. Dispersion: Ground Point Round 16 Test Firing Versus Theory, at 50 Feet Downrange

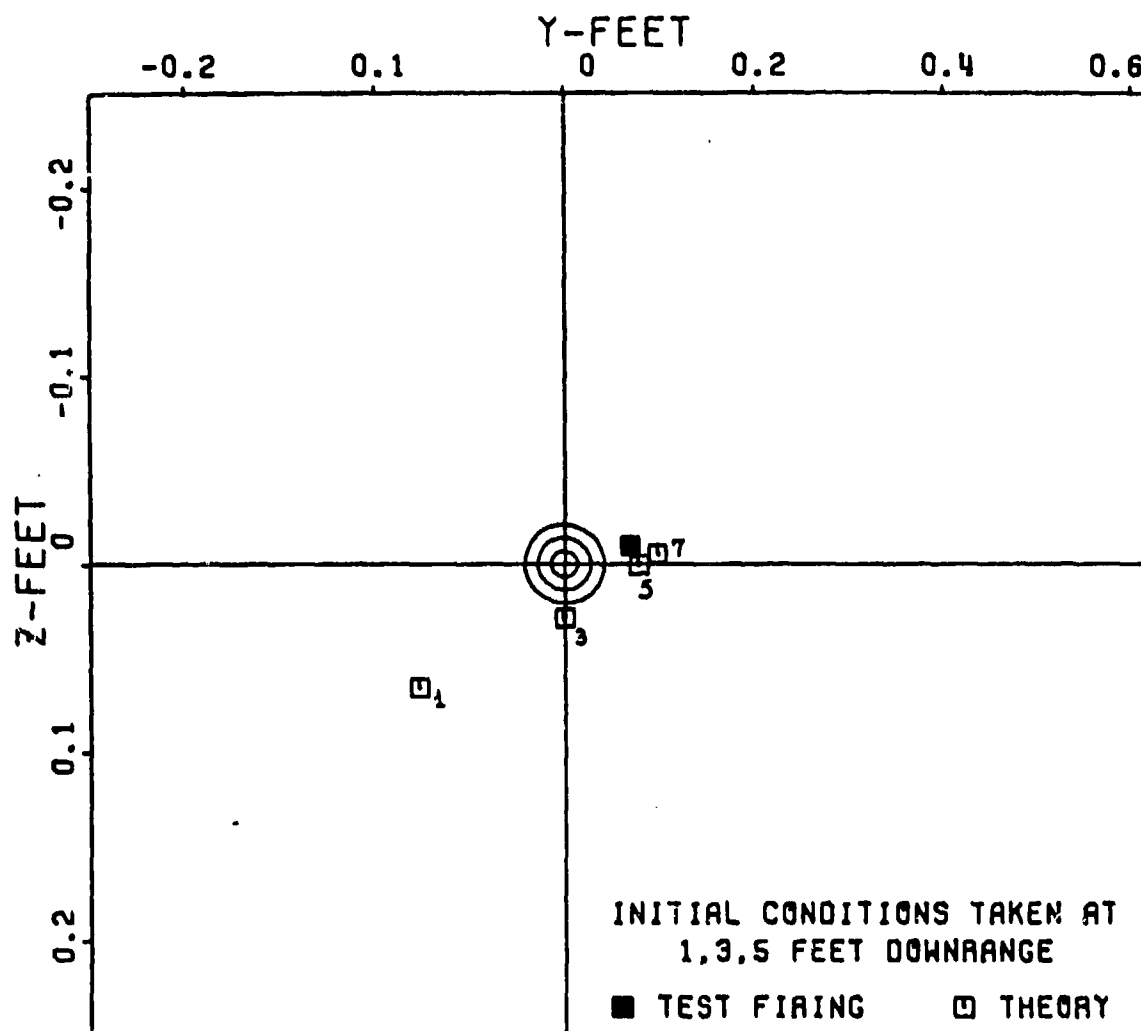


Figure 70. Dispersion: Ground Point Round 17 Test Firing Versus Theory at 50 Feet Downrange

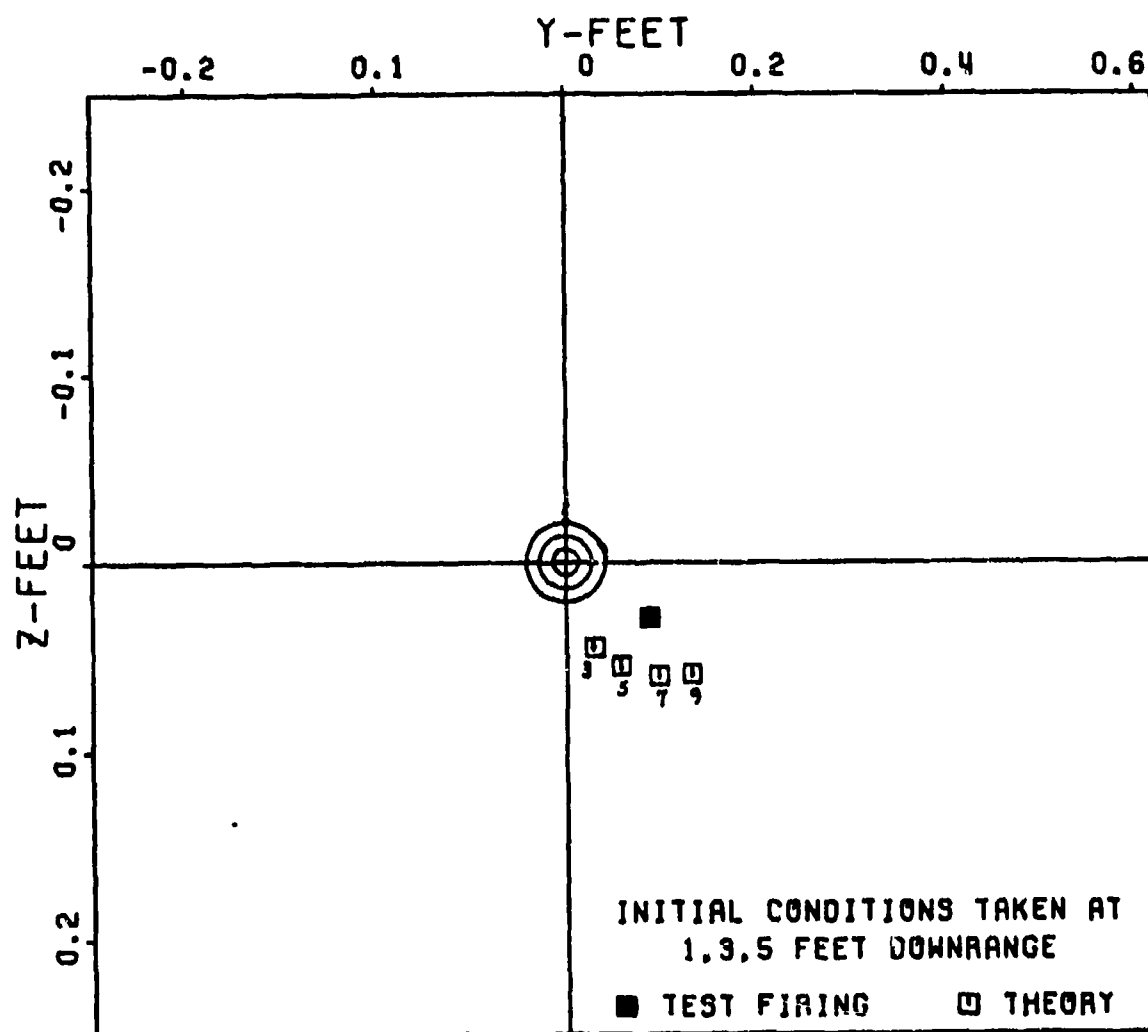


Figure 71. Dispersion: Ground Point Round 19 Test Firing Versus Theory at 50 Feet Downrange

cause disturbances to the flechette and alter the initial conditions. In addition, asymmetric sabot separation can influence the initial conditions. Therefore, the positions downrange of 1, 3, 5, and 7 feet were photographed to show the flight transition sequence. Figures 72-79 illustrate the flight transition sequence for the 8 flechette test rounds. In every sequence the sabot begins to separate, in varying degrees, 1 foot downrange. At 3 feet downrange, the sabot is nearly completely separated, but in some cases the sabot particles pose interference problems with the fins. By 5 and 7 feet downrange the sabot has completely separated and the flechette is in free flight. The correspondence between the flight transition sequence and dispersion results can be seen in each individual round. Figure 64 indicates that the initial conditions for round 4 occur somewhere between 1 and 3 feet downrange judging by the dispersion of the actual tested round. Figure 72 verifies this fact in that the sabot has separated from the flechette between 1 and 3 feet downrange. The y-coordinate in the dispersion vector does not accurately agree with the theory for this case. However, besides computational error other physical factors can influence dispersion. Contributions by fin asymmetries and other configurational asymmetries can be important but are unable to be detected or accounted for. Throughout this analysis this must be kept in mind to partially account for any discrepancy between the actual test firing and the theory and 6-D computations. Figure 65 indicates the initial conditions for round 6 occur between 3 and 5 feet downrange. Figure 73 verifies this choice showing separation occurring around 3 feet but with sabot particles very close to the fins causing possible interference and delaying the initial conditions location. The initial conditions location for round 7 is difficult to accurately choose since the y-coordinate does not accurately agree, Figure 66. It is safe to say that the initial conditions occur sometime around 3 feet and Figure 74 verifies this choice. The z-coordinate for round 8 is not as accurate as would be desired, Figure 7, but the y-coordinate indicates initial conditions occurring between 3 and 5 feet downrange. Figure 75 agrees with this choice indicated interference with the fins at 3 feet delaying the initial conditions. Initial conditions for round 14 are chosen between 3 and 5 feet downrange, Figure 68. Figure 76 indicates possible fin interference tending to verify the choice. Figures 69 and 77 indicate and verify the choice of initial conditions in the immediate vicinity of 3 feet downrange for round 16. Possible fin interference at 3 feet downrange, Figure 78, round 17, verifies a choice of initial conditions between 3 and 5 feet, Figure 70. A similar situation occurs for round 19 in Figures 71 and 79. It is often difficult to choose initial condition positions accurately due to slight discrepancies between theory and test

TCP VIEW



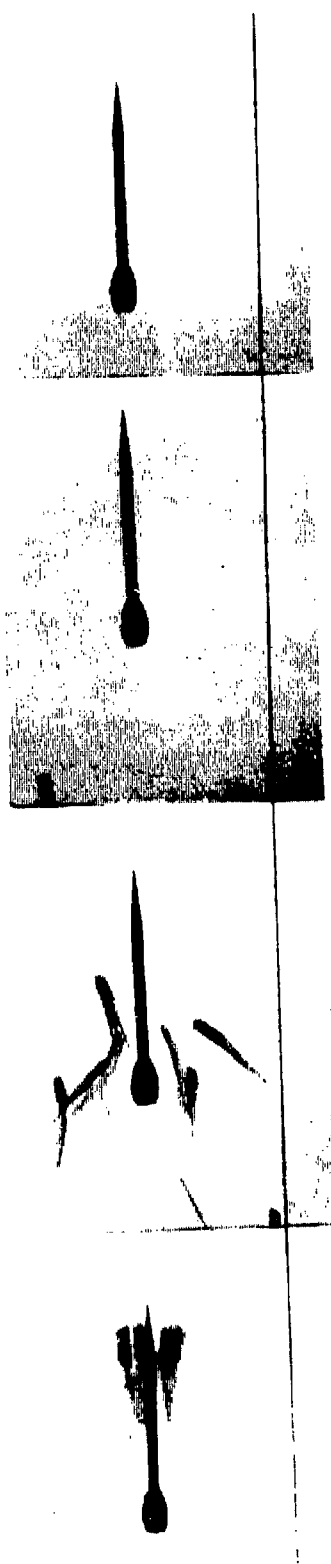
SIDE VIEW



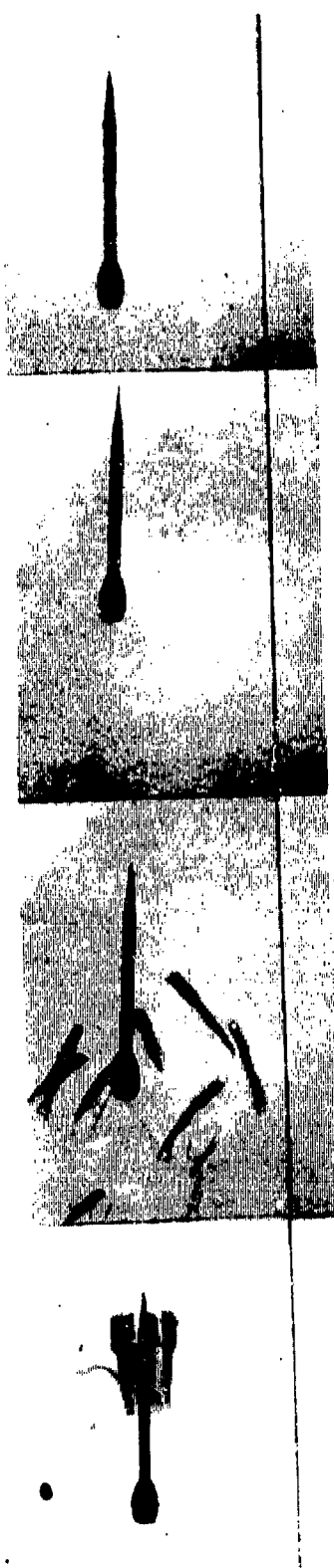
1 FT      3 FT      5 FT      7 FT  
 POSITION DOWNRANGE

Figure 72. Flight Transition Sequence  
 Round 4

TOP VIEW



SIDE VIEW



1 FT 3 FT 5 FT 7 FT  
POSITION DOWNRANGE

Figure 73. Flight Transition Sequence  
Round 6



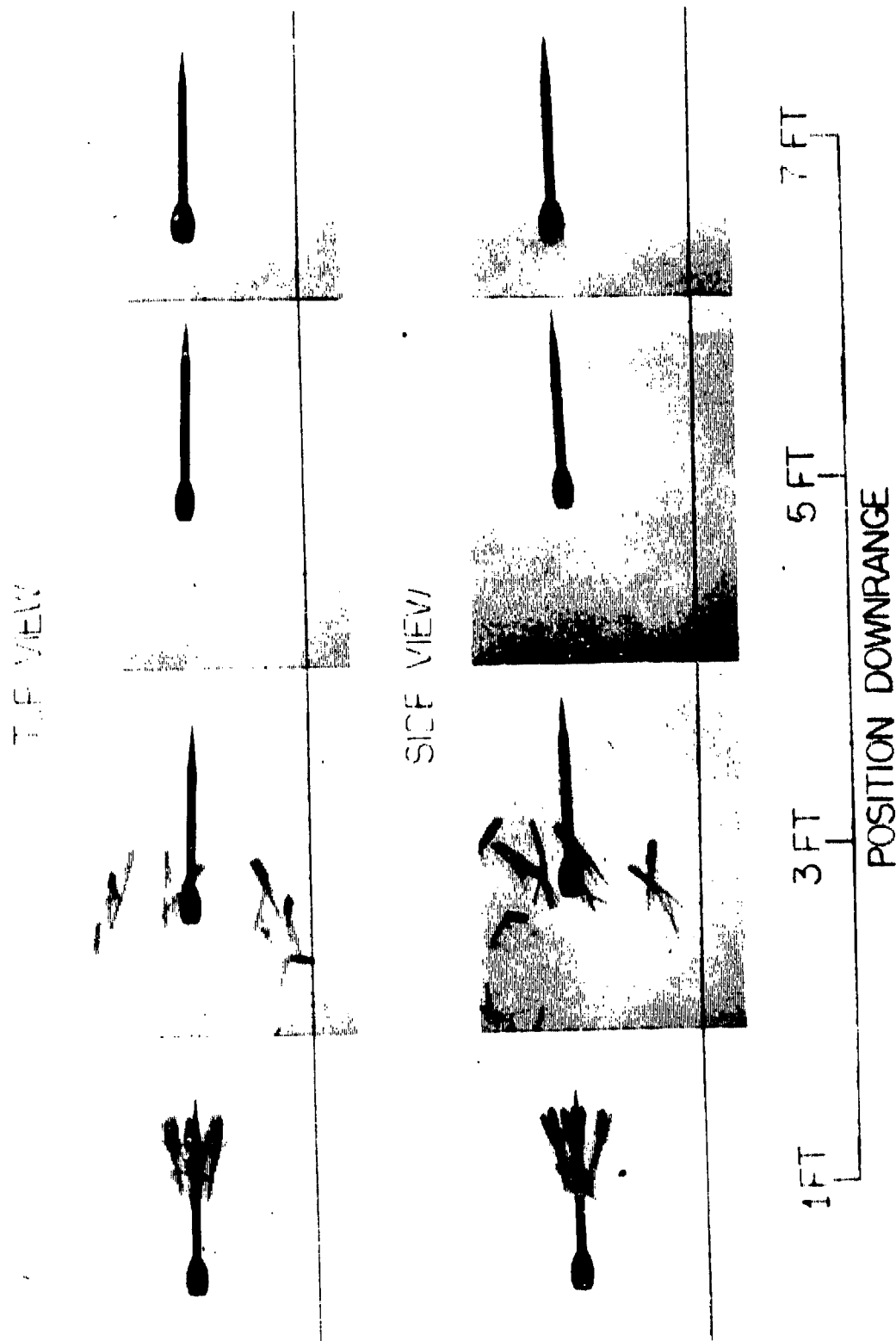
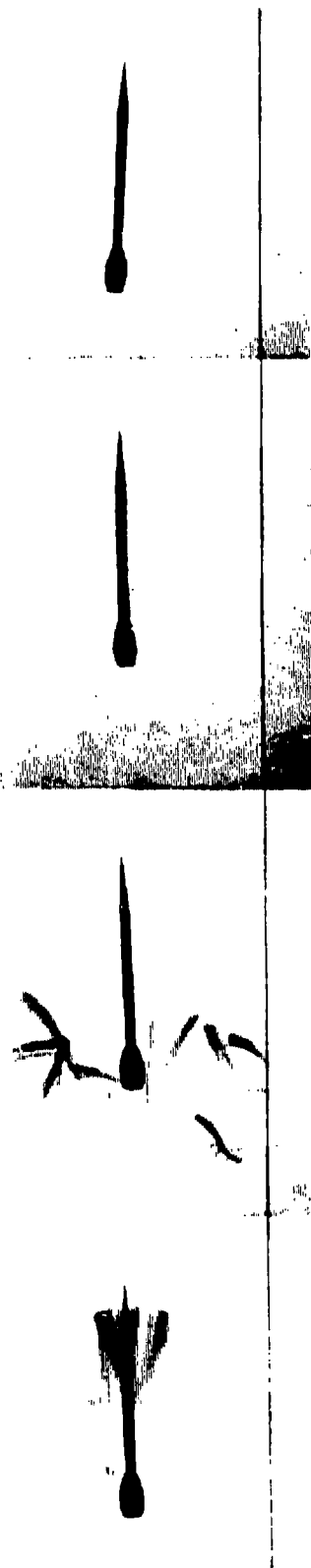
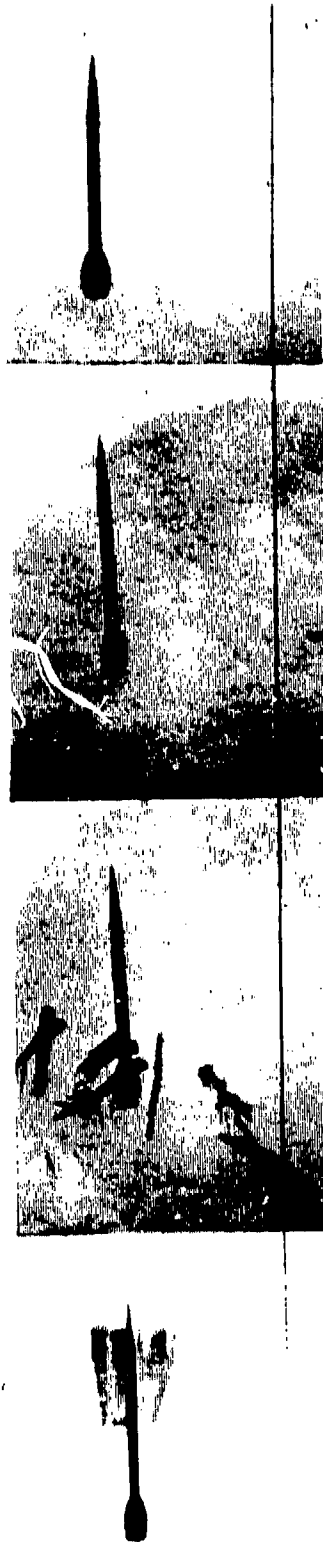


Figure 74. Flight Transition Sequence Round 7

TCP VIEW



SIDE VIEW



1 FT      3 FT      5 FT      7 FT

POSITION DOWNRANGE

Figure 75. Flight Transition Sequence Round 8

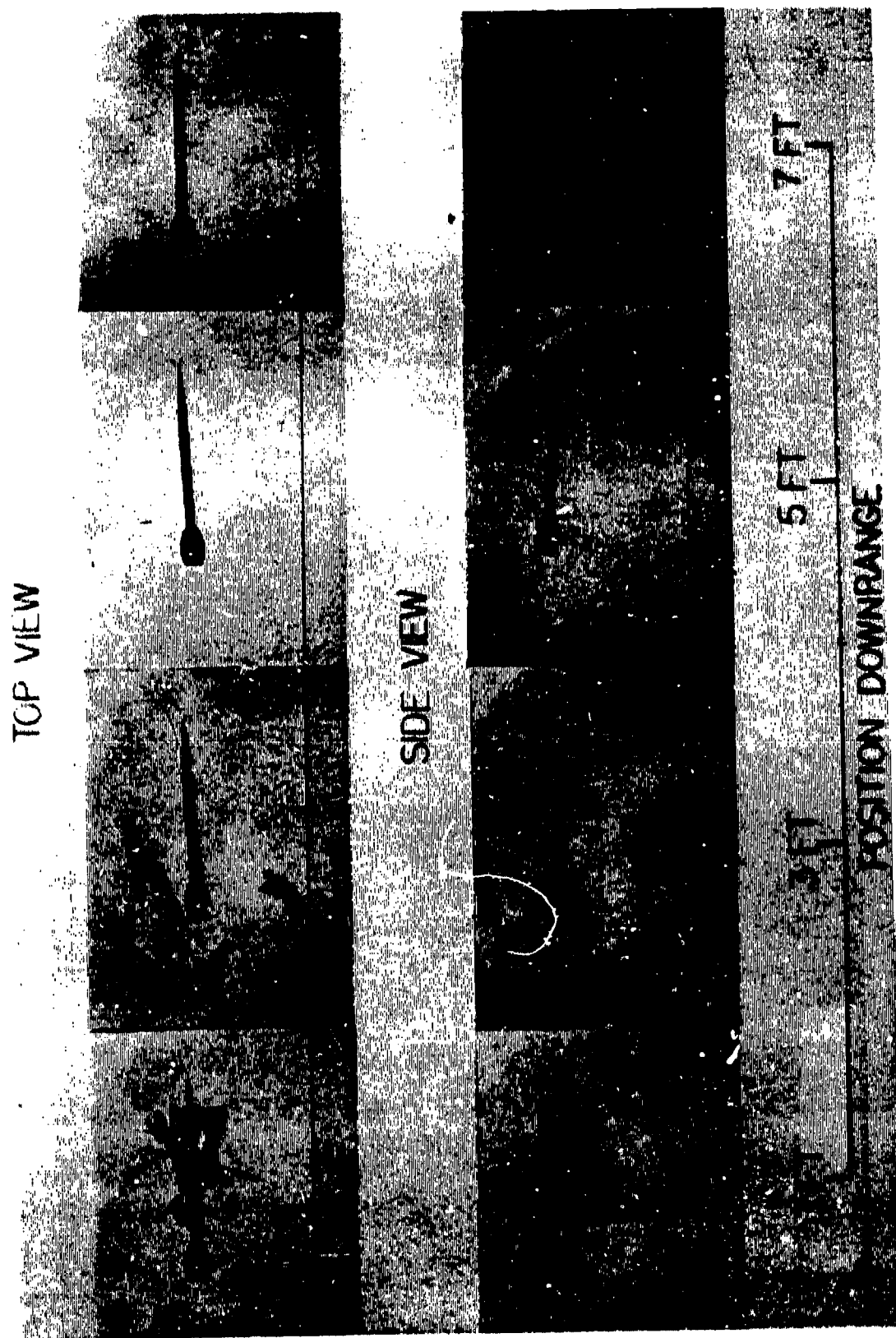
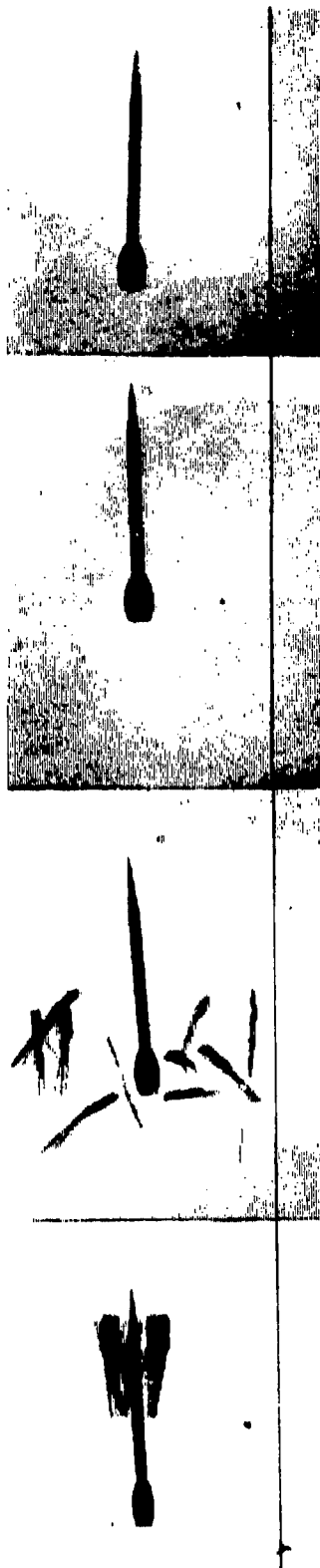
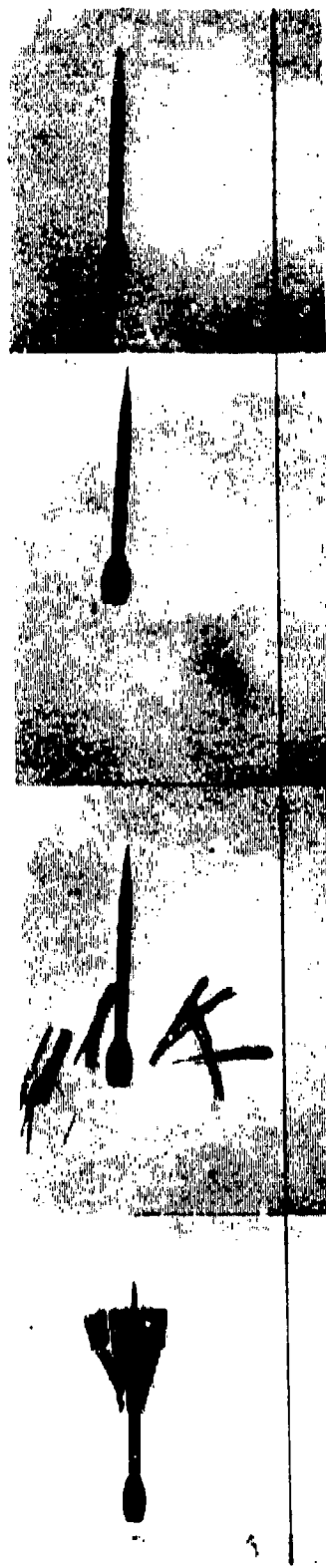


Figure 76. Flight Transition Sequence Round 14

TOP VIEW



SIDE VIEW



7 FT

5 FT

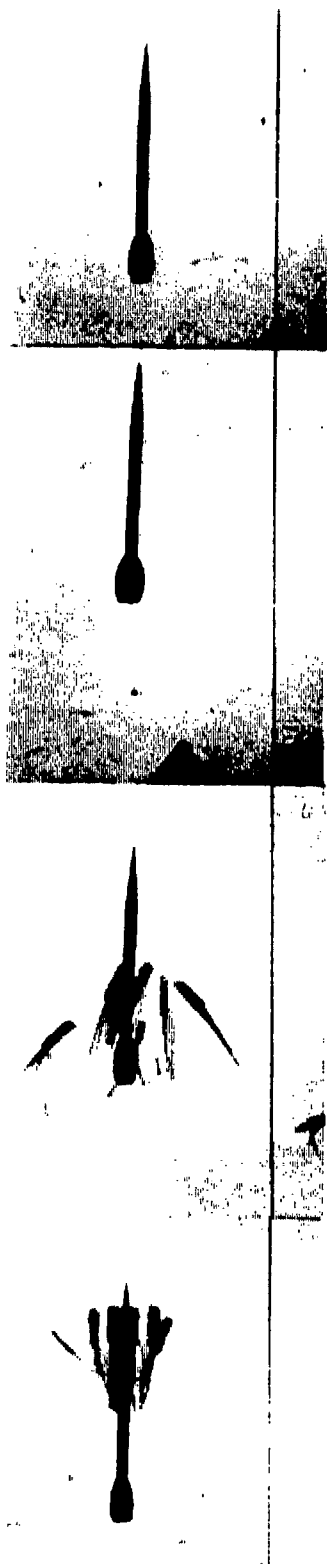
3 FT

1 FT

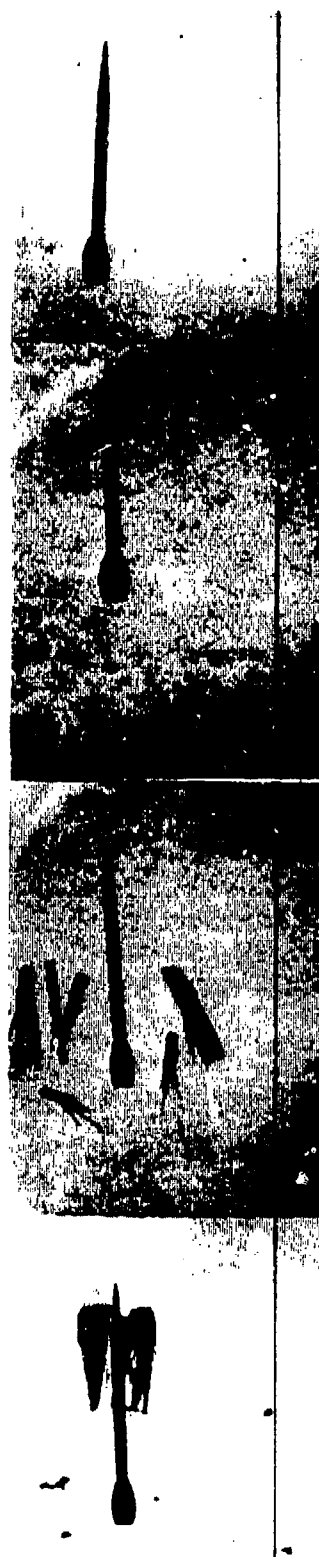
POSITION DOWNRANGE

Figure 77. Flight Transition Sequence Round 16

TCP VIEW



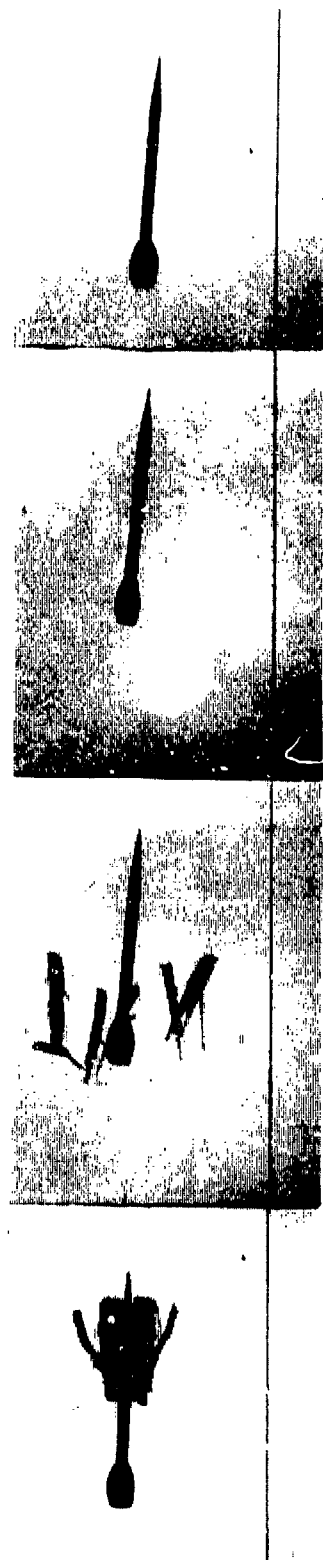
SIDE VIEW



1 FT 3 FT 5 FT 7 FT  
POSITION DOWNRANGE

Figure 78. Flight Transition Sequence Round 17

TOP VIEW



SIDE VIEW



1 FT 3 FT 5 FT 7 FT  
POSITION DOWNRANGE

Figure 79. Flight Transition Sequence Round 19

firings. However, the discrepancies are of the order 0.05 feet, which shows up large in Figures 64-71 due to the scale chosen, but is within the error expected from the validation of theory section.

The influence of sabot separation can be readily seen by inspection of Figures 72-79, 1 and 3 feet downrange. In every case, the flechette and sabot are at nearly a zero angle of attack at 1 foot, but has changed angle of attack noticeably by 3 feet downrange. This would indicate that fin interference or asymmetric sabot separation is causing the noticeable effect. It can be concluded that dispersion is dependent upon the initial conditions that the initial conditions are a function of sabot separation and that the theory can predict what the initial conditions are and where they occur.

#### DISPERSION THEORY VERSUS FIRST MAXIMUM YAW HYPOTHESIS

A popular theory to predict the dispersion of flechette is the First Maximum Yaw Hypothesis. This theory relates the dispersion magnitude to the first maximum yaw magnitude by a nearly linear relationship. Other initial conditions such as angular rate,  $\dot{\alpha}_0$ , and translational velocity,  $\dot{S}_0$  are said not to effect dispersion. To disprove this theory and strengthen the position of the theory ascribing to dispersion due to initial conditions  $\dot{S}_0, \dot{\alpha}_0, \dot{\alpha}_0$ , the First Maximum Yaw theory was applied to Frankford Arsenal data. Figure 80 shows a plot of dispersion magnitude versus first maximum yaw magnitude. Clearly no linear relationship exists between dispersion and first maximum yaw. In fact, the plotted data resembles a random shotgun blast. Figures 81, 82, and 83 employ the theory to the first maximum yaw hypothesis. Again the plot substantiates the findings of Figure 80. The disproval of the first maximum yaw hypothesis comes as no surprise since the dispersion theory contradicts it and the 6-D computations, which integrate the actual equations of motion, validated the dispersion theory. Therefore, dispersion could never accurately be predicted by a theory involving only first maximum yaw.

The influence of initial conditions,  $\dot{S}_0, \dot{\alpha}_0$ , and  $\dot{\alpha}_0$  and dispersion for the actual test firings are expected to be different from that in the validation of theory section because of the different ranges in the initial conditions. For example,  $\dot{S}_0$  only in the validation section was  $(100 + 100i)$  ft/sec. In the actual test firings,  $\dot{S}_0$  only ranged as high as 20.0 ft/sec.

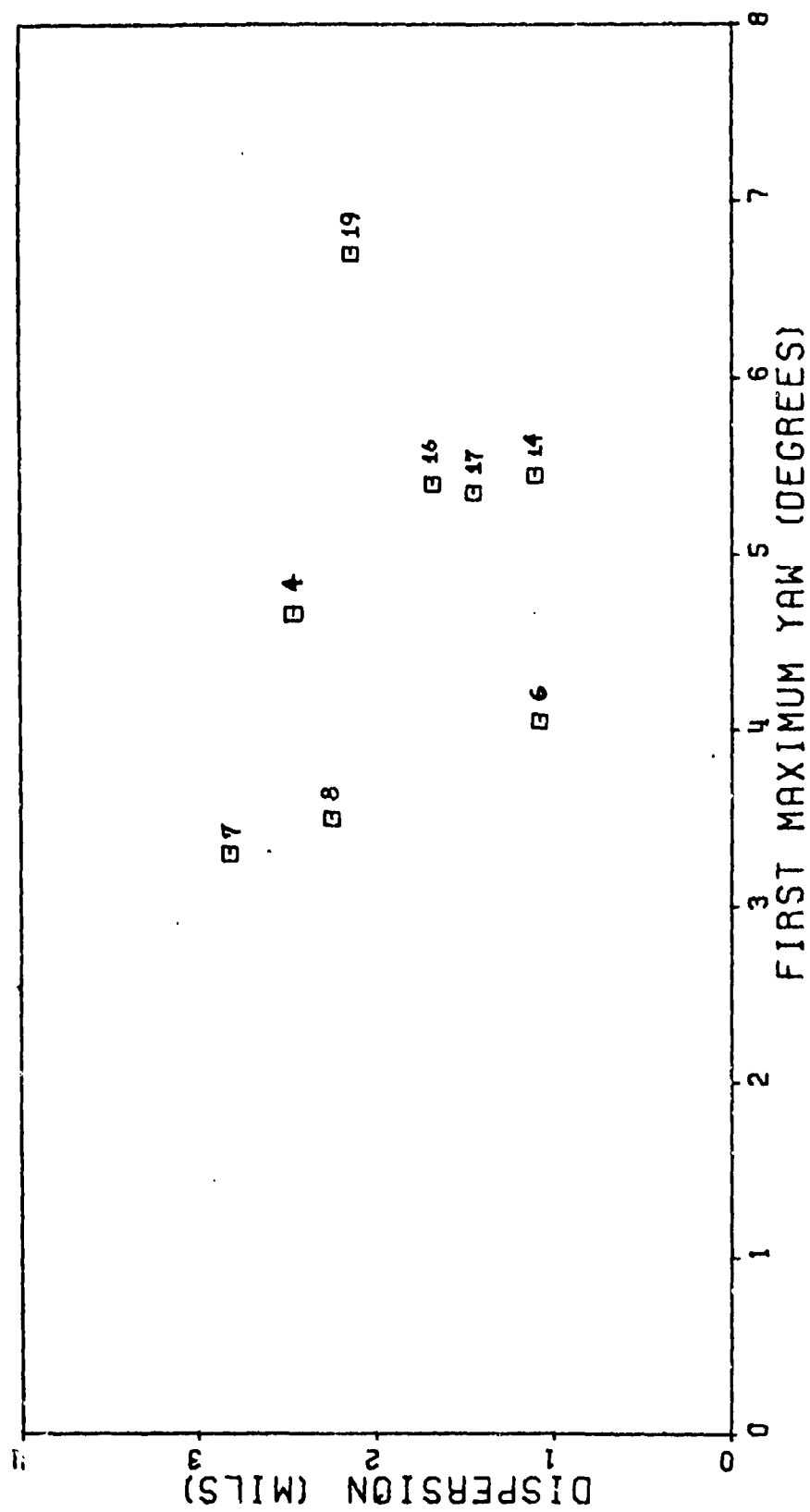


Figure 80. Dispersion Versus First Maximum Yaw,  
Frankford Test Firing Results



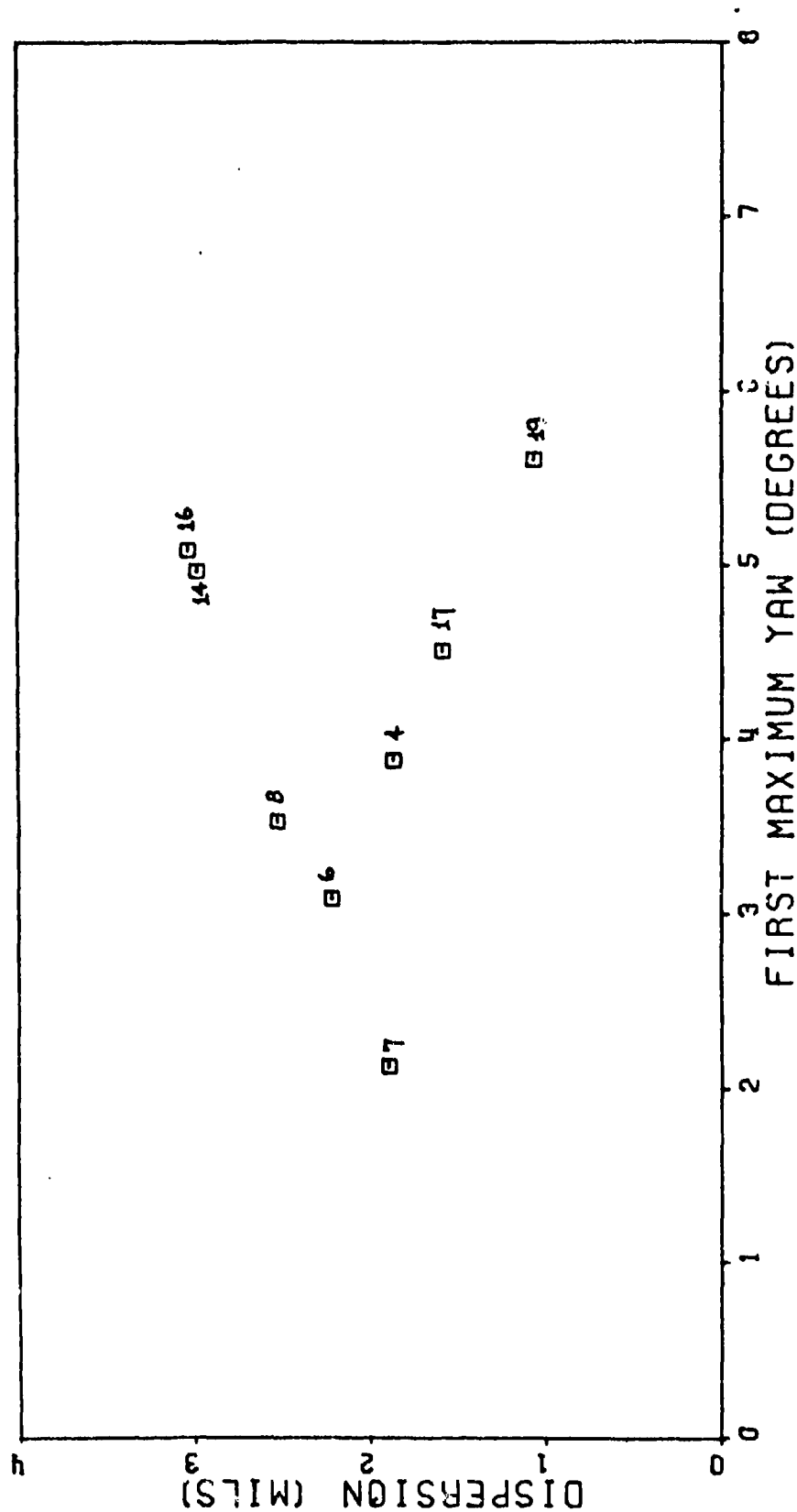


Figure 81. Dispersion Versus First Maximum Yaw, Theory-Initial Conditions, 1 Foot Downrange

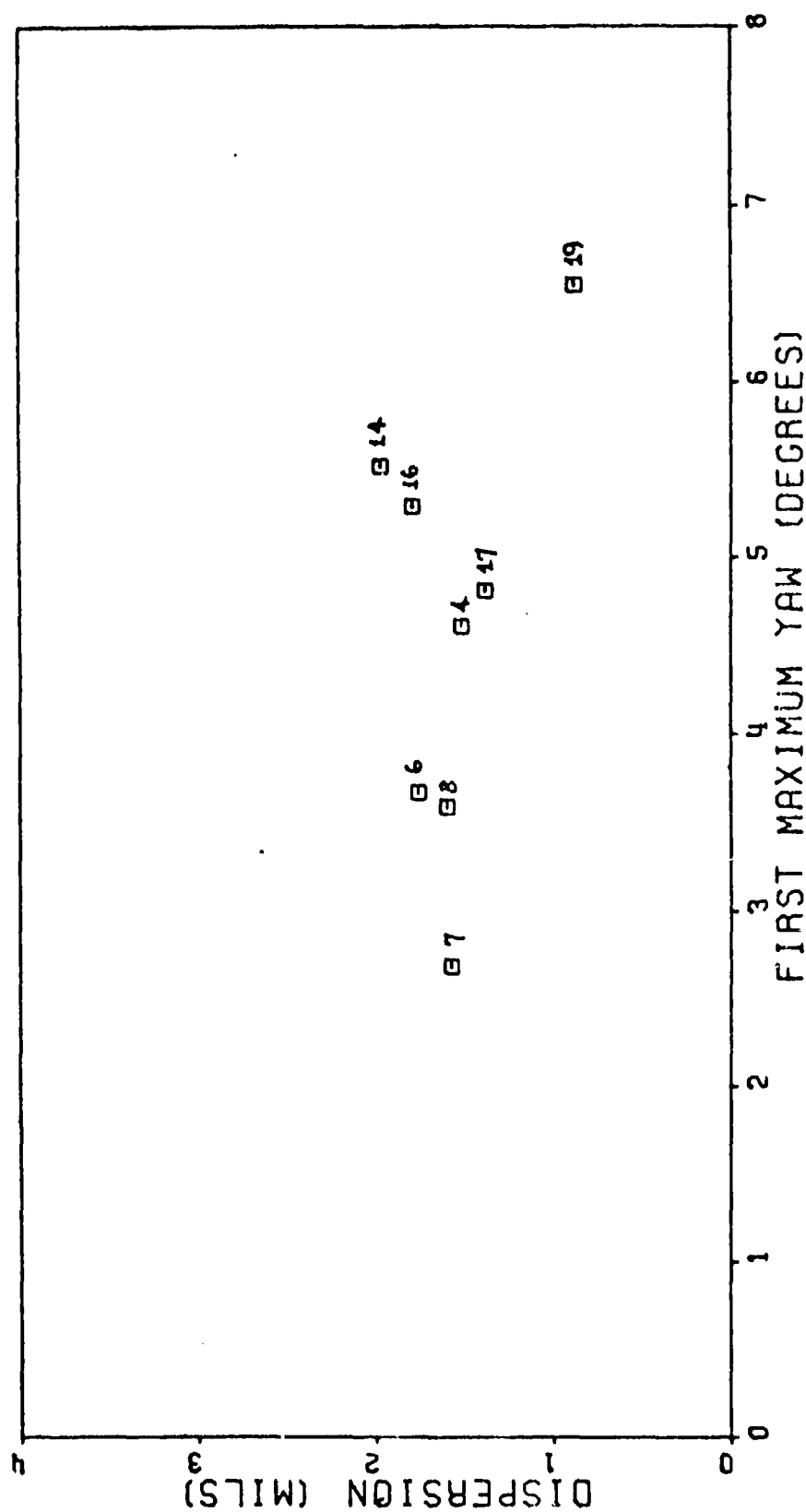


Figure 82. Dispersion Versus First Maximum Yaw, Theory-Initial Conditions, 3 Feet Downrange

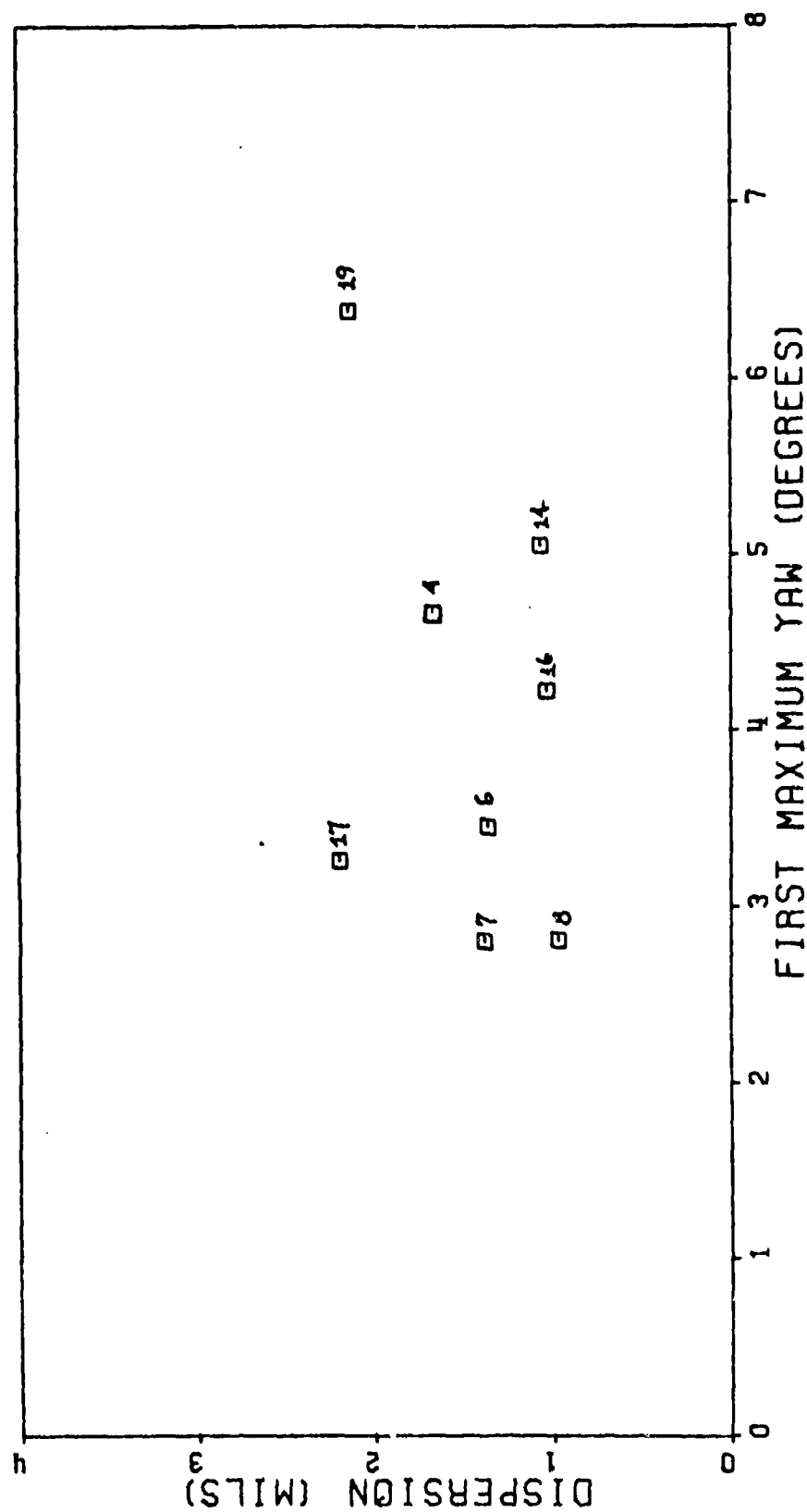


Figure 83. Dispersion Versus First Maximum Yaw, Theory-Initial Conditions, 5 Feet Downrange

Of course, the large value was only to validate the theory. However,  $\vec{S}_0$  is a very important contributor to dispersion. In the reduced equation 24, employed to calculate the theory column in Table 22,

$$\overrightarrow{J.A.} (\text{mils}) = 1000 \left[ \frac{\vec{S}_0}{x} + \frac{\vec{S}_0}{u} - \frac{I_y}{\text{mud}} A \left( \vec{\alpha}_0 - \vec{\alpha}_0 \frac{ipL_x}{I_y} \right) \right]$$

for round 4, 1 foot downrange,

$$1000 \frac{\vec{S}_0}{u} = (1.1007 + 1.9134i) \text{ mils}$$

where as,

$$\overrightarrow{J.A.} = (1.329 - 1.302i) \text{ mils}$$

Since this is typical of the 8 rounds tested,  $\vec{S}_0$  has a profound effect on dispersion for these rounds.

Similarly, for this particular case,

$$1000 \frac{\vec{S}_0}{x} = (0.0160 + 0.0004i) \text{ mils}$$

$$1000 \vec{\alpha}_0 \frac{ipL_x A}{\text{mud}} = (-0.01437 + 0.00214i) \text{ mils}$$

$$-1000 \vec{\alpha}_0 \frac{I_y A}{\text{mud}} = (-0.206075 - 1.383672i) \text{ mils}$$

Obviously,  $\vec{S}_0$  and  $\vec{\alpha}_0$  are by far the greatest contributors to dispersion for this case. Inspection of all the other 31 cases in Table 22 agrees with this general pattern.  $\vec{S}_0$  can be nearly eliminated, of course, by accurate setup of the test equipment so that the gun barrel is set exactly at coordinates (0,0). Any  $\vec{S}_0$  then would occur from displacement due to the blast.

Figure 84 illustrates the dependence of the Jump Angle, and hence dispersion, upon angular rate and angle of attack.

Although  $\vec{S}_0$  and  $\vec{\alpha}_0$  contribute the most to the Jump Angle, the combination of  $\vec{S}_0$  and  $\vec{\alpha}_0$  can have a noticeable influence. From the test firings,  $\vec{S}_0$  was found to have a negligible effect on dispersion. Therefore, it is neglected in Figure 84 to simplify the plot. It is evident from Figure 84 that various combinations of  $\vec{\alpha}_0$  and  $\vec{\alpha}_0$  yield zero dispersion. It is possible that large values of  $\vec{\alpha}_0$  and  $\vec{\alpha}_0$  can combine to yield zero dispersion; an impossibility with the first maximum yaw hypothesis. If  $\vec{\alpha}_0$  and  $\vec{\alpha}_0$  are able to balance to give zero dispersion, then this idea can be expanded to include the entire equation.

The governing equation used throughout this dispersion analysis section is:

$$\vec{J.A.} = 1000 \left[ \frac{\vec{S}_0}{x} + \frac{\vec{S}_0}{u} - \frac{I_y}{mud} A \left( \vec{\alpha}_0 - \vec{\alpha}_0 \frac{ipL_x}{L_y} \right) + \frac{ig}{2} \left( \frac{x}{u^2} \right) \right]$$

Eliminating the constant gravity term,

$$\vec{J.A.} = 1000 \left[ \frac{\vec{S}_0}{x} + \frac{\vec{S}_0}{u} - \frac{I_y}{mud} A \left( \vec{\alpha}_0 - \vec{\alpha}_0 \frac{ipL_x}{L_y} \right) \right]$$

Setting  $\vec{J.A.}$  to zero, the idea behind Figure 84 is expanded to include  $\vec{S}_0$ ,  $\vec{S}_0$ .

$$\frac{\vec{S}_0}{x} + \frac{\vec{S}_0}{u} = \frac{I_y}{mud} A \left( \vec{\alpha}_0 - \vec{\alpha}_0 \frac{ipL_x}{L_y} \right)$$

rearranging

$$m \left[ \vec{S}_0 \left( \frac{u}{x} \right) + \vec{S}_0 \right] = \frac{A}{d} (\vec{\alpha}_0 L_y - \vec{\alpha}_0 ipL_x)$$

A dimensional analysis of the equations finds that both sides have units of momentum. Going one step farther it can be said that to obtain zero dispersion: initial transverse momentum = initial momentums that causes dispersion. The size of initial conditions can be huge, Figure 84, but if they can combine to balance, zero dispersion results. The way the initial conditions combine, determine the magnitude of the imbalance or

dispersion. It should be noted that this dispersion discussed is round to round dispersion and that the inconsistency of the momentum imbalance from round to round causes a dispersion pattern (a set of rounds). The next section will highlight this principle in the evaluation of physical factors affecting dispersion.

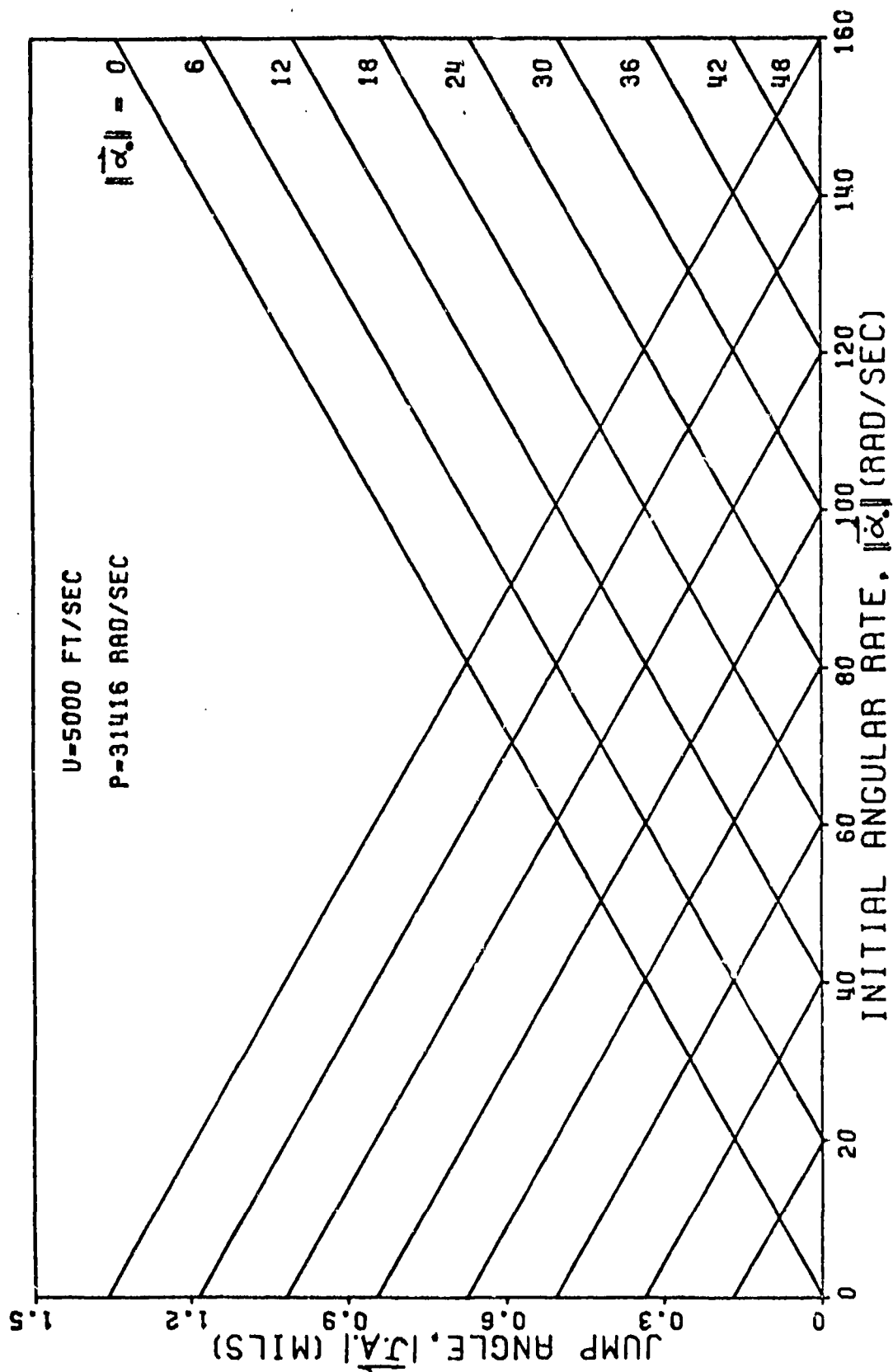


Figure 84. Jump Angles For Various Initial Conditions

## SECTION VI

### PHYSICAL EVALUATION OF DISPERSION

Initial momentum imbalance has been shown to cause dispersion. Initial conditions determine the magnitude of the imbalance. What causes these initial conditions to occur is the subject of this final section. Initial conditions occur somewhere between 0 and 5 feet downrange to different degrees of magnitude due to various conditions. These conditions are:

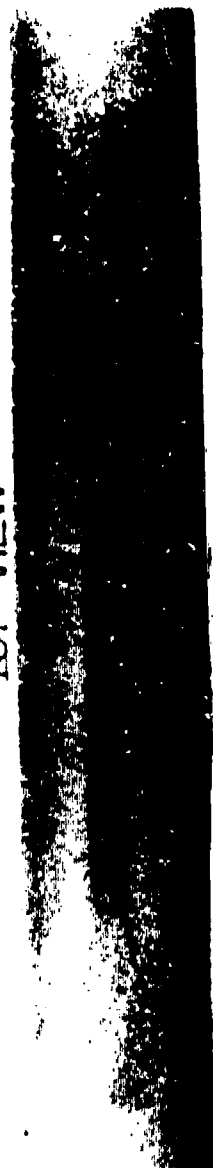
1. Fin or body asymmetry
2. In-bore mal-alignment
3. Asymmetric blast
4. Asymmetric sabot separation
5. Sabot-fin interference
6. Fin or body damage

Fin or body asymmetries can cause dispersion magnitudes to range as much or greater than those in the Validation of Theory section for aerodynamic asymmetries. These asymmetries can be overcanted or bent fins, damaged nose cone, or even body deformities. Figure 85 which shows in-bore mal-alignment also shows a slightly bent body, concave downward. In-bore mal-alignment can be attributed to warping and/or the entire flechette at some angle of attack. Clearly, if this flechette were fired, the in-bore angle of attack would produce an  $\vec{\alpha}_0$  outside the gun barrel even before sabot separation. With the flechette at some angle of attack, the blast can cause a large  $\vec{\alpha}_0$  and an  $\vec{S}_0$  and  $\vec{S}_0$ . The blast itself is a chief catalyst in causing the initial conditions. An asymmetric blast can indeed impart influence on the initial conditions, but a symmetric blast can also. Given an initial angle of attack due to some disturbances the symmetric blast can cause significant  $\vec{\alpha}_0$ ,  $\vec{\alpha}_0$ ,  $\vec{S}_0$  and  $\vec{S}_0$ . Figure 86 shows a typical blast region with the flechette outlined in the picture. The momentum principle discussed in the previous section goes hand-in-hand with this blast region. It is here that the transverse and angular-momentum is imparted to the flechette. Figure 87 illustrates a typical flechette in the blast region. Coming out of the barrel at some angle of attack, the blast catches the flechette and induces some angular rate. At the



same time, the flechette is translated laterally giving an  $\dot{S}_0$  and  $\dot{S}_0$ . If these contributions cancel each other out; that is, if initial transverse momentum equals initial angular momentum then the dispersion is zero. If they do not cancel, dispersion results. The sketch is highly simplified in that the blast itself is all-engulfing as in Figure 86. Of course, the transition sequence of sabot separation, fin interference, and possible fin damage must not be forgotten. The transition sequence occurs in the blast region, however, and is not considered separate from the blast. When separation occurs, the sabot particles are apt to interfere with the fin section and cause possible damage. Once the sabot has separated and cleared the fins, the blast has had its greatest effect and the initial conditions can be determined. After the flechette has moved down-range, it assumes a supersonic free flight, Figure 88.

TOP VIEW



SIDE VIEW



Figure 85. Flechette In-Bore Position



Figure 86. Typical Flechette Blast Region

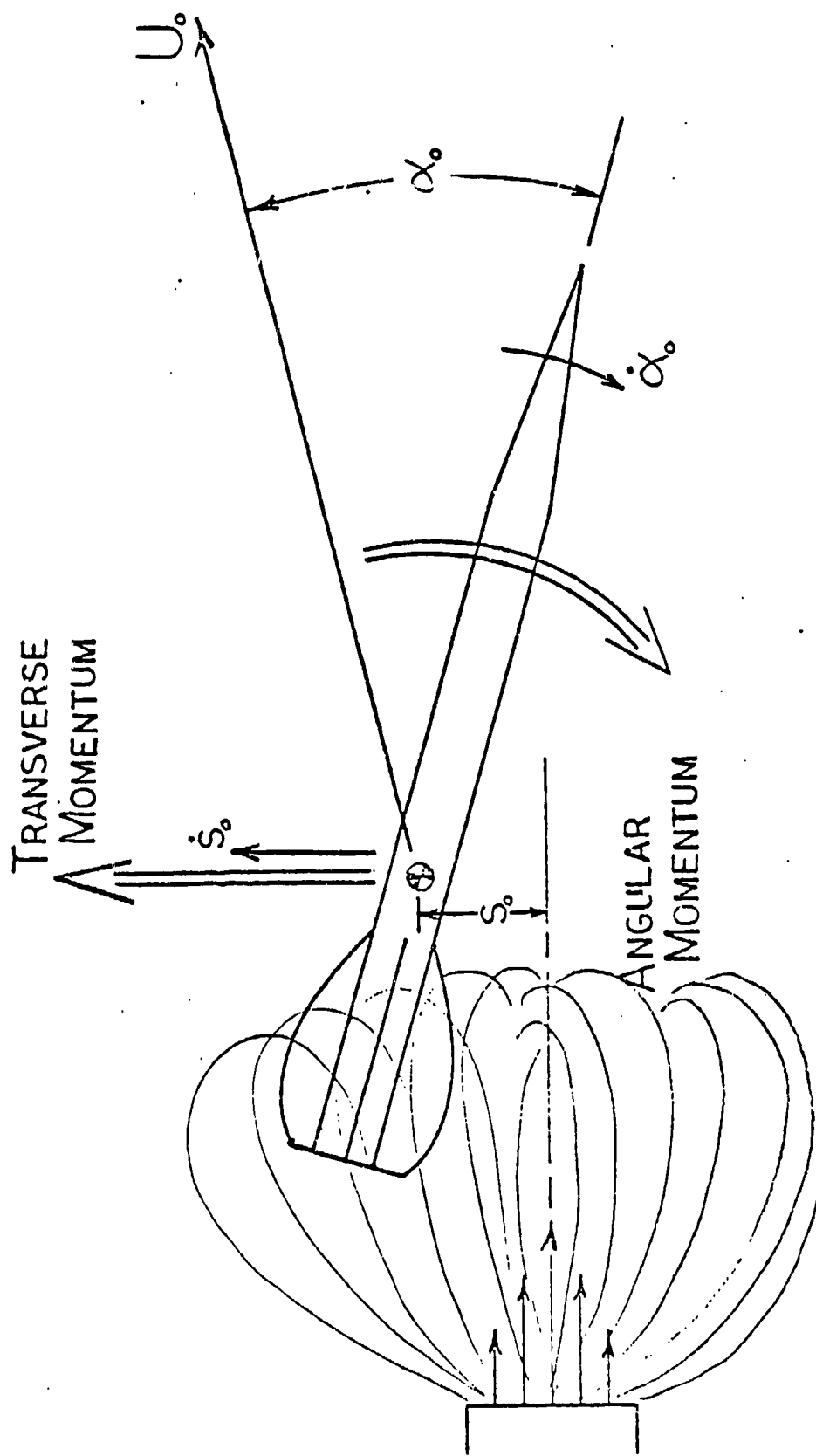


Figure 87. Muzzle Blast Effects

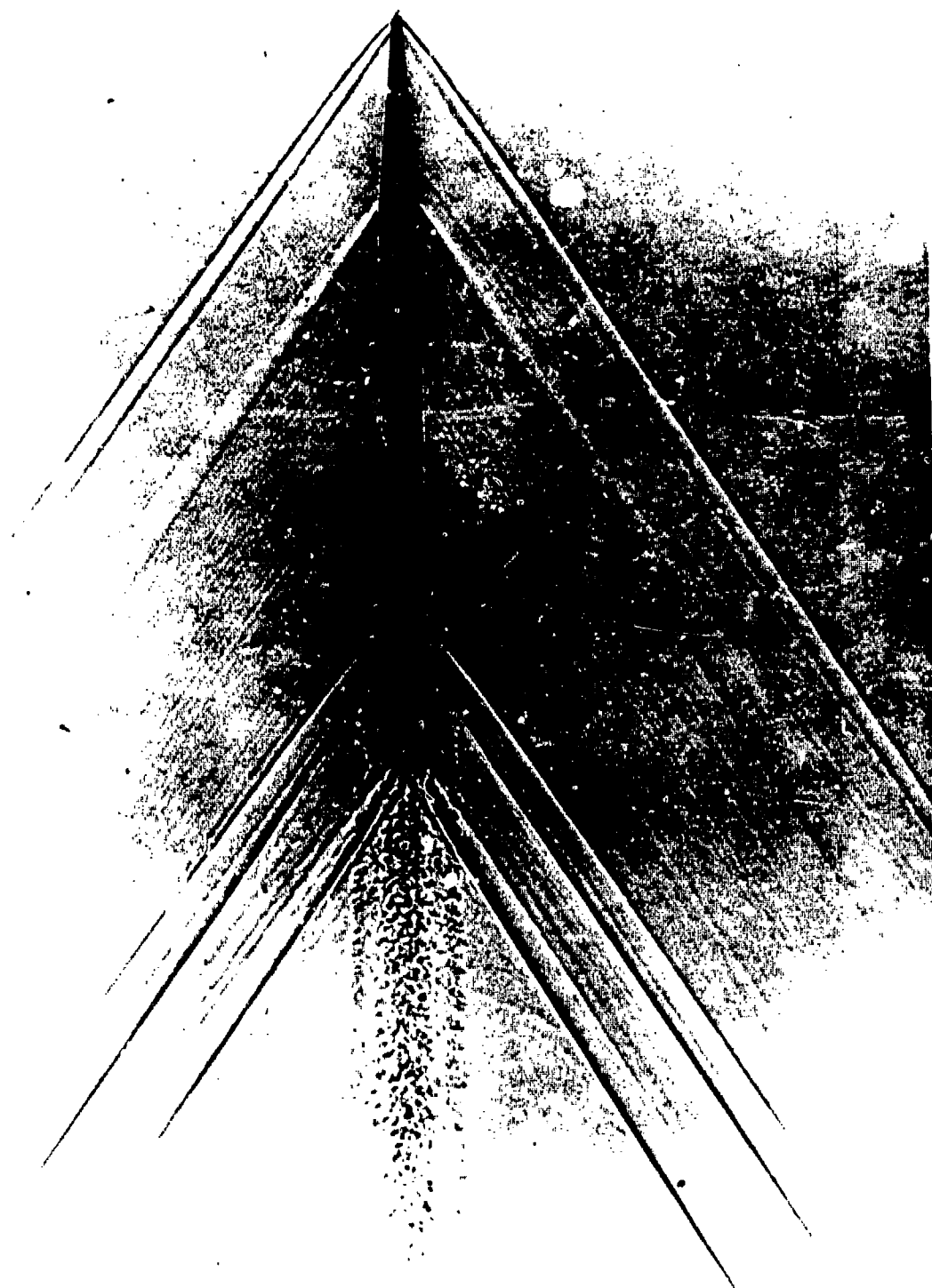


Figure 88. Supersonic Free Flight, Ground Point Flechette

## SECTION VII

### CONCLUSIONS

A complete Jump and Dispersion Theory has been developed for free flight vehicles. Three governing equations have been determined to accommodate high, low, and very low roll rates. The theories were found to be accurate with six-degree-of-freedom numerical computations of the equations of motion and therefore reliably predict the jump and dispersion of flechettes. The theory validation included 201 case runs in four phases. The first phase validated the theory with respect to restoring and damping moments. The effect of these moments on dispersion was found to depend on the initial conditions. The second phase validated the theory with respect to Magnus forces and moments. The effect of Magnus was found to be very small and not of any consequence unless the total dispersion of any given round was of the same order of magnitude as the Magnus effect. Phase three validates the theory with respect to aerodynamic asymmetries and roll rate. All three theories were validated in this phase and found quite accurate considering the large dispersions encountered. Aerodynamic asymmetries causing a trim angle of 1 degree had little effect on the dispersion of flechettes. Slower rolling bodies were shown to have, in general, increasingly larger dispersion values as roll rate decreased. It can be concluded that for free flight vehicles prone to aerodynamic asymmetries and fin damage, a high roll rate is essential to lower dispersion and increase accuracy. The fourth phase validates the theory with respect to gravity. The theory indicates a lateral contribution to dispersion from gravity in addition to the obvious vertical contribution. For the flechette, the lateral contribution was found to be minimal and was neglected in this analysis.

Free flight data was obtained from Frankford Arsenal to correlate with the theory. Angular and translational data was fitted and put into initial condition form. The initial condition data was applied to the theory and compared to target data for the rounds tested. The theory was found to agree favorably in magnitude with the test firings. As a result, the method used to analyze the data can be considered a valid method. Photographs of the test firings were taken to include the flight transition sequence in the blast region. The pictures further verify the analysis method of the initial conditions by allowing agreement between the chosen initial conditions and the position downrange where they were selected.

The evaluation of the free flight dispersion against the theory also disproves the First Maximum Yaw hypothesis. A plot

of jump angle versus first maximum yaw of actual test data produced a shotgun blast pattern with no relationship evident between dispersion and first maximum yaw. In addition, a plot of jump angle versus angular rate for various initial angles of attack indicates an infinite amount of combinations of initial conditions to yield a given jump angle. Thus, zero dispersion has an infinite set of possible initial conditions. It was found for zero dispersion that a unique physical condition holds: to obtain zero dispersion, initial transverse momentum = initial angular momentum. These momenta are imparted to the flechette in the blast region where the body and especially the fins are subject to disturbances. Momentum imbalance is the reason dispersion occurs. The initial conditions only determine the magnitude of imbalance or dispersion. This dispersion is round to round dispersion. Inconsistency in the imbalance results in a dispersion pattern. The initial conditions were found not to occur until after the sabot separation and the blast has had its greatest effect. The factors causing the existence of initial conditions were found to be not only the blast and sabot separation sequence, but also fin and body asymmetries and bore mal-alignment. In order to decrease dispersion, these physical factors causing initial conditions must be kept at a minimum. The most important aspect would be to protect the fins from asymmetries, damage, and interference from the separating sabot. These initial conditions can never realistically be eliminated but if kept minimal, dispersion is reduced.

## APPENDIX

This appendix contains mass parameters and stability coefficients for the Ground Point Flechette. Table A-1 lists values for mass, diameter, axial and transverse moments of inertia. Figures A-1 through A-8 present stability coefficients used in this analysis versus Mach number.  $C_{z_\alpha}$ ,  $C_{M_\alpha}$ ,

$C_{M_q} + C_{M_\alpha}$  were provided by Frankford Arsenal.  $C_{z_{p\beta}}$ ,  $C_{M_{p\beta}}$ ,

$C_{Y_E}$ ,  $C_{Z_E}$ ,  $C_{M_E}$ ,  $C_{N_E}$  were nominal values of the coefficients following the same trends of  $C_{z_\alpha}$  and  $C_{M_\alpha}$  for Mach number.

$C_{M_\alpha}$  and  $C_{M_q}$   $C_{M_\alpha}$  were verified in the University of Notre Dame supersonic wind tunnel (Reference 16).

TABLE A-1

### FLECHETTE PARAMETERS

mass = 0.000046 slugs

diameter = 0.006 feet

$I_x$  = 0.000000000217 slugs-ft<sup>2</sup>

$I_y$  = 0.000000036421 slugs-ft<sup>2</sup>



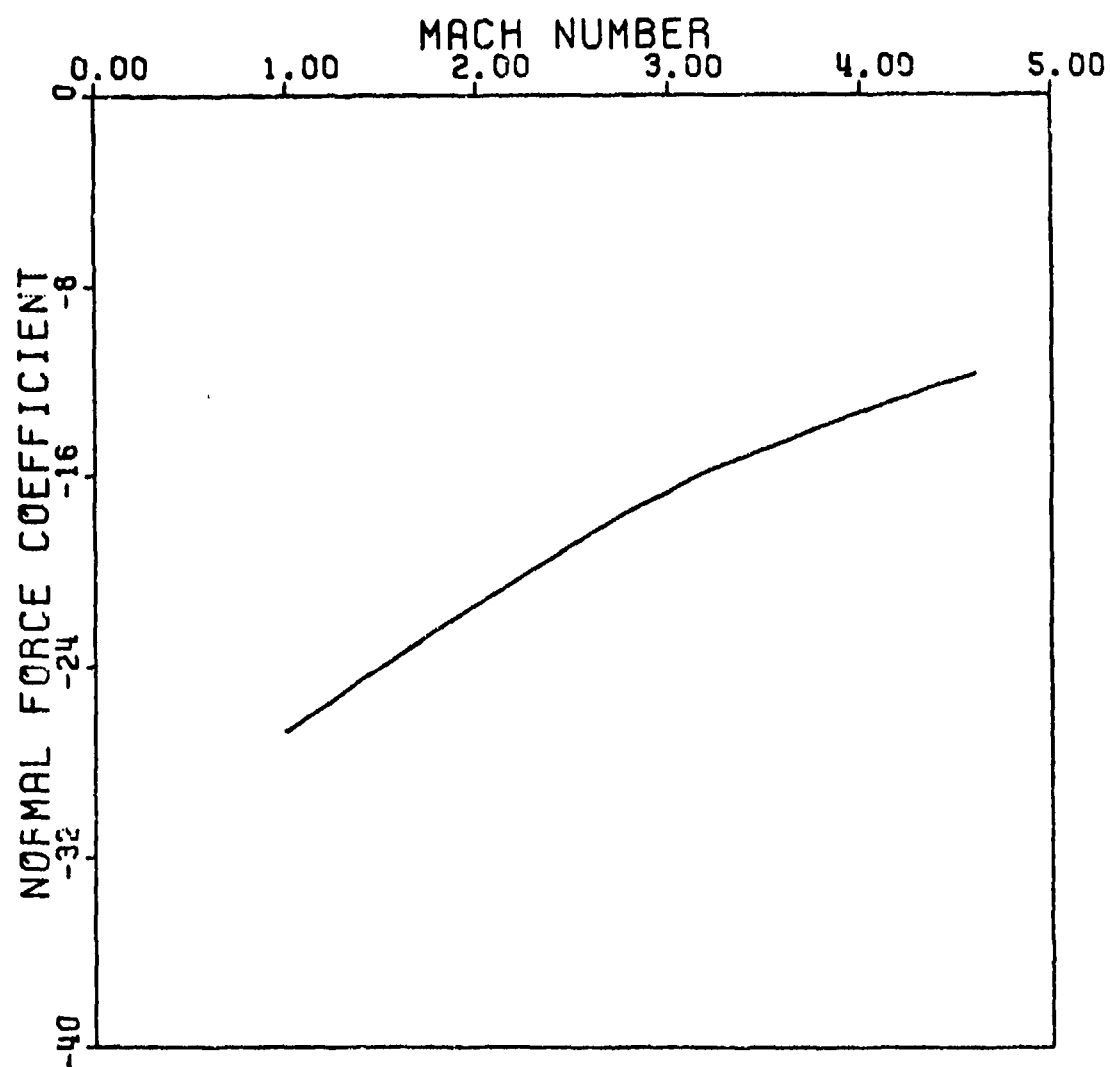


Figure A-1.  $C_{z_{\alpha}}$  Versus Mach Number  
Producibility Ground Point

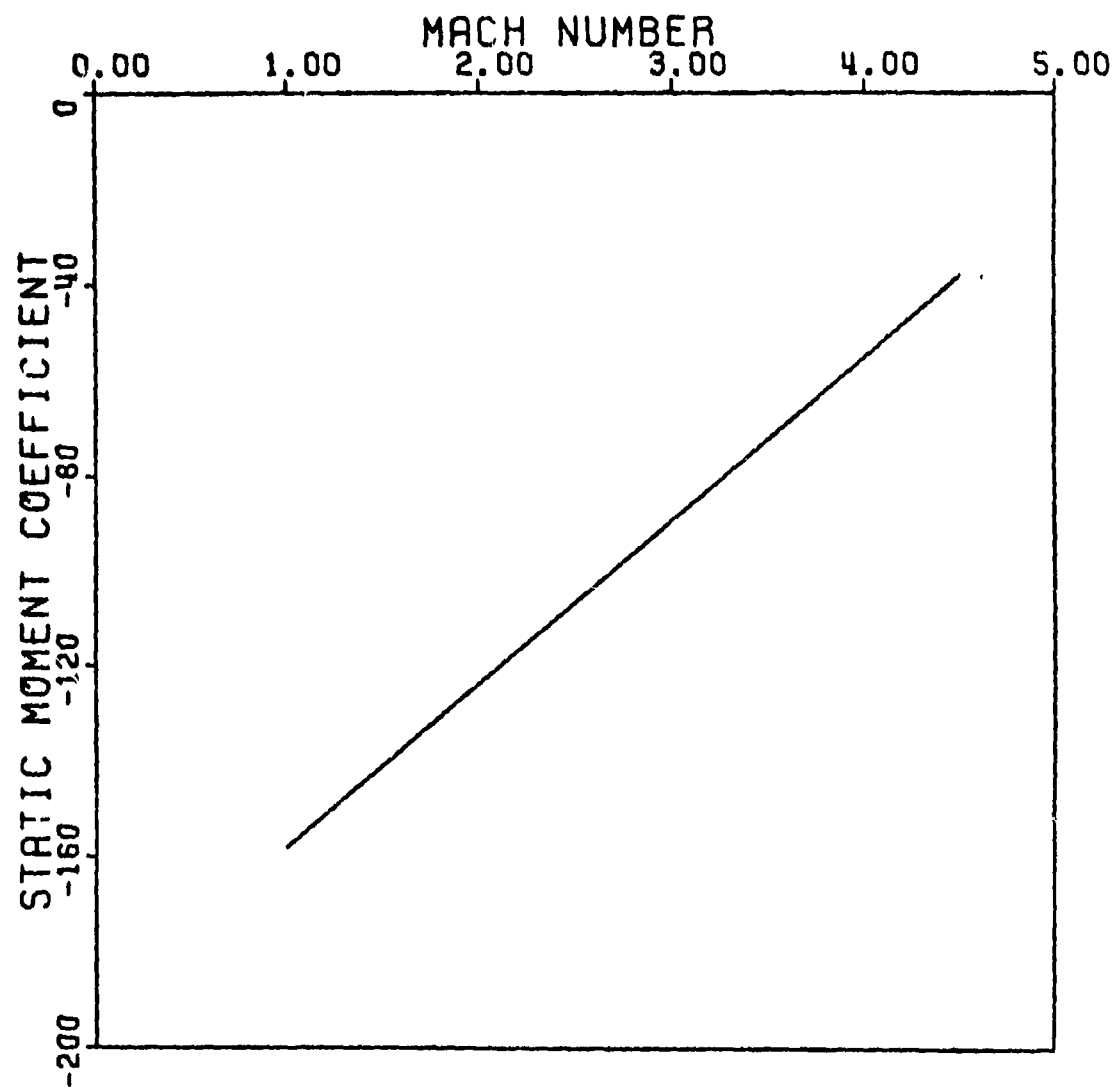


Figure A-2.  $C_{M_\alpha}$  Versus Mach Number  
Producibility Ground Point

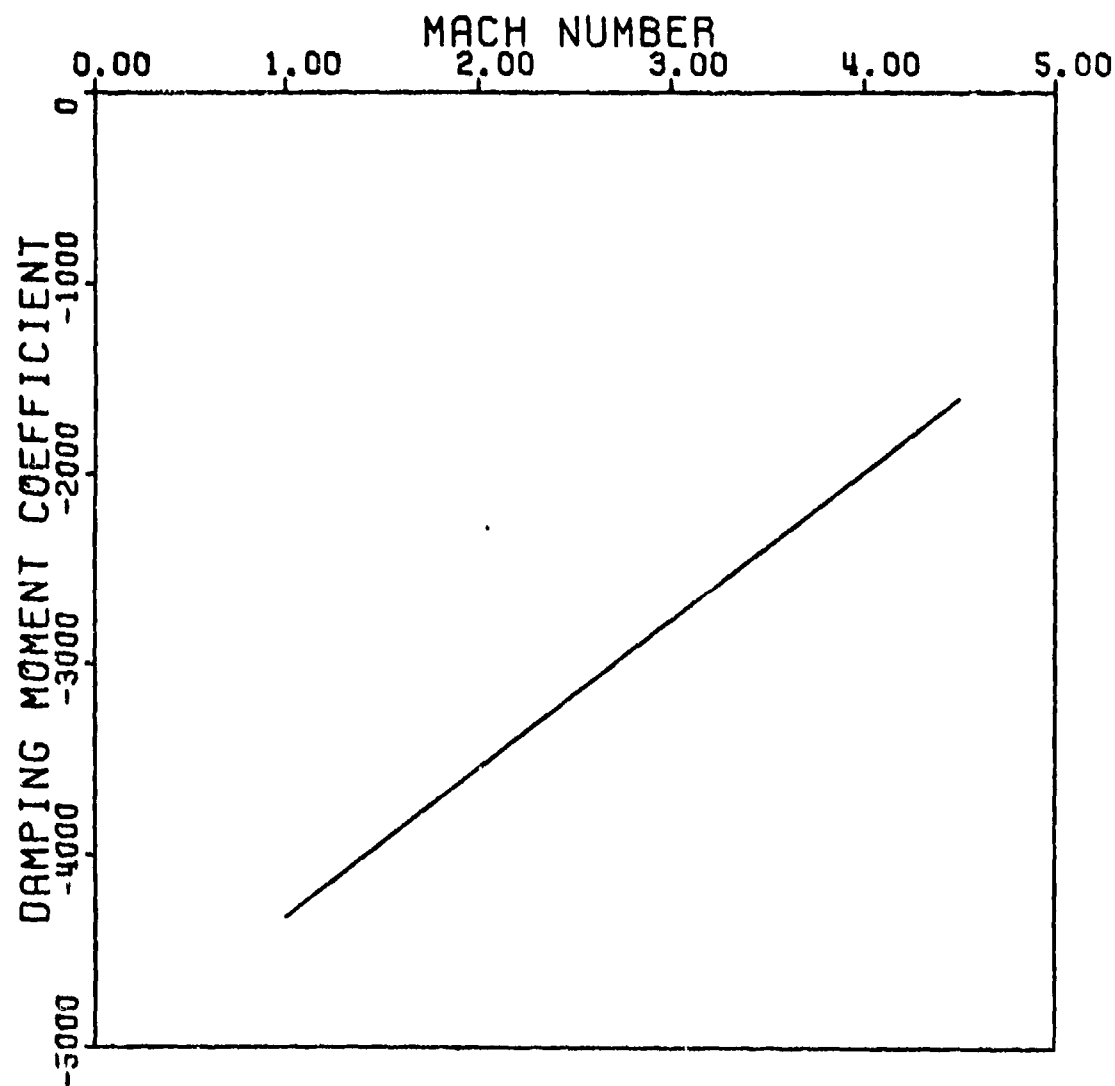


Figure A-3.  $C_{M_q} + C_{M_\alpha}$  Versus Mach Number  
Producibility Ground Point

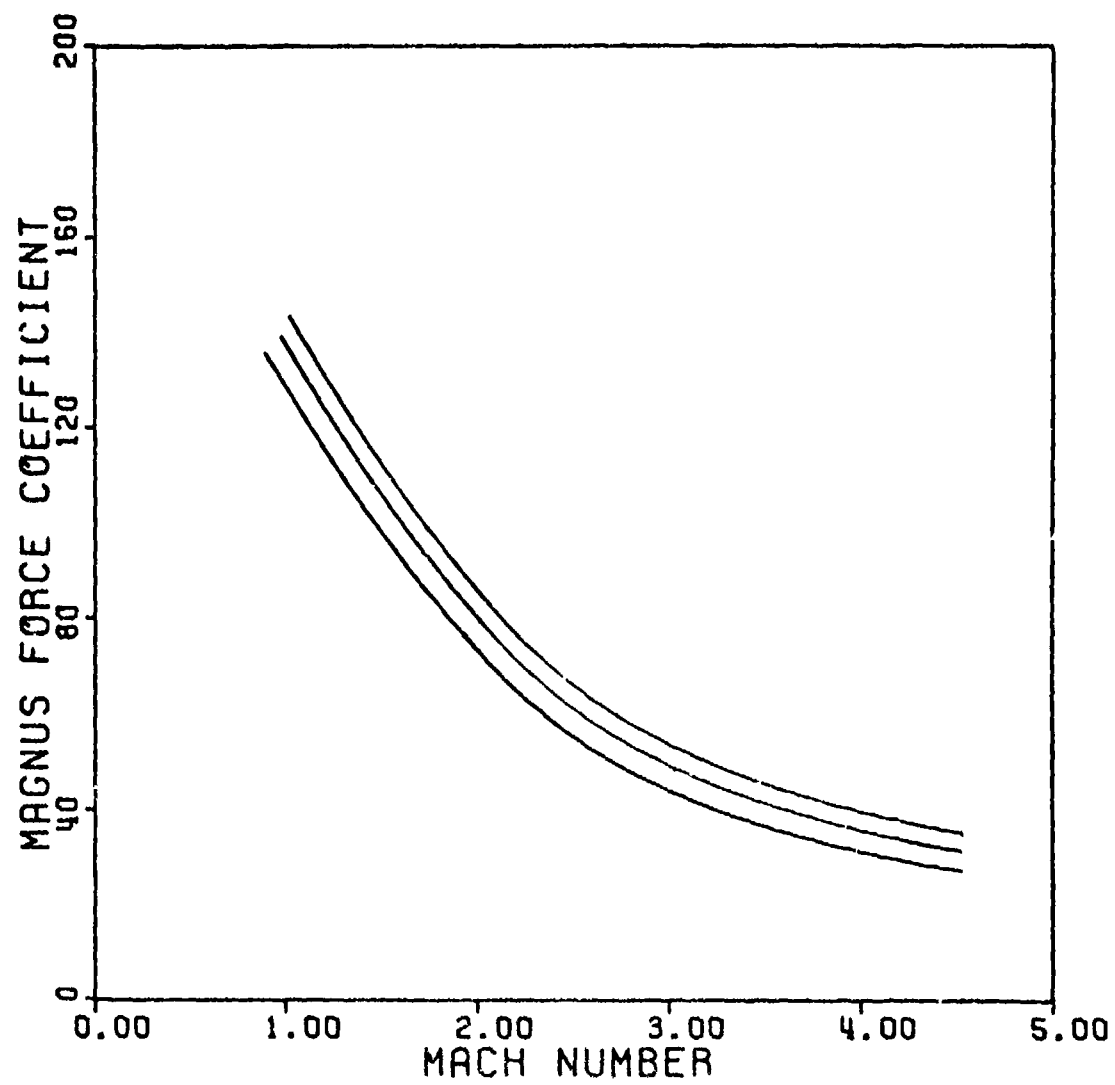


Figure A-4.  $C_{z_{pB}}$  Versus Mach Number  
Producibility Ground Point

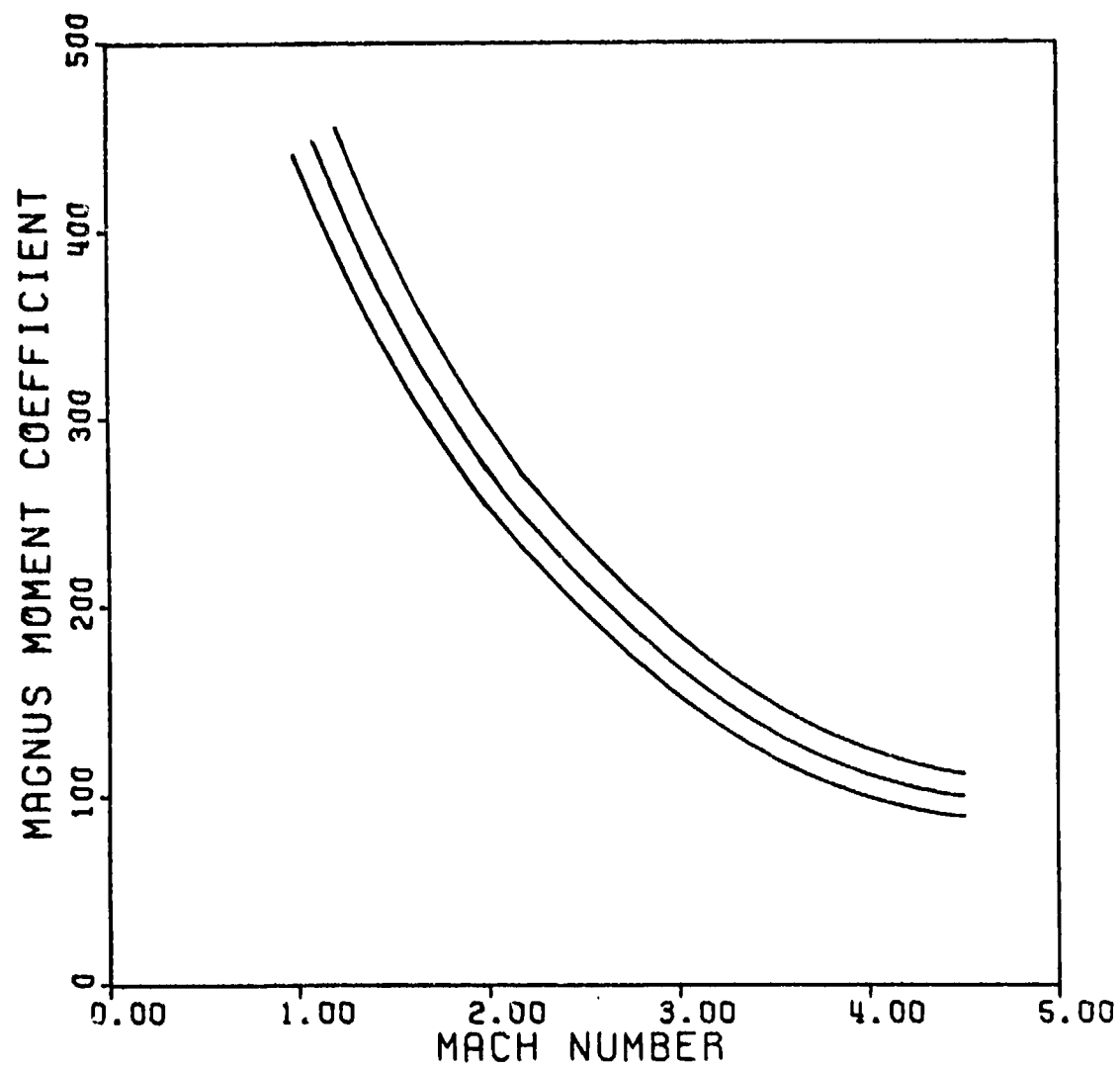


Figure A-5.  $C_{M_{p\beta}}$  Versus Mach Number  
Producibility Ground Point

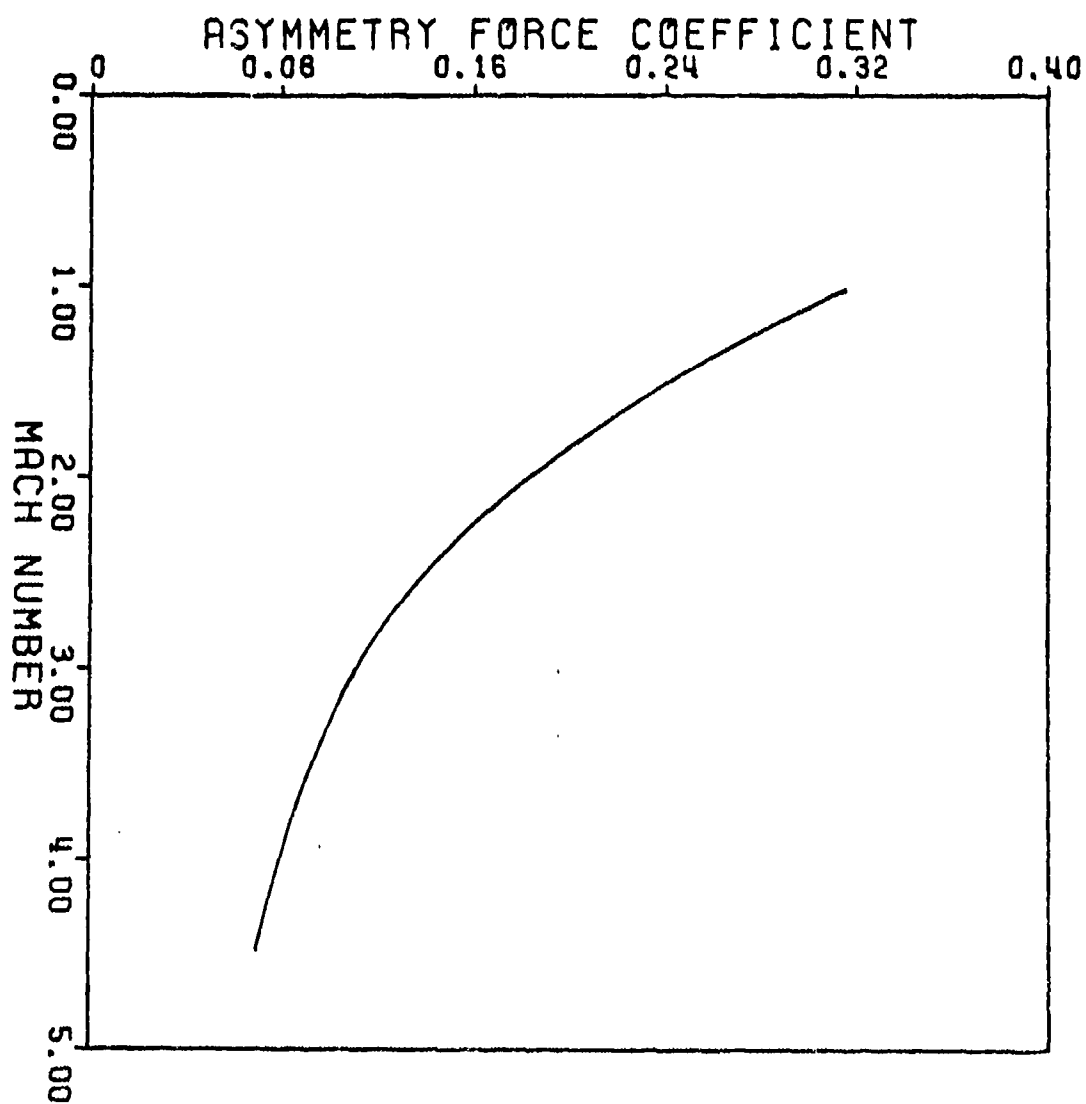


Figure A-6.  $C_{YE}$  ,  $C_{ZE}$  Versus Mach Number  
Producibility Ground Point

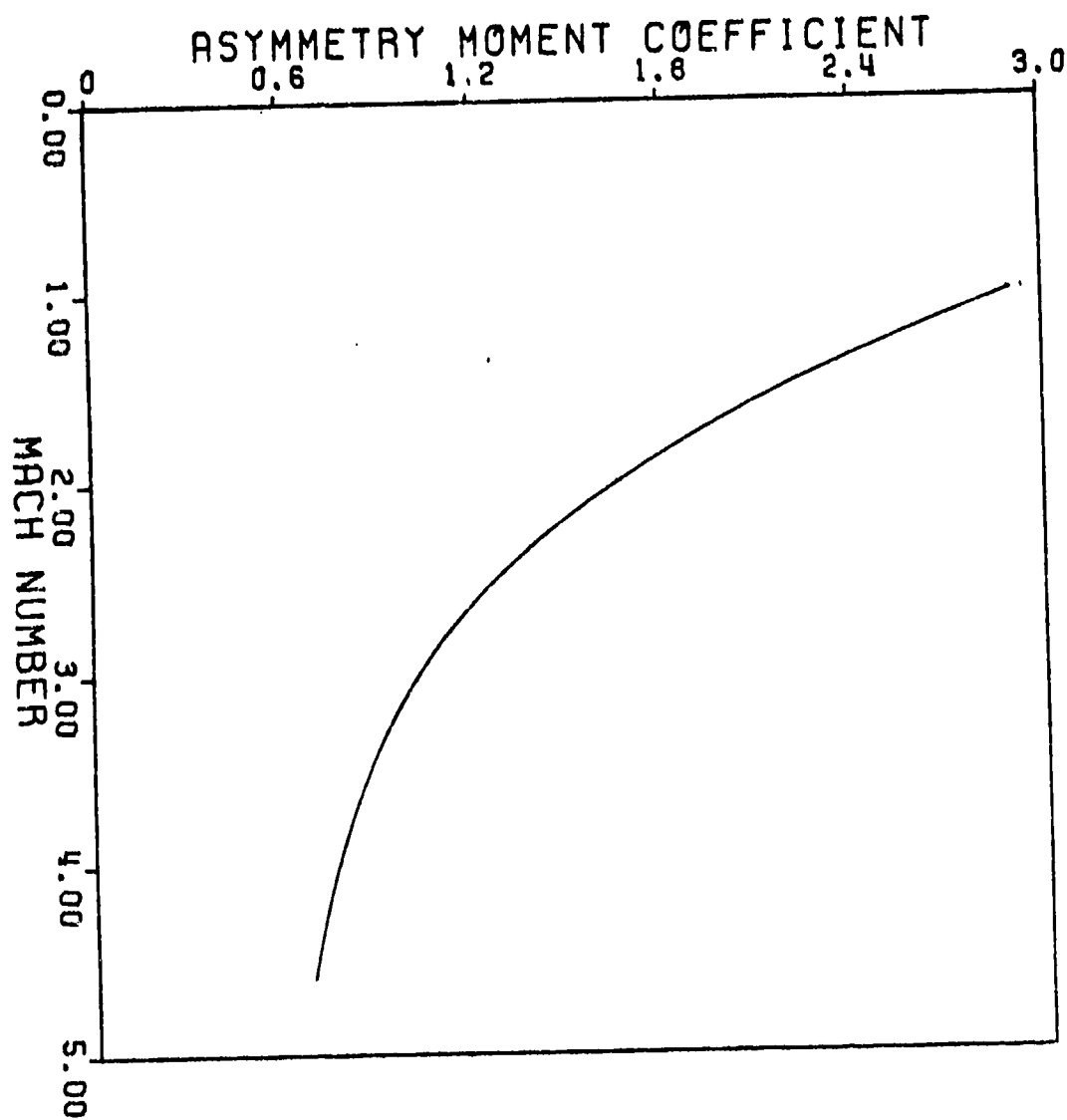


Figure A-7.  $C_{ME}$  Versus Mach Number  
Producibility Ground Point

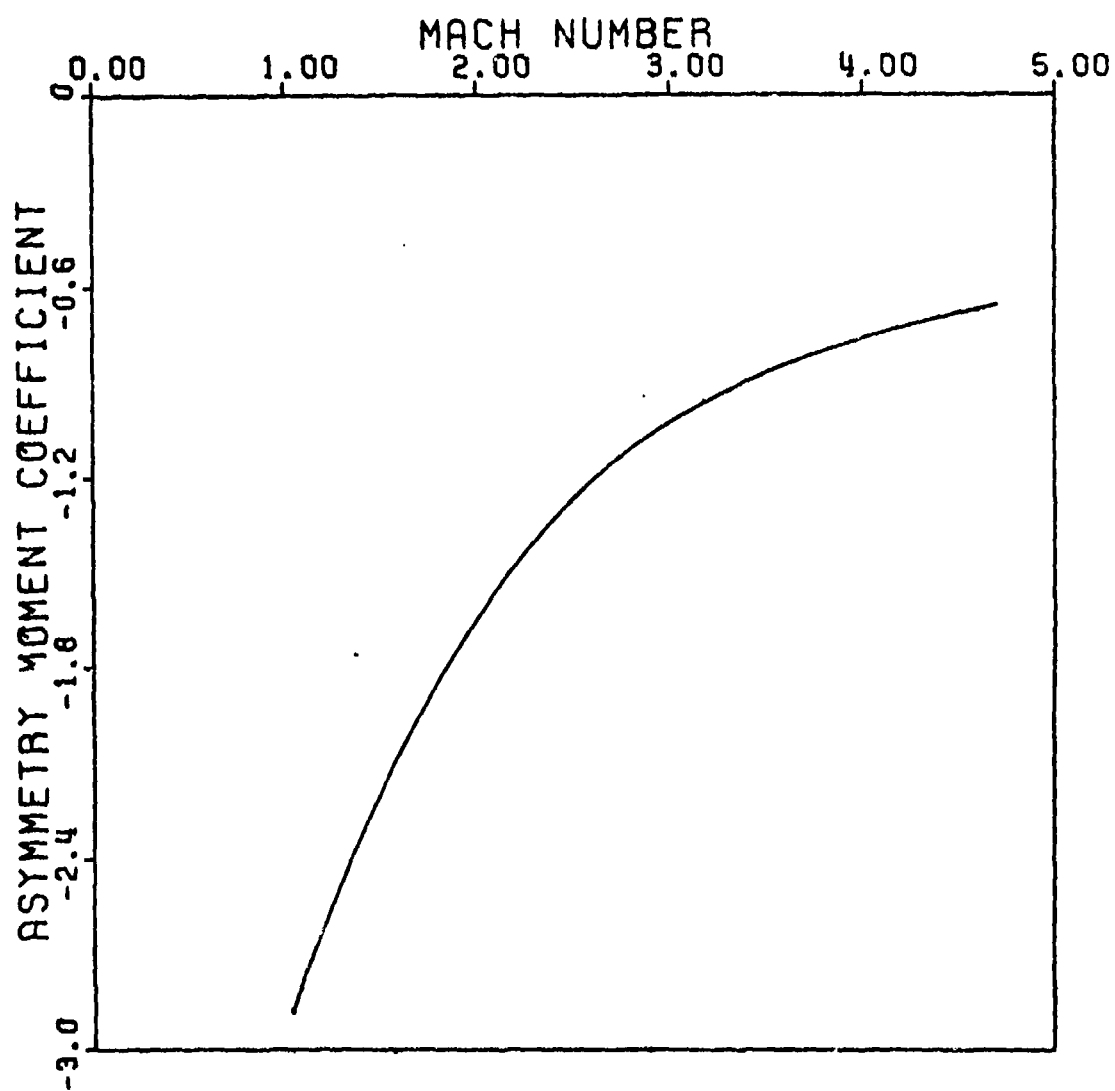


Figure A-8.  $C_{NE}$  Versus Mach Number  
Producibility Ground Point



## REFERENCES

1. Fowler, R. M., Gallop, E. G., Lock, C. N. M., and Richmond, N. W., "Aerodynamics of a Spinning Shell" Phil. Trans. Royal Society, London, 1920.
2. Sterne, T. E., "On Jump Due to Bore Clearance," BRL Report No. 491, 29 Sept 1944.
3. Murphy, C. H., "Comments on Projectile Jump," BRL Report No. 1071, April 1957.
4. Kent, R. H., "First Memorandum Report on 3.3 inch Design Data Firings in Connection with O. B. Program 2627-3," BRL 14 May 1920.
5. Zaroodny, S. J., "On Jump Due to Muzzle Disturbances," BRL Report No. 703, June 1949.
6. Murphy, C. H., Bradley, J. W., "Jump Due to Aerodynamic Asymmetry of a Missile with Varying Roll Rate," BRL Report No. 1077, May 1959.
7. Nicolaides, J. D., "On the Free Flight Motion of Missiles Having Slight Configurational Asymmetries," BRL Report No. 858, June 1953.
8. Nicolaides, J. D., McAllister, L. D., "A Note on the Contribution of Configurational Asymmetries to the Free Flight Motion of Missiles," Journal of the Aeronautical Sciences, Vol. 19, No. 12, Dec 1952.
9. Nicolaides, J. D., "Free Flight Dynamics," Text, Aerospace Engineering Department, University of Notre Dame, 1964.
10. Ingram, C. W., "A Computer Program for Integrating the Six-Degree-of-Freedom Equations of Motion of a Symmetrical Missile," Aerospace Engineering Dept, University of Notre Dame, 1970.
11. Ingram, C. W., Daniels, P., "A Spin Scale Theory for Rigid Body Integration Using the Frick Slip Frame," AIAA Journal, Vol. 5, No. 1 Jan 1967.
12. Ingram, C. W., "Analytical Program for the Evaluation and Reduction of Dispersion and Jump of Fin Bodies," U.S. Army Frankford Arsenal Contract No. DAAA25-71-C0447, August 1972.

# REFERENCES (CONCLUDED)

13. Eikenberry, R. S., "Wobble, Analysis of Missile Dynamic Data," Prepared for Sandia Corp, Albuquerque, N. M. 1969.
14. Ingram, C. W., Nicolaides, J. D. Eikenberry, R. S., Lijewski, L. E., "A Computer Program to Fit the Initial Angular Data from Test Firing of Flechettes," Prepared for U.S. Army, Frankford Arsenal, Phila Pa, 1973.
15. Piddington, M., "The Aerodynamic Characteristics of a Spin Projectile," BRL Memo Report No. 1594, Ballistics Research Laboratory, Aberdeen Proving Ground, Md, Sept 1964.
16. Garsik, M., "Dynamic Supersonic Wind Tunnel Testing," Masters Thesis, University of Notre Dame, Aerospace Dept, May 1974.